SYNTHESIS OF PINCER-LIGATED METAL COMPLEXES FOR DEHYDROGENATION, NITROGEN REDUCTION, AND OLED APPLICATIONS

by

ANDREA FRANCES KOSLOW CASURAS

A dissertation submitted to the

School of Graduate Studies

Rutgers, The State University of New Jersey

In partial fulfillment of the requirements

For the degree of

Doctor of Philosophy

Graduate Program in Chemistry and Chemical Biology

Written under the direction of

Professor Alan S. Goldman

And approved by

_____

_____

_____

_____

New Brunswick, New Jersey

January 2019

ABSTRACT OF THE DISSERTATION

SYNTHESIS OF PINCER-LIGATED METAL COMPLEXES FOR DEHYDROGENATION, NITROGEN REDUCTION, AND OLED APPLICATIONS

By

ANDREA FRANCES KOSLOW CASURAS

Dissertation Director: Alan S. Goldman

After the initial development of pincer complexes in the 1960's, a significant amount of research has been placed into the understanding and applications of pincer complexes. To this day, new applications of pincer-ligated complexes are being discovered. While most commonly used in catalysis, recently pincer-ligated complexes have expanded to other fields, such organic light-emitting devices (OLEDs). This thesis will focus on the synthesis of several pincer-ligated complexes and their application towards dehydrogenation, nitrogen reduction, and OLEDs.

Synthesis of the reported Nishibayashi molybdenum-dimer, the (^{tBu}PNP)MoNCl, and the (^{tBu}PPP)MoNCl complexes were attempted for use in electrochemical nitrogen reduction. Due to the ability of the Nishibayashi complexes to reduce dinitrogen to ammonia chemically, we synthesized them in attempt to do the reduction electrochemically instead. In addition, synthesis of (^{tBu}PPP)RuNCl and (^{tBu}PPP)ReNCl complexes were attempted for comparison to the molybdenum analogue. Lastly, we attempted to synthesize a pyrene-PNP ligand for potential ligand-electrode interactions.

After the attempt reported here, the pyrene-PNP ligand was successful synthesized by a different route in our laboratory.

After DFT calculations and experiments showed that ruthenium was not a good choice for nitrogen reduction, the (^{tBu}PPP)Ru complex was then considered for dehydrogenation work. Several new (^{tBu}PPP)Ru complexes were synthesized and characterized via NMR. Preliminary studies have shown that the (^{tBu}PPP)RuH_4 complex is an effective catalyst for alcohol dehydrogenation and has good potential for alkane dehydrogenation as well.

Another aspect of dehydrogenation work is the acceptor that is used during catalysis. With the goal of doing dehydrogenation electrochemically, benzoquinone was chosen as a potential acceptor. The interactions of benzoquinone, and several benzoquinone derivatives, with (^{tBu}PCP)IrH_2/H_4 were studied. It was observed that quinones are extremely efficient hydrogen acceptors; however, the excess quinone can then strongly bind to iridium, inhibiting any alkane dehydrogenation. We were able to achieve a slow production of ketone from alcohol dehydrogenation, showing that, while strong, the quinone-metal bond can be broken, allowing catalysis.

While (^{tBu}PCP)Ir complexes are extremely well known in the literature for catalysis, their photoluminescence is not usually considered. Several different (^{tBu}PCP)Ir complexes with polycyclic aromatic ligands were studied for their photoluminescence. By making small variations on the polycyclic ligand, we were able to observe the effects these variations had on the emission wavelength. Additionally, each complex was mixed with

polymethylmethacrylate (PMMA) and spin coated on a glass surface to examine their performance and lifetime in the solid state, as they would be in an OLED.

Acknowledgements

I would first, and foremost, like to thank my advisor Professor Alan Goldman for allowing me to explore a plethora of project ideas and supporting me through all my work. During my Ph.D., I came across several difficult situations in my outside life and Alan was always there to lend an ear and help me push through. Also, he allowed me the freedom to develop my leadership skills through managing lab safety, lab cleaning, and, particularly, with the move to the new building. With this freedom to take charge and manage the group, I discovered my love of management and leadership. I cannot thank him enough for this.

I also wish to thank Professors Deirdre O'Carroll, Ralf Warmuth, and Frieder Jäekle for serving on my thesis committee. Additionally, I would like to thank Professor Karsten Krogh-Jespersen for serving on my original committee and giving me guidance my first two years as a graduate student. Also Dr. Jing Lee, for sitting on my OFRP committee last minute.

I would also like to thank Dr. Lawrence Williams, Dr. Evelyn Erenrich, and the RISE program for helping me discover my love of science and pushing me to go to graduate school. Dr. Evelyn Erenrich and the RISE program showed me how to be a scientist and a graduate student. Even now, seven years later, Dr. Erenrich is supporting my future by allowing me to work with the RISE program to give back to undergraduates what it was the program gave me.

I owe sincere gratitude to Dr. Tom Emge, for his guidance with X-ray cyrstallographics, Dr. Nagarajan Murali, for NMR expertise, and Dr. Gene Hall, for teaching me all about mass spectrometry.

Without the support of CENTC I would not be where I am today. Through the collaborations with Dr. Alexander Miller, Dr. Pat Holland, Dr. Jim Mayer, and Dr. Bill Jones, along with the rest of CENTC, I was able to learn how to collaborate with other university and develop a project across multiple disciplines. Additionally, CENTC supported the LEEDAR program, which allowed me to go into high-school to inspire and teach students about chemistry. Something I started doing in my undergraduate university and was ecstatic to continue.

I would like to thank Dr. Geeta Govindarajoo for all her support and knowledge about teaching. Through teaching her class over the past five years I developed a love for teaching and working with students. She taught me how to interact with students and inspire them. She is the one who confirmed my passion for being a mentor and a leader to others.

I would especially like to thank the other members of the Goldman group, past and present. Special thanks to Dr. Katie Field and Dr. David Laviska, who introduced me to organometallic chemistry and taught me Schlenk techniques. Additionally, I would like to thank the current members of the group (Benjamin Gordon, Tariq Bhatti, Bo Li, Arun Shada, Boris Sheludko, and Soumyadipa Das). Particularly, I would like to thank Ben and Boris for being an amazing support to me and always being there when I needed them.

I would like to thank Dr. Nicholas Lease. Without Nick's support and friendship, I would have never made it through my Ph.D. As a friend, has always supported and stood beside me. Even on the bad days he was there to help me along and cheer me up. As a coworker, he would always help and discuss research. Through his expertise, I was able to develop my own knowledge and skill beyond what I expected.

I would like to thank my family for their love and support. I would like to thank my father, sister, and grandmother for always being there and truly supporting me through life. I would especially like to thank my mother, Janice Koslow, for turning me into the woman I am today. Through her love and support I have been able to achieve many things. Without her constantly pushing me to be a better person and a strong individual, I would not be in graduate school.

Finally, I would like to thank my boyfriend Jim Hadfield for all his love and support throughout my Ph.D. Despite the long distance and the constant four-hour drives to see each other, he has stood by me and always made me believe that I can achieve anything. His never-ending support helped motivate me through this difficult process and has kept me positive and excited for the future. I love him with all my heart and I am extremely thankful he is in my life.

Dedication

To my boyfriend, my mother, and most importantly, Booger.

Table of Contents

List of Figures

List of Schemes

List of Tables

Chapter 1

Introduction

"Pincer" ligands are a class of tridentate ligands that are identified by their meridional configuration. First developed in 1976 by Moulton and Shaw[1], pincer ligands have developed into a valuable tool for tuning the reactivity and selectivity of metal catalysts. Using a pincer-ligand provides the metal complex with high thermal stability (>240^{o}C) and easy tunability through both steric and electronic modifications (Figure 1.1). For example, changing the R group influences the reactivity of the pincer complex.[2,3] Changing from a *tert*-butyl to an *iso*-propyl will change the sterics of the complexes; with a less bulky R group, the complex will be less stable, however, it will be more reactive.[4] If one changes the L_t group from a phosphorous to a nitrogen, both the sterics and the electronics change, and this can allow the ligand to become hemilabile.[5,6] One can also change the X linker from the more common CH_2 to an O.[7] The smaller atomic radius of O results in shorter bond lengths, pulling the P atoms away from the metal center, allowing for easier substrate coordination. Lastly, one can place different atoms in the L_i position to change the electronics and trans-influence of that central atom, or place different substituents at Y, allowing for finer tuning of electronics or the ability to tether the catalyst to a solid support or electrode.[8-11]

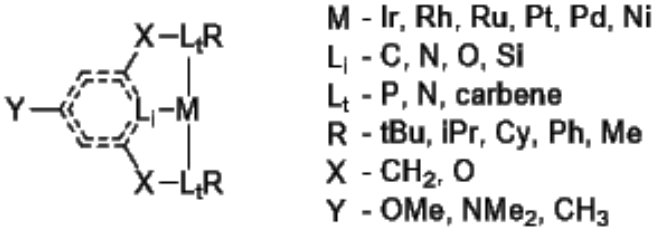

Figure 1.1: Variations for Pincer Ligands

One of the first pincer complexes developed by Moulton and Shaw was a (κ^3-2,6-(tBu$_2$PCH$_2$)$_2$C$_6$H$_3$)IrHCl complex.[1] Their ligand was soon abbreviated to ^{tBu}PCP and since then all pincer complexes have been abbreviated based on the atoms bound to the metal center and any non-carbon linkers (Figure 1.2). When duplications occur (use of the same three atoms bound to the metal), the complexes are given different names (i.e. "Phebox", "Macho", etc.). Traditionally, pincer ligands contain neutral donor atoms such as P, O, N, and S with a central anionic carbon, most commonly as part of a phenyl ring.[12-16] However, since their discovery, an extremely wide range of pincer ligands have been developed that incorporate new and unique structures.

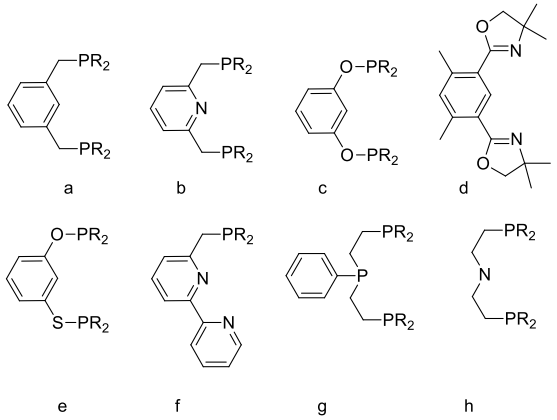

Figure 1.2: Various Pincer-Ligands (a) PCP (b) PNP (c) POCOP

(d) NCN = "Phebox" (e) PSCOP (f) PNN (h) PNP = "Macho"

Pincer-ligated metal complexes have been used in a wide variety of applications (i.e. fundamental organometallics, catalysis, materials chemistry etc.). The first report of reactivity was in 1983 by Kaska and Jensen.[16] In their report, they show that (^{tBu}PCP)RhHCl can be dehydrohalogenated at room temperature and the resulting intermediate undergoes C-H activation of either the solvent or one of the *tert*-butyl groups on the phosphorous arms (Scheme 1.1). While they were not able to extend this reactivity to catalysis, the discovery that pincer-metal complexes had the ability to perform C-H activation inspired scientists to further explore the potential of pincer-metal complexes.

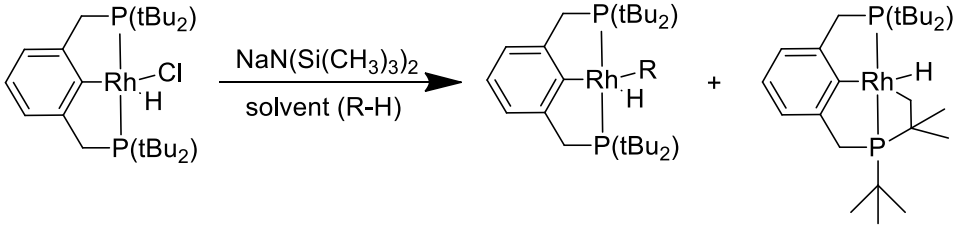

Scheme 1.1: C-H Activation by (^{tBu}PCP)RhHCl

It wasn't until over a decade later that the first report of transfer dehydrogenation was published. In 1996, Kaska and Jensen reported that the (^{tBu}PCP)IrH_2 pincer complex could dehydrogenate cyclooctane using *tert*-butylethylene (TBE) as a sacrificial hydrogen acceptor (Scheme 1.2).[18] Only a few years later, our laboratory reported the dehydrogenation of n-octane using (^{iPr}PCP)IrH_2 and TBE (Scheme 1.3).[19] Mechanistic studies suggest initial coordination of the TBE to the catalyst, followed by a 1,2-insertion into the Ir-H bond. The reductive elimination of the alkane gives the 14 e^- (PCP)Ir species that can oxidatively add the alkane. Subsequent β-hydride elimination and olefin

dissociation generate the olefin product and regenerate the starting catalyst (Scheme 1.4).[20,21]

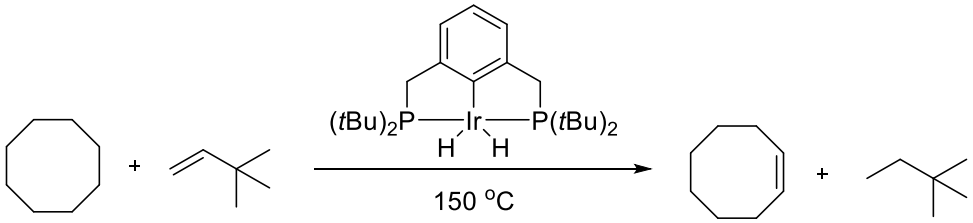

Scheme 1.2: Transfer Dehydrogenation of Cyclooctane using (^{tBu}PCP)IrH$_2$

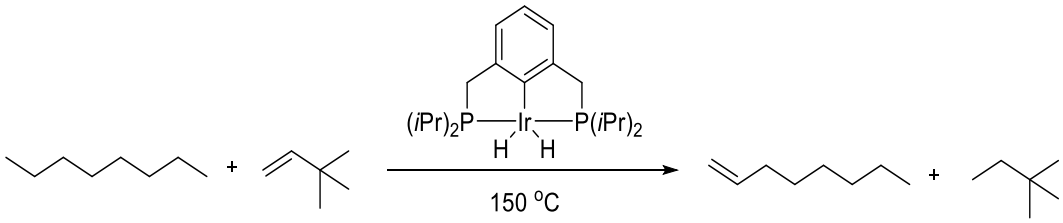

Scheme 1.3: Transfer Dehydrogenation of n-Octane using (^{tBu}PCP)IrH$_2$

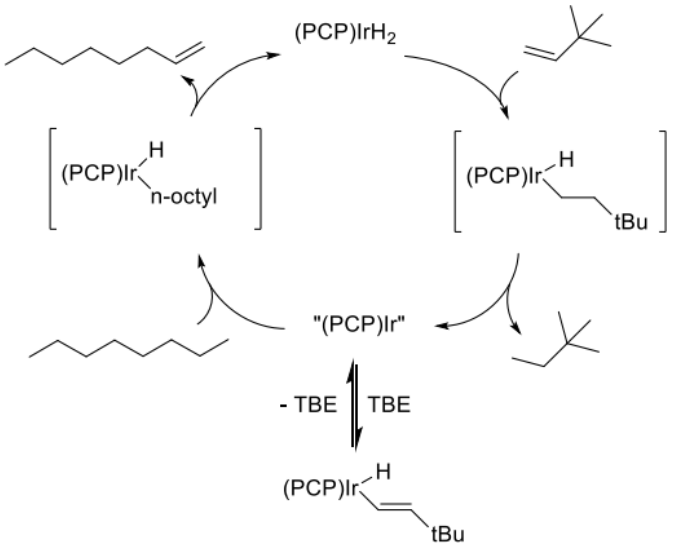

Figure 1.3: Mechanism of Transfer Dehydrogenation using (^{tBu}PCP)IrH$_2$

Since the first report, pincer-metal complexes have been studied in a wide variety of C-H activations. In 2006, our group, along with Brookhart, reported the use of pincer catalysts for transfer dehydrogenation in combination with a Schrock molybdenum olefin metathesis catalyst to affect alkane metathesis.[22] Our group has also shown the ability of pincer complexes to C-H activate aryl and vinyl substrates.[21] Lastly, pincer catalysts have the ability to form C-C bonds, such as via the Suzuki biaryl and Heck olefin arylation coupling reactions.[23]

Other than C-H activation, pincer complexes have been shown to react with a wide variety of small molecules (Figure 1.4). They can successfully activate O-H bonds, performing alcohol dehydrogenation to aldehydes and ketones[24]; they can react with O_2[25], N_2[26-28], and CO[29]; and they can activate both C-F[30] and N-H[31] bonds. For most pincer-iridium complexes, N_2 binds and inhibits further reactivity, however recent reports show that pincer-molybdenum and pincer-iron complexes can reduce the N_2 to ammonia.[26-28] The cleavage of dinitrogen to form metal nitrides and produce ammonia is one of the most sought-after reactions in chemistry today.

While mostly known for their catalytic properties and small molecule activation, it is worth noting other fields of science that pincer complexes have begun to reach. Over the past decade, pincer-metal complexes have begun to appear in both materials and biochemical research. They have been involved in the study of enzymes,[32] surfactants,[33] polymers, and OLED design.[34] The wide range of applications for pincer-metal complexes stems back to the high stability and tunability the pincer ligand provides. Between unique

ligand design, different metal-ligand combinations, and a wide variety of applications, there is still a lot to discover about pincer-metal complexes and their reactivities.

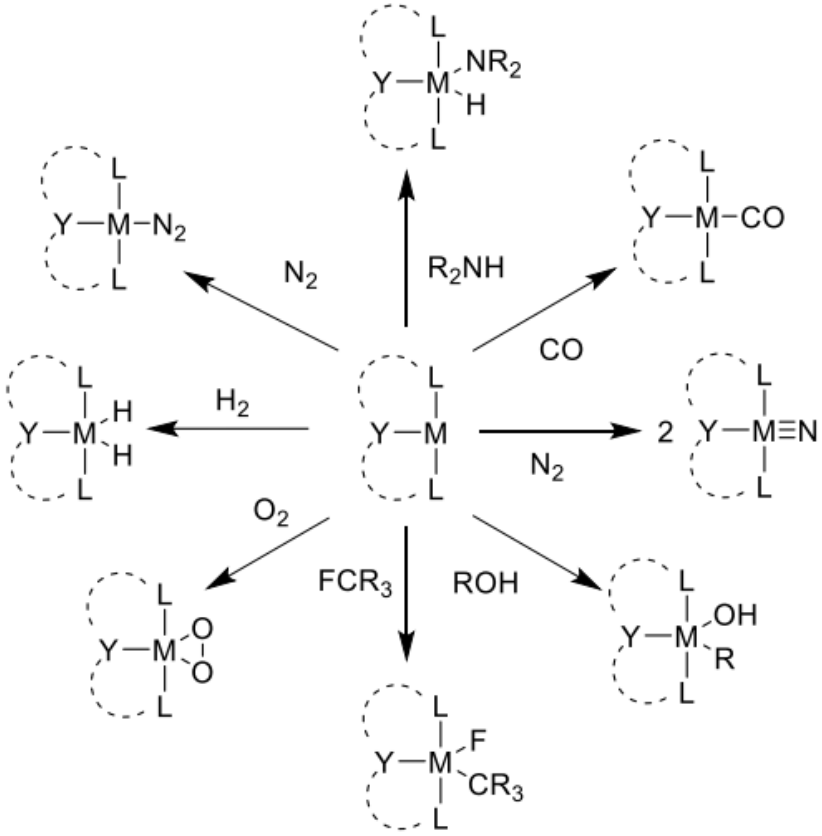

Figure 1.4: Small Molecule Activation using Pincer-Metal Complexes

1.2: Research Goals of this Thesis

While numerous pincer-metal complexes have been developed, the full range of their reactivities and applications are unknown. In order to advance and improve pincer-metal chemistry, one must look to improve not only the catalyst itself, but also explore novel reactions/conditions using known catalysts. The aim of this thesis is to synthesize reported pincer-metal complexes and explore their reactivity in a new way.

Chapter 2 discusses the synthesis of pincer-metal catalysts for use in electrochemical nitrogen reduction. In the first part, early experimental and DFT results on several pincer-metal complexes showed that molybdenum is the best metal of choice for nitrogen reduction. Nishibayashi has reported several pincer-Mo complexes that reduce nitrogen to ammonia chemically.[35,36] This chapter focuses on the synthesis of several of these pincer-Mo complexes to attempt nitrogen reduction in an electrochemical setting. Additional synthetic efforts were made towards novel pyrene-PNP ligand that would allow for direct interactions between the pincer-ligand and electrode in the electrochemical process.

Chapter 3 discusses the synthesis and reactivity of (^{tBu}PPP)Ru complexes. First reported in 2012, the (^{tBu}PPP)$RuCl_2$ complex was never studied for reactivity or catalysis.[37] This chapter focuses on the synthesis and characterization of several (^{tBu}PPP)Ru complexes. Additionally, initial dehydrogenation studies show the potential the (^{tBu}PPP)RuH_4 complex has as a catalyst for alkane and alcohol dehydrogenation.

Chapter 4 discusses the well-known cyclooctane transfer-dehydrogenation reaction using (^{tBu}PCP)IrH_2. Since its discovery, this reaction has most commonly been done using TBE or NBE as a sacrificial hydrogen acceptor. This chapter focuses on the possibility of using para-quinones as a non-sacrificial hydrogen acceptor, avoiding the production of chemical waste. Ideally using electrochemistry, the para-quinone could act as a hydrogen acceptor and then be regenerated through the loss of two protons and two electrons.

Chapter 5 focuses on the extremely well studied (^{tBu}PCP)Ir complex and explores its use in an entirely different field of science, OLEDs. Using the (^{tBu}PCP)Ir framework, several (^{tBu}PCP)Ir(ppy)H and (^{tBu}PCP)Ir(ppy)Cl complexes (ppy=2-phenylpyridine) were synthesized and characterized. The effects of different electronics on the emission wavelength and intensity were studied by making small changes to the phenylpyridine ligand.

1.3: References

1) Moulton, C. J.; Shaw, B. L. *J. Chem. Soc., Dalton Trans*. **1976**, 1020.
2) Punji, B.; Emge, T. J.; Goldman, A. S. *Organometallics* **2010**, *29*, 2702.
3) Adams, J. J.; Lau, A.; Arulsamy, N.; Roddick, D. M. *Organometallics* **2011**, *30*, 689.
4) Choi, J.; MacArthur, A. H. R.; Brookhart, M.; Goldman, A. S. *Chem. Rev.* **2011**, *111*, 1761.
5) Flores, J. A.; Haibach, M. C.; Goldman, A. S. ACS: 2012, INOR 8
6) Nishiyama, H.; Niwa, E.; Inoue, T; Ishima, Y.; Aoki, K. *Organometallics* **2002**, *21*, 2572.
7) Göttker-Schnetmann, I.; White, P. S.; Brookhart, M. *Organometallics* **2004**, *23*, 1766.
8) Gupta, M.; Hagen, C.; Flesher, R. J.; Kaska, W. C.; Jensen, C. M. *Chem. Commun.* **1996**, 2083.
9) Hermann, D.; Gandelman, M.; Rozenberg, H.; Shimon, L.J.W.; Milstein, D. *Organometallics* **2002**, *21*, 812.
10) Haibach, M.C.; Wang, D.Y.; Emge, T.J.; Krogh-Jespersen, K.; Goldman, A.S.; *Chem. Sci.* **2013**, *4*, 3683.
11) Maclnnis, M.C.; MacLean, D.F.; Lundgren, R.J.; McDonald, R.; Turculet, L. *Organometallics* **2007**, *26*, 6522.
12) Albrecht, M.; van Koten, G. Angew. *Chem. Int. Ed.* **2001**, *40*, 3750-3781.
13) Morales-Morales, D. *Rev. Soc. Quim. Méx.* **2004**, *48*, 338-346.
14) Roddick, D. M. *Top. Organomet. Chem.* **2013**, *40*, 49-88.
15) Asay, M.; Morales-Morales, D. *Dalton Trans*. **2015**, *44*, 17432-17447.
16) van der Boom, M. E.; Milstein, D. *Chem Rev.* **2003**, *103*, 1759-1792.
17) Nemeh, S.; Jensen, C.; Binamira-Soriaga, E.; Kaska, W. C. *Organometallics* **1983**, *2*, 1442-1447.
18) Gupta, M.; Hagen, C.; Flesher, R. J.; Kaska, W. C.; Jensen, C. M. *Chem. Commun.* **1996**, 2083.
19) Liu, F.; Pak, E. B.; Singh, B.; Jensen, C. M.; Goldman, A. S. *J. Am. Chem. Soc.* **1999**, *121*, 4086.
20) Renkema, K. B.; Kissin, Y. V.; Goldman, A. S. *J. Am. Chem. Soc.* **2003**, *125*, 7770.
21) Kanzelberger, M.; Singh, B.; Czerw, M.; Krogh-Jespersen, K.; Goldman, A. S. *J. Am. Chem. Soc.* **2000**, *122*, 11017.
22) Goldman, A. S.; Roy, A. H.; Huang, Z.; Ahuja, R.; Schinski, W.; Brookhart, M. *Science* **2006**, *312*, 257.
23) Albrecht, M.; van Koten, G. *Angew. Chem., Intl. Ed.* **2001**, *40*, 3750.
24) Kundu, S.; Choi, J.; Wang, D. Y.; Choliy, Y.; Emge, T. J.; Krogh-Jespersen, K.; Goldman, A. S. *J. Am. Chem. Soc.* **2013**, *135*, 5127.
25) Boisvert, L.; Goldberg, K. *I. Acc. Chem. Res.*, **2012**, *45*, 899.
26) Silantyev, G.A.; Förster, M.; Schluschaβ, B.; Abbenseth, J.; Würtele, C.V.; Holthausen, M.C.; Schneider, S. *Angew, Chem.* **2017**, *56*, 5872.
27) Klopsch, I.; Finger, M.; Würtele, C.; Milde, B.; Werz, D.B.; Schneider, S. *J. Am. Chem. Soc.* **2014**, *136*, 6881.
28) Schendzielorz, F.S.; Finger, M.; Volkmann, C.; Wurtele, C.; Schneider, S. *Angew. Chem.* **2016**, *55*, 11417.

29) Lee, D. W.; Jensen, C. M.; Morales-Morales, D. *Organometallics* **2003**, *22*, 4744.
30) Choi, J.; Wang, D. Y.; Kundu, S.; Choliy, Y.; Emge, T. J.; Krogh-Jespersen, K.; Goldman, A. S. *Science* **2011**, *332*, 1545.
31) Balaraman, E.; Gnanaprakasam, B.; Shimon, L. J. W.; Milstein, D. *J. Am. Chem. Soc.* **2010**, *132*, 16756.
32) Rankin, J; Mauban, R; Fellner, M; Desguin, B; McCracken, J; Hu, J; Varganov, S; Hausinger, R. *Biochemistry* **2018**, *57*, 3244-3251.
33) Davidi, I; Patra, D; Hemida-Merino, D; Portale, G; Rotello, V; Raviv, U; Shenhar, R. *Macromolecules* **2014**, *47*, 5774-5783.
34) Liao, J; Rajakannu, P; Liu, S; Lee, G; Chou, P; Jen, A; Chi, Y. *Inorg. Chem.* **2018**, *57*, 8287-8298.
35) Tanaka, H.; Arashiba, K.; Kuriyama, S.; Sasada, A.; Nakajima, K.; Yoshizawa, K.; Nishibayashi, Y. " *Nat. Commun.* **2014**, *5*, 3737-3737.
36) Arashiba, K.; Kinoshita, E.; Kuriyama, S.; Eizawa, A.; Nakajima, K.; Tanaka, H.; Yoshizawa, K.; Nishibayashi, Y. *J. Am. Chem. Soc.* **2015**, *137*, 5666-5669
37) Gilbert-Wilson, R; Field, L; Bhadbhade, M. *Inorg. Chem.* **2012,** *51,* 3239-3246.

Chapter 2

Synthesis of Rhenium, Ruthenium, and Molybdenum Pincer-Ligated Complexes for Nitrogen Reduction

Abstract:

The Haber-Bosch process is the main industrial method used to synthesize ammonia today. It is estimated that in 2008, the Haber-Bosch process sustained every 1 out of 2 people, and today that number is probably closer to 2 out of 3.[1] While necessary, the Haber-Bosch process is highly inefficient, requiring high temperatures and pressures, as well as having a very low per-pass conversion. A potential alternative to the Haber-Bosch process would be to catalytically reduce nitrogen to ammonia through use of electrochemistry. This process would be cheaper, requiring significantly lower temperatures and pressures, and could be run from sustainable energy sources. To achieve this, a catalyst capable of electrochemically splitting nitrogen must be developed. Here we report the synthesis of several of the reported Nishibayashi molybdenum complexes to attempt electrochemical nitrogen reduction. We also attempt the synthesis of Re and Ru pincer-complexes, and a pyrene-PNP pincer ligand, for comparison with that of the Nishibayashi complexes.

2.1: Introduction

It is estimated that globally, close to 60% of the nitrogen in human tissue is derived from synthetic fertilizer.[1] Developed in the 1900s, the Haber-Bosch process produces almost all the synthetic fertilizer used today.[2] However, the Haber-Bosch process is extremely energy intensive, accounting to almost 2% of the world's total energy consumption.[3] This large amount of energy derives from the tremendously high temperatures (>300°C) and pressures (>125 atm) required. Additionally, the process itself is not very efficient, resulting in a very low per-pass conversion rate (ca. 15%).[4] Lastly, a large portion of the energy required goes into the production of the H_2 gas required before the process can even begin.

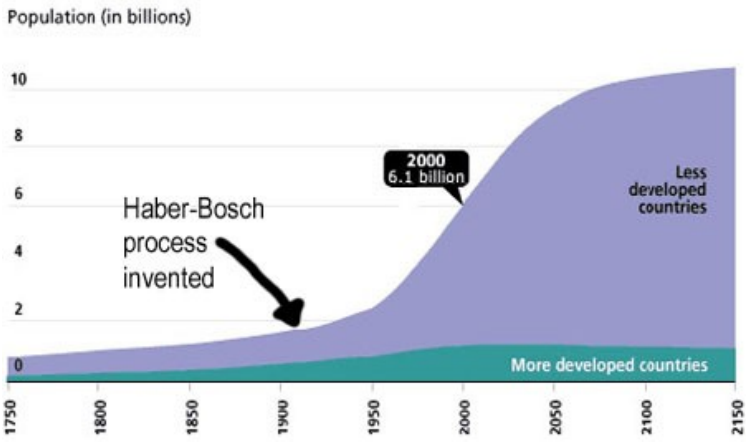

Figure 2.1: Effect of Haber-Bosch Process on World Population[5]

An ideal route to ammonia would be electrochemical, effectively the reaction of N_2 with H_2O to give O_2 as a by-product, driven by a renewable electrical power source (Figure 2.2). This could be complementary with renewable energy since production rates could be varied to accommodate mismatches in supply and demand. While we have yet to achieve an ideal route using water, our collaborators have been able to demonstrate

that the reduction of nitrogen to ammonia can be done in organic solvents with a different proton and electron source.[6]

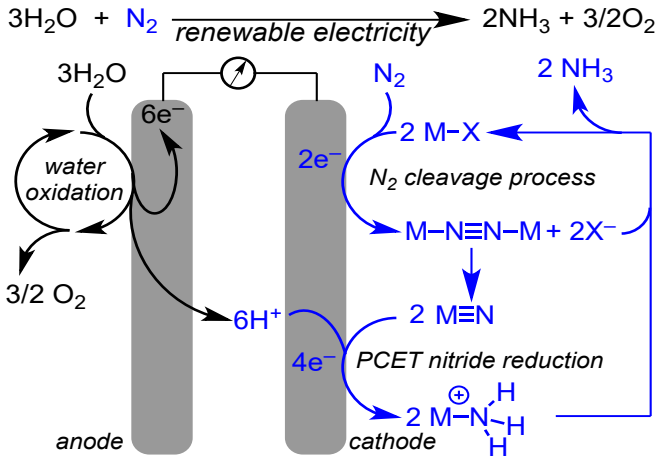

Figure 2.2: Electrochemical Approach to N_2 Reduction[7]

Ammonia itself can be used as a fertilizer, however, ammonium nitrate and urea are more commonly used.[8] To make ammonium nitrate and urea, nitrogen is first reduced to ammonia and then re-oxidized to make the desired compound. Using an electrochemical approach, we could potentially bypass the need to first make ammonia, which means a significant reduction in the amount of energy required.[9,10]

$$N_{2(g)} + 6H^+_{(aq)} + 6e^- \longrightarrow 2NH_{3(aq)} \quad E° = +0.092\ V \quad (3)$$

$$n = 6,\ \Delta G° = -nFE° = +157\ \text{kcal mol}^{-1}$$

$$^{n}/_{2}\,H_2O_{(l)} \longrightarrow {}^{n}/_{4}\,O_2 + nH^+_{(aq)} + ne^- \quad -E° = -1.23\ V \quad (4)$$

$$n = 2,\ \Delta G° = -nFE° = -1\ \text{kcal mol}^{-1}$$

$$N_{2(g)} + 3O_{2(g)} + 2H^+ + 2e^- \longrightarrow 2HNO_{3(aq)} \quad E° = +1.24\ V \quad (5)$$

Figure 2.3: Energy Savings by Direct Oxidation of N_2 to HNO_3

When approaching the mechanism behind nitrogen reduction, there are three main pathways that can be considered: N_2 cleavage, distal, and alternating pathways. If one looks at the FeS clusters in nitrogenase enzymes, they would observe the reduction of dinitrogen to ammonia with the H^+ coming from water molecules and the electron coming from ATP hydrolysis.[11-13] It is currently unknown whether these nitrogenase enzymes go through the distal or alternating path, however, current evidence supports the latter.[14-16]

In an attempt to replicate the nitrogenase enzymes, in 2003 Yandulov and Schrock reported the first molecular catalyst capable of reducing N_2 to NH_3 chemically.[17,18] Since this first report, the work of Peters and Nishibayashi has expanded our knowledge of nitrogen reduction chemistry, focusing primarily on iron and molybdenum catalysts.[19-28]

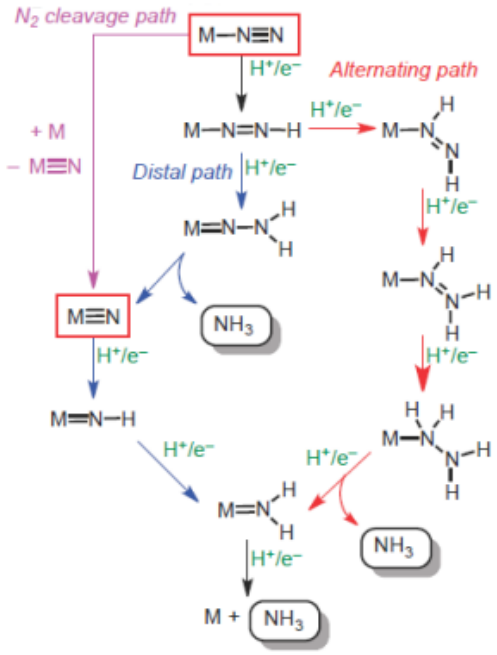

Figure 2.4: Possible Pathways for Dinitrogen Reduction

Looking further into the mechanism of their catalysts, both Schrock and Peters demonstrated that the reduction of nitrogen can go through the distal pathway. Using both computational and mechanistic work, they showed their catalysts proceed through both the high energy diazenido (M-NHNH) and hydrazideo (M-NNH_2) intermediates. To confirm this, they were able to isolate both intermediates and characterize them. Nishibayashi also saw this mechanism type with his (PNP)Mo-dimer. However, while these catalysts were able to reduce nitrogen to ammonia, they suffered from low turnovers and had a significant production of H_2 from a side reaction between the acid proton source and the reductant.

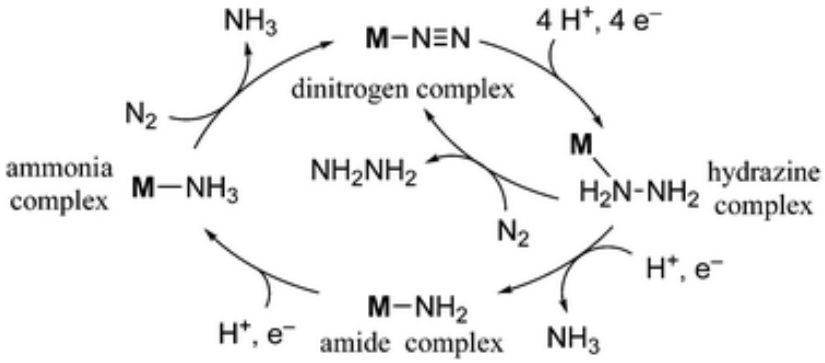

Figure 2.5: Alternating Path Mechanism Seen in the Work of Schrock and Peters

Since 2003, a main focus of nitrogen reduction research has been developing a catalyst that has high turnovers of ammonia. To date, the most successful catalyst is (^{tBu}PNP)MoI_3, developed by Nishibayashi.[28] It is capable of up to 450 turnovers of ammonia per metal center which is a significant increase to the previous record of 63 turnovers held by Peters.[18-20] Additionally, Nishibayashi has shown that in contrast to the Schrock and Peters catalysts, his molybdenum nitride catalysts go through the nitrogen

splitting pathway. Using two metal centers, his catalysts can split the dinitrogen into two metal-nitride complexes. From here the nitride can be reduced to ammonia and, upon the addition of another dinitrogen and (PNP)Mo fragment, ammonia is released and the cycle repeated (Figure 2.7).

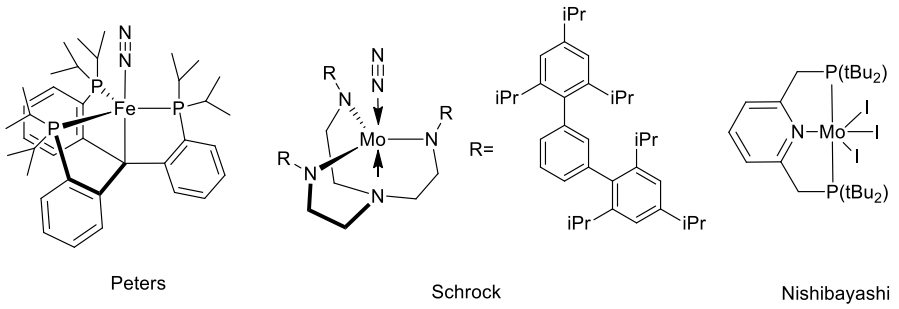

Figure 2.6: Peter's, Schrock's, and Nishibayashi's Nitrogen Reduction Catalysts

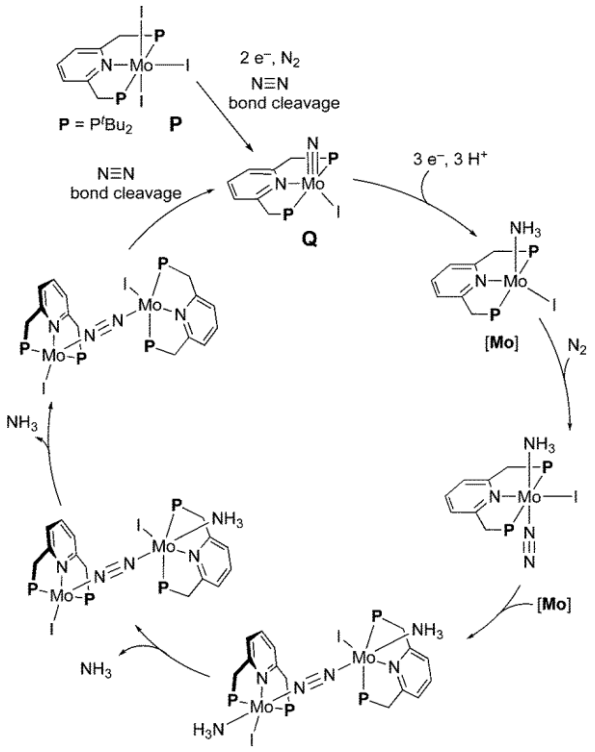

Figure 2.7: Nitrogen Splitting Mechanistic Pathway Observed with the (PNP)MoI$_3$ Complex[28]

As previously stated, in hopes of improving the ability of the catalyst to reduce nitrogen, as well as reducing the side production of H_2, we have decided to use an electrode as our source of electrons. While there are reports of electrocatalytic heterogeneous reduction of N_2, there are fewer reports of electrocatalytic homogeneous reduction.[29,30] The earliest report of electrocatalytic homogeneous reduction was in 1985 by Pickett.[31,32] In this report he showed that using a W-N_2 complex, he could reduce nitrogen to ammonia at -2.5 V vs. ferrocene. While he was successful at producing ammonia, the reduction could only proceed stepwise because the tungsten complex required a strong acid to be protonated. In 2012, Schrock attempted electrochemical reduction of nitrogen with his catalyst, however he found that his complex was protonated on the ligand and this prevented any catalytic activity.[33] Finally, in 2016 Peters reported his catalyst to produce ammonia at -2.6 V vs. ferrocene, however he was only able to achieve a stoichiometric amount of ammonia.[34] So far, no molecular catalyst has been reported to catalytically reduce dinitrogen to ammonia using electrochemistry.

Due to the high reactivity of the Nishibayashi (^{tBu}PNP)Mo complex, we decided to pursue a catalyst that could work electrochemically through the nitrogen cleavage pathway. In this pathway, the dinitrogen could be split into two metal nitrides that could then undergo proton coupled electron transfer (PCET) to produce ammonia. Through this pathway we can avoid the high energy intermediates that were observed by Schrock and Peters. With this in mind, we hoped to develop pincer-metal catalysts that can split dinitrogen and produce ammonia electrocatalytically.

2.2: Attempted Synthesis of (^{tBu}PPP)Re and (^{tBu}PPP)Ru Nitride Complexes

In the early stages of the nitrogen reduction project, it was decided to screen numerous metal complexes to learn how the metal and ligand influence the nitrogen reduction cycle. Many different pincer-metal complexes that had been previously made in our lab were sent off for testing with our collaborators Dr. Alexander Miller (UNC), Dr. Pat Holland, and Dr. James Mayer (Yale). Initial results showed that iridium and rhodium were not good choices of metal for nitrogen reduction.[35] The most promising metals were rhenium, ruthenium, iron, osmium and molybdenum. Our laboratory attempted the synthesis of iron and osmium nitrogen complexes; however, these were unsuccessful.

The first two complexes to show some promise were (H-Macho)$RuCl_2$ and (Macho)$ReCl_2$. Our collaborators at UNC observed that the (H-Macho)RuN complex was able to go from a nitride to ammonia very easily, however was unable to split nitrogen initially to form the nitride (Figure 2.8 Bottom).[36] To obtain the nitride complex, it had to be synthesized via an azide. In contrast, additional work at UNC in collaboration with Sven Schneider, found that the (Macho)$ReCl_2$ could easily split the nitrogen to form the nitride electrochemically, however it was then unable to complete the cycle to form ammonia (Figure 2.8 Top).[37]

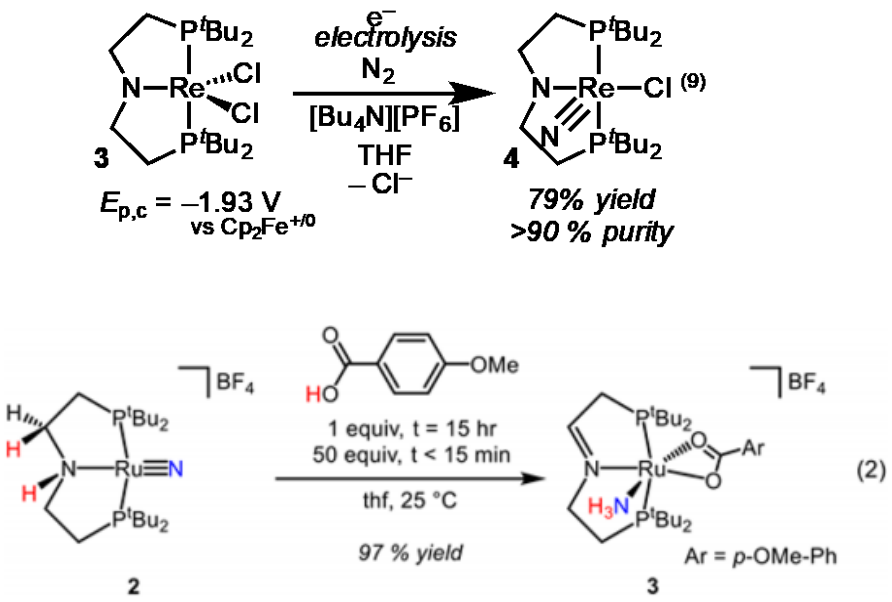

Figure 2.8: (Macho)Re and (Macho)Ru Nitrogen Reduction Results

To explain why this was observed, DFT calculations were performed on the complexes. As one can observe in the table, it became apparent that the (H-MACHO)RuN_2 and the (MACHO)ReNCl complexes were extremely stable. This explains why each complex was unable to perform the full cycle of nitrogen to ammonia. Further experimental work done at Yale suggests that the (MACHO)ReNCl complex was not only too stable to be reduced to ammonia, it was also too stable to be oxidized to a nitroxide species. Further calculations were done on various other complexes using a different metal center and/or a different ligand backbone to help direct us for future synthetic efforts (Table 2.1).

Table 2.1: DFT Calculations Exploring the M-N_2 and MN Energies for Different Pincer-M Combinations by Dr. Faraj Hasanayn and Dr. Karsten Krogh-Jesperson

M (G = 0.0 for 2 M + 2 N2)	n	Ox. state	d e-'s	2 M-N_2	2 MN + N2	Rxn: 2 M-N2 = 2 MN + N2
(^{tBu}POCOP)MoI	0	2	4	3.4	-32.0	-35
(^{tBu}POCOP)MoI$^-$ anion	-1	1	5	-15.4	-56.2	-41
(^{tBu}PONOP)MoI	0	1	5	-6.8	-49.0	-42
(MACHO)Ru	0	1	7	-41.2	8.0	49
(MACHO)Os	0	1	7	-50.2	-20.8	29
(MACHO)ReCl	0	2	5	-13.4	-56.6	-43
(^{tBu}PCP)Ru	0	1	7	-47.0	30.8	78
(^{tBu}PCP)Os	0	1	7	-49.6	6.8	56
(^{tBu}PCP)ReCl	0	2	5	-5.2	-53.0	-48
(Phebox)Ru	0	1	7	-3.6	48.2	52
(Phebox)Os	0	1	7	-31.8	23.8	56
(Phebox)ReCl	0	2	5	-17.2	-39.2	-22
(MACHO-H+)Ru	+1	1	7	-48.4	12.6	61
(MACHO-H+)Os	+1	1	7	-63.4	-27.8	36
(MACHO-H+)ReCl	+1	2	5	-5.4	-48.0	-43
(MACHO-H)Ru	0	0	8	-67.0	14.2	81
(MACHO-H)Os	0	0	8	-73.4	-7.8	66
(MACHO-H)ReCl	0	1	6	-39.4	-49.4	-10
(imine-PNP)Ru	+1	1	7	-47.0	22.4	69
(imine-PNP)Os	+1	1	7	-58.4	-13.6	45
(imine-PNP)ReCl	+1	2	5	-5.2	-40.6	-35
(PpyNP)Ru	0	0	8	-36.0	44.0	80
(PpyNP)Os	0	0	8	-37.2	18.6	56
(PpyNP)ReCl	0	1	6	-7.6	-51.8	-44

Before the DFT calculations were performed, it was shown that one of the difficulties with the (H-MACHO)RuN to (MACHO)RuNH_3 transition was the ability for the ligand to provide hydrogen atoms (Figure 2.9).[36] After donating the atoms to the nitride, the catalyst could then lose ammonia and rebind nitrogen. However, with the now unprotonated pincer ligand, there were no protons available to make ammonia. All attempts to hydrogenate the pincer were unsuccessful. From here we decided to pursue

Re and Ru complexes with innocent pincer ligands, ones that would not participate in the reaction.

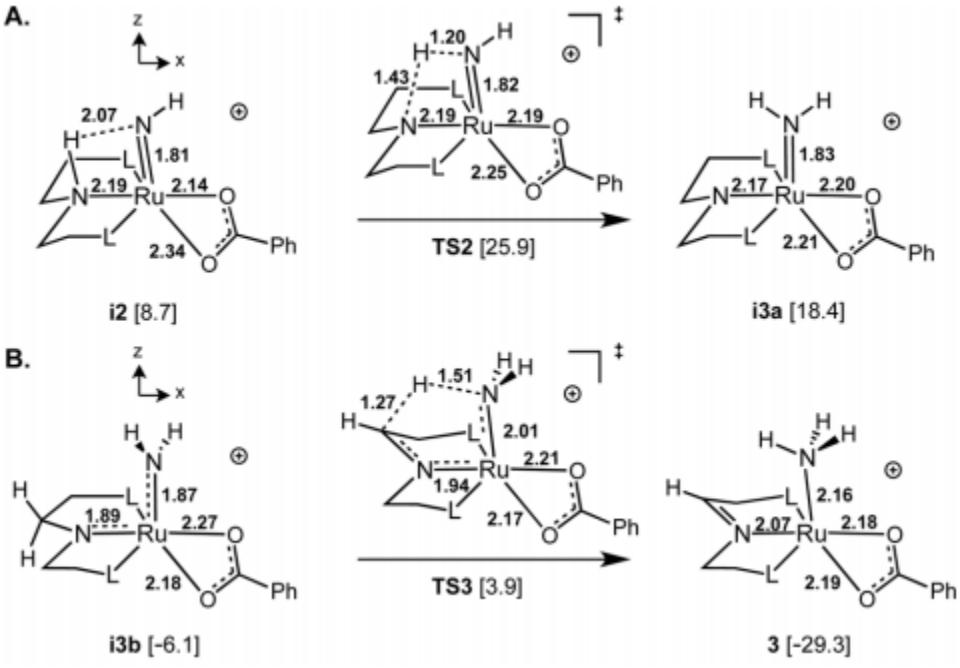

Figure 2.9: Ability of the H-Macho Ligand to Donate Protons to the Nitride

While several different ligands were chosen, our lab decided to focus on the ^{tBu}PPP ligand, seen in the Nishibayashi (^{tBu}PPP)Mo complex. We attempted the synthesis of (^{tBu}PPP)Ru and (^{tBu}PPP)Re nitride complexes. However, before isolation and purification, we received the results of the DFT calculations and it was decided that all future efforts would be with molybdenum complexes. Here is a report of the synthetic efforts that did occur. The (^{tBu}PPP)$RuCl_2$ complex obtained would be used for later studies on dehydrogenation (See Section 3.4).

2.2.1 Attempted Synthesis of (^{tBu}PPP)ReN

To synthesize the (^{tBu}PPP)$ReCl_3$ complex, $Cl_3Re(PPh_3)_2Acn$ was mixed with PPP ligand in THF. The reaction was refluxed for 1 hour and then solvent was removed via vacuum. Unexpectedly the ^{31}P NMR showed only free PPh_3 in solution, no new complexes or free PPP ligand. Also, the ^{1}H NMR had peaks ranging from -8 to 21 ppm. The PPh_3 production means that the starting material reacted, however the lack of other ^{31}P peaks and the wide range of ^{1}H peaks indicates a paramagnetic species. This suggests that we did not make the expected 16 e^- diamagnetic (^{tBu}PPP)$ReCl_3$ complex.

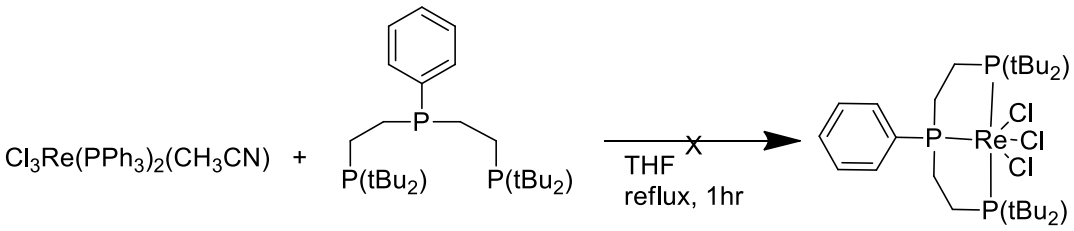

Scheme 2.1: Attempted Synthesis of (^{tBu}PPP)$ReCl_3$

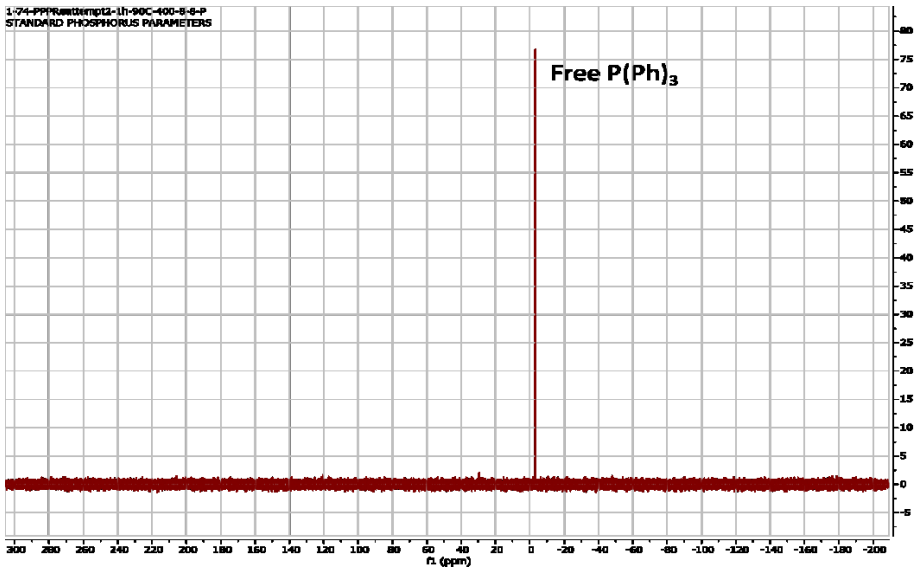

Figure 2.10: ^{31}P NMR Showing Only Free $P(Ph)_3$

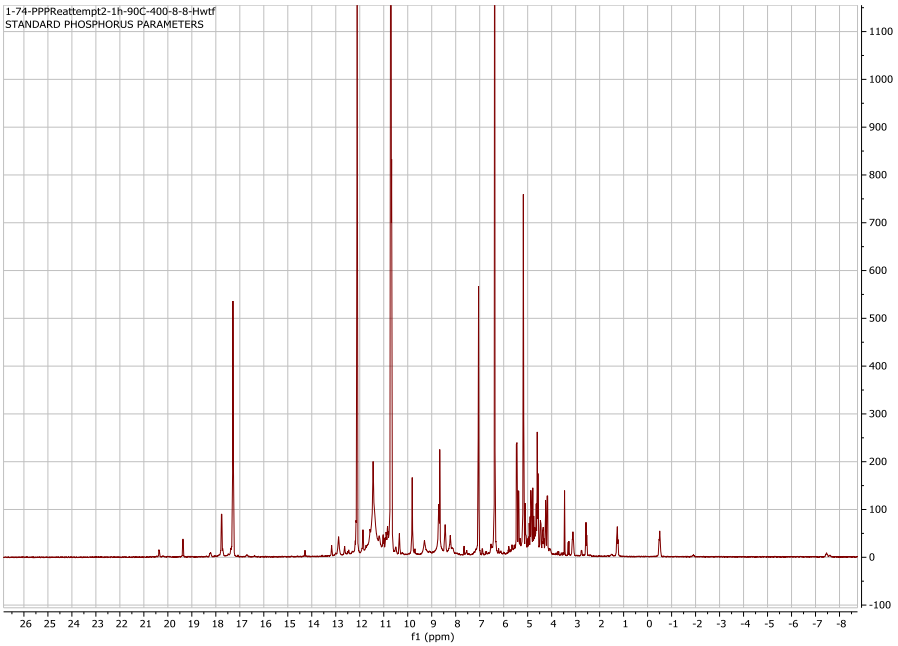

Figure 2.11: ^{1}H NMR of Unknown Product after Attempted (^{tBu}PPP)ReCl$_3$ Synthesis

Due to this unexpected result we checked the quality of our starting material using a known synthesis of the (Macho)ReCl$_2$ complex.[38] The reaction worked as reported, confirming our starting material had not gone bad. Since we confirmed our starting material was good, and saw the production of PPh$_3$ in solution, we decided to move on and attempt to synthesize the (PPP)Re nitride complex. We hoped that the unknown paramagnetic product would react with Me$_3$SiN$_3$ to give the nitride product. However, after adding the Me$_3$SiN$_3$ and heating the reaction multiple diamagnetic complexes were observed. Due to the inability to characterize the paramagnetic product in Scheme 2.1 and the appearance of multiple diamagnetic products after adding Me$_3$SiN$_3$, no further effort was placed into making the (^{tBu}PPP)ReN complex. At this point we decided to move onto the (^{tBu}PPP)Ru complex instead.

2.2.2 Attempted Synthesis of (^{tBu}PPP)RuNCl

For the (^{tBu}PPP)$RuCl_2$ complex, the first attempted synthesis was done in a fashion similar to the reported synthesis for (^{tBu}PPP)$MoCl_3$. A mixture of [(cymene)$RuCl_2$]$_2$ and PPP ligand was dissolved in THF. The solution was heated for 24 hours and a single unknown product was observed in the ^{31}P NMR at δ 36 and δ 24; signals too far upfield for a pincer-metal complex. After this a different synthetic route was found in the literature, reported by Leslie et. al. in 2012.[39] For this synthesis, $Ru(PPh_3)_3(Cl)_2$ and PPP ligand are dissolved in THF. The reaction stirs at room temperature overnight and a light orange solid precipitates out. Hexane is then added to the reaction mixture to facilitate further precipitation. After filtering out and drying the precipitate a dry, orange powder is obtained. This synthesis worked as reported and the ^{1}H and ^{31}P NMR of the dry powder showed a pure product with values that matched those reported by Leslie et. al.

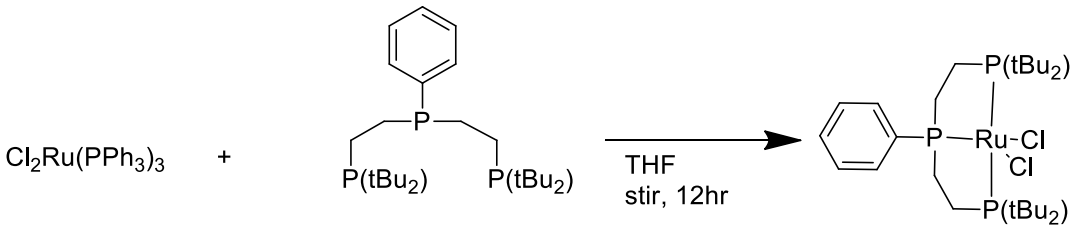

Scheme 2.2: Synthesis of (^{tBu}PPP)$RuCl_2$

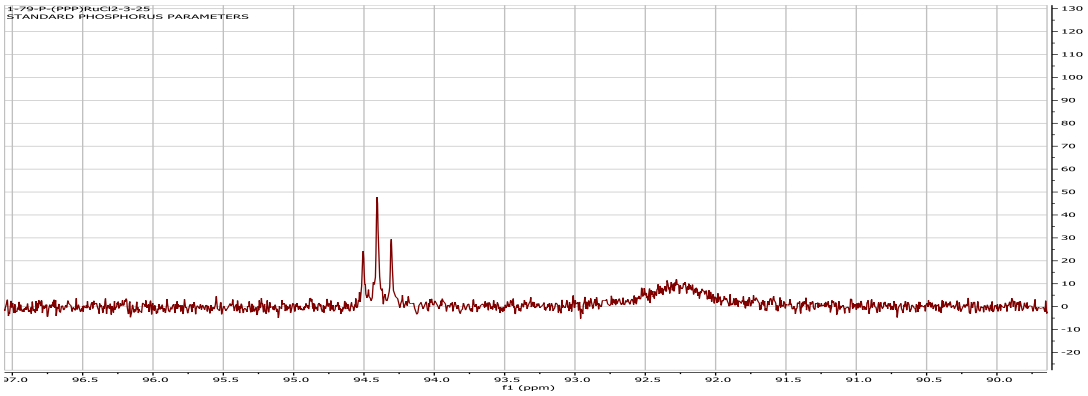

Figure 2.12: ^{31}P NMR of (^{tBu}PPP)RuCl$_2$

Next, we attempted to make the nitride complex via an azide. For this reaction, triemethylsilyl azide is mixed with the (^{tBu}PPP)RuCl$_2$. The low solubility of the (^{tBu}PPP)RuCl$_2$ resulted in a very slow reaction that turned green after 4 days. The solution still had starting material in the bottom, so it was transferred to a smaller flask for better stirring. After stirring for an additional 24 hours, the ^{31}P NMR showed three broad signals at δ 92.99, δ 67.02, and δ 33.14 in a 1:1:1 ratio. The far upfield shift of the phosphorous at δ 33.14 suggests that one of the phosphorous arms dissociated from the metal center resulting in a signal close to that of the free ligand at δ 34.0.

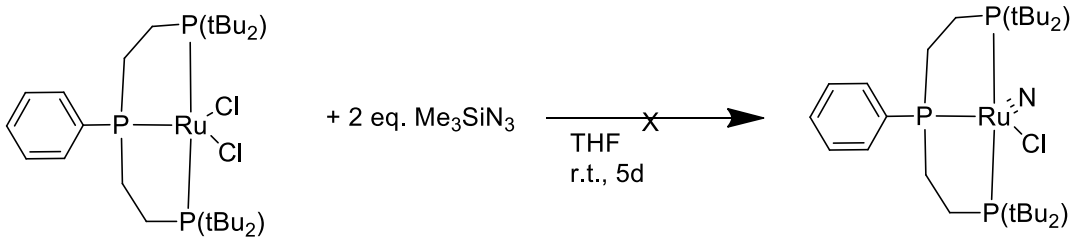

Scheme 2.3: Attempted Synthesis of (^{tBu}PPP)RuNCl

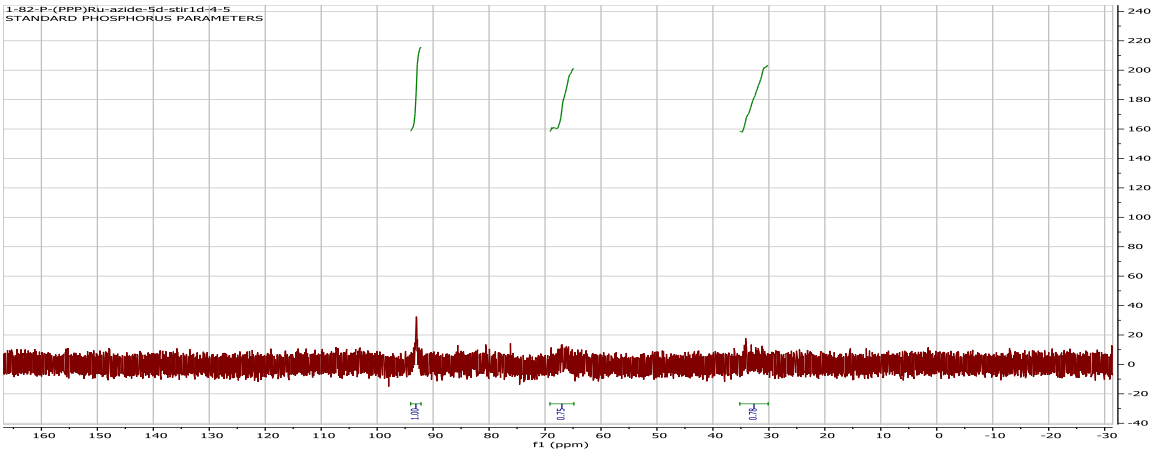

Figure 2.13: ^{31}P NMR of Unknown Complex Formed During the Attempted Synthesis of (^{tBu}PPP)RuNCl

At this point, the DFT calculations on the individual metal-pincer complexes were finished. As stated previously, the DFT calculations showed that ruthenium made extremely stable M-N_2 complexes and rhenium made extremely stable MN complexes. These calculations were confirmed by the experiments done by our collaborators at Yale and UNC. Literature reports, along with the DFT calculations, showed that molybdenum was an ideal choice of metal for the nitrogen reduction catalysts. It was decided that all future synthetic efforts would be focused on pincer-molybdenum complexes and all work on (^{tBu}PPP)Ru and (^{tBu}PPP)Re was ended.

2.3: Synthesis of Nishibayashi Pincer-Molybdenum Catalysts

After we discovered the issues with using Re and Ru as nitrogen reduction catalysts, we decided to go back and synthesize some known pincer-molybdenum complexes that could bring nitrogen to ammonia chemically. Since these complexes have shown they can go through the full cycle, they would be the best starting point to see if

our hypothesis of nitrogen reduction through electrochemical means was plausible. At the time the most successful molybdenum catalysts were the (PNP)Mo-dimer and (PNP or PPP)MoNCl complexes developed by Nishibayashi.[24,26] Since we knew these complexes could produce ammonia chemically, we decided to use them for electrocatalytic dinitrogen reduction. However, it was soon discovered that working with molybdenum is significantly different than our usual work with iridium, and many additional precautions and procedures needed to be implemented in order to result in a successful synthesis.

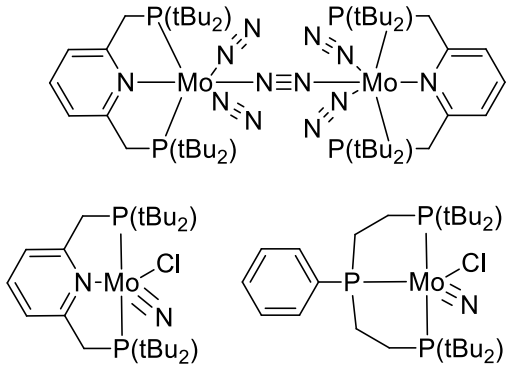

Figure 2.14: Nishibayashi Nitrogen-Reduction Catalysts

2.3.1 Attempted Synthesis of Nishibayashi (PNP)Mo-Dimer

The first targeted complex was the Nishibayashi (PNP)Mo-dimer. For this complex, $Mo(THF)_3(Cl)_3$ was dissolved in THF. To this solution, PNP ligand was added. The solution was then heated at 50°C for 24 hours under nitrogen. Solvent was pulled off via vacuum and then THF was added. Hg/Na 5% was added to the solution and the reaction was left to stir for 24 hours at room temperature with nitrogen bubbling through the solution. The

color change went from orange to blue to green. ^{31}P NMR of the crude solution showed the (PNP)Mo-dimer with three side products and free ligand. All attempts to isolate the product led to decomposition. Additionally, if left to sit in solution, the complex would decompose within 24 hours.

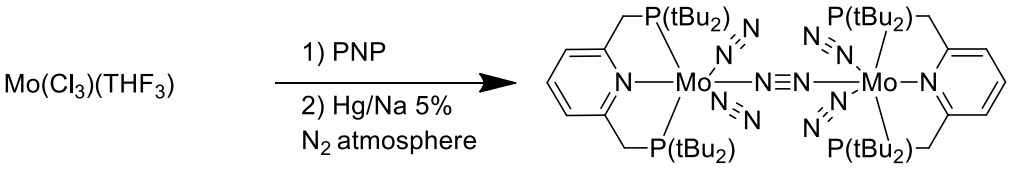

Scheme 2.4: Synthesis of Nishibayashi (^{tBu}PNP)Mo-Dimer

Later work in our laboratory showed that the percentage of sodium in the Ha/Na amalgam has a significant effect on the reaction. Originally, the Hg/Na 5% was chosen due to its commercial availability, however soon we started making the amalgam in our laboratory allowing us a lower percentage of sodium. With this we were able to observe better reactivity and less decomposition with other catalysts. It is likely that the high production of side products and free ligand seen in the synthesis of the Nishibayashi dimer, along with the decomposition after 24 hours in solution, was due to the Hg/Na 5%. Additionally, it was later discovered that molybdenum complexes have an extreme sensitivity to trace water, much more than that of iridium. While the THF used for the synthesis was distilled, the solvents used for workup were only stored over sieves. It is likely that there were still trace amounts of water in these solvents, resulting in the decomposition during workup.

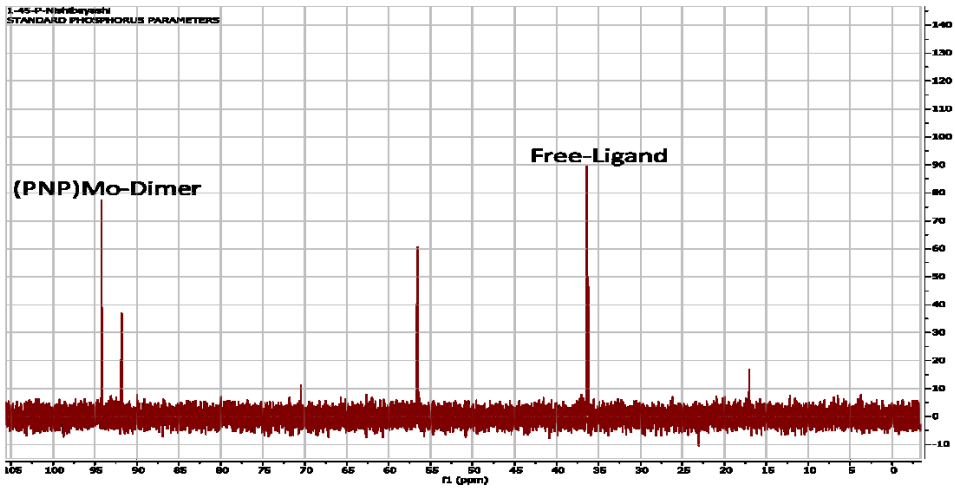

Figure 2.15: ^{31}P NMR of Nishibayashi (PNP)Mo-Dimer

At this point it seemed like we would not be able to obtain the (PNP)Mo-dimer. Due to this we then moved onto the (^{tBu}PPP)MoNCl and the (^{tBu}PNP)MoNCl complexes also reported by Nishibayashi. These complexes had a simpler synthesis, using azide instead of nitrogen and Hg/Na amalgam, and showed greater reactivity than the (^{tBu}PNP)Mo-dimer. In addition, we also targeted the (^{tBu}PPP)$MoCl_3$ and (^{tBu}PNP)$MoCl_3$ complexes for our collaborators to test. Nishibayashi has shown that these complexes can be made into active catalysts in the presence of reducing agent and nitrogen. This can be seen with this (^{tBu}PNP)MoI_3 catalyst (Figure 2.7).[28]

2.3.2 Synthesis of (^{tBu}PNP)MoNCl

To synthesize the (^{tBu}PNP)MoNCl, we followed the synthetic routes reported by Nishibyashi.[24] The first step for this synthesis is to make the (^{tBu}PNP)$MoNCl_2$ complex. In a Schlenk, Me_3SiN_3 is added to a solution of $Mo(Cl)_3(THF)_3$ in THF. The solution is then heated at 50^{o}C for 1 hour. The solvent is then removed via vacuum and the residue is

dissolved in THF. To this ^{tBu}PNP ligand is added and the mixture is stirred at 50^{o}C for 4 hours. In contrast to the reported route, the solution was cooled to room temperature and then immediately stored in the freezer at -45^{o}C. After a few weeks in the freezer, orange crystals crashed out of solution. These crystals were collected via filtration; however, it was found that upon warming to room temperatures the crystals disintegrated into a light orange powder. However, the (^{tBu}PNP)MoNCl$_2$ powder is very stable and can last for months stored under argon or nitrogen.

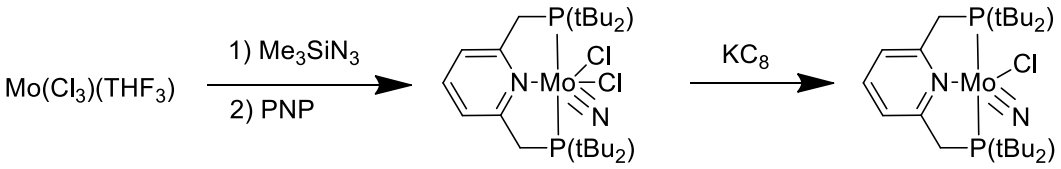

Scheme 2.5: Synthesis of (^{tBu}PNP)MoNCl

The (^{tBu}PNP)MoNCl$_2$ complex was confirmed by MALDI TOF mass spectroscopy. The MS data showed a parent peak of 542 m/z, suggesting a loss of chloride under ionization. Comparing the peaks and isotope splitting to a theoretical simulation showed strong similarities (Figure 2.16). Additionally, the ^{31}P NMR showed only some excess free ligand, confirming the product is paramagnetic. From the MS data and ^{31}P NMR we were confident that the (^{tBu}PNP)MoNCl$_2$ was synthesized.

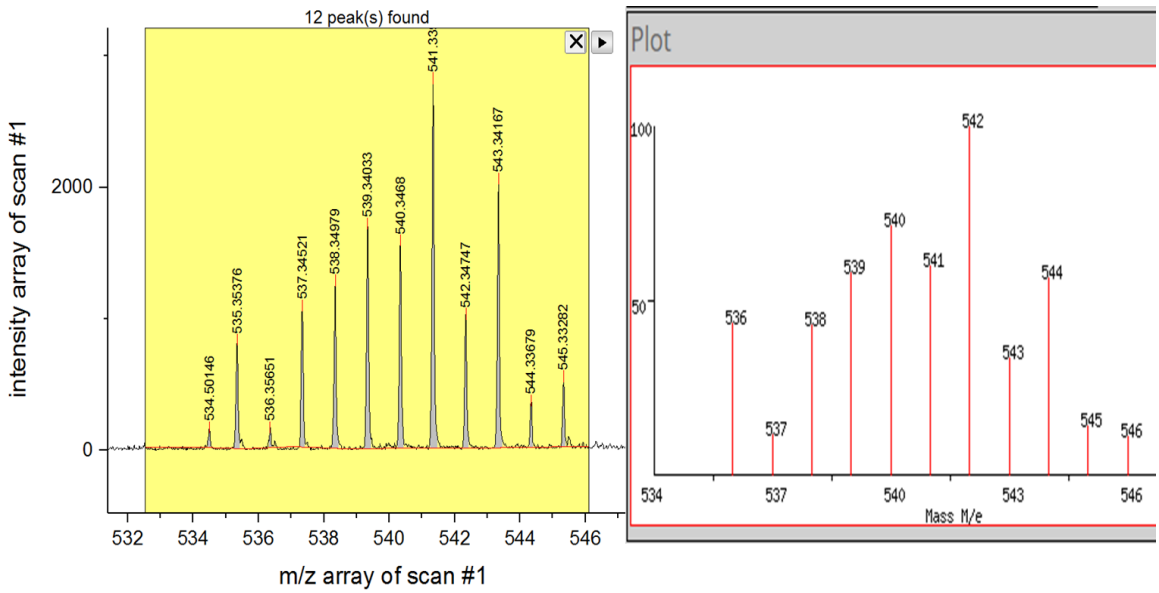

Figure 2.16: Mass Spec. Data for (PNP)MoNCl$_2$. Experimental (Left) Theoretical (Right)

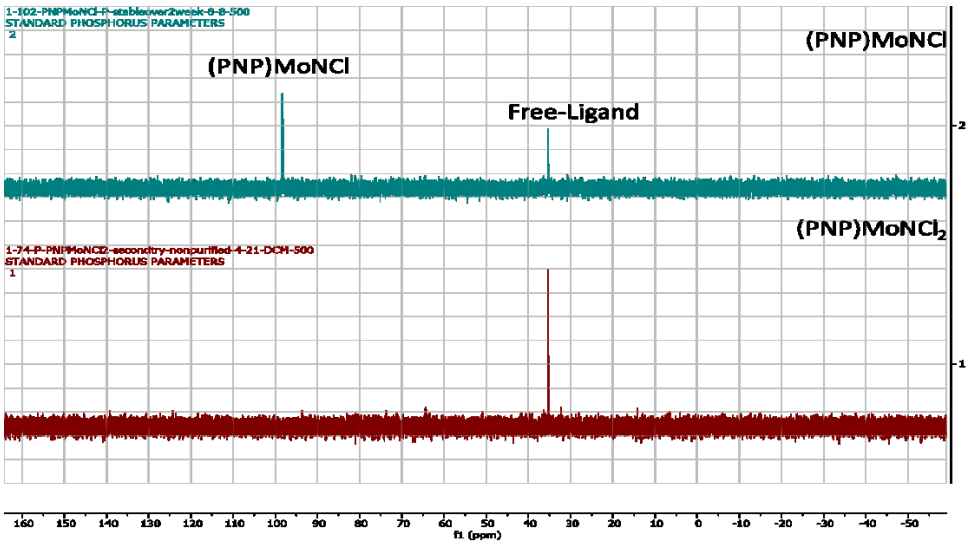

Figure 2.17: ^{31}P NMR of (PNP)MoNCl$_2$ and (PNP)MoNCl

To make the (^{tBu}PNP)MoNCl complex, (^{tBu}PNP)MoNCl$_2$ is mixed with KC_8 and left to stir overnight. A crude ^{31}P NMR shows a complete conversion to the (^{tBu}PNP)MoNCl complex. The solution was filtered, and the complex was isolated as a dark brown/green powder. Unfortunately, after several days the solid decomposed to molybdenum black.

This suggested that the (^{tBu}PNP)MoNCl complex was not stable for a long period of time and mostly likely would not survive the trip to our collaborators. For this reason, the (^{tBu}PNP)MoNCl$_2$ complex was isolated, purified, and sent for testing.

In addition to the (^{tBu}PNP)MoNCl, we hoped to send out the parent (^{tBu}PNP)MoCl$_3$ complex. Nishibayashi has shown that the tri-halogen complexes can convert to the nitride in situ and perform nitrogen reduction. We followed the reported synthesis by Nishibayashi and obtained an orange/brown solid. ^{31}P NMR had no signals, showing a paramagnetic product as expected. Very preliminary electrochemical studies have been performed on the (^{tBu}PNP)MoCl$_3$. However, it is still too early to draw any conclusions.

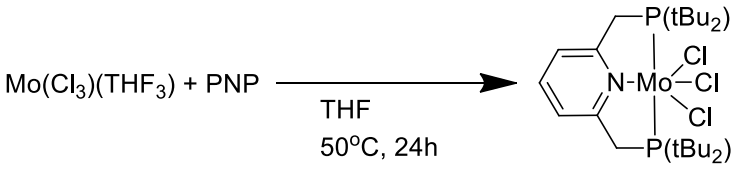

Scheme 2.6: Synthesis of (^{tBu}PNP)MoCl$_3$

2.3.3 Synthesis of (^{tBu}PPP)MoNCl

Concurrently, we also synthesized the (^{tBu}PPP)MoNCl complex. Since we knew both the (^{tBu}PPP)MoNCl and the (^{tBu}PNP)MoNCl complexes reduced nitrogen chemically, it would be a great opportunity to see if the different ligands affected the catalysts in an electrochemical setting. The PPP ligand has the additional π-accepting ability that can stabilize the broad range of oxidations state for the molybdenum.[26] Due to this, Nishibayashi found that, chemically, the (^{tBu}PPP)MoNCl works better than its PNP analogue. We hoped this extra stability would solve a lot of the decomposition issues we

were having with the PNP complex and help the complex do electrochemical nitrogen reduction.

The (^{tBu}PPP)MoNCl complex is synthesized in the same manner as the PNP analogue. One issue with the PPP complexes in comparison to the PNP complexes is they tend to turn out as an oil and can require significant purification efforts to obtain the pure-solid. For this reason, the (^{tBu}PPP)MoNCl$_2$ complex was not isolated. After confirmation of the loss of PPP signal in the ^{31}P NMR, KC_8 was added to the reaction mixture to make the (^{tBu}PPP)MoNCl complex. After reacting, the solution was filtered, and a brown solid was isolated. ^{31}P NMR shows product peaks at δ 120.6 and δ 92.5, consistent with Nishibayashi's reported complex.

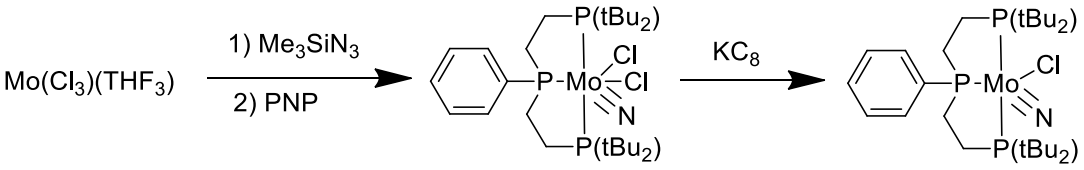

Scheme 2.7: Synthesis of (^{tBu}PPP)MoNCl

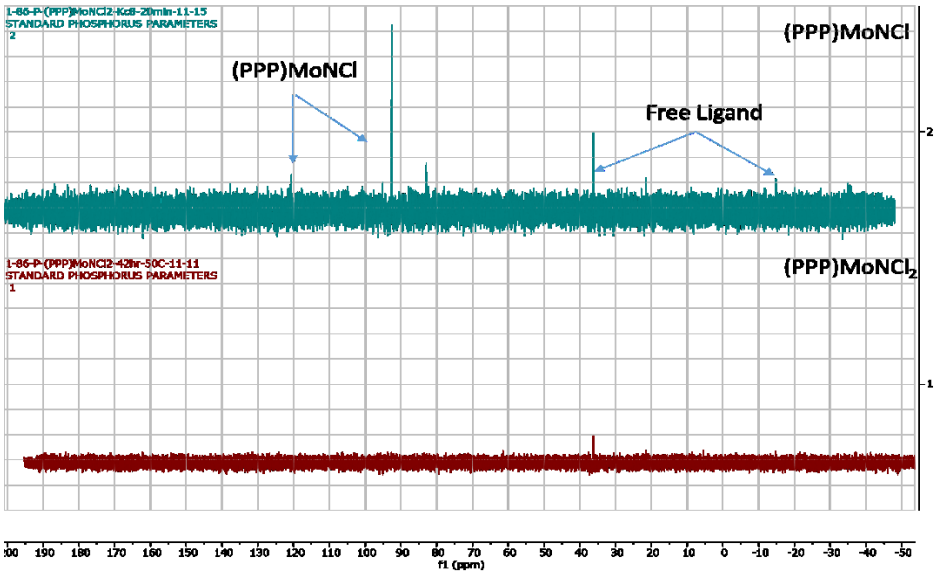

Figure 2.18: ^{31}P NMR of (^{tBu}PPP)MoNCl$_2$ and (^{tBu}PPP)MoNCl

We also synthesized the (^{tBu}PPP)MoCl$_3$ complex for electrochemical study. Following the reported synthetic procedure,[26] we isolated a paramagnetic brown solid. The (^{tBu}PPP)MoCl$_3$ complex was confirmed by MALDI TOF mass spectroscopy. The MS data showed a parent peak at 653 m/z. Additionally, there was a smaller signal at 619 m/z which equals the loss of a chloride ion during ionization (Figure 2.19). The ^{31}P NMR showed only some excess free ligand, confirming the product is paramagnetic. From the MS data and ^{31}P NMR we were confident that the (^{tBu}PNP)MoCl$_3$ was synthesized.

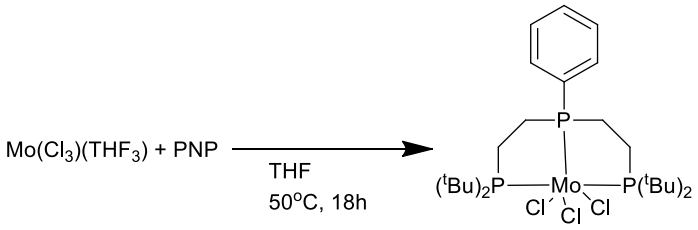

Scheme 2.8: Synthesis of (^{tBu}PPP)MoCl$_3$

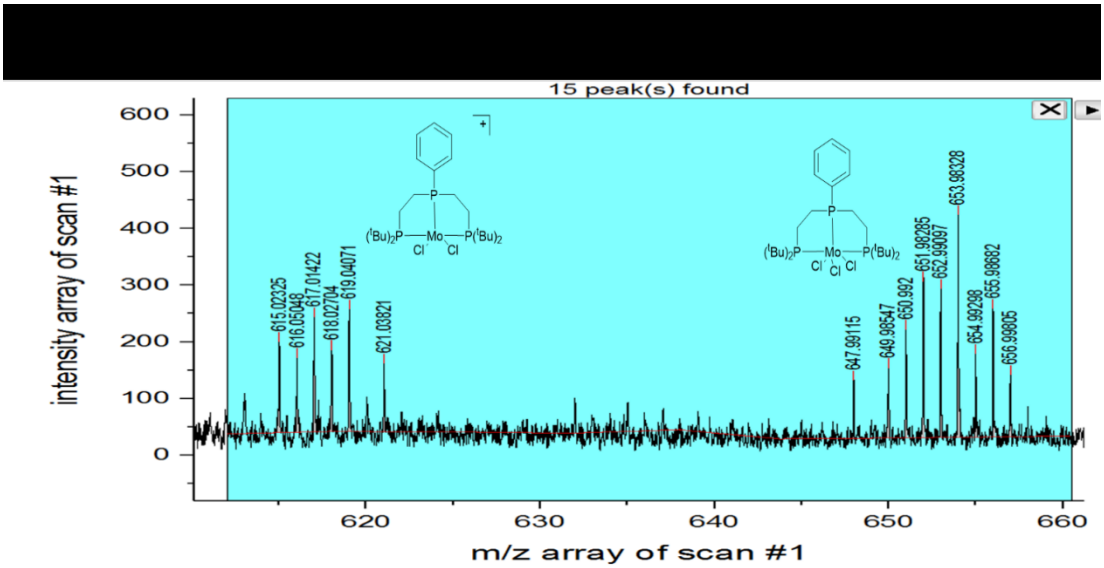

Figure 2.19: Mass Spec. Data for (^{tBu}PPP)MoCl$_3$*

2.4: Attempted Synthesis of a Pyrene-PNP Pincer Ligand

Another idea brought up in the collaboration, was developing a pincer-molybdenum complex that had a pincer-ligand backbone with the ability to attach to an electrode surface. The best example of this idea being performed with a pincer ligand is one reported in 2011 by Brookhart and Meyer. In this paper, they attach a pyrene to the backbone of a POCOP pincer ligand.[40] With the addition of this pyrene, they were able to perform electrochemical reduction of CO_2 to $HCOO^-$. The pyrene allowed for close proximity through pi interactions between the pyrene and the carbon nanotube surface. This allowed for better reactivity and increased current density. With this in mind, we set out to synthesize a pyrene version of the ^{tBu}PNP ligand.

* Each number is shifted by three mass compared to the actual due to machine calibration issues

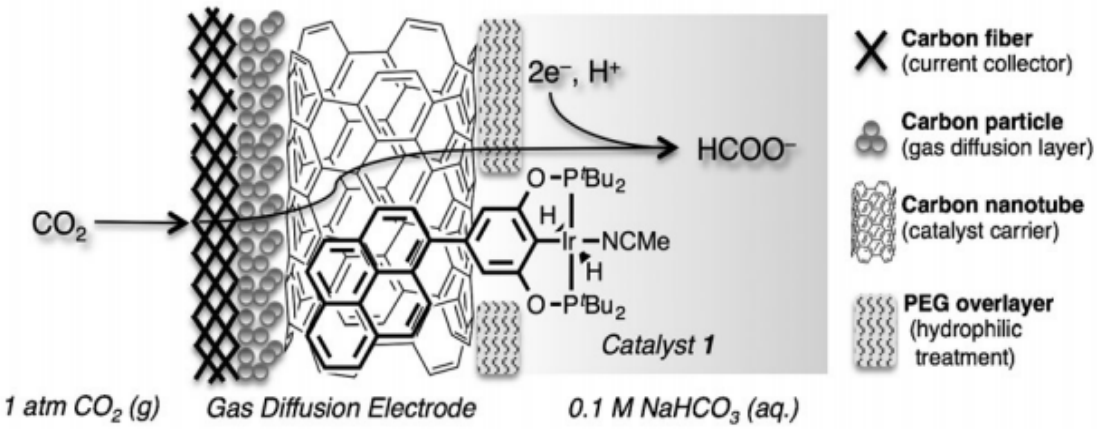

Figure 2.20: (Pyrene-POCOP)Ir Complex Developed by Brookhart and Meyer

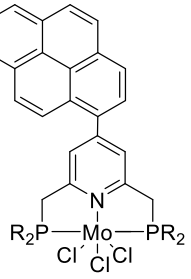

Figure 2.21: Target Pyrene-PNP Complex

Due to the big differences between PNP and POCOP synthesis, it was not possible for us to follow a synthetic route similar to that of Brookhart and Meyer. An initial synthetic route was set up that started with chelidamic acid, a very cheap and stable starting material. For this reaction, $SOCl_2$ could be used to substitute a chloride for each -OH group. After, methanol could be used to convert the two acyl chlorides to esters. From here the esters could be reduced to alcohol groups which could then be converted to bromines, which could go on to the desired phosphine arms. As for the leftover chloride

on the pyridine ring, it could be converted to a boronic acid and a Suzuki Coupling reaction could be done with monobromopyrene to allow for the pyrene backbone (Scheme 2.9).

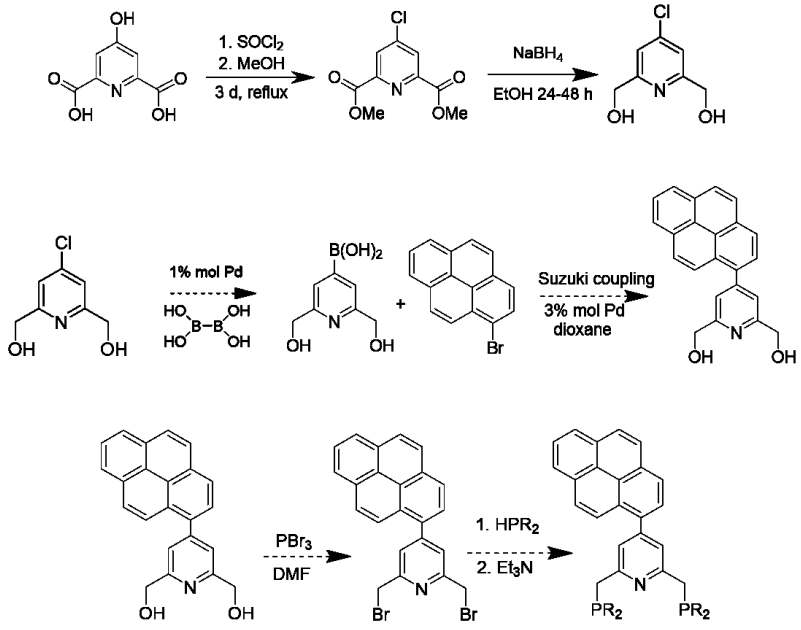

Scheme 2.9: Suggested Synthesis for Pyrene-PNP

For the first step of the synthesis, we initially tried using $SOCl_2$ and methanol to obtain the desired dimethyl 4-chlorodipicolinate.[41] The reaction was successful, however it often did not go to full completion and left the alcohol group on the pyridine ring. After further literature searching, another route was discovered using PCl_5 in place of $SOCl_2$.[42] Using this synthetic method, we were able to obtain the desired product in 70% yield with absolutely no presence of the -OH product. Due to this, and $SOCl_2$ being very hazardous volatile liquid, we decided for all future synthesis, PCl_5 would be our chloride source in this first step.

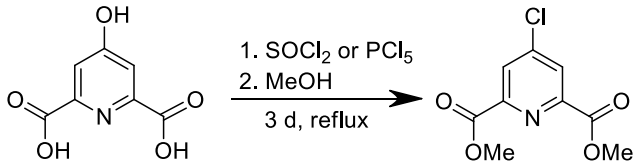

Scheme 2.10: Dimethyl 4-chlorodipicolinate Synthesis

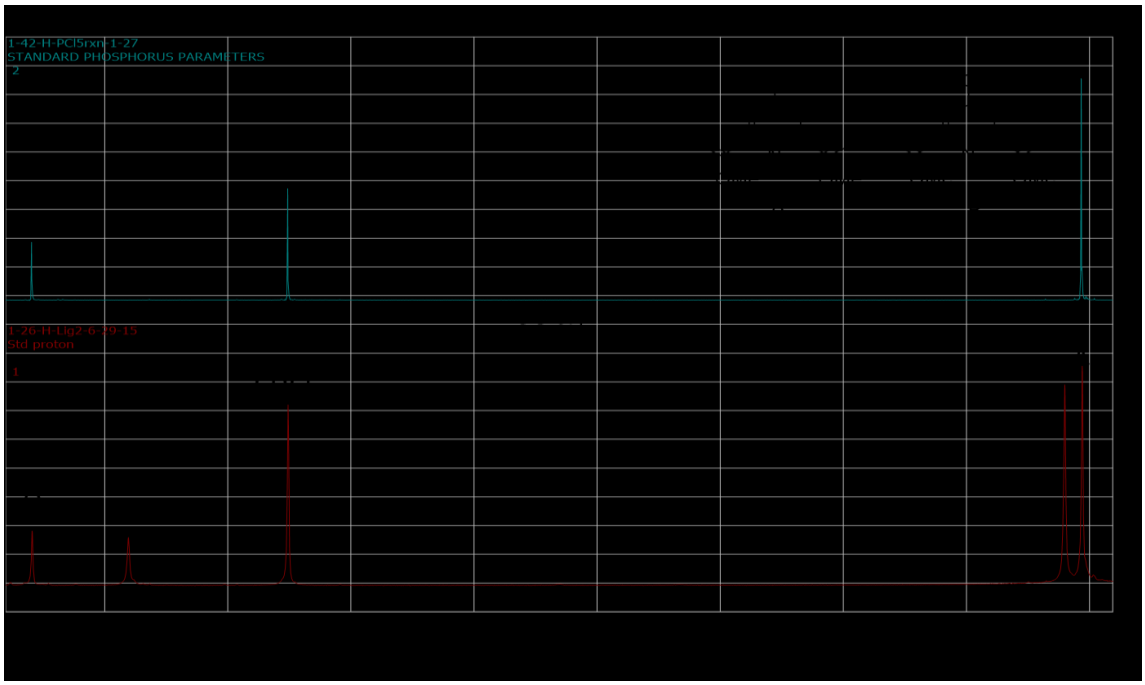

Figure 2.22: ^{1}H NMR Comparison of using $SOCl_2$ and PCl_5 in Reaction

The second step of our proposed synthesis was to then reduce the esters to alcohol groups. In order to do this, we added sodium borohydride.[43] After reflux overnight, it was observed that solid had crashed out and ^{1}H NMR showed decomposition of the compound. We then decided to look back on our synthetic route for other possible options. Furthermore, when looking at our synthesis, it was difficult to find any reported

synthetic work for the conversion of the chloride to a boronic acid for the Suzuki coupling. Due to this, a completely new synthetic route was developed.

In the second synthetic route we would convert the chloride to an iodide and then do a Suzuki coupling with 1-pyreneboronic acid.[41] This method was chosen because iodide is a significantly better leaving group than chloride and will be much more likely to perform oxidative addition. Additionally, there is literature precedence of Suzuki coupling between 1-pyreneboronic acid and iodobenzene.[44] After the Suzuki coupling, the ester could be reduced and converted to a pyrene as suggested in Synthetic Route #1 (Scheme 2.9).

Scheme 2.11: New Synthetic Plan for Pyrene-PNP

The first new step of this route is to substitute the chloride with an iodide. For this substitution, the chloride compound is dissolved in acetonitrile. Then sodium iodide and acetyl chloride are added. The reaction mixture is then sonicated for one hour, keeping the temperature under 50^{o}C. Since our sonicator does not have a temperature controller, the water was changed every 15 minutes to keep the temperature low. After

one hour, ^{1}H NMR showed only 43% conversion to the iodide substituted compound. Neither sonicating for longer times nor adding fresh reactants resulted in a higher conversion. In fact, both conditions would lead to some reversal in the reaction, often resulting in lower conversions.

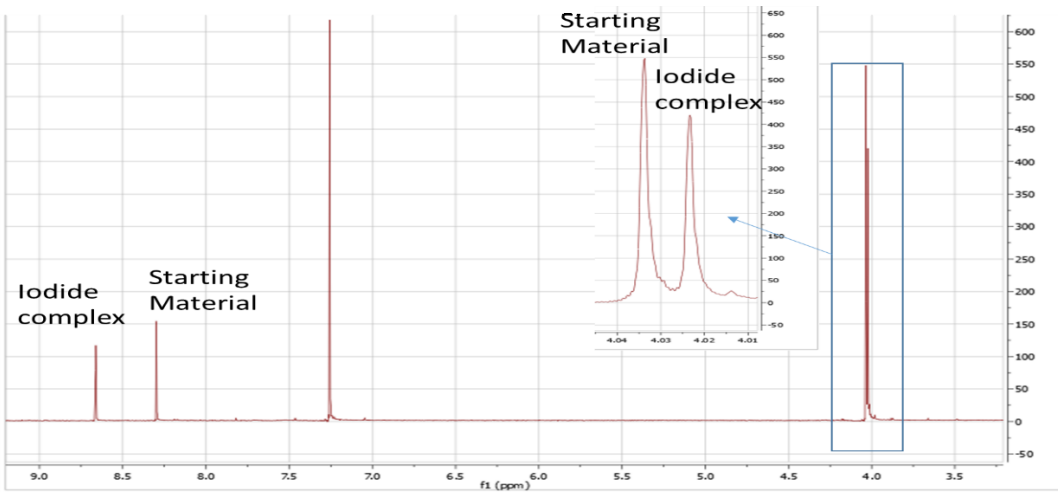

Figure 2.23: ^{1}H NMR Showing Mixed Products After reacting with NaI

Since we were unable to obtain the iodide compound in high yields and could not reach a conversion higher than 43%, we went back to the literature to revise our synthesis again. We found a paper that reports a Suzuki coupling using dimethyl 4-chlorodipicolinate. In their synthesis they couple the compound with 1-napthylboronic acid, a substrate very similar to our own.[45] Additionally, they were then able to reduce the esters to alcohols using sodium borohydride, which is the following step in our planned synthetic route. Following the same procedure reported by Hamasakai et. al. we attempted our Suzuki coupling with 1-pyreneboronic acid.

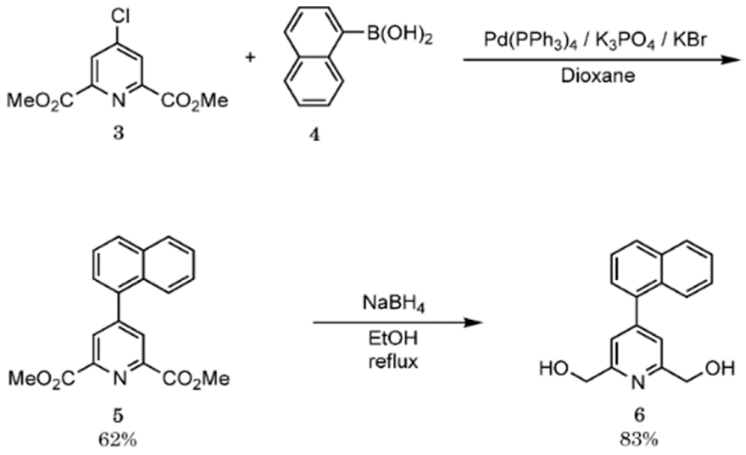

Figure 2.24: Reported Suzuki Coupling and Ester Reduction by Hamasaki et. al.

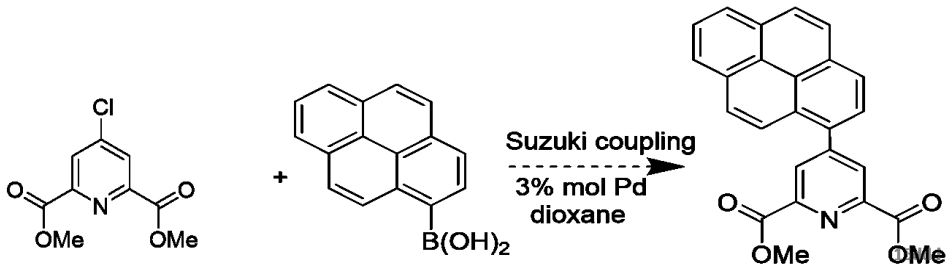

Scheme 2.12: Attempted Suzuki Coupling with 1-pyreneboronic acid

The reaction was run under typical Suzuki coupling conditions. However, during workup it was discovered that the addition of the pyrene to the compound introduced solubility issues. Multiple extractions and numerous washings with several different solvents eventually led to isolation of a brown solid. In the ^{1}H NMR we could observe a lot of pyrene and PPh_3O, resulting from the $Pd(PPh_3)_3$ used in reaction. However, complete conversion to a new product could be observed with NMR values near that of predicted spectra for the dimethyl 4-pyrene-dipicolinate. At this time, we could not confirm the correct product had been made due to issues with isolation and purification.

However, work performed later in our lab produced a similar complex with diethyl ester groups instead of dimethyl esters. The difference in spectra between the two complexes should be minimal for the pyridine and pyrene hydrogens. Comparing the two spectra shows extremely similar pyridine and pyrene proton signals. The methyl protons of our complex are slightly more upfield than the CH_2 groups yet far more downfield than the CH_3 group on the ethyl, as would be expected when comparing the two complexes. This comparison helped us identify our proton peaks and confirm our synthesis was successful.

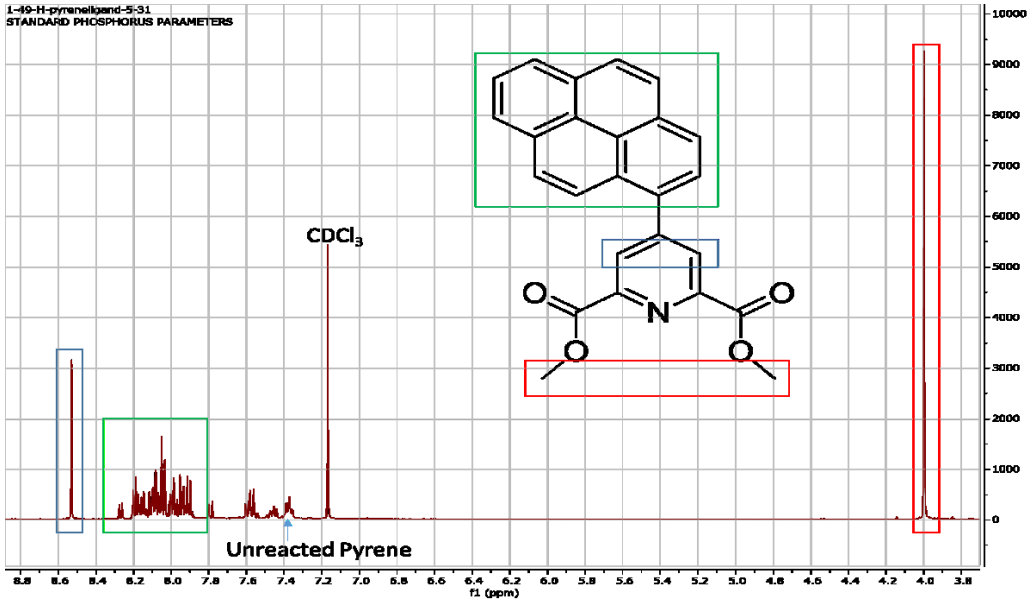

Figure 2.25: ^{1}H NMR of dimethyl 4-pyrene-dipicolinate

At this point the project was handed off to another member in the laboratory. Through a lot of editing and optimization of the synthetic route our laboratory was eventually able to obtain the pure pyrene-PNP ligand and successfully synthesize the

desired (pyrene-PNP)$MoCl_3$ and (pyrene-PNP)MoII complexes for electrochemical study (Scheme 2.13).[†]

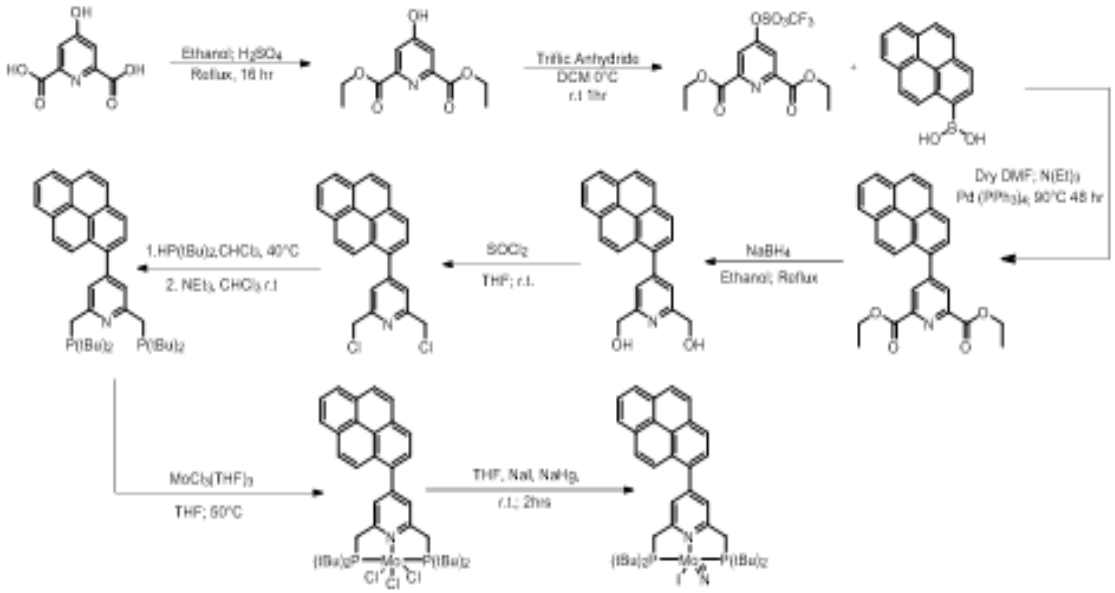

Scheme 2.13: Optimized Synthetic Scheme by Benjamin Gordon

[†] The optimization and editing of the synthetic route was performed by Benjamin Gordon. He synthesized and obtained the pure pyrene-PNP ligand and went on to synthesize the (pyrene-PNP)Mo complexes.

2.5: Summary

With the goal of electrochemical nitrogen reduction, some synthetic efforts were made to synthesize (^{tBu}PPP)Ru and (^{tBu}PPP)Re nitride complexes. However, initial experimental results on other Re and Ru complexes, along with DFT calculations, led us to refocus our efforts towards pincer-molybdenum complexes.

From there several reported Nishibayashi pincer-Mo complexes were synthesized. It was discovered that these complexes have an extreme sensitivity to moisture which is why most isolation attempts ended in decomposition. Once isolated, it was found that the pincer-MoNCl complexes were not stable over a long period of time. Due to this, the more stable pincer-$MoCl_3$ and pincer-$MoNCl_2$ complexes were synthesized for electrochemical studies by our collaborators.

Lastly, we reported an attempt to synthesize a pyrene-PNP ligand. After several modifications, we successfully synthesized dimethyl 4-pyrene-dipicolinate. However, solubility issues prevented us from isolating the product and moving on to the next step of reducing the ester and converting it to the desired phosphine. Later work in our laboratory focused on optimizing and editing the synthetic pathway to deal with the solubility issues and, eventually, the pyrene-PNP ligand was isolated. Using this, the (pyrene-PNP)$MoCl_3$ and (pyrene-PNP)MoNCl complexes were synthesized and isolated for future electrochemical studies.

2.6: Experimental

General Methods. All pincer-metal manipulations were carried out under argon using standard glovebox and Schlenk techniques, except for the (PNP)Mo-dimer which was carried out under nitrogen. All synthetic efforts of the pyrene-PNP ligand were performed in open air with anhydrous solvents unless noted otherwise.

Anhydrous solvents were purchased from Sigma-Aldrich and degassed by purging with argon. All solvents were stored over 3 Å molecular sieves in the glovebox. THF was distilled prior to use to ensure dryness. Deuterated solvents were degassed via freeze-pump-thaw cycles, dried over activated Al_2O_3, and stored over 3 Å molecular sieves prior to use. $Mo(Cl_3)(THF_3)$ was either purchased commercially or synthesized following literature procedure.[46] (^{tBu}PNP),[47] $Cl_3Re(PPh_3)_2Acn$,[38] (^{tBu}PPP)$RuCl_2$,[39] (^{tBu}PNP/PPP)$MoCl_3$,[22,26] and (^{tBu}PPP)$MoNCl_2$[26] were prepared according to literature methods. Unless noted above, all other reagents were purchased commercially and used as received.

All ^{1}H and ^{31}P NMR spectra were recorded on 400 MHz and 500 MHz Varian spectrometers. Chemical shifts are reported in ppm. The ^{1}H NMR signals are referenced to the residual solvent signals, and the ^{31}P NMR signals are referenced to an external standard of $P(CH_3)_3$.

All mass spec. were performed by Dr. Gene Hall. DFT Calculations were performed by/under the supervision of Dr. Faraj Hasanayn and Dr. Karsten Krogh-Jesperson.

^{tBu}PPP-Re and Ru Complexes

Revised synthesis of ^{tBu}PPP ligand[37]: Revised synthesis of ^{tBu}PPP ligand: The reported method of ^{tBu}PPP synthesis was followed with one revision. Divinylphenylphosphine was purchased from Sigma-Aldrich. Since it was purchased instead of synthesized it was dissolved only in THF for the synthesis instead of 50:50 ether/THF as in the reported method.

Failed Synthesis (^{tBu}PPP)RuCl$_2$:

10 mg of [(cymene)RuCl$_2$]$_2$ was mixed with 1.1 eq of PPP in THF. The reaction was heated at 50^{o}C overnight. ^{31}P NMR shows one species at 36 and 24 ppm, too far upfield for a (^{tBu}PPP)Ru monomer. It is likely a dimeric species was made. No attempt was made to characterize this product.

Failed Synthesis of (^{tBu}PPP)RuClN:

30 mg of (^{tBu}PPP)RuCl$_2$ was mixed with 2 eq. of Me_3SiN_3 in THF. Low solubility of the (^{tBu}PPP)RuCl$_2$ resulted in a very slow reaction. The solution turned green after 4 days. The solution still had starting material in the bottom, so it was transferred to a smaller flask for better stirring. After stirring for an additional 24 hours, the ^{31}P NMR showed three broad signals at 92.99, 67.02, and 33.14 ppm in a 1:1:1 ratio, suggesting one of the phosphorous arms dissociated from the metal center. No effort was made to isolate or characterize this product.

Failed Synthesis of (^{tBu}PPP)$ReCl_3$:

78 mg of $Cl_3Re(PPh_3)_2Acn$ was mixed with 46 mg of PPP ligand in 1 mL THF in a J-Young NMR tube. The reaction was refluxed for 1 hour. Solvent was removed via vacuum. ^{31}P NMR shows no signals suggesting a paramagnetic product that is not the expected (^{tBu}PPP)$ReCl_3$.

Failed (PPP)Re nitride synthesis:

10 mg (PPP)$ReCl_3$ was mixed with 4 eq. of Me_3SiN_3 in 0.5 ml THF. The reaction was heated at 50°C for 4 hours. The ^{31}P showed multiple products. No further attempt was made to synthesize this product.

Modified Nishibayashi Methods[20,22,24]

Modified Synthesis of (^{tBu}PNP)Mo-Dimer Complex:

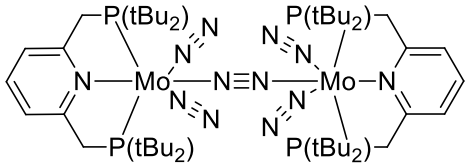

0.416 g of $Mo(THF)_3(Cl)_3$ was dissolved in 15 mL of THF. To this solution, 0.443 g of PNP ligand was added to the solution. The solution was then heated at 50°C for 24 hours under nitrogen. Solvent was pulled off via vacuum and then 20 mL of THF was added. 4.6 g of Hg/Na 5% was added to the solution and the reaction was left to stir for 24 hours at room temperature with nitrogen bubbling through the solution. The color change went from

orange to blue to green. ^{31}P NMR of the crude solution mixture showed some (PNP)Mo-dimer with three side products and free ligand. All attempts to isolate the product led to decomposition. ^{31}P NMR (202 MHz, THF) δ 94.16 (s).

Modified Synthesis of (tBuPPP)MoNCl:

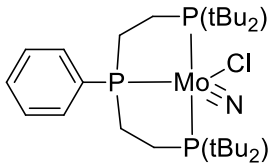

To a previously made solution of (^{tBu}PPP)MoNCl$_2$ was added 1 eq. of KC8. The solution was stirred at room temperature for 24 hours. The solution was then filtered through a syringe filter and washed with THF. Solvent was removed in vacuo and a brown solid was isolated. A clean ^{1}H NMR was not obtained. ^{31}P NMR (202 MHz, THF) δ 120.66 (s, 1P), 92.57(s, 2P).

Modified Synthesis of (^{tBu}PNP)MoNCl$_2$:

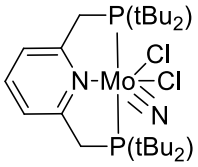

369 mg of Mo(THF)$_3$(Cl)$_3$ and 1.1 eq µL of trimethylsilylazide in 20 mL THF were stirred at 50^{o}C for 1 hour. The solvent removed via vacuum and the residue was re-dissolved in 20 mL THF. 488 mg of PNP ligand was then added to the solution and the mixture was stirred at 50^{o}C for 4 hours. This solution was then filtered via cannula filter and the solution was placed in the glovebox freezer (-45^{o}C) for one week. The product crashed out of solution

as orange crystals that dissolve to powder at room temperature. The product was collected via filtration. ^{31}P NMR shows no peaks due to the products paramagnetic qualities. MS (m/z): 541.3 (M^+).

Attempted Synthesis of (^{tBu}PNP)MoNCl:

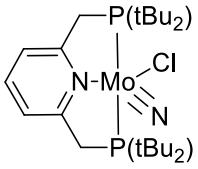

A suspension of 20 mg (^{tBu}PNP)$MoNCl_2$ and 1 eq. of KC_8 in 0.5 mL THF was made in a J-Young NMR tube. The NMR tube was stirred at room temperature overnight. The crude solution showed full conversion to the desired product, however all attempts at isolation resulted in decomposition. A clean ^1H NMR was not obtained. ^{31}P NMR (202 MHz, THF) δ 98.99 (s).

Pyrene-PNP Ligand Synthesis

1) dimethyl 4-chlorodipicolinate using $SOCl_2$:

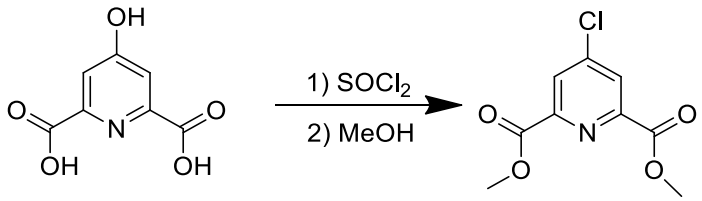

0.687 g chelidamic acid was dissolved in excess thionyl chloride and refluxed for three days. The solution was concentrated via vacuum. The residue was then cooled to 0°C and an excess of methanol was added. The flask was left to stir and slowly warm up to room temperature. The reaction was left to stir for three days at room temperature. The

product was then extracted using $NaHCO_3$ and EtOAc. Yield: 22%. ^1H NMR (300 MHz, Chloroform-*d*) δ 8.34 (s, C*H*, 2H), 4.08 (s, CH_3, 6H).

2) dimethyl 4-chlorodipicolinate using PCl_5:

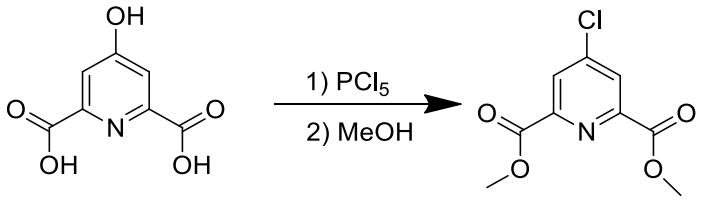

1.7 g of chilademic acid was dissolved in chloroform. 7.08 g of PCl_5 was added to the reaction and it was left to reflux for 3 days. Solvent was removed via vacuum. The residue was cooled to 0°C and then an excess of methanol was added. This was let to warm slowly to room temperature and then stirred for three days. Solvent was removed via vacuum and then the yellow residue was washed with methanol to yield a white product. Yield: 70%. ^1H NMR (500 MHz, Chloroform-*d*) δ 8.34 (s, C**H**, 2H), 4.07 (s, C**H**$_3$, 6H).

3) 4-chloro-2,6-bis(hydroxymethyl)pyridine

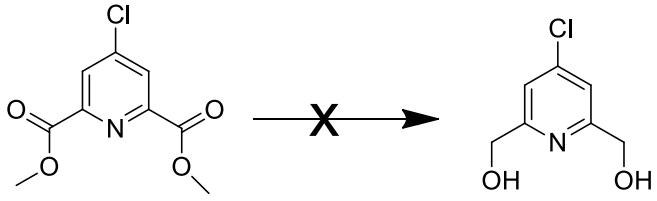

100 mg dimethyl 4-chlorodipicolinate was dissolved in 5 mL of dry methanol. The solution was cooled to 0°C and 4 eq. of $NaBH_4$ was added. The reaction was left to warm to room temperature and stirred at room temperature for 3 hours. The reaction was then refluxed

for overnight. At this point it was observed that a lot of solid had crashed out of solution. NMR showed decomposition of the compound.

4) dimethyl 4-iododipicolinate:

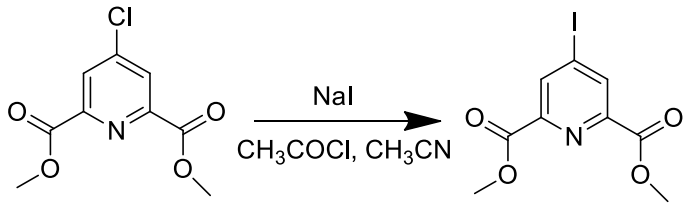

25 mg of dimethyl 4-chlorodipicolinate was mixed with excess NaI in acetyl chloride (3 mL) and dry acetonitrile (2.9 mL). The mixture was sonicated one hour, changing the water every 15-20 min. to stay under 50°C. A color change from white to bright orange was observed. By ^{1}H NMR there was only a 40% conversion to the iodine product. The excess salt was filtered out and the solvent was removed. Fresh reagents and solvent were added. After sonicating for another hour, NMR showed the reaction went in reverse to only 10% of the iodine complex. Iodine Complex: ^{1}H NMR (500 MHz, Chloroform-*d*) δ 8.66 (s, C**H**, 2H), 4.02 (s, C**H**$_3$, 6H). Chloride Complex: ^{1}H NMR (500 MHz, Chloroform-*d*) 8.29 (s, C**H**, 2H), 4.03 (s, C**H**$_3$, 6H).

5) dimethyl 4-pyrene-dipicolinate:

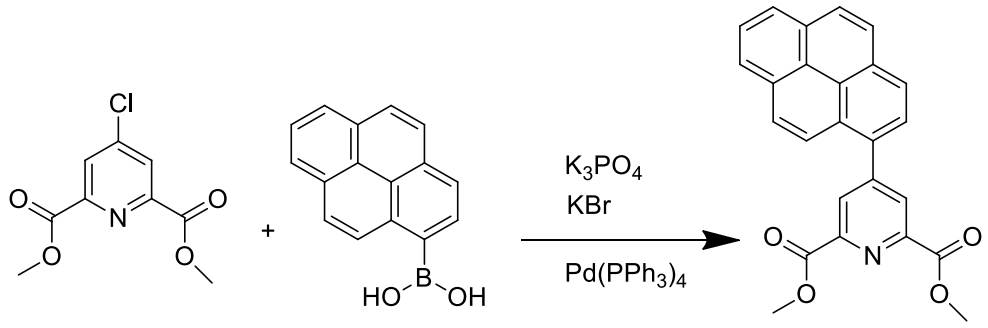

0.260 g of dimethyl 4-chlorodipicolinate was mixed with 0.440 g pyrene-1-boronic acid, 0.761g K_3PO_4, 0.286g KBr, 0.281 g $Pd(PPh_3)_4$, in 30mL of dioxane. The reaction was heated at 80°C for 8 hrs. The reaction was tracked by TLC. For workup, 0.1M KOH was added to quench the solution and caused solid to precipitate. The product was: Extracted with ether (x3). Extracted again via ether and water (x3). Washed with $CHCl_3$, benzene, and hexane (x3 each). This resulted in brown solid. The large excess of Pd resulted in a lot of phosphine oxide making isolation difficult. ^{1}H NMR (300 MHz, Acetone-d_6) δ 8.56 (s, C**H**, 2H), 8.34 – 7.93 (m, C**H**(pyrene) 9H), 4.03 (s, C**H**$_3$, 6H).

2.7: NMR

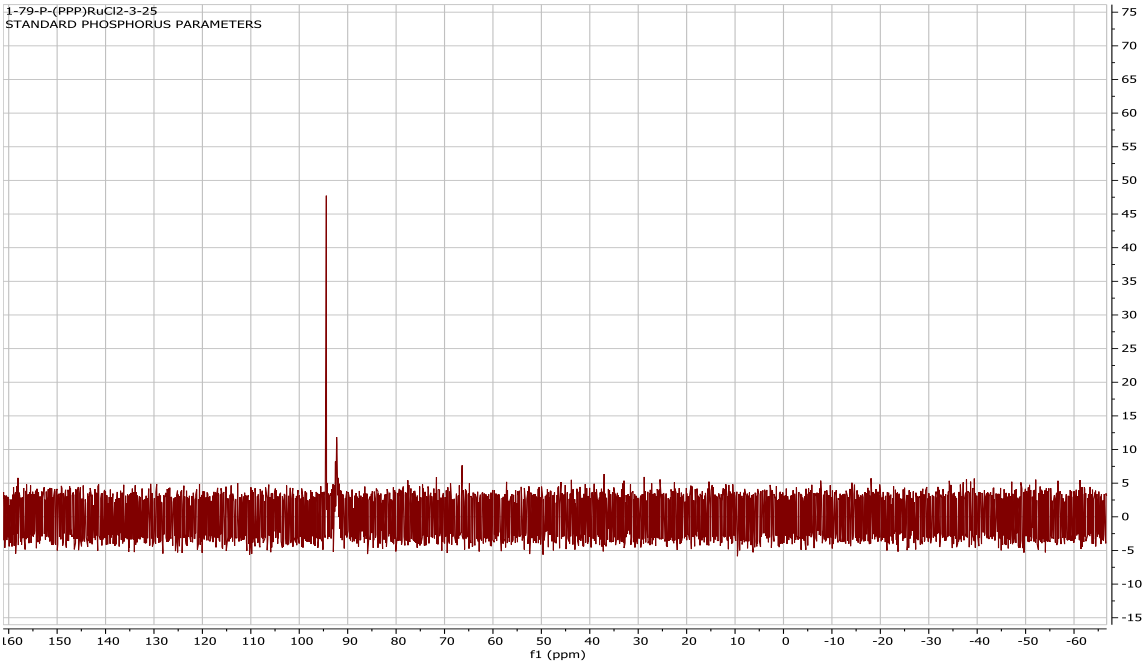

Figure 2.26: ^{31}P Spectra of (^{tBu}PPP)RuCl$_2$

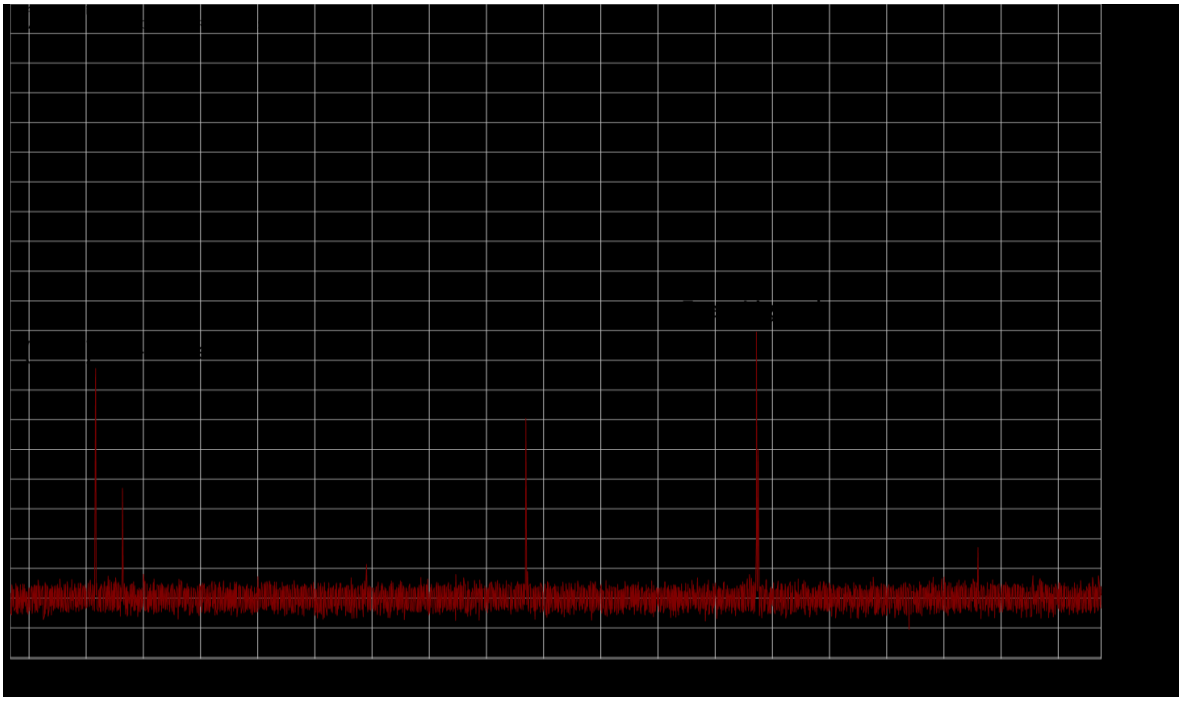

Figure 2.27: ^{31}P Spectra of (^{tBu}PNP)Mo-Dimer

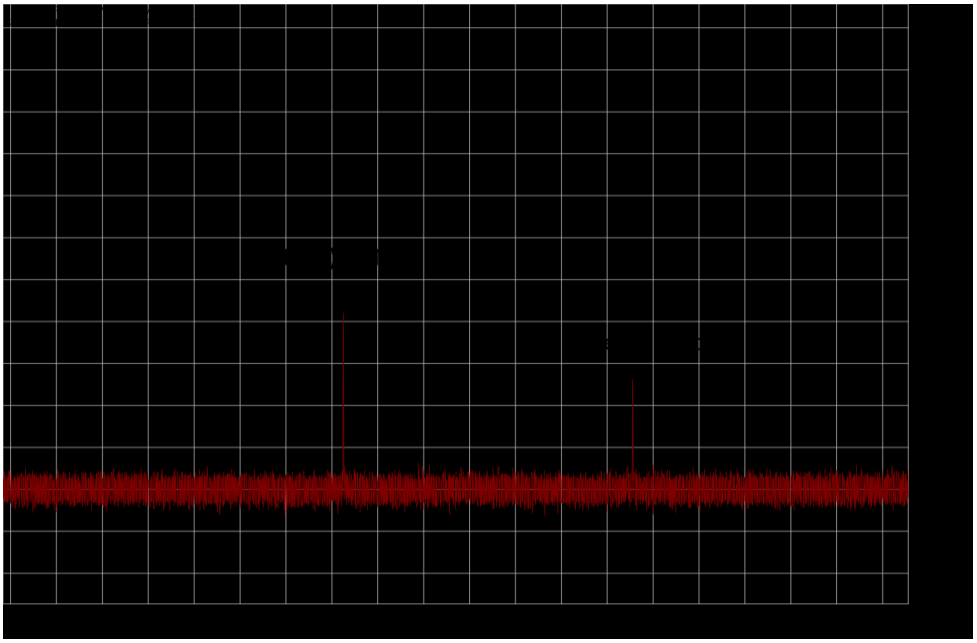

Figure 2.28: ^{31}P Spectra of (^{tBu}PNP)MoNCl

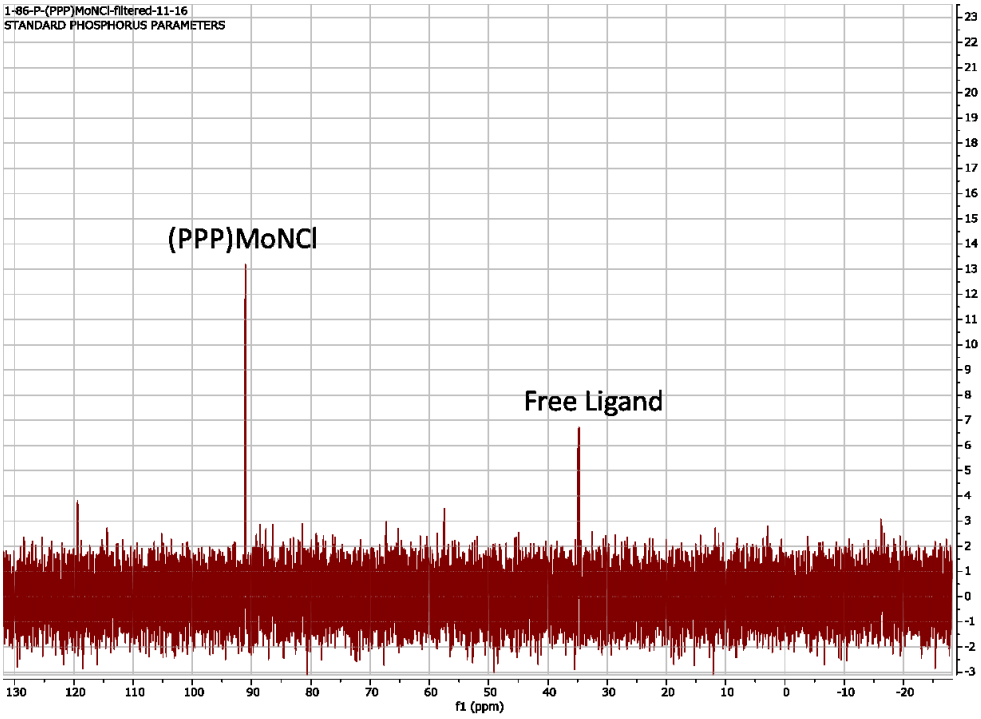

Figure 2.29: ^{31}P Spectra of (^{tBu}PPP)MoNCl

Pyrene-Ligand Synthesis

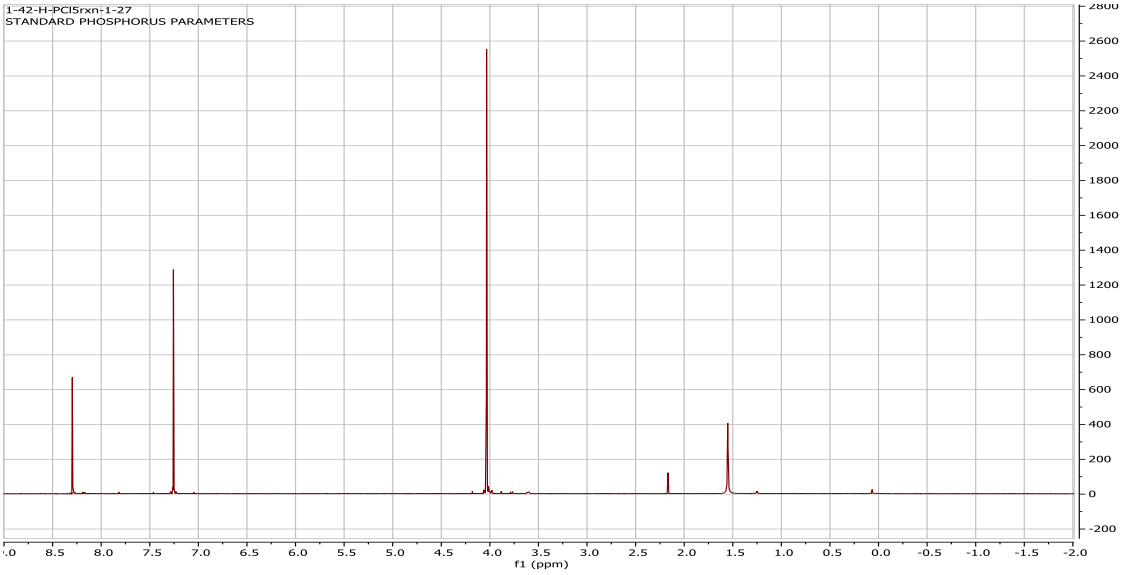

Figure 2.30: ^{1}H Spectra of Dimethyl 4-chlorodipicolinate

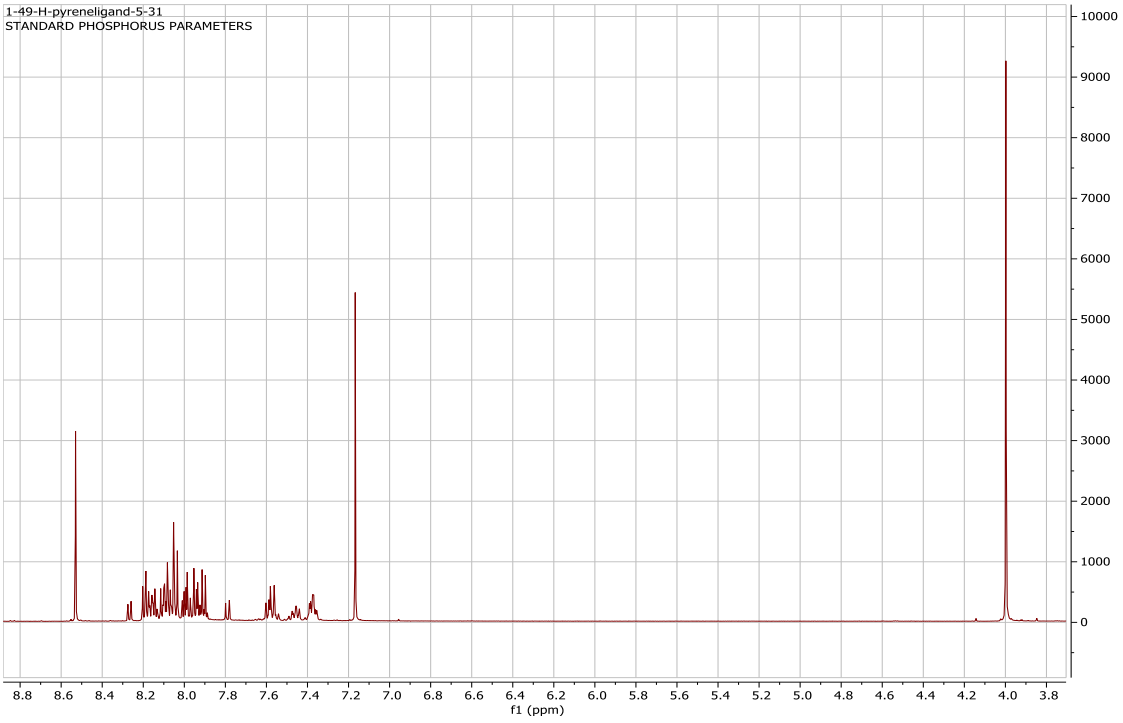

Figure 2.31: ^{1}H Spectra of Dimethyl 4-pyrene-dipicolinate

2.8: References

1. Fryzuk, M. “Ammonia transformed.” *Nature*, Feb 2004, *427*, 498-499.
2. Erisman, J. W; Sutton, M. A; Galloway, J; Kilmont, Z; Winiwarer, W. “How a century of ammonia synthesis changed the world.” *Nat. Geosci.* **2008**, *1*, 636-639.
3. Peplow, M. “A fixation with nitrogen.” *Chemistry World*, *48*, April 18, 2013. https://www.chemistryworld.com/feature/a-fixation-with-nitrogen/6076.article (Last Accessed Nov 8, 2018)
4. Appl, M. “Ammonia” in *Ullmann’s Encyclopedia of Industrial Chemistry:* Wiley-VCH Verlag GmbH & Co. KGaA, 2000.
5. Schmidhuber, J. “Haber & Bosch.” http://people.idsia.ch/~juergen/haberbosch.html (Last Accessed Nov 8, 2018)
6. Lindley, B.M.; Appel, A.M.; Krogh-Jespersen, K.; Mayer, J.M.; Miller, A.J.M. *ACS Energy Letters* **2016**, 698-704.
7. Image Created by Dr. Brian Lindley at UNC
8. Ashcraft, R.W.; Raman, S.; Green, W.H. *J. Phys. Chem. B,* **2007**, *111*, 11968.
9. Argonne National Laboratories ATcT enthalpies of formation based on version 1.118 of the Thermochemical Network, http://atct.anl.gov/Thermochemical Data/version 1.118/index.php (Last Accessed Nov 8, 2018).
10. “Feeding the World in the 21st Century: Grand Challenges in the Nitrogen Cycle” National Science Foundation Report; Nicolai Lehnert, PI; November 9-10, 2015. Executive summary online: https://www.nsf.gov/mps/che/workshops/n_cycle_workshop_executive_summary_november_2015.pdf
11. Seefeldt, L. C.; Hoffman, B. M.; Dean, D. R. "Electron transfer in nitrogenase catalysis" *Current Opinion in Chemical Biology* **2012**, *16*, 19-25.
12. *The Metal-Driven Biogeochemistry of Gaseous Compounds in the Environment*; Kroneck, P. M. H.; Sosa Torres, M. E., Eds.; Springer: Dordrecht, 2014.
13. Holland, P. L. "Nitrogen Fixation" In *Comprehensive Coordination Chemistry II*, McCleverty, J., Meyer, T. J., Eds.; Elsevier, Oxford, 2004; Vol. 8, p 569-599.
14. Hoffman, B. M.; Lukoyanov, D.; Yang, Z.-Y.; Dean, D. R.; Seefeldt, L. C. *Chem. Rev.* **2014**, *114*, 4041-4062.
15. Hu, Y.; Ribbe, M. "The interstitial carbide of the nitrogenase M-cluster: insertion pathway and possible function" In *Iron Sulfur Clusters in Chemistry and Biology*, Rouault, T., Ed.; Walter de Gruyter GmbH & Co KG, 2014
16. Bjornsson, R.; Lima, F. A.; Spatzal, T.; Weyhermüller, T.; Glatzel, P.; Bill, E.; Einsle, O.; Neese, F.; DeBeer, S. *Chem. Sci.* **2014**, *5*, 3096-3103.
17. Yandulov, D. V.; Schrock, R. R. *Science* **2003**, *301*, 76-78.
18. Anderson, J. S.; Rittle, J.; Peters, J. C. *Nature* **2013**, *501*, 84-87.
19. Creutz, S. E.; Peters, J. C. *J. Am. Chem. Soc.* **2014**, *136*, 1105-1115.
20. Anderson, J. S.; Cutsail, G. E.; Rittle, J.; Connor, B. A.; Gunderson, W. A.; Zhang, L.; Hoffman, B. M.; Peters, J. C. *J. Am. Chem. Soc.* **2015**, *137*, 7803-7809.
21. Schrock, R. R*Chem. Commun.* **2003**, 2389-2391.
22. Arashiba, K.; Miyake, Y.; Nishibayashi, Y. *Nature Chem.* **2011**, *3*, 120-125.

23. Kuriyama, S.; Arashiba, K.; Nakajima, K.; Tanaka, H.; Kamaru, N.; Yoshizawa, K.; Nishibayashi, Y. *J. Am. Chem. Soc.* **2014**, *136*, 9719-9731.
24. Tanaka, H.; Arashiba, K.; Kuriyama, S.; Sasada, A.; Nakajima, K.; Yoshizawa, K.; Nishibayashi, Y. " *Nat. Commun.* **2014**, *5*, 3737-3737.
25. Nishibayashi, Y. "Recent Progress in Transition-Metal-Catalyzed Reduction of Molecular Dinitrogen under Ambient Reaction Conditions" *Inorg. Chem.* **2015**
26. Arashiba, K.; Kinoshita, E.; Kuriyama, S.; Eizawa, A.; Nakajima, K.; Tanaka, H.; Yoshizawa, K.; Nishibayashi, Y. *J. Am. Chem. Soc.* **2015**, *137*, 5666-5669.
27. Tanaka, H.; Nishibayashi, Y.; Yoshizawa, K. *Acc. Chem. Res.* **2016**, acs.accounts.6b00033-acs.accounts.00036b00033.
28. Arashiba, K.; Eizawa, A.; Tanaka, H.; Nakajima, K.; Yoshizawa, K.; Nishibayashi, Y. *Bull. Chem. Soc. Jpn.* **2017**, *90*, 1111–1118.
29. Licht, S.; Cui, B. C.; Wang, B. H.; Li, F. F.; Lau, J.; Liu, S. Z. *Science* **2014**, *345*, 637-640.
30. Kordali, V.; Kyriacou, G.; Lambrou, C. " *Chem. Commun.* **2000**, 1673-1674.]
31. Pickett, C. J.; Talarmin, J. *Nature* **1985**, *317*, 652-653.
32. Pickett, C. J.; Ryder, K. S.; Talarmin, J. *J. Chem. Soc., Dalton Trans.* **1986**, 1453-1457.
33. Munisamy, T.; Schrock, R. R. *Dalton Trans.* **2012**, *41*, 130-137.
34. Del Castillo, T. J.; Thompson, N. B.; Peters, J. C. *J. Am. Chem. Soc.* **2016**, *138*, 5341-5350.
35. Connor, G.; Lease, N.; Casuras, A.; Holland, P. L.; Goldman, A. S.; Miller, A. J. M.; Mayer, J. M. *Dalton Trans.* **2017**, *46*, 14325-14330.
36. Lindley, B. M.; Bruch, Q.; Lease, N.; Goldman, A. S.; Hasanayn, F.; Miller, A. J. M. *J. Am. Chem. Soc.* **2017**, *139*, 5305−5308.
37. Lindley, B. M.; Alten, R. S; Finger, M; Schendzielroz, F; Wurtele, C; Miller, A. J; Siewert, I; Schneider, S. *J. Am. Chem. Soc.* **2018**, *140*, 7922-7935.
38. Klopsch, I.; Finger, M.; Würtele, C.; Milde, B.; Werz, D.B.; Schneider, S. *J. Am. Chem. Soc.* **2014**, *136*, 6881.
39. Gilbert-Wilson, R; Field, L; Bhadbhade, M. *Inorg. Chem.* **2012,** *51,* 3239-3246.
40. Kang, P; Zhang, S; Meyer, T; Brookhart, M. *Angewadte Chem.* **2014**, *53*, 8709-8713.
41. Nakamura, T; Mizukami, S; Tanaka, N; Kikuchi, K. *An Asian Journal* **2013**, *8*, 2685-2690.
42. Pellet-Rostaing, S; Miguirditchian, M; Chapron, S; Marie, C; Arrachart, G; Gracia, S. *Tetrahedron* **2015**, *71*.
43. Luning, U; Baumstark, R; Muller, M. *Liebigs Ann. Chem.* **1991**, 987-988.
44. Maitra, U; Maity, M. *J. Mater. Chem. A.* **2014**, *44*, 18952-18958.
45. Otsuka, M; Umezawa, K; Tamanoi, F; Naka, H; Hamasaki, A. *Bioorg. Med. Chem. Lett.* **2003.**
46. Stoffelbach, F., Saurenz, D. & Poli, R. *Eur. J. Inorg. Chem.* **2001**, 2699–2703.
47. Kawatsura, M. & Hartwig, J. F. *Organometallics* **2001**, *20*, 1960–1964.

Chapter 3

Synthesis of (^{tBu}PPP)Ru Complexes for Dehydrogenation

Abstract:

The activation of inert chemical bonds by pincer-ligated metal complexes has been an important area of research for decades. Ruthenium pincer-complexes have many beneficial qualities in comparison to other pincer-metal complexes. For example, they have high electron transfer ability, high coordination to hetero-atoms, and low redox potentials. In 2013, pincer-ruthenium complexes represented almost 13% of the total research on pincer-metal complexes and the percentage has continued growing since.[1] Herein we report the synthesis and characterization of novel (^{tBu}PPP)Ru complexes. Preliminary studies show that the (^{tBu}PPP)RuH_4 complex has catalytic activity for the dehydrogenation of alcohols and alkanes, making it the first reported L_3-type pincer-ruthenium complex to perform alkane dehydrogenation.

3.1: Introduction

Using pincer-ligated metal complexes for homogeneous catalysis has many advantages. Two of the biggest advantages are the ability to fine-tune the catalytic activity through choice of metal and choice of ligand. Pincer ligands have a wide variety of structures that help fine tune the electronics and sterics around the metal center. Due to the large range of possibilities for pincer ligands, the known combinations of metal-pincer complexes are extremely varied and always increasing.

One of the more common metals seen in catalysis is ruthenium. Ruthenium complexes exhibit high electron transfer ability, high coordination to hetero-atoms, low redox potentials, and have shown to have unique reactivity in comparison to other metals. In a recent review on ruthenium pincer complexes, Milstein points out that ruthenium catalysts can be found with a wide variety of pincer ligands that can be classified into three major groups: L_2X, L_3, and LX_2.[2] Milstein's own research primarily focuses on the L_3 type pincers (i.e. PNP and PNN).[3-5] Work using L_2X type ligands can be seen in the work of Roddick[6] and Baratta[7], using PCP and CNN. Lastly, LX_2 ligands such as SiNSi are very rare, but have been reported.[8,9]

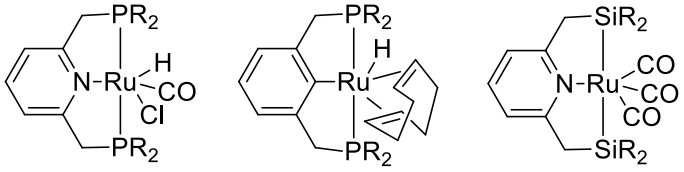

L_3 Type: Milstein L_2X Type: Roddick LX_2 Type: Tobita

Figure 3.1: Types of Pincer-Ligands

Due to the wide variety of pincer ligands used with ruthenium, numerous catalysts have been developed for a wide range of applications. Ruthenium has shown the ability to activate many types of bonds (i.e. C-H, O-H, B-H, H-H, Si-H, etc.)[10-15] It can activate C=O bonds in aldehydes, ketones, and even CO_2.[16-18] Lastly, pincer-ruthenium complexes have been shown to be extremely proficient for hydrogenation and dehydrogenation chemistry.[6,19-21]

Early work on alkane dehydrogenation is dominated by pincer-iridium and pincer-rhodium complexes. However, recently researchers have begun exploring the use of pincer-ruthenium complexes instead. In 2011, Roddick reported the dehydrogenation of cyclooctane using his PCP-ruthenium complex (Scheme 3.1).[6] His complex was the first efficient ruthenium catalyst for transfer alkane dehydrogenation under thermal conditions. Currently, (PCP)Ru complexes are the only pincer-ruthenium catalysts reported for alkane dehydrogenation.[6,22]

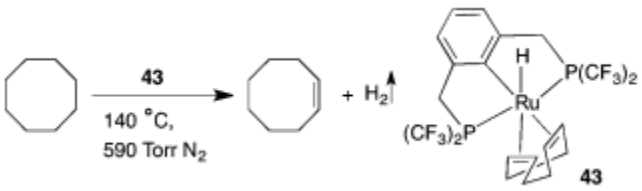

Scheme 3.1: (PCP)Ru(COD)(H) Alkane Dehydrogenation

More commonly, pincer-ruthenium catalysts are used for the dehydrogenation of alcohols. Alcohol dehydrogenation can be performed with or without a sacrificial hydrogen acceptor. While using an acceptor lowers the overall energetics of the reaction,

allowing for higher reactivity and turnovers, it has the downfall of producing a stoichiometric amount of waste.

Since the 1970s, ruthenium has been a focus for acceptorless dehydrogenation. The first major report was by Robinson in 1975 with his $[Ru(OCOCF_3)_2(CO)(PR_3)_2]$ catalyst.[23] More recently, in 2011, Milstein was able to perform effective alcohol dehydrogenation using his (PNX)Ru(H)(BH_4) catalyst (Scheme 3.2).[24]

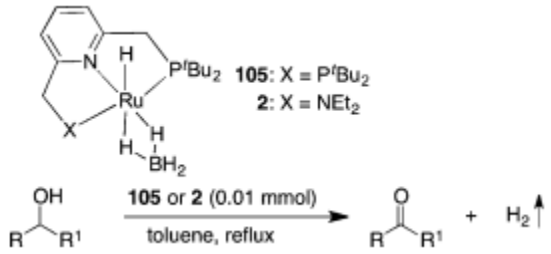

Scheme 3.2: (PNP)RuH(BH_4) Alcohol Acceptorless Dehydrogenation

Ruthenium is also very common in transfer dehydrogenation of alcohols, using a hydrogen acceptor. Pincer-ruthenium complexes catalyze transfer dehydrogenation effectively, having better reactivities when compared to other ruthenium complexes. In the past two decades numerous pincer-ruthenium complexes have been studied for transfer dehydrogenation. Using a (CNN)Ru complex, Baratta was able to reach a TOF of 1.5×10^6 for the transfer dehydrogenation of cyclohexanone to cyclohexanol.[7] However, to achieve such a high TOF, the reaction needed to be under basic conditions. The general mechanism for dehydrogenation is shown in Figure 3.2.[2]

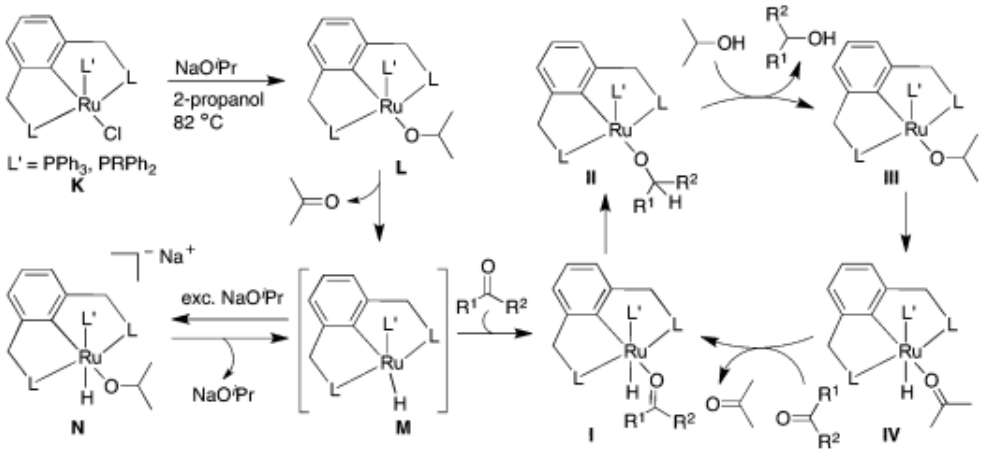

Figure 3.2: Mechanism for Alcohol Transfer Dehydrogenation using (PCP)Ru(Cl)(L)

Chen and coworkers have made some progress on transfer dehydrogenation without base, however the reaction rate is significantly slower than catalysis with base.[25] Development of a pincer-ruthenium catalyst that can perform transfer dehydrogenation efficiently without a base is still a sought-after goal in catalysis chemistry.

With such a wide range of reactivity, it is important to continually research different metal-ligand combinations. While many pincer ligands can be observed with a combination of phosphorous, carbon, and nitrogen, it is much less common to see PPP-pincer ligands in ruthenium chemistry. The Field group has shown significant work using tripodal tetradentate ligands with ruthenium.[26,27] In some of his more recent work, he discovered that using isopropyl groups on the phosphine arms allowed for one of the arms to become hemilabile.[28] When he switched to *tert*-butyl groups, the third phosphine arm would no longer bind to the ruthenium center, forming a (PPP)Ru pincer complex. For comparison with this PP_3-type ligand, Field also synthesized a ($P^{Ph}P_2^{tBu}$) type pincer ligand (This will be referred to as ^{tBu}PPP for the rest of this chapter). However, the

synthesis and characterization of the (^{tBu}PPP)RuCl$_2$ complex was used solely for comparison purposes.

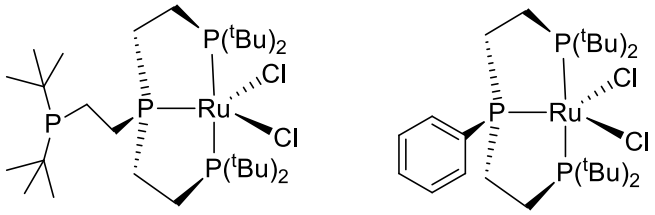

PP_3 $P^{Ph}P_2{}^{tBu}$ (aka. ^{tBu}PPP)

Figure 3.3: Complexes Synthesized by Field et. al. in 2012

Since the report in 2012, Field has continued work with his PP_3 ligands and has not shown any interest in the chemistry of the (^{tBu}PPP)RuCl$_2$ pincer complex. Herein we synthesize the Field (^{tBu}PPP)RuCl$_2$ complex and explore its reactivity. We focus on the synthesis and characterization of several new (^{tBu}PPP)Ru complexes. Additionally, we report some preliminary results showing the potential (^{tBu}PPP)RuH$_4$ has for both alkane and alcohol dehydrogenation.

3.2: Synthesis and Characterization of (^{tBu}PPP)RuHCl

Originally the purpose of synthesizing (^{tBu}PPP)RuCl$_2$ was for comparison to the (^{tBu}PPP)MoCl$_3$ and (Macho)RuCl$_2$ catalysts for nitrogen reduction (Section 2.2). A reported synthesis by Field et. al was followed and a pure product was obtained.[28]

After discovering that ruthenium was not a good metal for nitrogen reduction, we decided to explore other potential uses for the (^{tBu}PPP)RuCl$_2$. The use of pincer-ruthenium catalyst for alkane dehydrogenation is relatively rare in literature. Currently, the only

reported catalysts are (PCP)Ru complexes.[6,33] Due to the use of a L_2X pincer ligands, these complexes go through a mechanism that involves a (PCP)Ru(H) intermediate (Figure 3.2). Exploring the use of an L_3 ligand, the pincer-ruthenium complex becomes isoelectronic with our (PCP)Ir catalysts, and therefore may go through a similar mechanism to the (PCP)Ir catalysts. While rare for ruthenium catalysts, two of the most common versions of pincer-iridium catalysts that can be observed in dehydrogenation literature is the (Pincer)IrH_2/H_4 and the (Pincer)Ir(CH_2=CH_2) complexes. We decided to attempt the synthesis of the isoelectronic (^{tBu}PPP)RuH_4 and (^{tBu}PPP)Ru(CH_2=CH_2). The first step towards making these complexes is adding a reducing agent to substitute the chlorides for a hydride. The hydride source can either be the reducing agent itself, or through the oxidative addition of H_2.

Our first attempt was using $NaEt_3BH$, a common reducing agent used in our laboratory. It was observed that upon addition of the $NaEt_3BH$ to the (^{tBu}PPP)$RuCl_2$ in THF there was an instant color change to bright orange. When using more than 1 eq. there were multiple products in solution at early time points. After 5-10 minutes, the reaction would completely convert to a single product. This will be discussed in Section 3.3. However, when only 1 eq. was used, we observed an instant reaction to a new product in 100% yield with the production of a white precipitate (NaCl). After isolation of the orange solid, we were able to use NMR to characterize the species as (^{tBu}PPP)RuHCl.

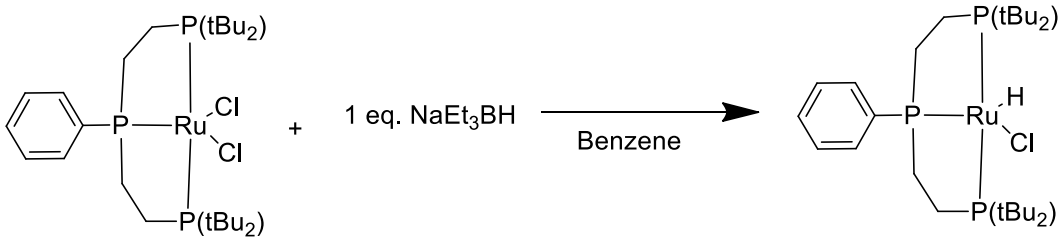

Scheme 3.3: Synthesis of (^{tBu}PPP)RuHCl using $NaEt_3BH$

The ^{31}P NMR showed a single species with a multiplet between δ 120.08 – 118.96, with an integration of one phosphorous, and a doublet at δ 80.57, with an integration of two phosphorous atoms and a *J* coupling of 20.4 Hz. The ^{1}H NMR showed sharp singles characteristic of a diamagnetic species. Four different peaks could be observed for the methylene linkers and the tert-butyl peaks overlap suggesting a fairly symmetrical complex. Lastly, a doublet of triplets can be observed at -28.91 ppm (J = 35.9 Hz, 17.9 Hz), corresponding to a single hydride on the complex. Due to the far upfield shift of the hydride along with the diamagnetic characteristic of the complex, it can be inferred that a single chloride is also on the metal, resulting in a 16 e^- (^{tBu}PPP)RuHCl species.

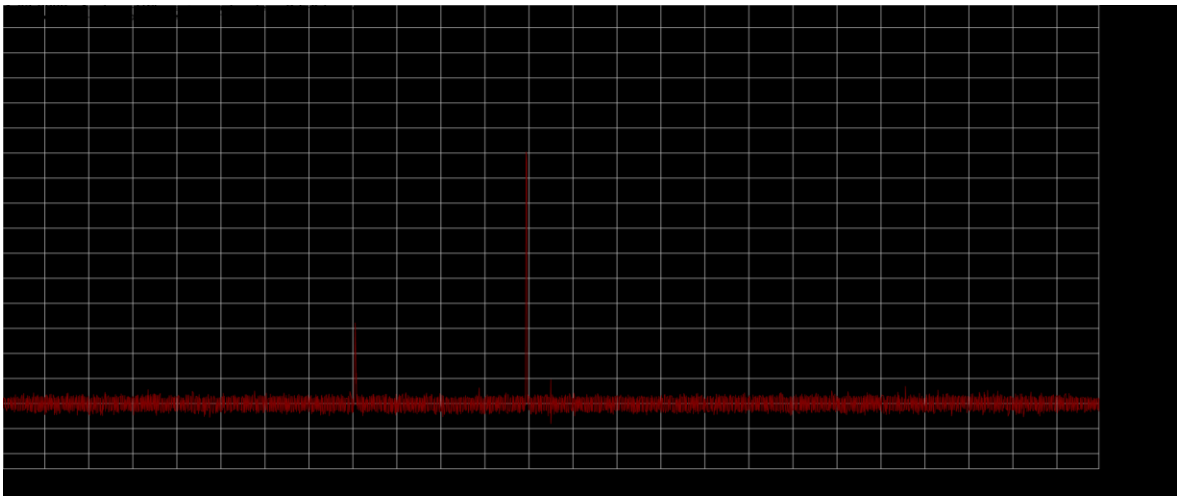

Figure 3.4: ^{31}P NMR of (^{tBu}PPP)RuHCl

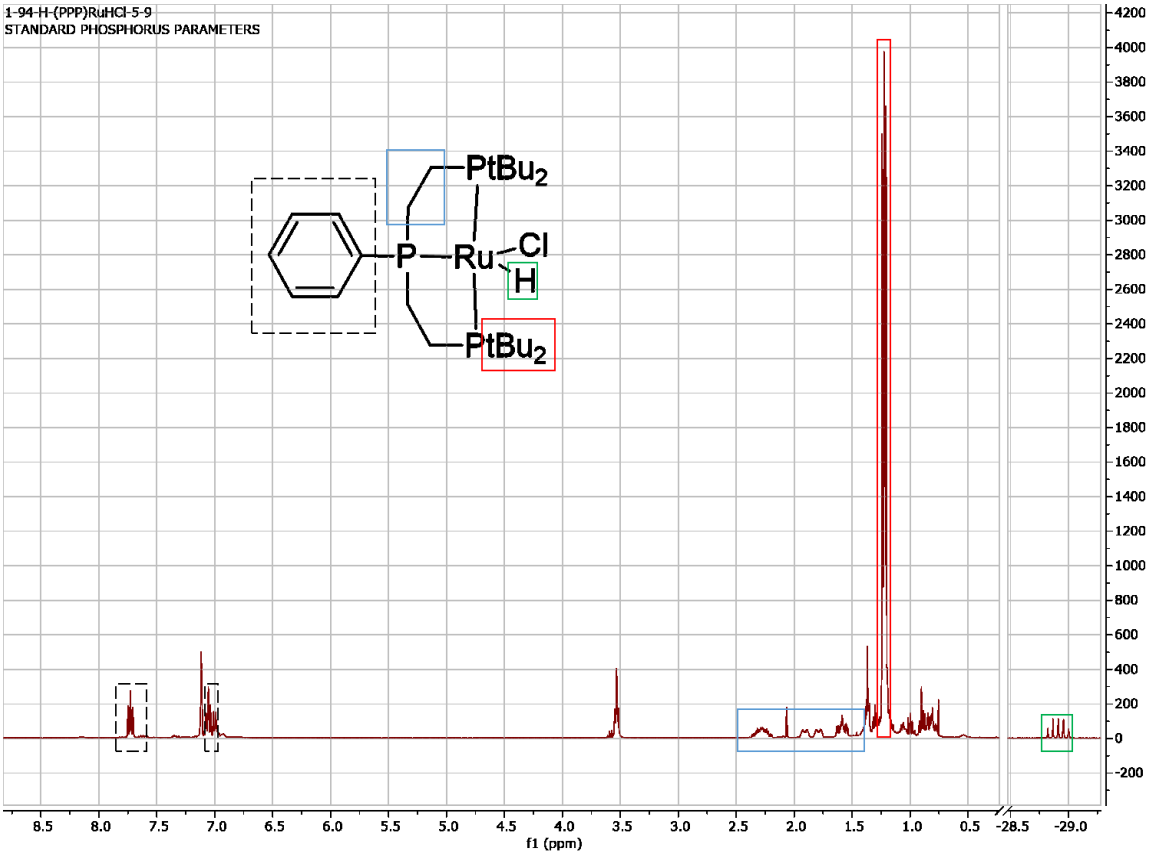

Figure 3.5: ^{1}H NMR of (^{tBu}PPP)RuHCl

3.2.1 Alternative Synthetic Route to (^{tBu}PPP)RuHCl using KtBuO and Isopropanol

The logical next step in our synthetic progression would be to add more reducing agent and H_2 atmosphere to synthesize the (^{tBu}PPP)RuH_4 complex. In our attempts to isolate the (^{tBu}PPP)RuH_4 complex and use it for catalysis, it was observed that the presence of any $NaEt_3BH$ both inhibits reactivity and leads to decomposition of the (^{tBu}PPP)RuH_4 to a different (^{tBu}PPP)Ru species (Section 3.3). Due to this, a new route was developed to synthesize (^{tBu}PPP)RuHCl using a different reducing agent.

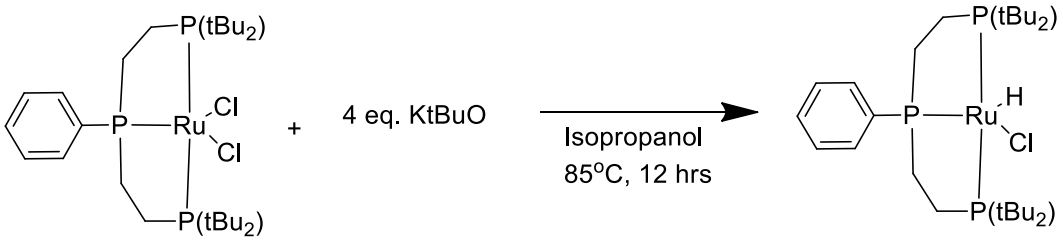

Scheme 3.4: Synthesis of (^{tBu}PPP)RuHCl using KtBuO and Isopropanol

For this synthesis, (^{tBu}PPP)$RuCl_2$ was mixed with 4 eq. of KtBuO in 0.5 mL of isopropanol. Low solubility of the starting material in isopropanol led to a slower reaction time than the reaction with $NaEt_3BH$. However, after five minutes all the starting material went into solution and a color change to bright orange was observed. The reaction was left to stir overnight, and the ^{31}P and ^{1}H NMR showed two (^{tBu}PPP)RuHCl isomers in a 1:1 ratio, neither of which match the previously synthesized complex. The reaction was then heated at 85°C overnight and a single (^{tBu}PPP)RuHCl species resulted. The ^{31}P NMR shows two signals, one multiplet between δ 121.06 – 119.35 (m) and one doublet at δ 86.68 with a *J* coupling of 15.9 Hz. The ^{1}H NMR shows a hydride signal at -30.60 ppm. The NMR suggests an (^{tBu}PPP)RuHCl species, however there is a significant difference in the shifts of the ^{31}P and hydride peaks in comparison to the previous reaction.

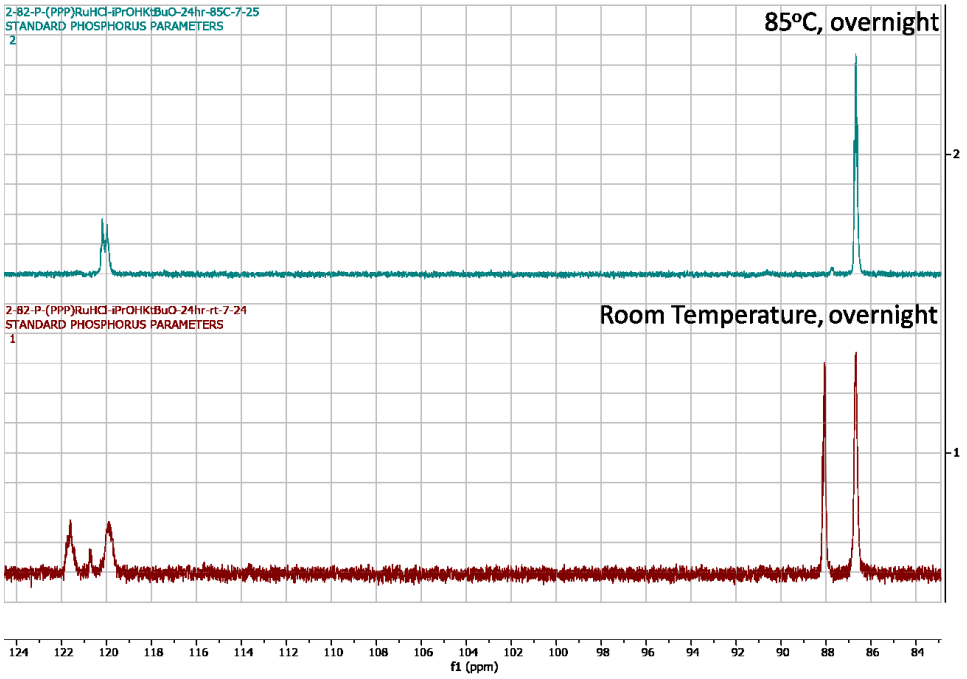

Figure 3.6: ^{31}P NMR of (^{tBu}PPP)RuHCl (top) Thermodynamic Product (bottom) Reaction Mixture of Thermodynamic Product and Unknown

To help confirm our structures and explain the differences, we compared our results to a very similar complex made by Field. et. al.[29] It was observed that when reacting their ($P^2P_3^{tBu}$)$RuCl_2$ complex with KH that two different isomers could be observed. In their kinetic ($P^2P_3^{tBu}$)RuHCl isomer, they observed a ^{31}P signal of δ 115.9 and δ 82.3 (*J* = 17 Hz). Additionally, their hydride signal was located at δ -30.61 (dt, *J* = 42 Hz, 18 Hz). In their thermodynamic ($P^2P_3^{tBu}$)RuHCl isomer, they observed a ^{31}P signal of δ 120.8 and δ 86.4 (*J* = 14 Hz) The hydride signal was located at δ -30.47 (dt, *J* = 43 Hz, 19 Hz). They observed both isomers at room temperature however after heating the solution the kinetic isomer converted to the thermodynamic isomer.

Through comparison of our complexes to those reported by Field we can observe several things. First, we can hypothesize that our HCl complex after heating is most likely a structure very similar to that of the thermodynamic isomer observed by Field. Comparing the NMR vales of these two complexes we can see they are nearly identical, within 1 ppm of both the phosphorous and hydride signals (Table 3.1). The kinetic product seen by Field most closely matches that of the complex made using $NaEt_3BH$.

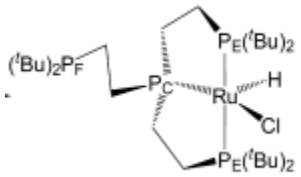

Figure 3.7: Field's (PP_3)RuHCl Thermodynamic Isomer

Table 3.1: Comparison of NMR Values of the Field (PP_3)RuHCl Isomers to Experimental (^{tBu}PPP)RuHCl Isomers

	Field Kinetic Isomer	Field Thermo. Isomer	$NaEt_3BH$ Product	KtBuO Therm. Isomer	KtBuO Unknown Isomer
^{31}P Signals	115.9, 82.3	120.8, 86.4	119, 80.57	121.6, 86.68	119.9, 88.08
Hydride Signal	-30.61	-30.47	-28.91	-30.60	-28.21

Field discovered that the ($P^2P_3{}^{tBu}$)$RuCl_2$ complex is an extremely distorted square-based pyramid.[29] We hypothesize that our complex is also extremely distorted, and the differences seen in NMR come from the level of complex distortion and location of the hydride and chloride. We know that in the distortion the phenyl group is located bent

towards one side of the complex. We believe that the kinetic product has the hydride on the same side as the phenyl while the thermodynamic product has the reverse (Figure 3.8). In these complexes the ethylene bridge in the pincer complex tends to be twisted so that one carbon is coming out of the plane while the other is behind. It is possible that the third unknown isomer that we see is a complex where the two carbons are in the same plane. This structure could be an intermediate between the kinetic and thermodynamic products. Without crystal structures of the complexes it is difficult to say exactly what the structures are, however with this comparison we can confidently say that they are (^{tBu}PPP)RuHCl.

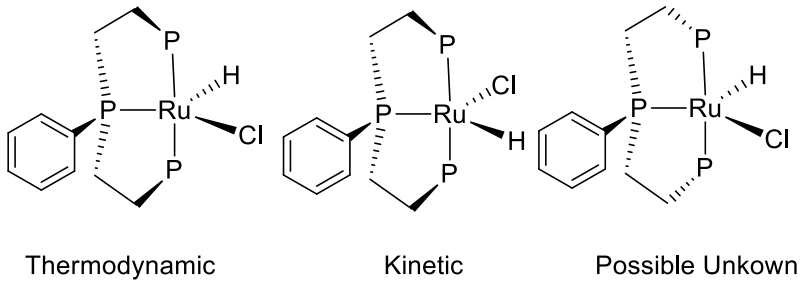

Figure 3.8: Proposed Structures for Observed Isomers

3.2.2 Alternative synthetic route to (^{tBu}PPP)RuHCl using $LiBH_4$

In attempting to make a (^{tBu}PPP)Ru(H)(BH_4) complex similar to one made by Field, another synthesis to a (^{tBu}PPP)RuHCl complex was discovered.[29] A suspension of $LiBH_4$ and (^{tBu}PPP)$RuCl_2$ in 0.5 mL benzene-d_6 was made. This reaction was left to stir at room temperature for five days. Like the previous reaction, two isomers were observed by ^{31}P NMR. The NMR tube was then heated at 70^{o}C for five days in attempt to obtain a single product. The reaction was left to cool and dark purple crystals suitable for

structural analysis crashed out of solution.

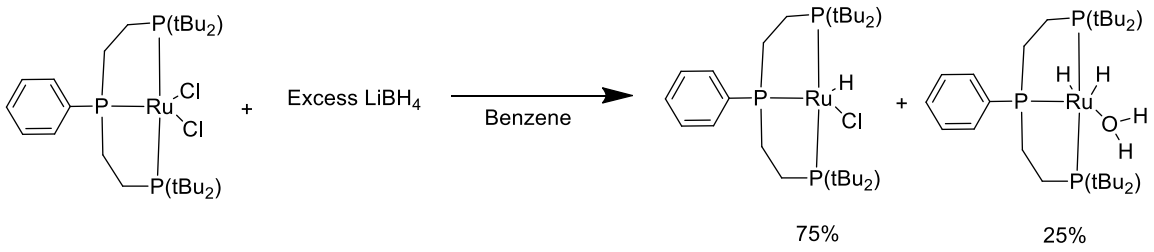

Scheme 3.5: Synthesis of (^{tBu}PPP)RuHCl using $LiBH_4$ in Benzene

Single crystal X-ray diffraction shows the crystal is a cocrystal with two different species in a 3:1 ratio. The major component is the expected (^{tBu}PPP)RuHCl species (Figure 3.9). The geometry of the (^{tBu}PPP)RuHCl is a distorted square-based pyramid, with three phosphines and the chloride forming the base and the hydrido ligand at the apex. The distortion comes from the significant difference between the small P2-Ru1-H1 bond angle of 75.83(18) compared to the Cl1A-Ru1-H1 bond angle of 124.58(18). These values are in close proximity to the values observed by Field in his (PP_3)RuHCl complex where the P2-Ru1-H1 bond angle is 72(2) and the Cl1-Ru1-H1 bond angle is 134(2).

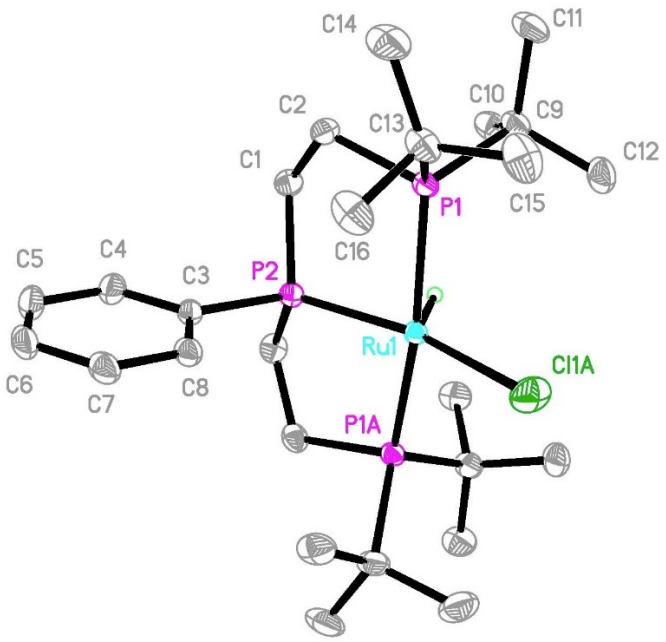

Figure 3.9: Crystal Structure of (^{tBu}PPP)RuHCl

Table 3.2. Selected Bond Lengths (Å) and Bond Angles (deg) for (^{tBu}PPP)RuHCl

Ru1-Cl1A	2.435(7)	Cl1A-Ru1-H1	124.48(18)
Ru1-P1	2.345(3)	P2-Ru1-Cl1A	159.60(2)
Ru1-P1A	2.345(3)	P1-Ru1-H1	82.784(16)
Ru1-P2	2.193(5)	P1A-Ru1-H1	82.783(16)
Ru1-H1	1.549(9)	P2-Ru1-P1A	84.099(8)
		P1-Ru1-P2	84.100(8)
		P1-Ru1-P1A	163.215(17)
		P1-Ru1-Cl1A	97.612(8)
		P1A-Ru1-Cl1A	97.613(8)
		P2-Ru1-H1	75.83(18)

The minor component of the crystal fits best with a (^{tBu}PPP)Ru(H)$_2$(H$_2$O) complex solvated by an additional water molecule. It is likely that this complex is due to some adventitious water in the solvent. The structure of this complex is an extremely distorted

octahedral complex with two hydrides in *cis*- coordination sites and the water *trans*- to one of the hydrides. X-Ray crystal structure and selected data for the (^{tBu}PPP)Ru(H)$_2$(H$_2$O) complex are available at the end of this chapter.

The NMR spectra of this complex suggest a (^{tBu}PPP)RuHCl complex with shifts very similar to that of the reaction using KtBuO. The ^{31}P shows a multiplet at δ 119.63 and a doublet at δ 87.05 with a *J* coupling of 17.3 Hz. The hydride in the proton NMR shows up at -29.41 ppm. The slight difference is most likely due to the difference in solvent. A minor product (~20%) can be seen at δ 116.38 and δ 96.50 with a hydride at -18.47 ppm. This product is most likely the (^{tBu}PPP)Ru(H)$_2$(H$_2$O) complex observed in the crystal.

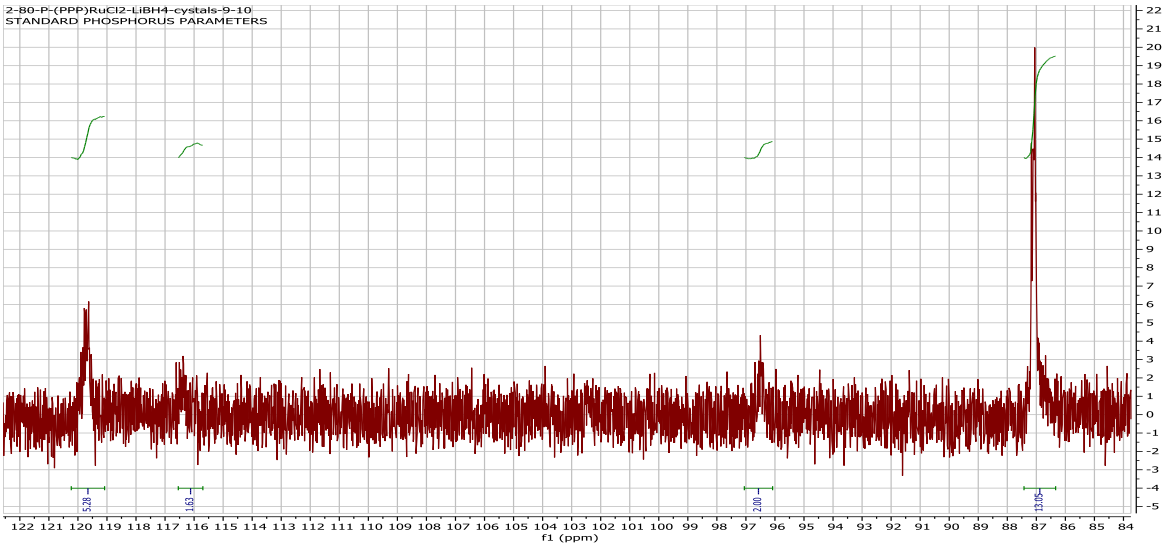

Figure 3.10: ^{31}P NMR of (^{tBu}PPP)RuHCl crystals

From the similarity in NMR and crystal structure, we can conclude that the structure obtained in 75% is that of the thermodynamic product. The NMR signals between the LiBH$_4$ reaction and KtBuO reaction are within 2 ppm of each other and this

difference can be explained by the different solvent effects of benzene versus isopropanol.

Table 3.3: NMR Comparison of Thermodynamic (^{tBu}PPP)RuHCl Isomers Obtained in KtBuO and $LiBH_4$ Reactions

	Thermo. Isomer KtBuO	Thermo. Isomer using $LiBH_4$
^{31}P Signals	121.6, 86.68	119.63, 87.05
^{1}H Hydride Signals	-30.60	-29.41

3.3: Synthesis and Characterization of $Na^+[(^{tBu}PPP)RuH_3]^-$, (^{tBu}PPP)Ru(H)(BH_4), and Unknown (^{tBu}PPP)RuH_3

While synthesizing the (^{tBu}PPP)RuHCl complex with $NaEt_3BH$, it was observed that when >1eq of $NaEt_3BH$ was added a new tri-hydride species could be observed. Additionally, the structure and/or composition of this trihydride changed significantly between benzene and THF solvent. NMR characterization was performed on each complex, however there is not enough information to confirm the structure of each trihydride. Here we report the characterization data and our best hypothesis of each structure.

3.3.1 Synthesis and Characterization of Na(^{tBu}PPP)RuH_3

A large excess (>15eq) of $NaEt_3BH$ was added to a solution of (^{tBu}PPP)$RuCl_2$ in THF and a slow color change to yellow was observed at room temperature over the course of 24 hours. Additionally, white precipitate (NaCl) crashed out of solution. The solution was filtered, but when the solvent was then removed via vacuum the complex decomposed.

The complex is not stable out of solution, so all NMR characterization had to be done on the crude solution which contains the excess $NaEt_3BH$ in addition to the Et_3B that was made.

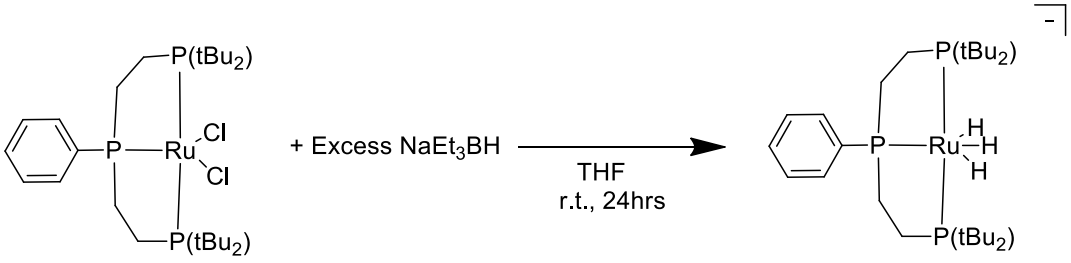

Scheme 3.6: Synthesis of (^{tBu}PPP)RuH_3^-

^{31}P NMR shows a single product with a doublet at δ 129.59 (2P) with a *J* coupling of 19.1 Hz and a broad multiplet at 120.06 ppm (1P). The ^{1}H NMR shows the appearance of three distinct hydrides: -8.78 – -9.22 (m, 1H), -10.20 – -10.56 (m, 1H), -13.34 (dtd, *J* = 25.0, 14.1, 11.9 Hz, 1H). Uniquely, this complex has three hydrides that do not exchange with each other.

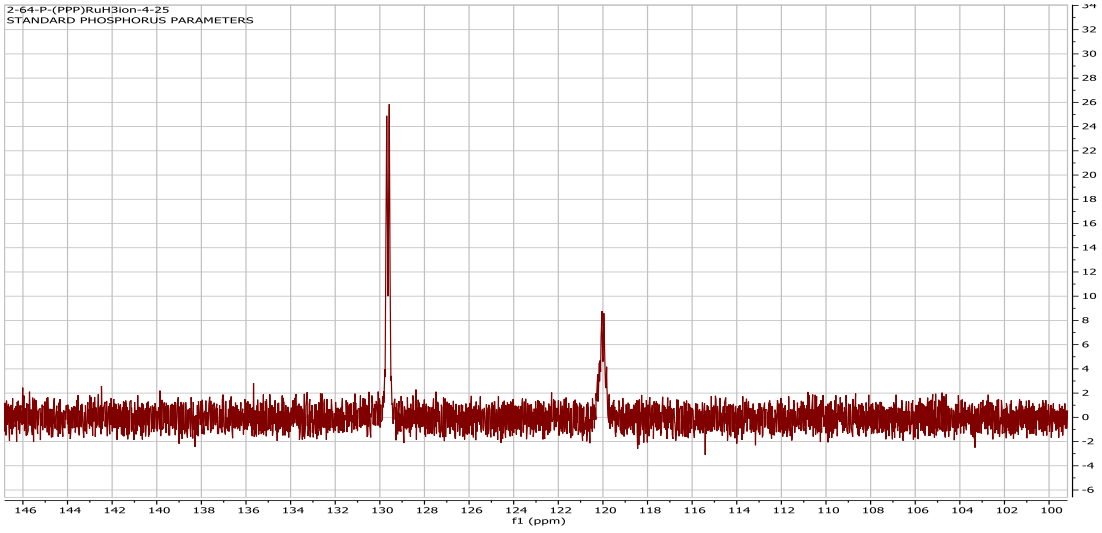

Figure 3.11: ^{31}P NMR of (^{tBu}PPP)RuH_3^-

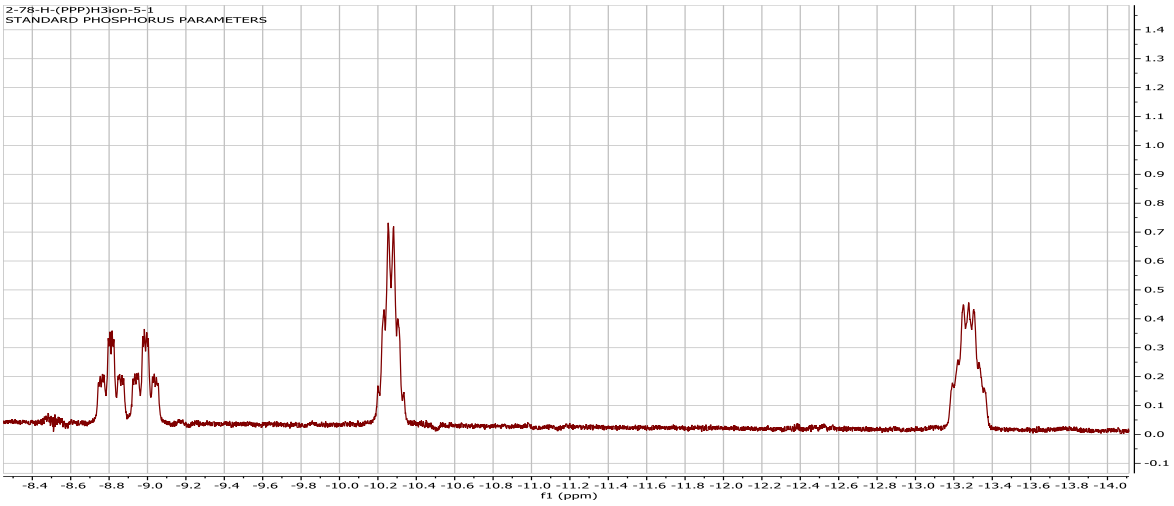

Figure 3.12: ^{1}H NMR: Hydride Signals of (^{tBu}PPP)RuH$_3^-$

If we compare the NMR values to the K[($P^2P_3^{tBu}$)RuH$_3$] reported by Field, we can see that the values come very close to each other (Table 3.4).[29] This leads us to believe that the complex made in THF solution is the trihydride anion.

Table 3.4: NMR Comparison of (^{tBu}PPP)RuH$_3^-$ and Field (PP$_3$)RuH$_3^-$

	K[($P^2P_3^{tBu}$)RuH$_3$]	Na[(^{tBu}PPP)RuH$_3$]
^{31}P Signals	131.6, 121.1	129.59, 120.06
^{1}H Hydride Signals	-9.1, -10.59, -13.7	-8.9, -10.3, -13.34

3.3.2 Synthesis of (^{tBu}PPP)Ru(H)(BH_4)

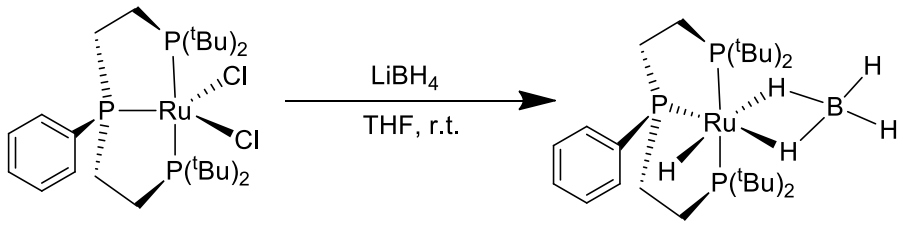

Scheme 3.7: Synthesis of (^{tBu}PPP)Ru(H)(BH_4)

In an attempt to confirm the (^{tBu}PPP)RuH_3^- complex we synthesized (^{tBu}PPP)Ru(H)(BH_4). To a solution of (^{tBu}PPP)$RuCl_2$ in THF, an excess of $LiBH_4$ was added. The solution was stirred for one hour. ^{31}P NMR showed a single species at δ124.05 (t, *J* = 15.8 Hz, 1P) and δ 102.11 (d, *J* = 14.8 Hz, 2P) with two corresponding hydride peaks in the ^{1}H NMR at δ -6.43 (bs, 2H, Ru-*H*-B) and δ -19.25 (dt, *J* = 38.4, 19.1 Hz, 1H, Ru-*H*). Due to the proteo-solvent, we were not able to identify the non-bridging hydrogens of the bound BH_4.

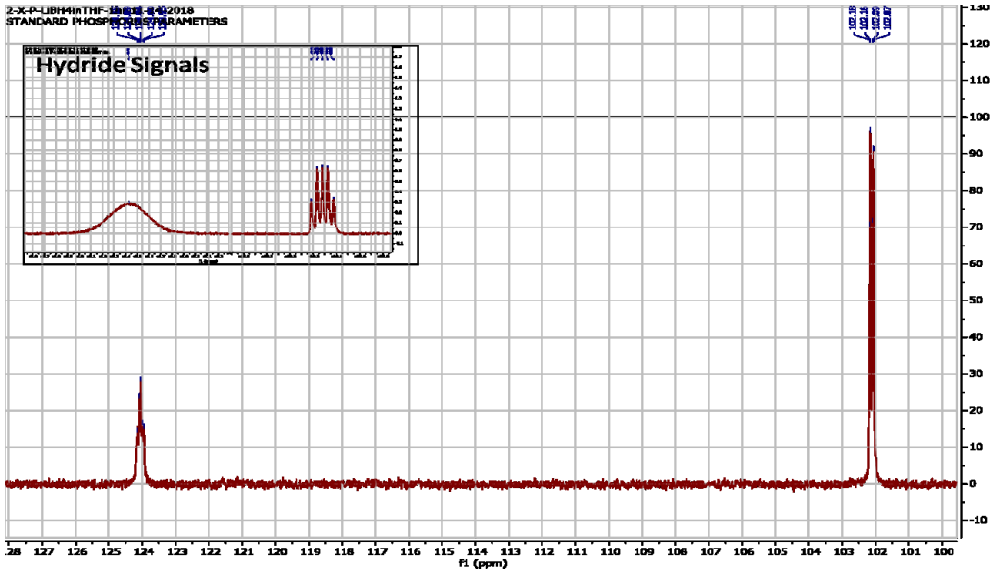

Figure 3.13: ^{31}P NMR of (^{tBu}PPP)Ru(H)(BH_4)

Based off a synthesis by Field, we hoped through the addition of KtBuO to (^{tBu}PPP)Ru(H)(BH_4) we could make (^{tBu}PPP)RuH_3^-. To a solution of (^{tBu}PPP)Ru(H)(BH_4) in THF/benzene, excess KtBuO was added, and the reaction was stirred for 24 hours. ^{1}H NMR showed several new minor species in the hydride region, however the (^{tBu}PPP)Ru(H)(BH_4) complex remained primarily unreacted.

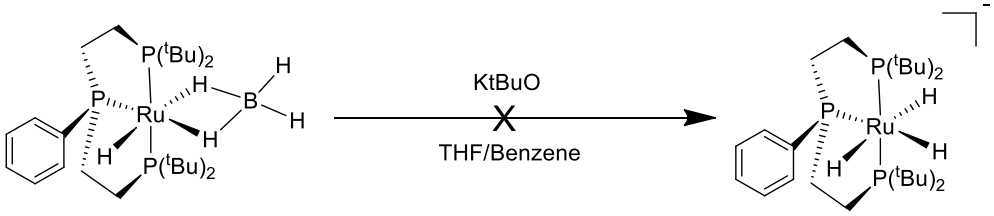

Scheme 3.8: Failed Synthesis of (^{tBu}PPP)RuH_3^-

3.3.3 Synthesis and Attempted Characterization of Unknown (^{tBu}PPP)RuH_3

In stark contrast to the (^{tBu}PPP)RuH_3 anion, an unknown (^{tBu}PPP)RuH_3 complex is formed immediately when 4 eq. of $NaEt_3BH$ is added to (^{tBu}PPP)$RuCl_2$ in benzene or toluene. The solution turns yellow with the formation of a white precipitate (NaCl). The complex was then isolated by filtration and the removal of solvent. Unlike the previous complex, this (^{tBu}PPP)RuH_3 complex is stable after vacuum, however all attempts to grow a crystal have been unsuccessful. All characterization performed was done via NMR.

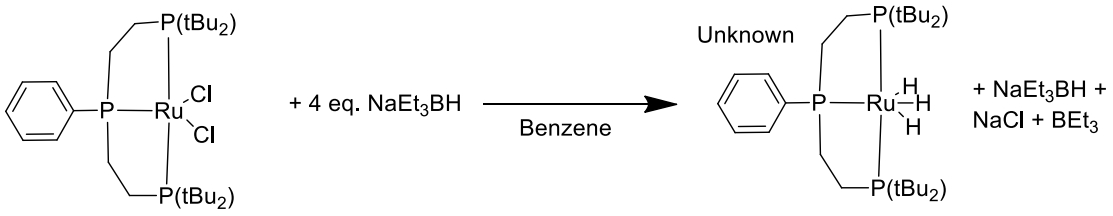

Scheme 3.9: Synthesis of Unknown (^{tBu}PPP)RuH$_3$

Comparison of NMR spectra shows that the central phosphorous atom is the most affected by the new complex. While the previous H_3 anion has peaks at δ 129.59 and 120.06 ppm, this new H_3 complex shows up at δ 127.76 – 126.67 and 101.26. The peak corresponding to the central phosphorous is shifted by almost 20 ppm while the outer phosphorous signals only shift by around 2 ppm. Additionally, all carbon peaks are shifted, however the most affected is the phenyl carbon bonded directly to the central phosphorous. This peak is shifted downfield 9 ppm in the ^{13}C NMR, from 137.38 ppm in the anion to 146.24 ppm in the new complex. Lastly, the ^{1}H NMR signals for this complex are all within 1 ppm of the anion, except for the hydrides. Whereas the anionic complex has three hydrides at -8.78 – -9.22, -10.20 – -10.56, -13.34 this new complex has three hydrides at -10.58, -11.30 – -11.48, and -14.54. The large *J* coupling of 61.7 Hz suggests that the most downfield hydride is located *trans*- to the central phosphorous in both complexes. This suggests that the differences in the two complexes mainly affect the central phosphorous and the hydride *trans*- to that phosphorous.

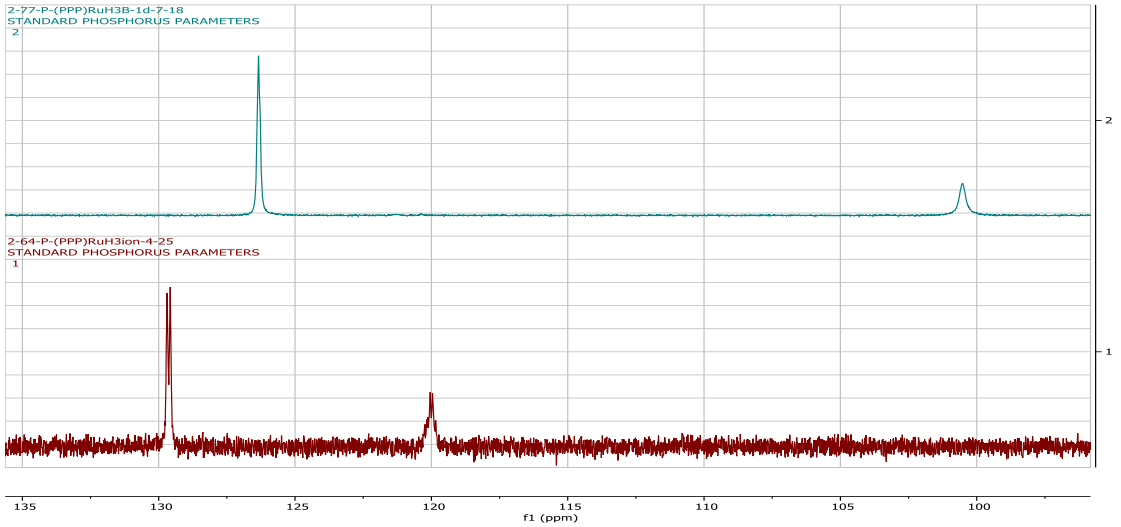

Figure 3.14: ^{31}P NMR Comparison of (^{tBu}PPP)RuH$_3^-$ (Top) and Unknown (^{tBu}PPP)RuH$_3$ (Bottom)

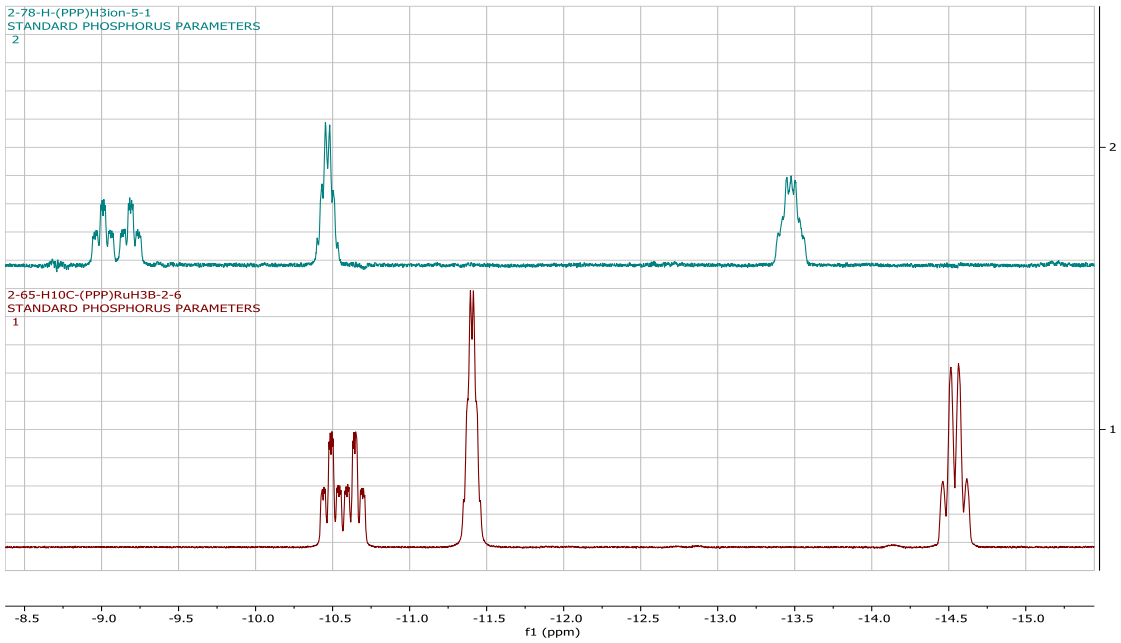

Figure 3.15: ^{1}H NMR Hydride Comparison of (^{tBu}PPP)RuH$_3^-$ (Top) and Unknown (^{tBu}PPP)RuH$_3$ (Bottom)

We have been unable to obtain a crystal structure for this complex, so it is difficult to know exactly what causes such a significant difference in NMR values between the use of THF and benzene as a reaction solvent. In an attempt to figure out the structure a few different tests were performed (Scheme 3.8). The unknown complex could be completely converted to the anionic complex with the addition of THF to the solution. Also, when H_2 is added to either complex, the (^{tBu}PPP)RuH_4 complex is formed (See Section 3.4). Conversely, when $NaEt_3BH$ was added to (^{tBu}PPP)RuH_4 in benzene, the unknown H_3 complex was made. Lastly, in attempt to isolate the structure CO was added to the unknown complex. This resulted in a (^{tBu}PPP)RuH_2CO complex, which was characterized by NMR

.

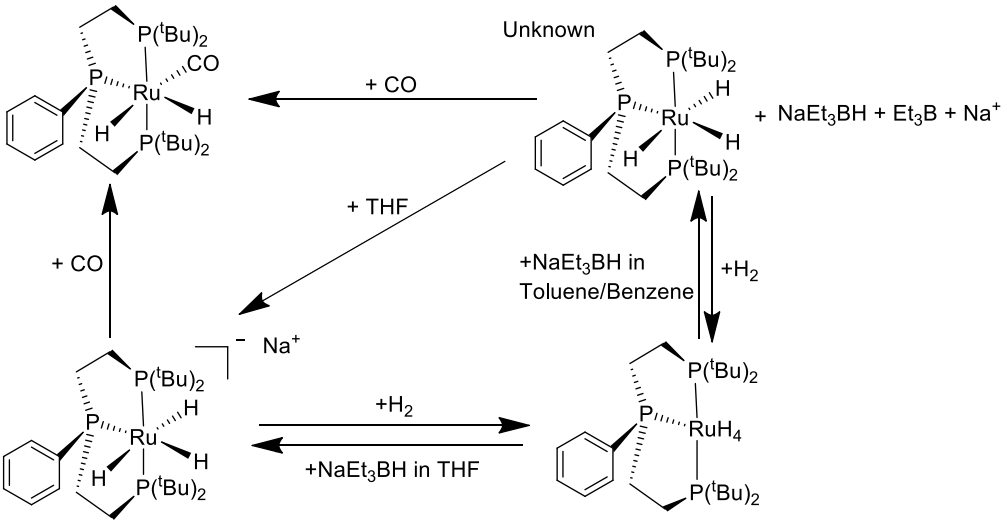

Scheme 3.10: Different Reactions of Unknown (^{tBu}PPP)RuH_3

At this point, our best hypothesis is that the hydrides are bridging between the metal center and another atom. While there are many examples of M-H-B bonds, this is

usually with BH_2L_2 complexes where two hydrides can be bridging. Additionally, there are no examples of $HBEt_3$ complexing to a metal center through a bridging hydride. This leaves us with the Na^+ in solution.

It is possible that the sodium in solution is held in close proximity to the two hydrides through weak bonding interactions. The third hydride is mostly likely the one nearest the phenyl group; the phenyl and t-butyl groups probably have too much steric crowding to allow the sodium to interact. When Field grew crystals of his H_3 anion, he did so in toluene, and found that the crystals were actually dimers that had bridging sodium atoms between two RuH_3 complexes.[29] It is possible that in THF the sodium atoms are able to bind to the THF, drawing them away from the metal, however in the lack of a coordinating solvent, the sodium interacts with the metal-hydrides, which is why we observe a difference in the NMR between THF and benzene/toluene. Additionally, Field showed that with his complex, he was unable to isolate the H_3 anion under a vacuum, however he could grow crystals in benzene or toluene. This could explain why the complex we synthesized in benzene could be isolated under vacuum; the sodium/solvent interactions stabilize the species. At this point, this is our best hypothesis, however a crystal structure would be necessary for confirmation.

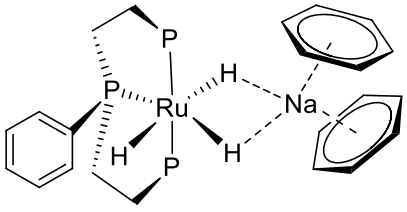

Figure 3.16: Suggested Structure of Unknown (^{tBu}PPP)RuH_3 Complex

3.4 Synthesis and Characterization of (^{tBu}PPP)RuH$_4$ and (^{tBu}PPP)Ru(CH$_2$=CH$_2$):

To perform dehydrogenation, we decided to make the two most common forms of catalyst seen in literature, the tetrahydride and ethylene complexes. First, to make the (^{tBu}PPP)RuH$_4$ complex, we started with (^{tBu}PPP)RuCl$_2$ in benzene and added 4 eq. of NaEt$_3$BH. The solution was then placed under H_2 atmosphere and allowed to stir for 24 hours. A color change to a light yellow was observed along with white precipitate (NaCl). The solution was filtered, however when attempting to isolate the solid via pulling solvent, the complex partially converted to the H_3 species. The H_3 anion was observable in the presence of THF, the unknown H_3 complex was observed in benzene. However, if the mixed products were then dissolved and placed under hydrogen atmosphere, the complexes would convert back to (^{tBu}PPP)RuH$_4$. It was also observed that if no vacuum was applied, but the solution was placed under argon atmosphere instead, the H_4 complex would still convert back to the H_3 species. Later studies showed that the conversion was due to the leftover NaEt$_3$BH and not the lack of H_2 atmosphere.

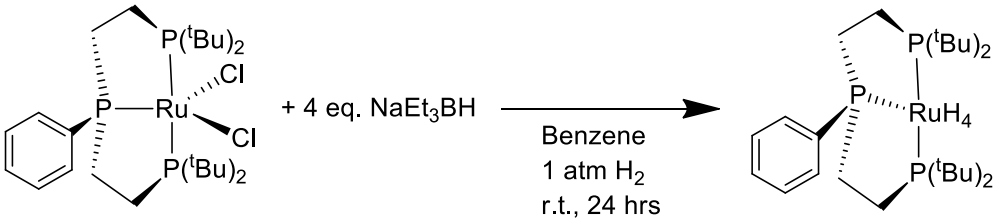

Scheme 3.11: Synthesis of (^{tBu}PPP)RuH$_4$

Characterization of the (^{tBu}PPP)RuH$_4$ complex was accomplished by NMR. Two distinct signals were observed in the ^{31}P NMR at δ 127.58 and 118.09. In addition, a single broad hydride peak was observed in the proton NMR at -8.24 ppm with an integration of four hydrogens.

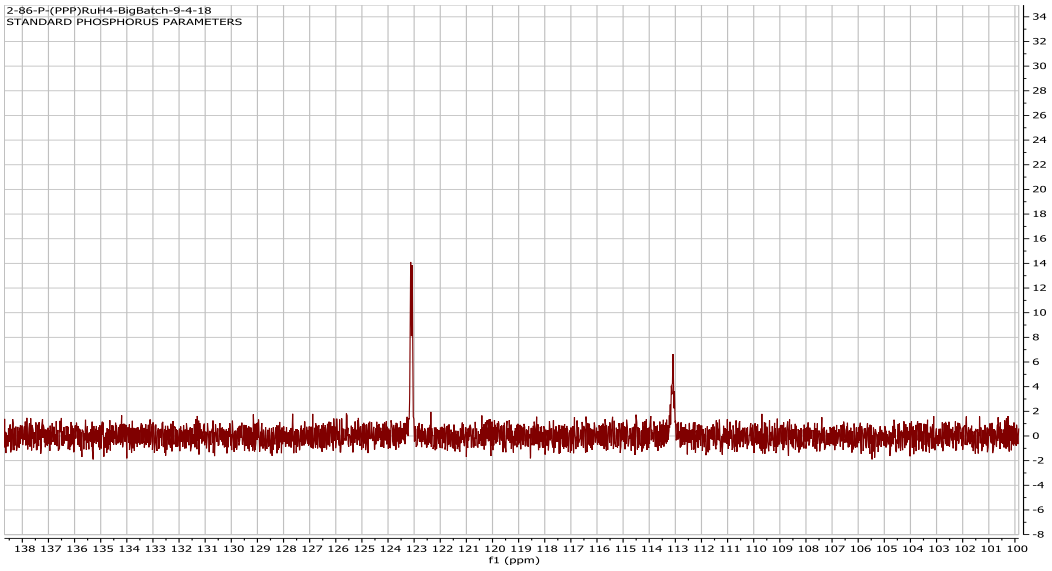

Figure 3.17: ^{31}P NMR of (^{tBu}PPP)RuH$_4$

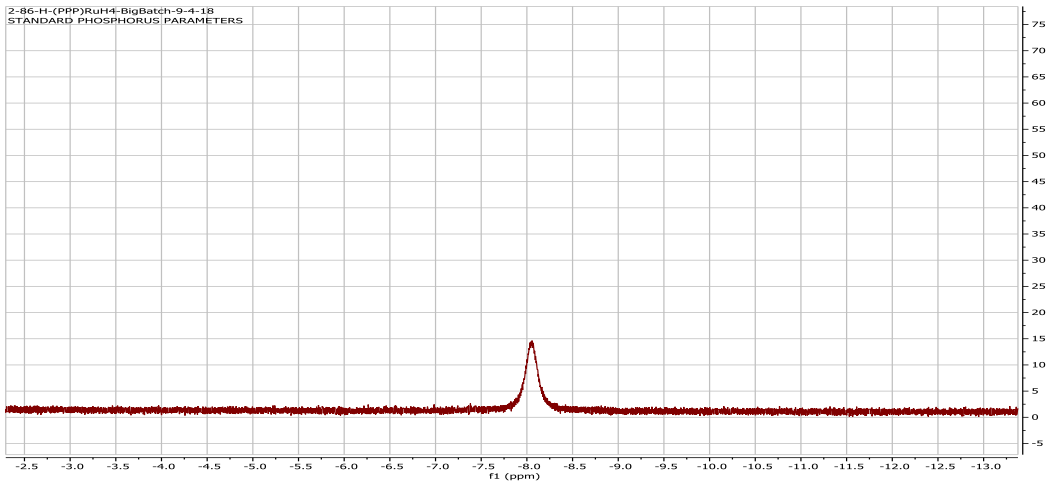

Figure 3.18: Hydride Signal of (^{tBu}PPP)RuH$_4$

Due to the inability to fully isolate the (^{tBu}PPP)RuH_4 complex, and its instability under a lack of H_2 atmosphere, we decided to move on to the ethylene complex for dehydrogenation. The solution of (^{tBu}PPP)RuH_4 complex was placed under ethylene atmosphere and an immediate color change to dark purple occurred. While attempting to isolate the complex, it was observed that it was only stable under a positive ethylene atmosphere. Similar to the (^{tBu}PPP)RuH_4 complex, once under argon atmosphere or after solvent was removed via vacuum, the complex changed into a new unknown. However, when recharged with ethylene, all the unknown complex converted back to (^{tBu}PPP)Ru(CH_2=CH_2). From the ^{1}H NMR we believe that the complex only has a single ethylene coordinated, however due to the inability to isolate the complex it was difficult to get a clean ^{1}H NMR (See Figure 3.38). It is possible that the complex is the bis-ethylene.

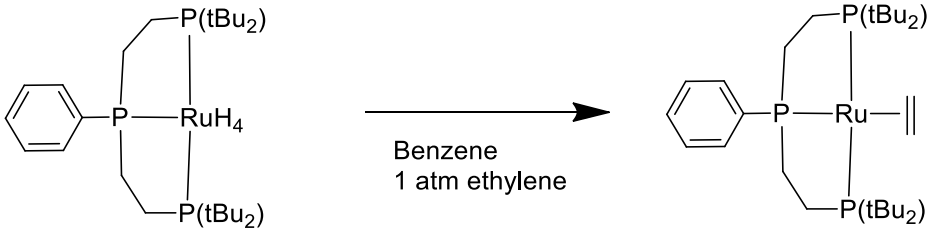

Scheme 3.12: Synthesis of (^{tBu}PPP)Ru(CH_2=CH_2)

To help confirm the structure, a mass spec. of the complex was taken, however the mass spec. showed a parent peak at 555 m/z that corresponds to the 14 e^- (^{tBu}PPP)Ru species. This shows the loss of the ethylene ligand, which does not help structure confirmation.

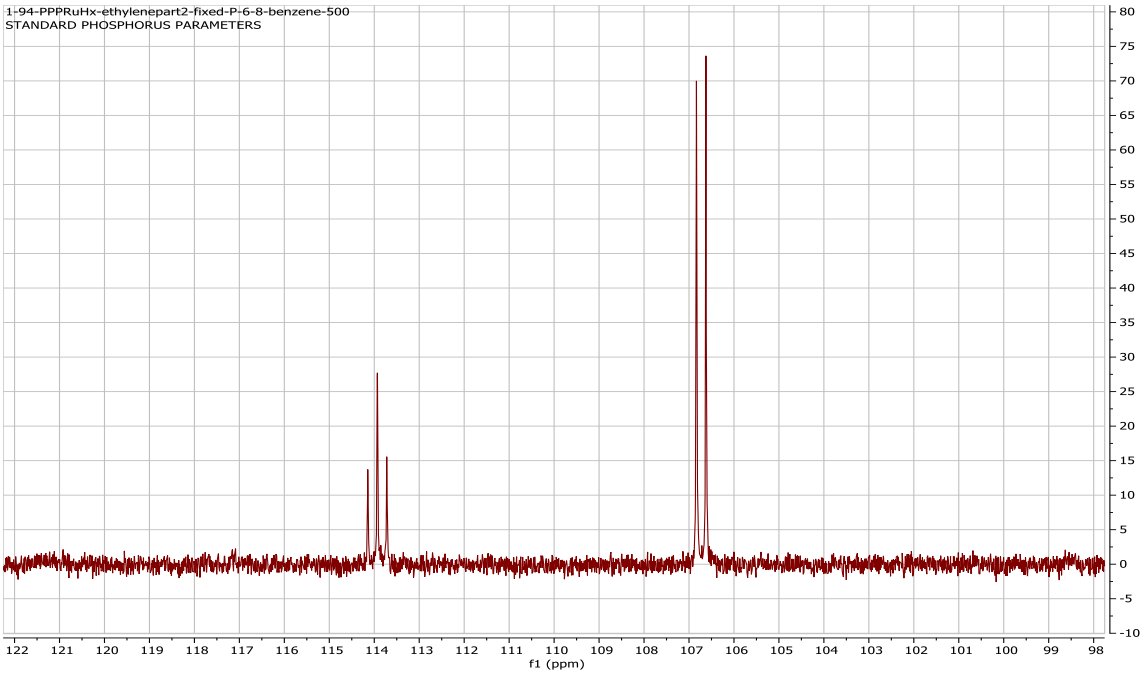

Figure 3.19: ^{31}P NMR of (^{tBu}PPP)Ru(CH_2=CH_2)

3.4.1 Dehydrogenation with Ethylene

With the characterization and identification of the (^{tBu}PPP)Ru complexes, we decided to try alcohol and alkane dehydrogenation to see if they could be used as catalysts. The first attempt was made with the (^{tBu}PPP)Ru(CH_2=CH_2) complex. Since this complex was only stable under ethylene atmosphere, we decided to use ethylene as the acceptor while attempting to dehydrogenate cyclooctane. NMR showed that the (^{tBu}PPP)Ru(CH_2=CH_2) reacted to form numerous products, however no cyclooctene was observed. It is possible that, as previously seen, the trace amounts of $NaEt_3BH$ left in solution inhibited the reaction by reacting with the metal center. Due to this we decided to go back and attempt synthesis without the use of $NaEt_3BH$.

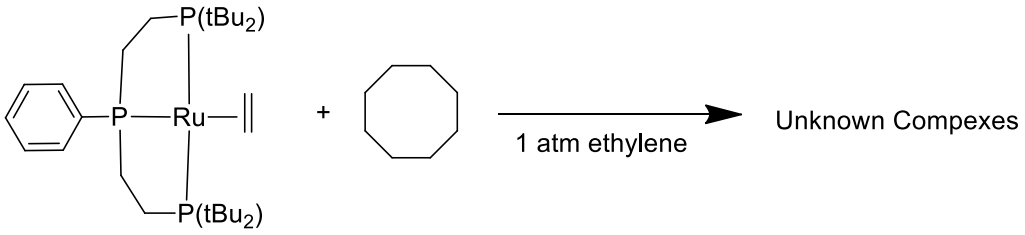

Scheme 3.13: Attempted COA Dehydrogenation using (^{tBu}PPP)Ru(CH_2=CH_2)

3.4.2 (^{tBu}PPP)RuH_4 without $NaEt_3BH$

Since it seemed that the presence of $NaEt_3BH$ causes the (^{tBu}PPP)RuH_4 to convert back to the H_3 complex in the absence of H_2 atmosphere and possibly inhibits catalysis of the (^{tBu}PPP)Ru(CH_2=CH_2) complex, we developed a new synthetic route for (^{tBu}PPP)RuH_4 without any borohydride containing reducing agent.

Work on a different pincer-Ru catalyst in our lab showed that using KtBuO and isopropanol, the Ru-Cl_2 complex could be converted to the H_4. As mentioned previously, doing this in the absence of H_2 atmosphere leads to the (^{tBu}PPP)RuHCl complex, however under H_2 atmosphere the reaction will go forward to produce the (^{tBu}PPP)RuH_4 species within 20 minutes. Unlike the reaction with $NaBEt_3H$, when solvent was removed via vacuum, the complex did not change. The (^{tBu}PPP)RuH_4 was then washed with hexane and isolated for use in catalysis. The NMR matched that of the (^{tBu}PPP)RuH_4 complex made via $NaEt_3BH$. This synthesis provided us with a method to obtain (^{tBu}PPP)RuH_4 without $NaEt_3BH$ and showed us that the (^{tBu}PPP)RuH_4 complex is in fact stable without H_2 atmosphere. This confirms the cause of the previous conversion back to the H_3 complex was the leftover $NaEt_3BH$ in solution.

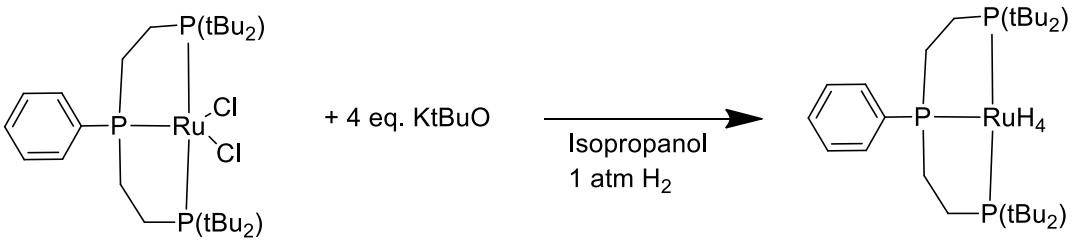

Scheme 3.14: Synthesis of (^{tBu}PPP)RuH$_4$ using KtBuO and Isopropanol

3.4.3 Dehydrogenation using (^{tBu}PPP)RuH$_4$

With the new synthetic route, we were able to obtain clean and pure (^{tBu}PPP)RuH$_4$. In addition, we found that the reaction could be run on a gram scale and the solid catalyst was stable up to one month in the glovebox. Due to this we decided to reattempt dehydrogenation with the (^{tBu}PPP)RuH$_4$ catalyst. The first reaction we attempted was the transfer dehydrogenation of isopropanol to *tert*-butyl ethylene (TBE). For this reaction (^{tBu}PPP)RuH$_4$ catalyst was dissolved in isopropanol, causing the solution to turn yellow. To this solution, 27.6 eq of TBE were added. The reaction was heated at 100^{o}C for 2 hours. After 2 hours, the NMR shows complete conversion of the TBE to TBA. When the reaction was performed at 40^{o}C the reaction was significantly slower, only showing 50% completion after 22 hours.

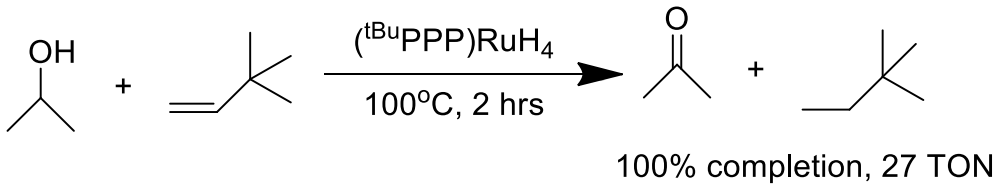

Scheme 3.15: Transfer Alcohol Dehydrogenation using (^{tBu}PPP)RuH$_4$

Currently, the large majority of reports using a L_3 pincer-ruthenium catalyst for alcohol transfer dehydrogenation use catalysts that have noninnocent pincer ligands that assist in hydride transfer or go through an active 16 e^- (Pincer)Ru(L) species. We believe that unlike the previously reported pincer-ruthenium catalysts, the (^{tBu}PPP)RuH_4 catalyst follows a mechanism very similar to (PCP)Ir. However, mechanistic studies need to be performed in order to confirm this hypothesis.

Since the (^{tBu}PPP)RuH_4 catalyst showed it could perform the dehydrogenation of an alcohol, we moved on to attempt alkane dehydrogenation. For this reaction we dissolved (^{tBu}PPP)RuH_4 catalyst in cyclooctane, turning the solution dark orange/red. To this 24 eq. of TBE were added. This reaction was run at 100^{o}C for 2 hours. After two hours 8 turnovers of TBE to TBA could be observed by NMR. Further heating of this solution did not result in any additional turnovers. In the ^{31}P NMR, one major species could be observed suggesting that the reaction forms a complex that inhibits further activity. It is possible that as the amount of cyclooctene increases, the 14 e^- (PPP)Ru intermediate reacts with cyclooctene to form a stable allyl complex that inhibits reactivity.

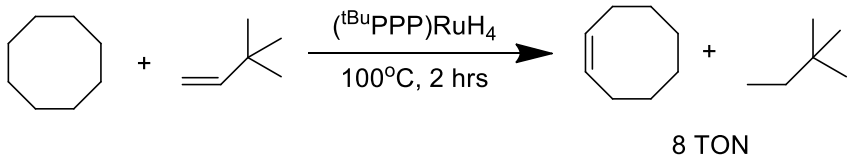

Scheme 3.16: COA Dehydrogenation with (^{tBu}PPP)RuH_4

When the reaction was attempted at 130°C the catalyst completely decomposed after 2 turnovers of TBE to TBA. More in-depth studies are necessary fully understand the

reactivity of the (^{tBu}PPP)RuH_4 catalyst and find optimal conditions to perform catalysis without decomposition. However, these preliminary results show that the (^{tBu}PPP)RuH_4 complex can successfully catalyze dehydrogenation of both alcohols and alkanes. Additionally, this is the first example of an L_3Pincer-Ru catalyst successfully performing alkane dehydrogenation.

3.5: Summary

A series of (^{tBu}PPP)Ru complexes were synthesized and characterized. Overall the synthesis and reactivity of the complexes are extremely facile and quick. With few exceptions, each synthesis could be performed within one hour at room temperature and resulted in 100% conversion to a new product. It was found that when $NaEt_3BH$ was used in synthesis, the $NaEt_3BH$ could react differently depending on solvent conditions. Additionally, the presence of any $NaEt_3BH$ in subsequent reactions caused the metal to preferably react with the leftover $NaEt_3BH$, causing the (^{tBu}PPP)RuH_4 and (^{tBu}PPP)$Ru(C_2H_4)_2$ complexes to be unstable unless under their corresponding atmospheres. However, a new synthetic route was developed that avoided the use of borohydrides resulting in a stable (^{tBu}PPP)RuH_4 catalyst. This catalyst was then screened for dehydrogenation and it was found that it could successfully perform alcohol and alkane dehydrogenation. Further studies are necessary to test the true scope of catalysis and find ideal reaction conditions. However, this is the first report of a pincer (PPP)Ru catalyst successfully dehydrogenating both alcohols and alkanes.

3.6: Experimental

General Methods. All pincer-metal manipulations were carried out under argon using standard glovebox and Schlenk techniques.

Anhydrous solvents were purchased from Sigma-Aldrich and degassed by purging with argon. All solvents were stored over 3 Å molecular sieves in the glovebox. THF was distilled prior to use to ensure dryness. Deuterated solvents were degassed via freeze-pump-thaw cycles, dried over activated Al_2O_3, and stored over 3 Å molecular sieves prior to use. (^{tBu}PPP)$RuCl_2$ was prepared according to literature methods.[28] Unless noted above, all other reagents were purchased commercially and used as received.

All ^{1}H and ^{31}P NMR spectra were recorded on 400 MHz and 500 MHz Varian spectrometers. Chemical shifts are reported in ppm. The ^{1}H NMR[‡] signals are referenced to the residual solvent signals, and the ^{31}P NMR signals are referenced to an external standard of $P(CH_3)_3$.

Laser desorption ionization mass spectrometry (LDI-MS) was carried out on an UltraflexIIIT^M time of flight (TOF-TOF) mass spectrometer (Bruker Daltonics, Inc., Billerica, MA, USA). Samples were irradiated with photons from a 355 nm Nd:YAG laser operating in the Smartbeam configuration with several 100 Hz shots in a random sample spot analysis. Bruker FlexControl was used to analyze all samples and all spectra were

[‡] In all the ^{1}H NMR reported here, it can be observed that not all the methylene peaks could be found. Each methylene peak is split multiple times so these peaks are often very broad. Additionally, these peaks can overlap with solvent and/or *tert*-butyl peaks. Any methylene peaks easily identified are reported.

processed offline using Bruker FlexAnalysis. All samples were diluted in toluene or benzene and 1-mL deposited on etched stainless-steel Bruker target plates.

Synthesis of (^{tBu}PPP)RuHCl using $NaEt_3BH$:

52 mg of (^{tBu}PPP)$RuCl_2$ was mixed with 1 eq. of $NaEt_3BH$ in 0.5 mL of benzene-d_6. An immediate change to orange was observed. Solvent was removed, and an orange solid was isolated. ^{31}P NMR (162 MHz, Benzene-d_6) δ 120.08 – 118.96 (m), 80.57 (d, *J* = 20.4 Hz). ^{1}H NMR (400 MHz, Benzene-d_6) δ 7.73 (t, *J* = 9.6 Hz, C**H**, 2H), 7.05 (t, *J* = 7.3 Hz, C**H**, 2H), 7.00 (d, *J* = 7.2 Hz, C**H**, 1H), 2.37 – 2.17 (m, C$\mathbf{H}_2$, 2H), 1.85 (m, C$\mathbf{H}_2$, 2H), 1.59 (dddd, *J* = 15.1, 12.9, 6.0, 3.9 Hz, C$\mathbf{H}_2$, 2H), 1.40 – 1.34 (m, C$\mathbf{H}_2$, 2H), 1.25-1.19 (m, C(C$\mathbf{H}_3$)$_3$, 36H), -28.91 (dt, *J* = 35.9, 17.9 Hz, Ru**H**, 1H).

Synthesis of (^{tBu}PPP)RuHCl using KtBuO and isopropanol:

46 mg of (PPP)$RuCl_2$ was mixed with 32.6 mg KtBuO in 0.5 mL isopropanol. After the starting material fully dissolved the solution changed from yellow to bright orange. The NMR tube was stirred overnight. Several species were observable by NMR so the reaction was heated at 85°C for 24 hours. One species was observable by ^{31}P NMR. ^{31}P NMR (202 MHz, Isopropanol) δ 121.07 – 118.27 (m), 89.38 – 83.23 (m). ^{1}H NMR (500 MHz, Isopropanol) δ -30.20 – -32.24 (m, Ru**H**, 1H).

Synthesis using $LiBH_4$:

A suspension of 20mg (^{tBu}PPP)$RuCl_2$ and 5.65 mg $LiBH_4$ was made in 0.5 mL of benzene or THF.

For benzene, (^{tBu}PPP)RuHCl Product: The reaction was stirred for 5 days. Two isomers were observable by NMR. The reaction was heated for 5 days and then cooled to room temperature. Purple crystals crashed out of solution. The crystal structure showed that the complex was (^{tBu}PPP)RuHCl (75%). ^{31}P NMR (162 MHz, Benzene-d_6) δ 117.93 (s), 85.33 (d, *J* = 17.3 Hz). ^{1}H NMR (400 MHz, Benzene-d_6) δ 7.70 (t, *J* = 8.5 Hz, C**H**, 2H), 7.26 – 7.15 (m, C**H**, 3H), 2.52 (s, C**H**$_2$, 2-6H), 1.98 – 1.74 (m, C**H**$_2$, 2H), 1.43 (overlapping triplets, *J* = 12.1, 6.4 Hz, C(C**H**$_3$)$_3$, 36H), -29.41 (dt, *J* = 45.9, 19.8 Hz, Ru**H**, 1H).

For THF, (^{tBu}PPP)Ru(H)(BH_4) Product: The reaction was stirred for 20 min. One product was observable by NMR. Due to proteo-solvent we were unable to specify the non-bridging protons on the BH_4. ^{31}P NMR (162 MHz, THF) δ 124.58 – 122.46 (m), 102.12 (dd, *J* = 14.4, 3.6 Hz). ^{1}H NMR (400 MHz, THF) δ 7.96 – 7.82 (m, C**H**, 2H), 7.38 (d, *J* = 4.5 Hz, C**H**, 3H), 1.41 (t, *J* = 6.0 Hz, C(C**H**$_3$)$_3$, 18H), 1.34 (t, *J* = 5.9 Hz, C(C**H**$_3$)$_3$, 19H), -6.46 (s, Ru**H**, 2H), -19.31 (dt, *J* = 38.4, 19.1 Hz, Ru**H**, 1H).

Synthesis of (^{tBu}PPP)RuH_4 using $NaEt_3BH$:

50 mg of (PPP)$RuCl_2$ was mixed with 3 eq. of $NaEt_3BH$ in 0.5 mL of benzene-d6. The reaction was stirred under hydrogen atmosphere for 48 hours. One species was observable by NMR. Attempts to pull vacuum resulted in the complex changing to the (PPP)RuH_3 complex. ^{31}P NMR (162 MHz, Benzene-d_6) δ 127.58 (d, *J* = 9.5 Hz), 118.09 (t, *J*

= 9.6 Hz). ^{1}H NMR (400 MHz, Benzene-d_6) δ 7.79 (tt, *J* = 7.9, 1.6 Hz, C**H**, 2H), 7.20 (t, *J* = 7.1 Hz, C**H**, 1H), 7.14 (d, *J* = 7.2 Hz, C**H**, 1H), 2.33 (dddtd, *J* = 21.6, 11.8, 8.7, 6.5, 5.9, 3.2 Hz, C**H**$_2$, 2H), 1.86 (dddt, *J* = 46.3, 13.5, 6.4, 3.1 Hz, C**H**$_2$, 2H), 1.69 – 1.57 (m, C**H**$_2$, 2H), 1.30 (t, *J* = 5.8 Hz, C(C**H**$_3$)$_3$, 18H), 1.02 (t, *J* = 5.8 Hz, C(C**H**$_3$)$_3$, 18H), -8.24 (s, Ru**H**, 4H).

Synthesis of (^{tBu}PPP)RuH$_4$ using KtBuO and isopropanol:

36 mg of (PPP)RuCl$_2$ was mixed with 30 mg of KtBuO in 0.5 mL THF. H_2 was bubbled through the solution and a color change yellow was observed after a few minutes. The reaction was stirred for 20 minutes. Solvent was removed, and the residue was washed with hexane. The mixture was filtered via cannula and the solvent was removed to produce a yellow/orange solid. NMR DATA: ^{31}P NMR (162 MHz, Benzene-d_6) δ 128.02 (d, *J* = 9.6 Hz), 118.01 (t, *J* = 9.9 Hz). ^{1}H NMR (400 MHz, Benzene-d_6) δ 7.80 (t, *J* = 8.4 Hz, C**H**, 2H), 7.17 (t, *J* = 7.8 Hz, C**H**, 2H), 7.09 (d, *J* = 7.6 Hz, C**H**, 1H), 2.41 – 2.20 (m, C**H**$_2$, 2H), 1.92 – 1.72 (m, C**H**$_2$, 2H), 1.50 – 1.31 (m, C**H**$_2$, 4H), 1.32 (t, *J* =6.1 Hz, C(C**H**$_3$)$_3$ 18H), 1.031 (t, *J* = 6.1 Hz, C(C**H**$_3$)$_3$, 18H), -8.24 (s, Ru**H**, 4H).

Synthesis of Unknown (^{tBu}PPP)RuH$_3$:

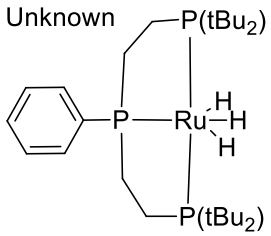

48.1 mg of (PPP)RuCl$_2$ was mixed with 4 eq. of NaEt$_3$BH in 0.5 mL of benzene-d6 in a J-Young NMR tube. Solution immediately turned yellow. Solvent was pulled by vacuum to afford a yellow solid. NMR DATA: ^{31}P NMR (202 MHz, Benzene-*d*$_6$) δ 127.76 – 126.67 (bs), 101.26 (bs). ^{1}H NMR (400 MHz, Benzene-*d*$_6$) δ 7.26 – 7.22 (m, C**H**, 2H), 6.97 – 6.92 (m, C**H**, 2H), 6.90 (d, *J* = 7.1 Hz, C**H**, 1H), 2.27 (dtt, *J* = 27.2, 14.3, 6.6 Hz, C**H**$_2$, 2H), 2.10 – 1.80 (m, C**H**, 2H), 1.18 – 1.10 (m, C(C**H**$_3$)$_3$, 18H), 1.02 – 0.97 (m, C(C**H**$_3$)$_3$, 18H), -10.58 (dtdd, *J* = 61.7, 20.5, 7.7, 3.6 Hz, Ru**H**, 1H), -11.30 – -11.48 (m, Ru**H**, 1H), -14.54 (dtd, *J* = 21.2, 20.8, 2.4 Hz, Ru**H**, 1H). ^{13}C NMR (126 MHz, Benzene-*d*$_6$) δ 137.38 (**C**-P), 128.86 (**C**H), 128.07 (**C**H), 125.21 (**C**H), 35.80 – 34.59 (m, **C**H$_2$), 31.59 (**C**(CH$_3$)$_3$), 30.42 (C(**C**H$_3$)$_3$), 30.33 (C(**C**H$_3$)$_3$), 28.02 (**C**H$_2$).

Synthesis of (^{tBu}PPP)RuH$_3^-$ using NaEt$_3$BH:

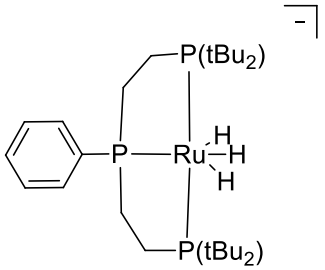

55 mg of (PPP)$RuCl_2$ was mixed with 20 eq. of $NaEt_3BH$ in 0.5 mL of THF in a J-Young NMR tube. Solution was stirred for 24 hours. Crude NMR shows one product. All attempts to isolate resulted in decomposition. NMR DATA: ^{31}P NMR (162 MHz, Benzene-d_6) δ 129.59 (d, *J* = 19.1 Hz), 120.06 (bs). ^{1}H NMR (400 MHz, Toluene-d_8) δ 8.37 – 8.28 (m, C**H**, 2H), 7.30 – 7.24 (m, C**H**, 2H), 7.23 – 7.19 (m, C**H**, 1H), 2.57 (q, *J* = 13.7, 11.7, C$\mathbf{H}_2$, Hz, 2H), 2.24 – 2.01 (m, C$\mathbf{H}_2$, 2H), 1.96 (m, C$\mathbf{H}_2$, 2H), 1.51 (t, *J* = 5.5 Hz, C(C$\mathbf{H}_3$)$_3$, 18H), 1.32 (t, *J* = 5.3 Hz, C(C$\mathbf{H}_3$)$_3$, 19H), -8.78 – -9.22 (m, Ru**H**, 1H), -10.20 – -10.56 (m, Ru**H**, 1H), -13.34 (dtd, *J* = 25.0, 14.1, 11.9 Hz, Ru**H**, 1H). ^{13}C NMR (126 MHz, Benzene-d_6) δ 146.24 (**C-**P), 139.15 (d, *J* = 14.4 Hz, **C**H), 132.24 (**C**H), 131.23 (**C**H), 39.89 (d, *J* = 24.2 Hz, **C**H_2), 37.68 (**C**$(CH_3)_3$), 36.17 – 35.79 (m, C(**C**H_3)$_3$), 35.48 (C(**C**H_3)$_3$), 31.26 (d, *J* = 27.2 Hz, **C**H_2).

Synthesis of (^{tBu}PPP)Ru(CH_2=CH_2):

52 mg of (PPP)$RuCl_2$ was mixed with 3 eq. of $NaEt_3BH$ in 0.5 mL of benzene-d_6 in a J-Young NMR tube. The reaction was stirred under hydrogen atmosphere for 48 hours. The atmosphere was then replaced with ethylene. Upon thawing the solution immediately turned dark purple. ^{31}P NMR (202 MHz, Benzene-d_6) δ 113.92 (t, *J* = 42.7 Hz), 106.72 (d, *J* = 42.8 Hz). ^{1}H NMR (500 MHz, Benznene-d_6) δ 7.45 (ddt, *J* = 9.7, 6.4, 1.6 Hz, C**H**, 2H), 6.91 – 6.84 (m, C**H**, 2H), 6.83 (s, C**H**, 1H), 2.96 – 2.89 (m, C$\mathbf{H}_2$=C$\mathbf{H}_2$, 3H), 2.13 (ddq, *J* = 20.4, 13.5, 6.9 Hz, C$\mathbf{H}_2$, 2H), 1.81 (h, *J* = 7.4 Hz, C$\mathbf{H}_2$, 3H), 1.61 – 1.39 (m, C$\mathbf{H}_2$, 3H), 1.38 – 1.25 (m, C$\mathbf{H}_2$, 2H), 1.15 – 1.11 (m, C(C$\mathbf{H}_3$)$_3$, 18H), 0.80 (dq, *J* = 7.8, 3.5 Hz, C(C$\mathbf{H}_3$)$_3$, 18H). MS (m/z): 555.0 (M^{++}).

Attempted dehydrogenation using (^{tBu}PPP)Ru(CH_2=CH_2):

Inside the glovebox, a mixture was made of 20 mM (^{tBu}PPP)Ru(CH=CH_2) in 0.5 mL of cyclooctane in a J-Young NMR tube. The NMR tube was placed under ethylene atmosphere and then heated for 1 hr. at 85°C. NMR showed no production of cyclooctane.

Synthesis of (^{tBu}PPP)RuH_2CO:

51.8 mg of (PPP)RuCl_2 was mixed with 4 eq. of NaEt_3BH in 0.5 mL of benzene-d_6 in a J-Young NMR tube. The solution immediately turned yellow. The atmosphere was replaced with CO and stirred overnight. Crude NMR Data shows one complex. NMR DATA: ^{31}P NMR (162 MHz, Benzene-d_6) δ 121.19 (d, *J* = 4.1 Hz), 100.37 (d, *J* = 10.6 Hz). ^{1}H NMR (400 MHz, Benzene-d_6) δ 7.44 (ddd, *J* = 9.3, 8.0, 1.4 Hz, C**H**, 2H), 7.01 (td, *J* = 7.6, 1.3 Hz, C**H**, 2H), 6.88 – 6.85 (m, C**H**, 1H), 1.77 (ddddd, *J* = 18.2, 9.1, 6.7, 4.5, 2.5 Hz, C**H**$_2$, 2H), 1.39 – 1.21 (m, C**H**$_2$, 2H), 1.00 – 0.95 (m, C(C**H**$_3$)$_3$, 23H), 0.93 – 0.88 (m, C(C**H**$_3$)$_3$, 18H), -8.13 (dd, *J* = 80.7, 1.6 Hz, Ru**H**, 1H), -10.94 (d, *J* = 24.6 Hz, Ru**H**, 1H).

General Procedure for Dehydrogenation:

Inside the glovebox, a mixture was made of 20 mM (^{tBu}PPP)RuH_4 and 440 mM TBE in 0.5 mL of isopropanol or cyclooctane in a J-Young NMR tube. The reaction was then heated. At designated times the NMR tube was cooled to room temperature and checked by ^{1}H NMR. The TON were calculated using the ratio of TBE to TBA in the NMR.

3.7: NMR

(^{tBu}PPP)RuHCl using $NaEt_3BH$:

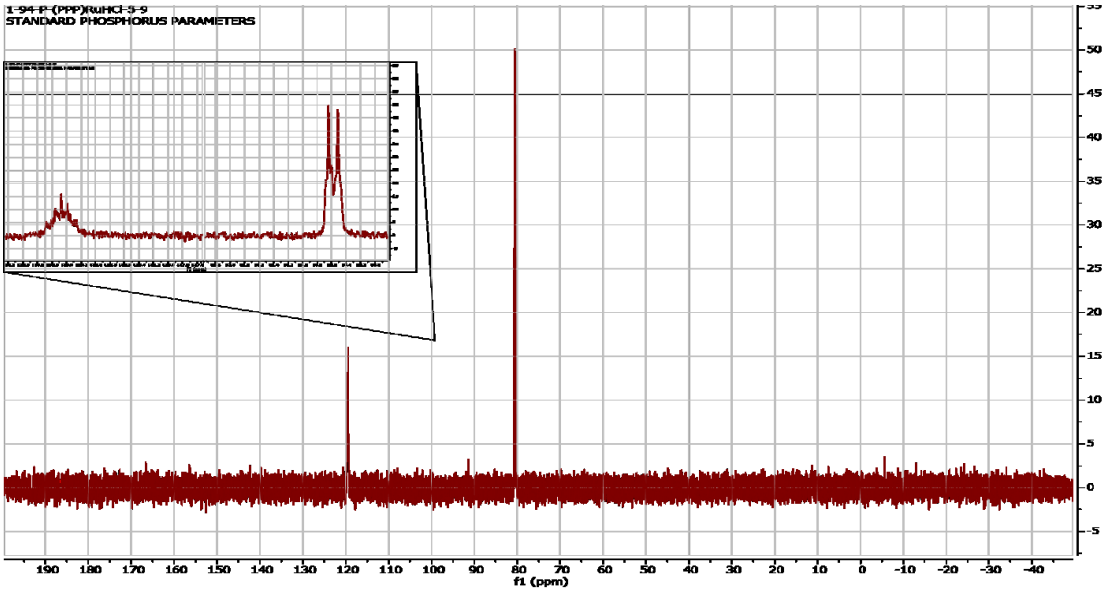

Figure 3.20: ^{31}P NMR of (^{tBu}PPP)RuHCl

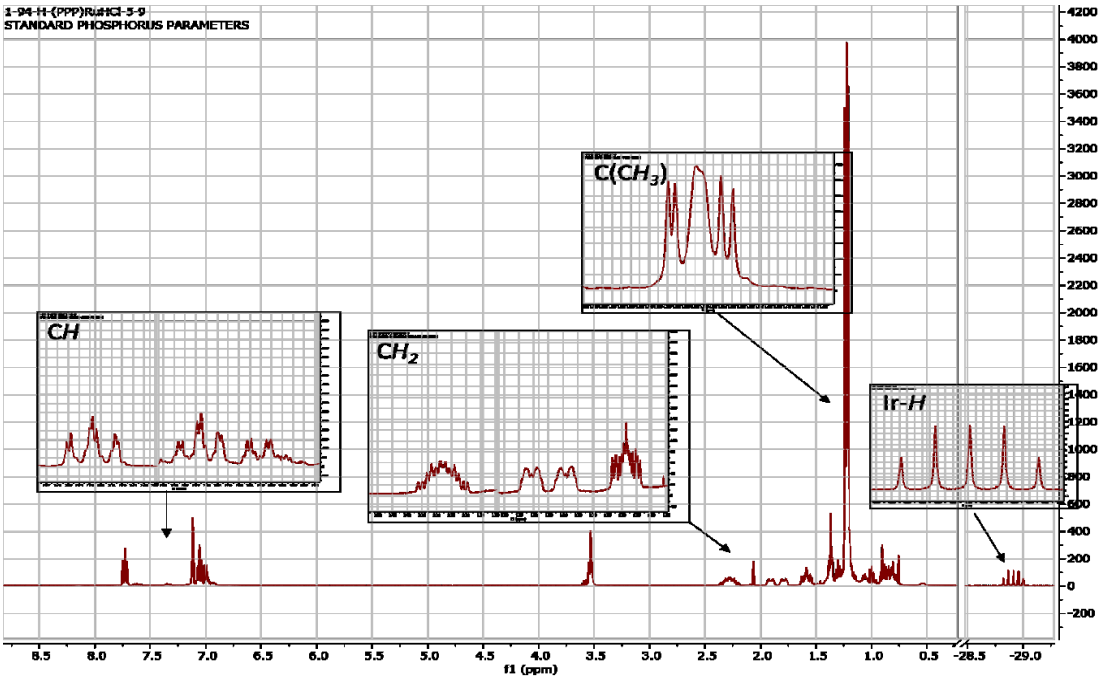

Figure 3.21: ^{1}H NMR of (^{tBu}PPP)RuHCl

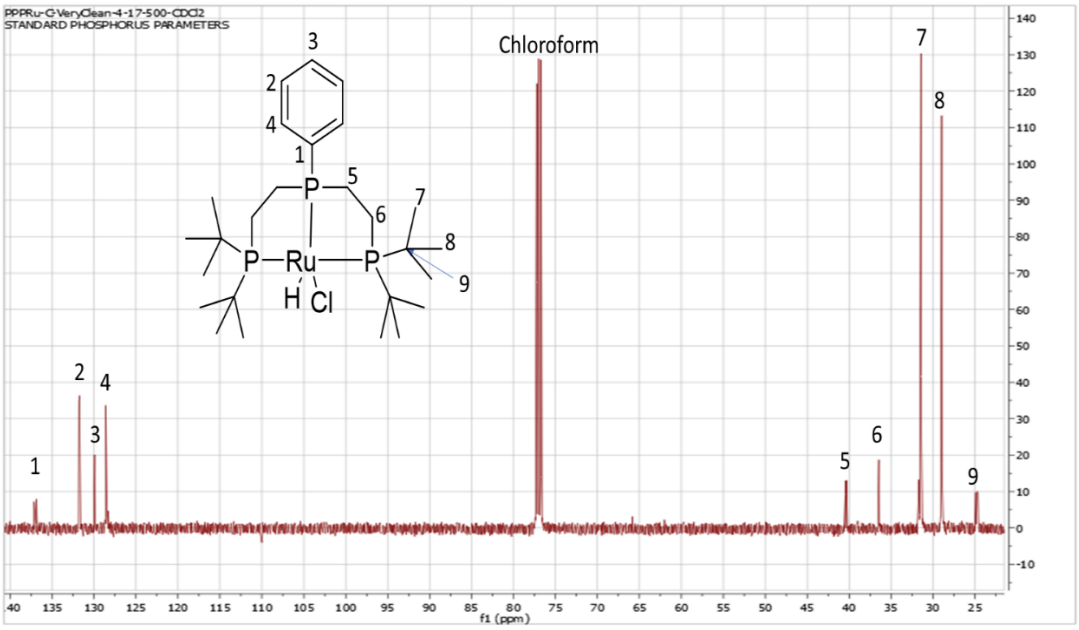

Figure 3.22: ^{13}C NMR of (^{tBu}PPP)RuHCl

(^{tBu}PPP)RuHCl using KtBuO and isopropanol:

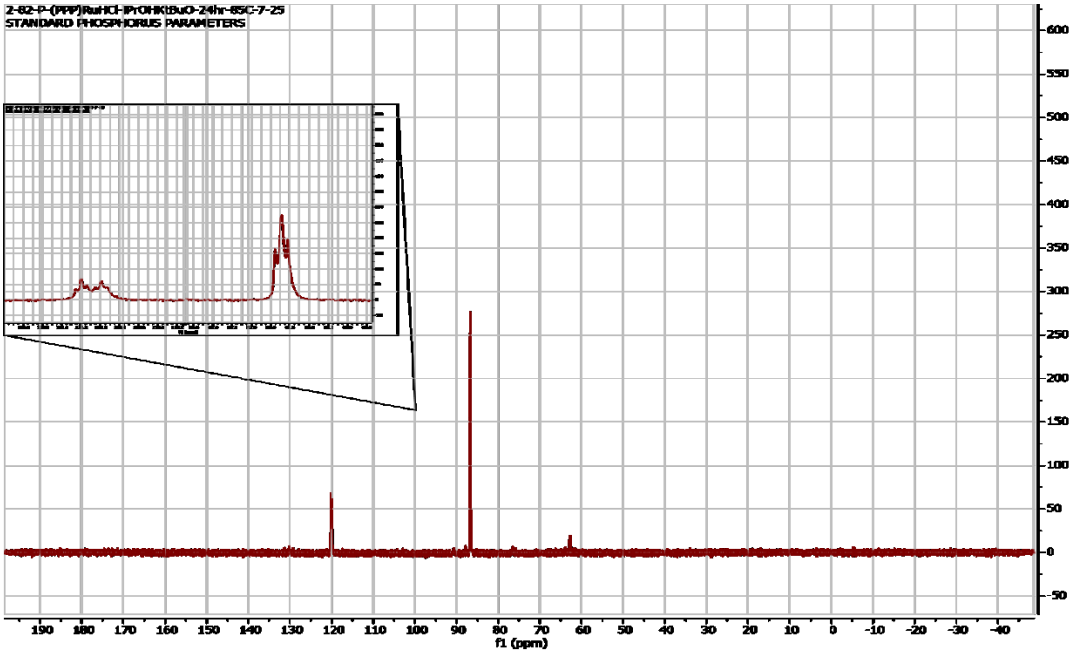

Figure 3.23: ^{31}P NMR of (^{tBu}PPP)RuHCl #2

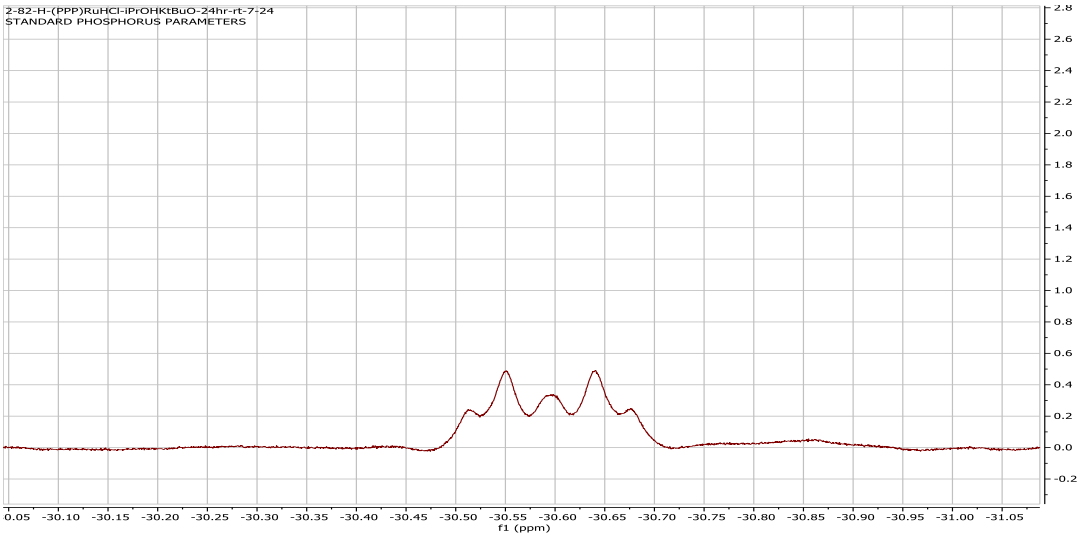

Figure 3.24: ^{1}H NMR of (^{tBu}PPP)RuHCl #2 Hydride[§]

[§] This reaction was run in proteo-solvent, so other ^{1}H NMR signals could not be distinguished

(^{tBu}PPP)RuHCl using $LiBH_4$:

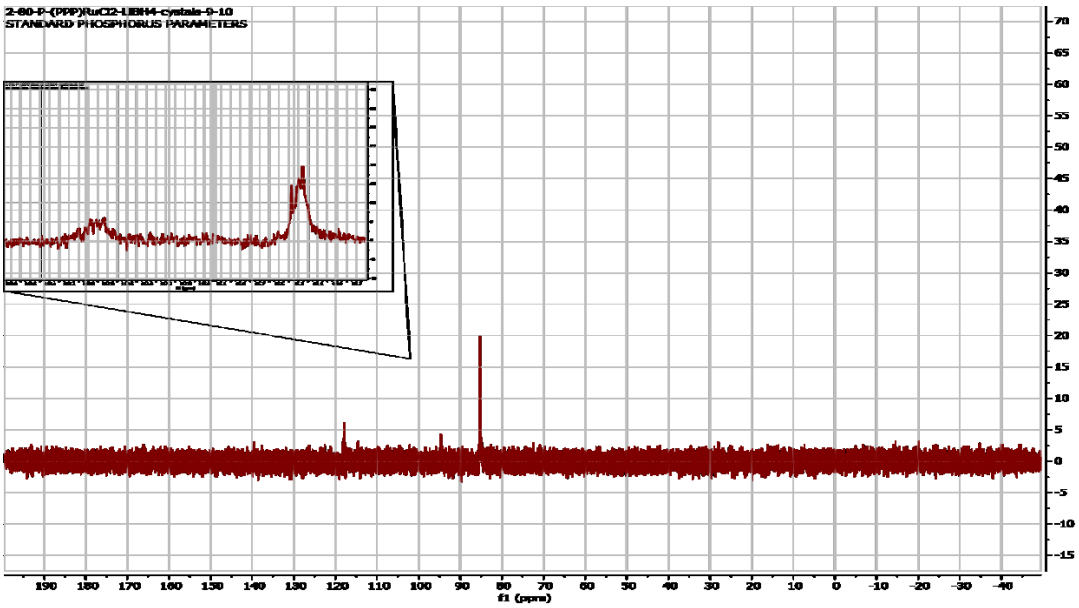

Figure 3.25: ^{31}P NMR of (^{tBu}PPP)RuHCl #3

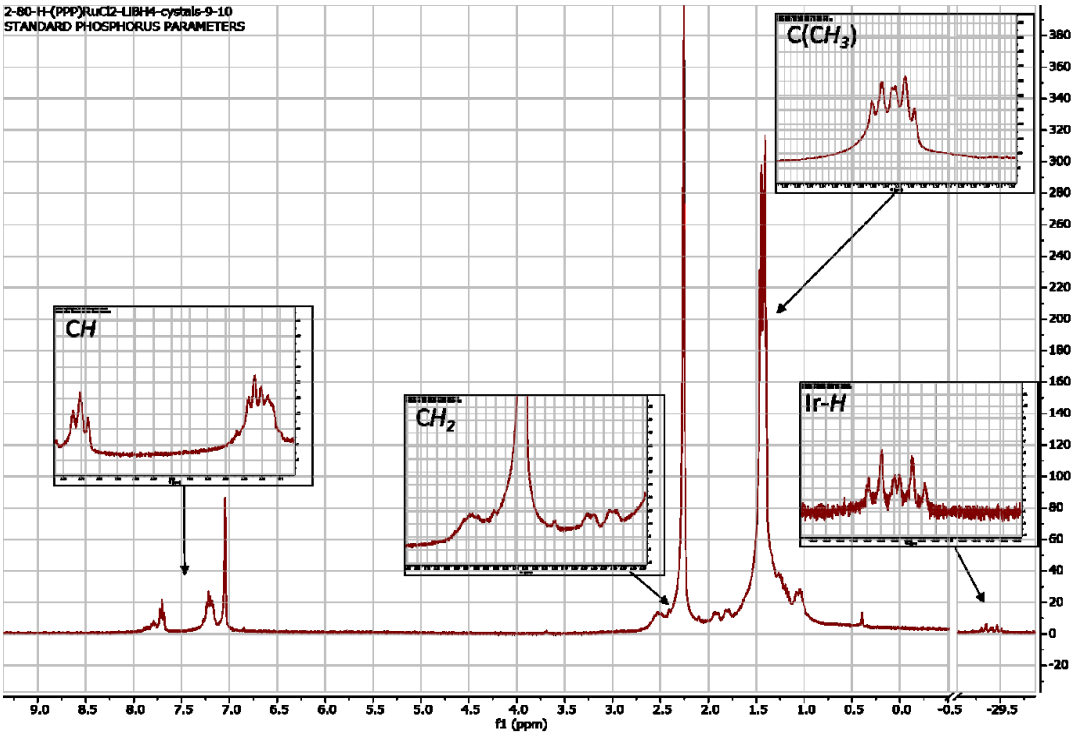

Figure 3.26: ^{1}H NMR of (^{tBu}PPP)RuHCl #3

(^{tBu}PPP)RuH$_3^-$

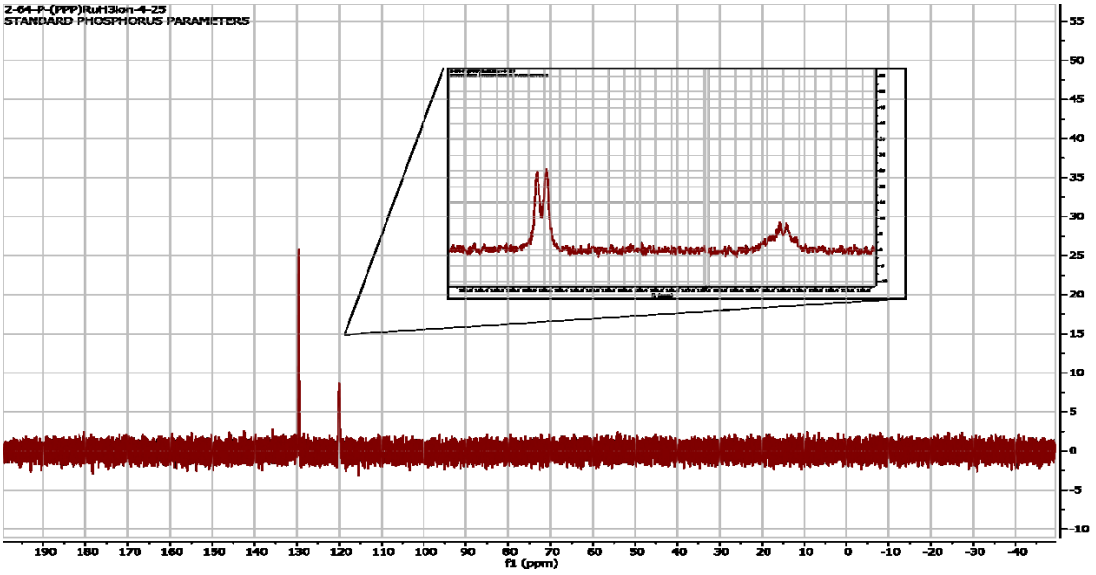

Figure 3.27: ^{31}P NMR of (^{tBu}PPP)RuH$_3^-$

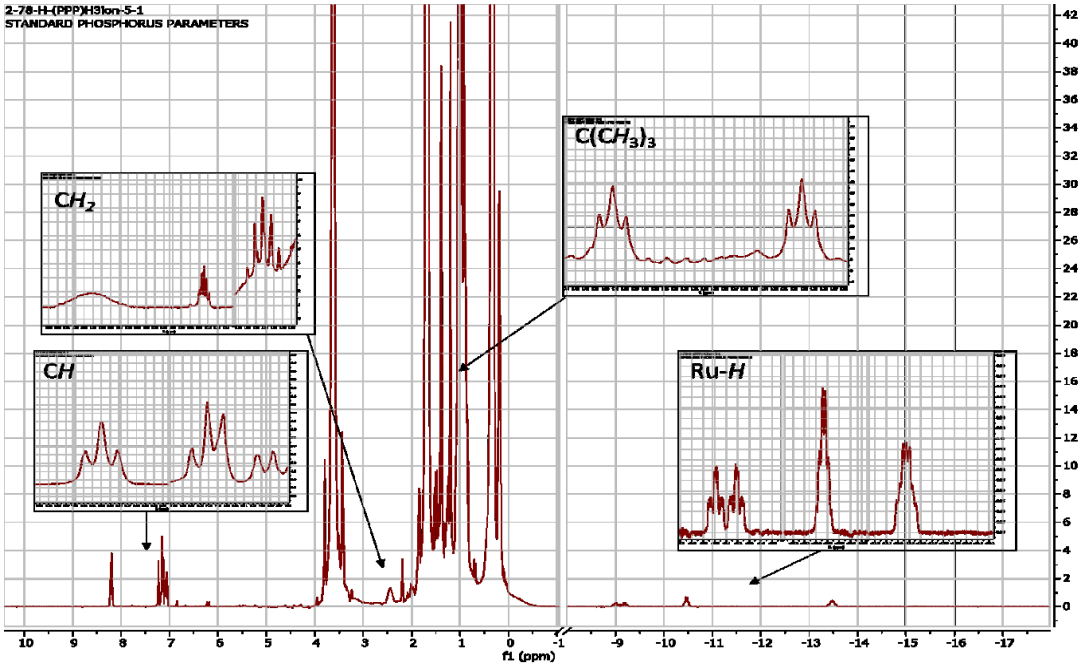

Figure 3.28: ^{1}H NMR of (^{tBu}PPP)RuH$_3^-$

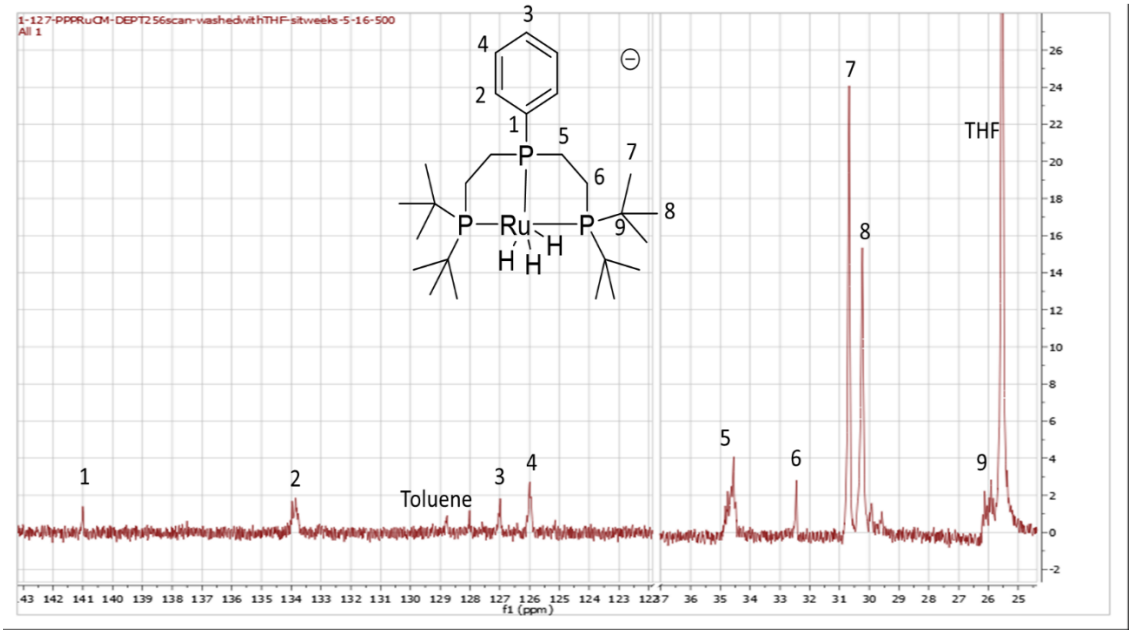

Figure 3.29: ^{13}C NMR of (^{tBu}PPP)RuH$_3^-$

Unknown (^{tBu}PPP)RuH$_3$:

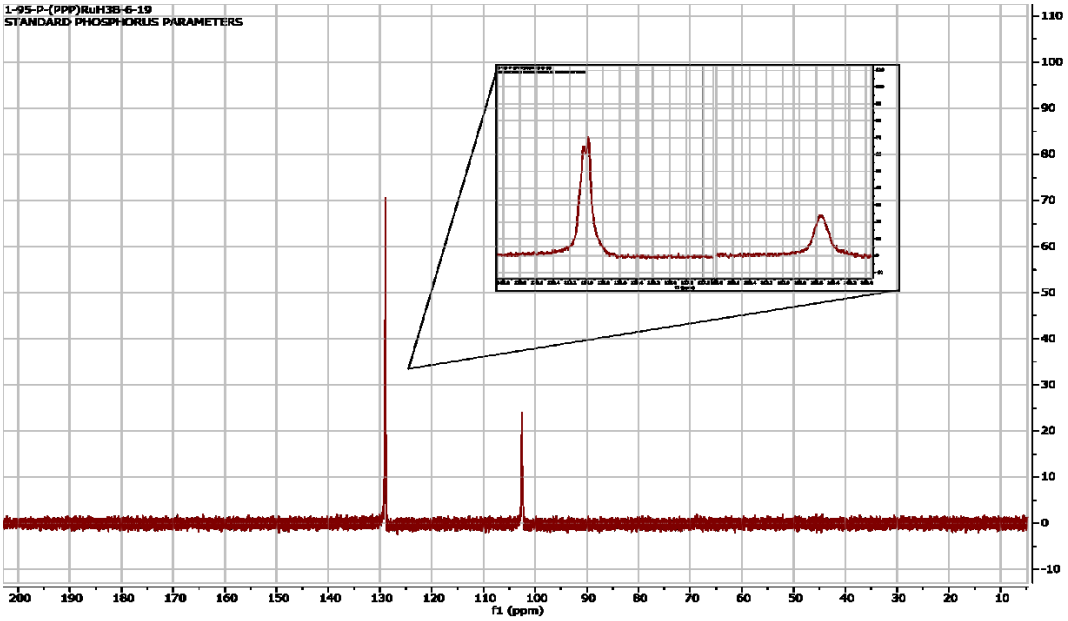

Figure 3.30: ^{31}P NMR of Unknown (^{tBu}PPP)RuH$_3$

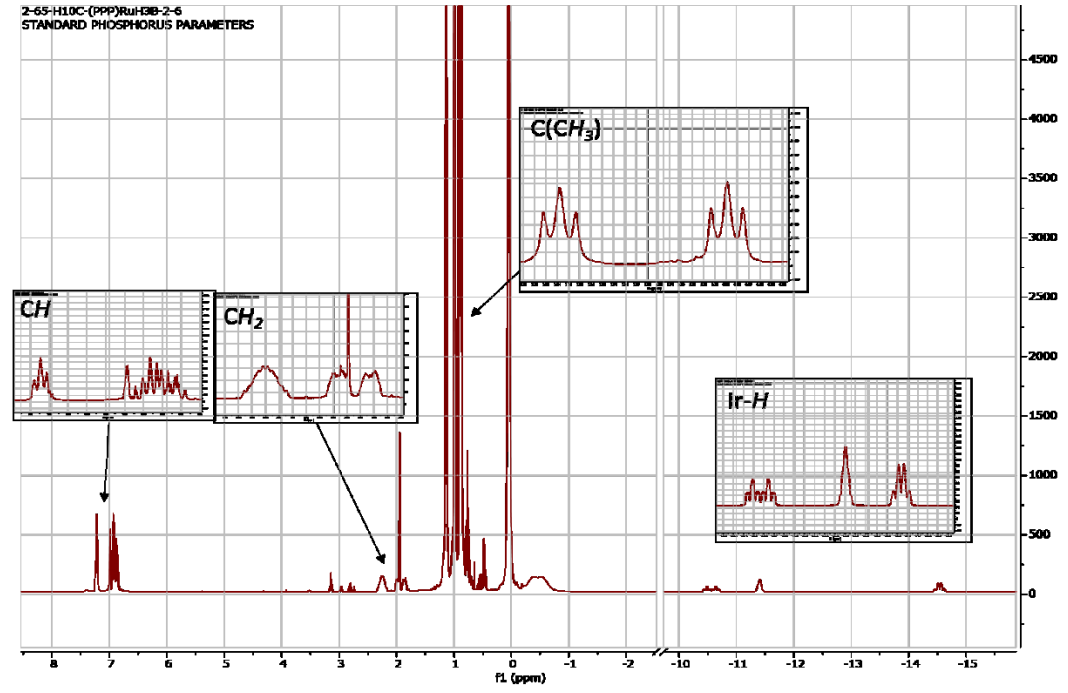

Figure 3.31: ^{1}H NMR of Unknown (^{tBu}PPP)RuH$_3$

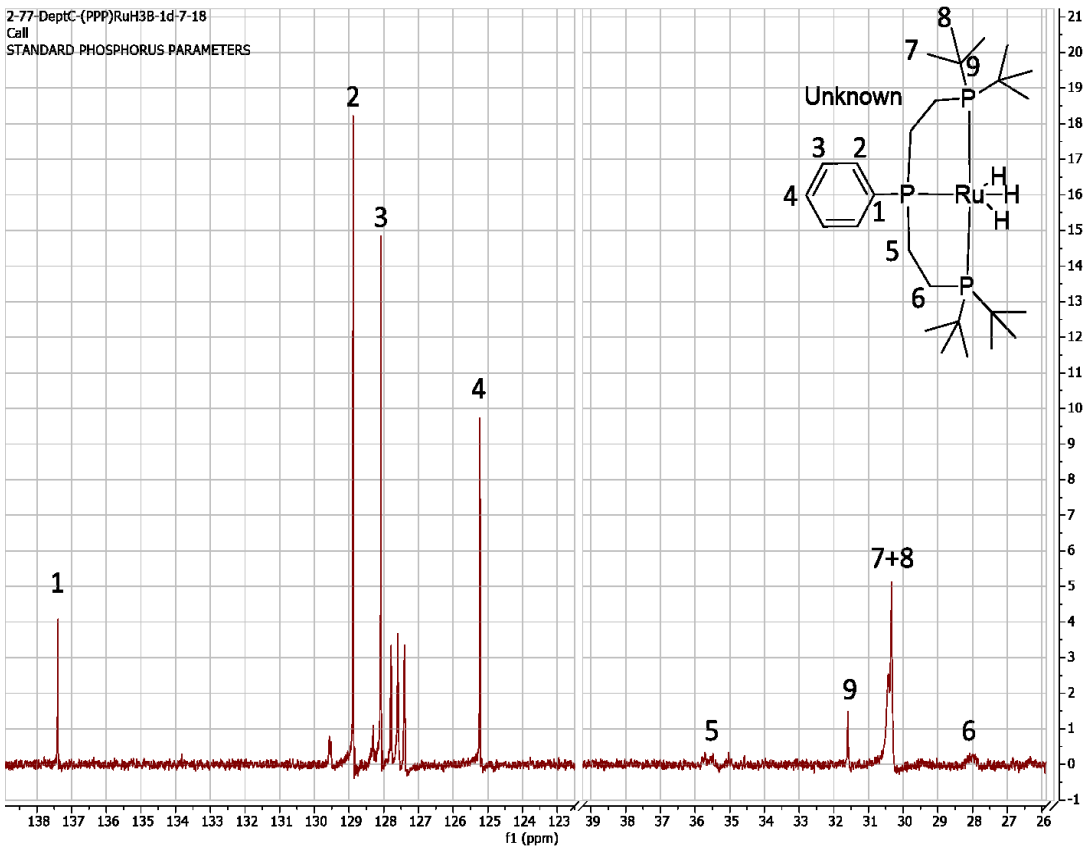

Figure 3.32: ^{13}C NMR of Unknown (^{tBu}PPP)RuH$_3$

(^{tBu}PPP)Ru(H)(BH_4)

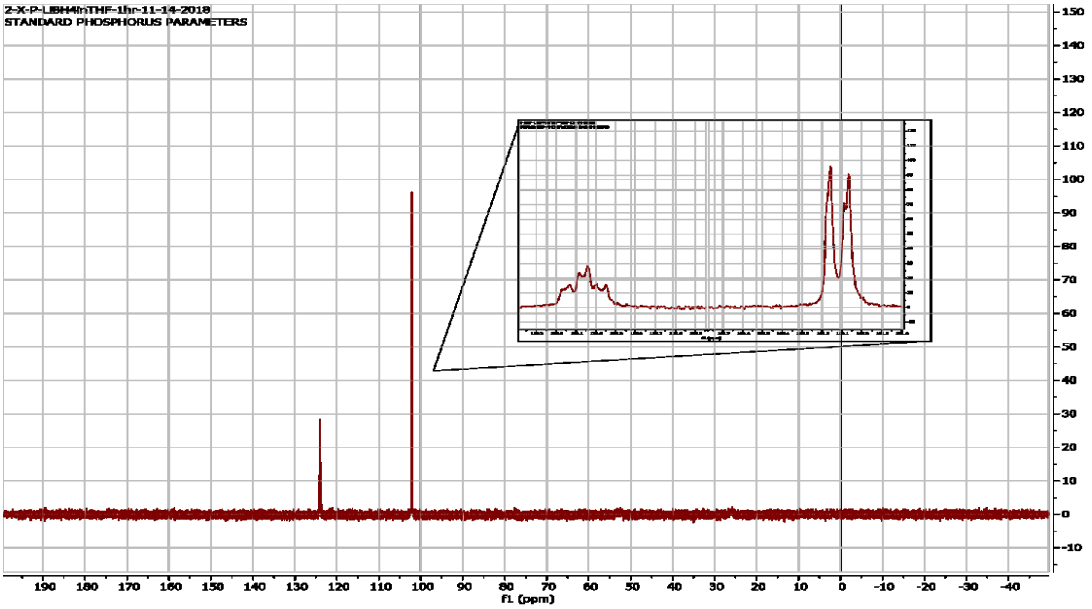

Figure 3.33: ^{31}P NMR of (^{tBu}PPP)Ru(H)(BH_4)

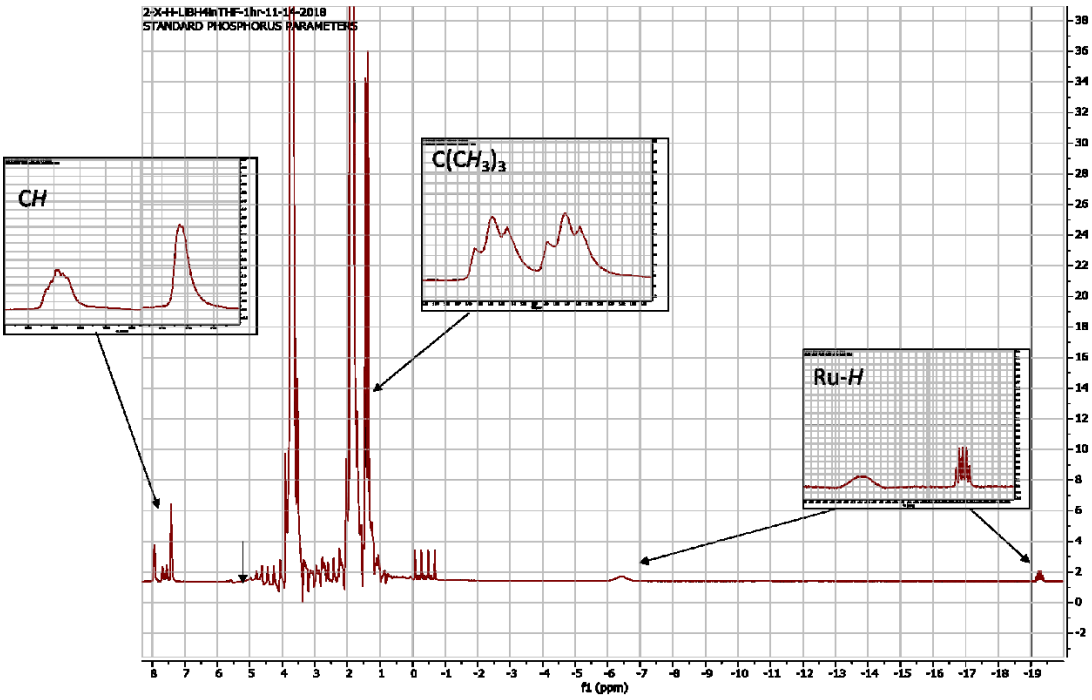

Figure 3.34: ^{1}H NMR of (^{tBu}PPP)Ru(H)(BH_4)

(^{tBu}PPP)RuH$_4$[**]

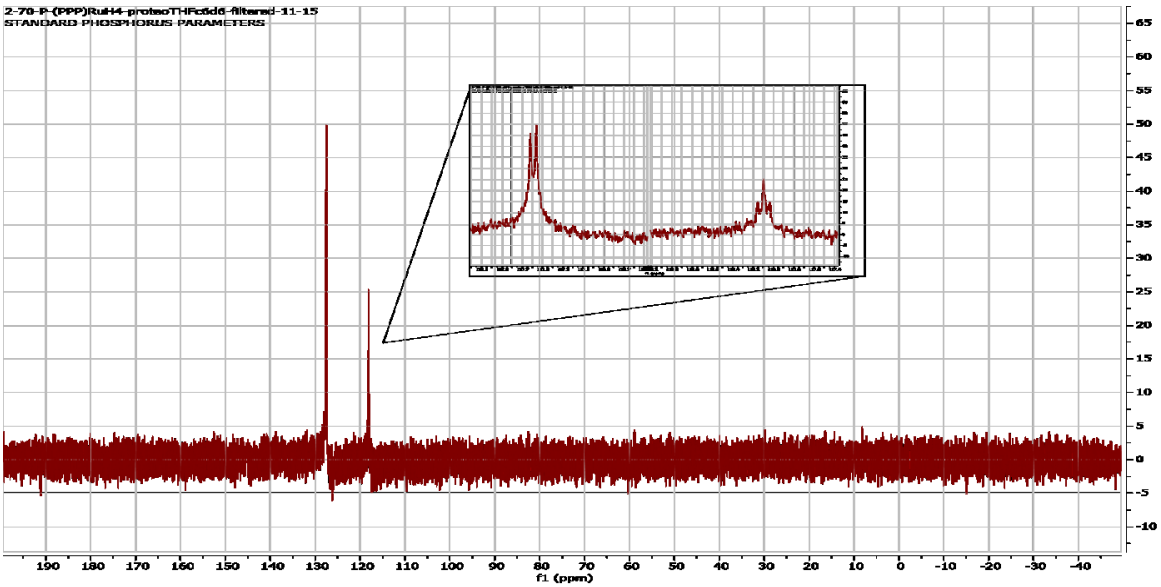

Figure 3.35: ^{31}P NMR of (^{tBu}PPP)RuH$_4$

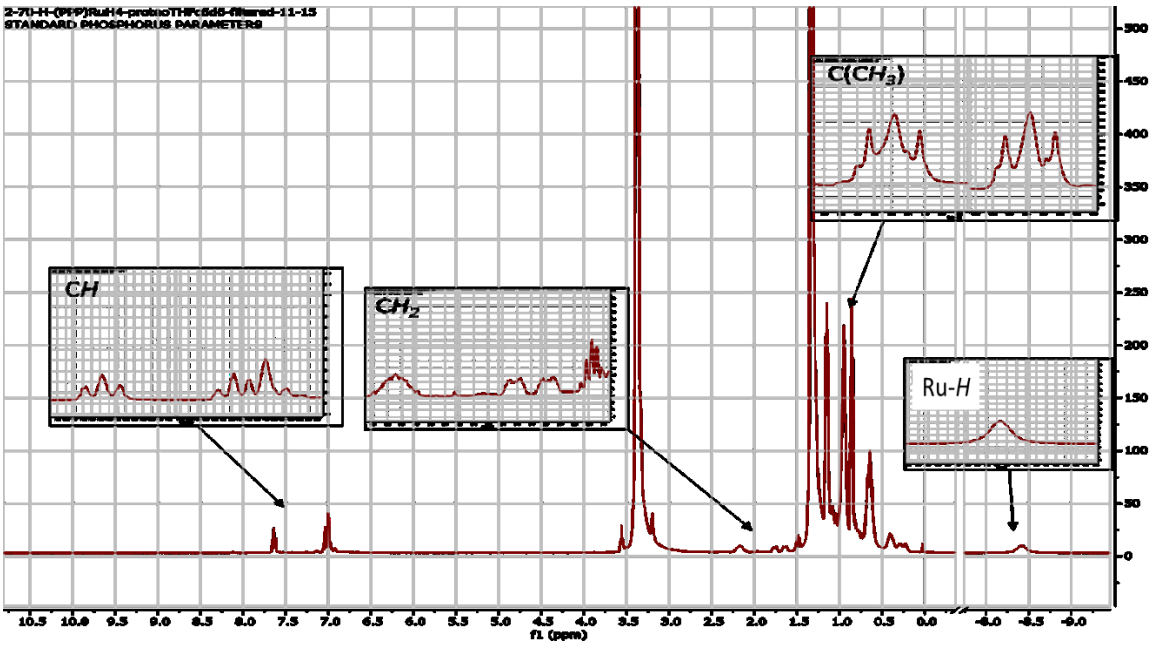

Figure 3.36: ^{1}H NMR of (^{tBu}PPP)RuH$_4$

[**] Both synthetic routes led to the same exact product so only one NMR is being shown

(^{tBu}PPP)Ru(CH_2=CH_2)

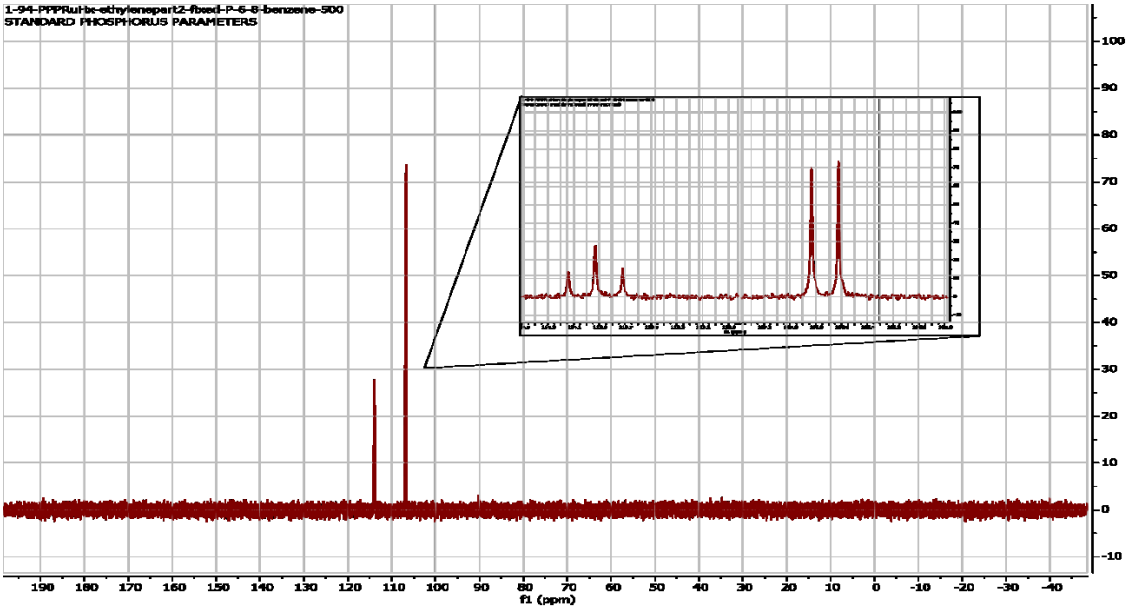

Figure 3.37: ^{31}P NMR of (^{tBu}PPP)Ru(CH_2=CH_2)

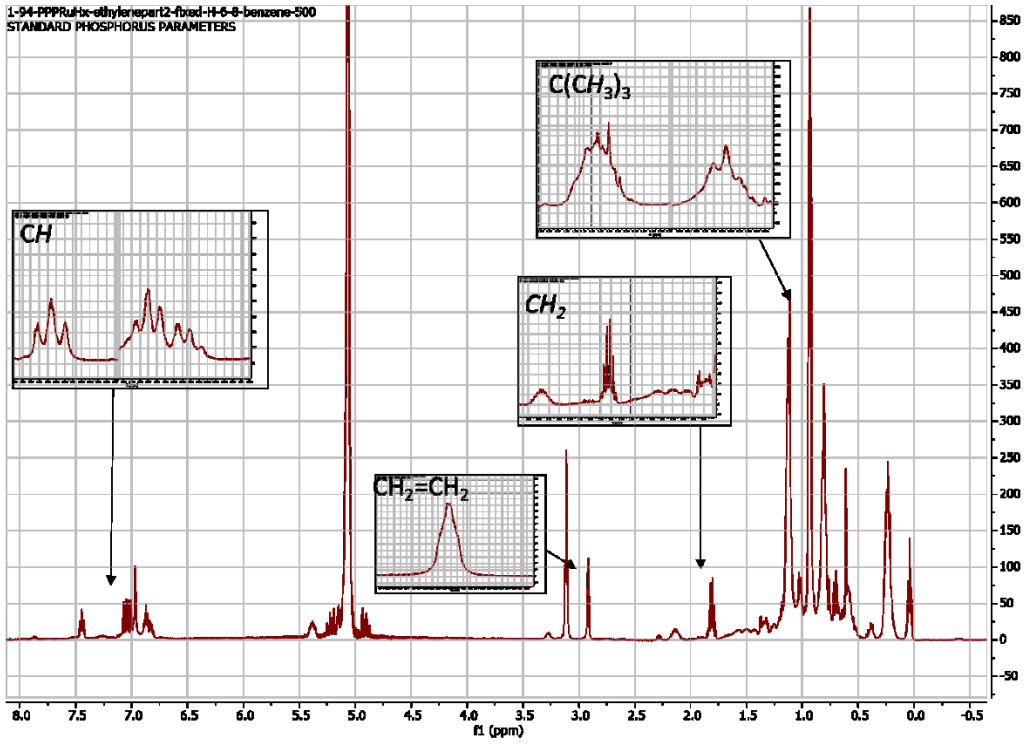

Figure 3.38: ^{1}H NMR of (^{tBu}PPP)Ru(CH_2=CH_2)

(^{tBu}PPP)RuH$_2$CO:

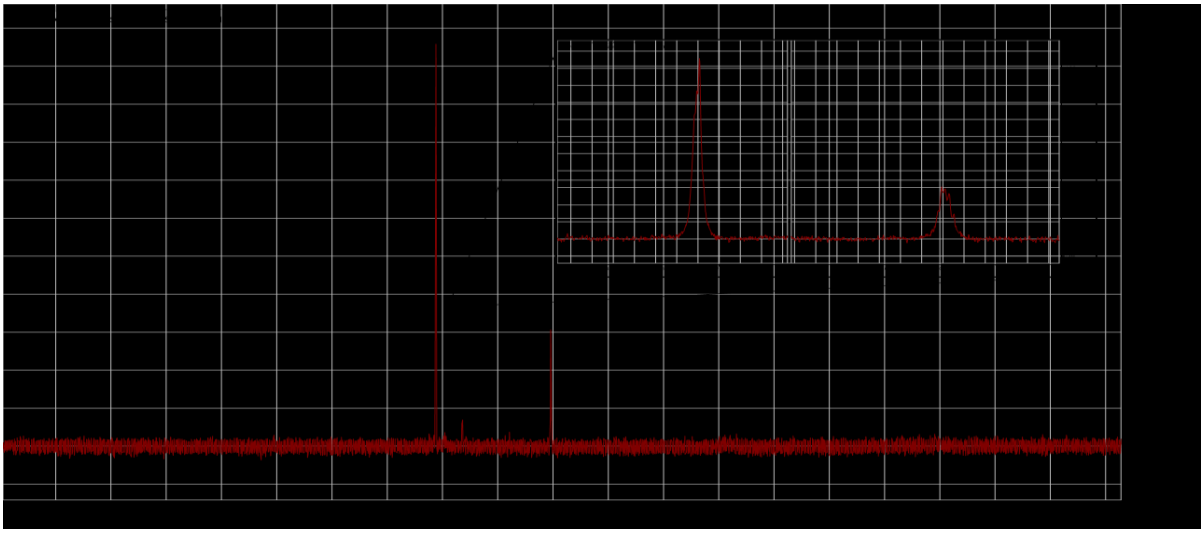

Figure 3.39: ^{31}P NMR of (^{tBu}PPP)RuH$_2$CO

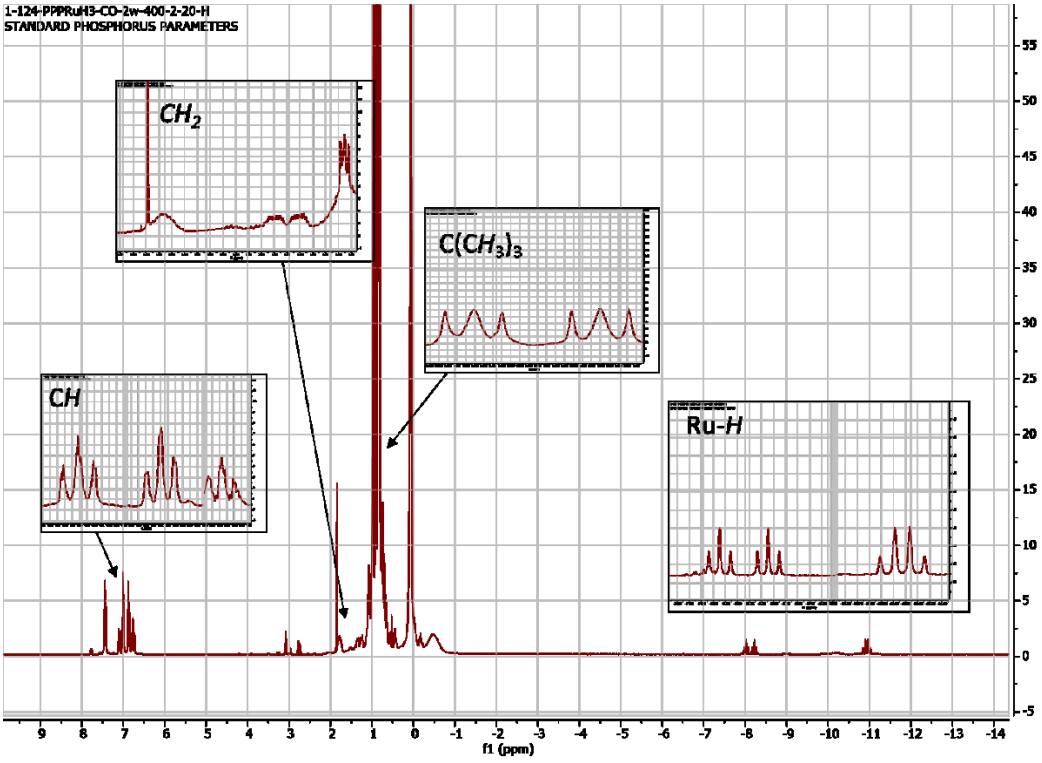

Figure 3.40: ^{1}H NMR of (^{tBu}PPP)RuH$_2$CO

3.8: References

1) Verpoort, F; Su, W; Ahmad, N; Younus, H. *Coord. Chem. Rev.* **2014**, *276*, 112-152.
2) Gunanathan, C; Milstein, D. *Chem. Rev.* **2014**, *114*, 12024-12087.
3) Zhang, J.; Leitus, G.; Ben-David, Y.; Milstein, D. *J. Am. Chem. Soc*. **2005**, *127*, 10840.
4) Gnanaprakasam, B.; Zhang, J.; Milstein, D. *Angew. Chem., Int. Ed.* **2010**, *49*, 1468.
5) Gunanathan, C.; Milstein, D. *Angew. Chem., Int. Ed.* **2008**, *47*, 8661.
6) Gruver, B; Adams, J; Warner, S; Arulsamy, N; Roddick, D. *Organometallics* **2011**, *30*, 5133-5140.
7) Baratta, W.; Chelucci, G.; Gladiali, S.; Siega, K.; Toniutti, M.; Zanette, M.; Zangrando, E.; Rigo, P. *Angew. Chem., Int. Ed.* **2005**, *44*, 6214.
8) Komuro, T.; Tobita, H. *Chem. Commun.* **2010**, *46*, 1136.
9) Zhang, Y.; Li, X.; Hong, S. H. *Adv. Synth. Catal.* **2010**, *352*, 1779.
10) Gunanathan, C.; Gnanaprakasam, B.; Iron, M. A.; Shimon, L. J. W.; Milstein, D. *J. Am. Chem. Soc.* **2010**, *132*, 14763.
11) Conner, D.; Jayaprakash, K. N.; Cundari, T. R.; Gunnoe, T. B. *Organometallics* **2004**, *23*, 2724.
12) Khaskin, E.; Iron, M. A.; Shimon, L. J. W.; Zhang, J.; Milstein, D. *J. Am. Chem. Soc*. **2010**, *132*, 8542.
13) Blum, O.; Milstein, D. J. *Organomet. Chem.* **2000**, *479*, 593−594.
14) Anaby, A.; Butschke, B.; Ben-David, Y.; Shimon, L. J. W.; Leitus, G.; Feller, M.; Milstein, D. *Organometallics* **2014**, *33*, 3716.
15) Gallagher, M.; Wieder, N. L.; Dioumaev, V. K.; Carroll, P. J.; Berry, D. H. *Organometallics* **2010**, *29*, 591.
16) Montag, M.; Zhang, J.; Milstein, D. *J. Am. Chem. Soc.* **2012**, *134*, 10325.
17) Huff, C. A.; Kampf, J. W.; Sanford, M. S. *Chem. Commun.* **2013**, *49*, 7147.
18) Huff, C. A.; Sanford, M. S. *ACS Catal.* **2013**, *3*, 2412.
19) Balaraman, E.; Gunanathan, C.; Zhang, J.; Shimon, L. J. W.; Milstein, D. *Nat. Chem.* **2011**, *3*, 609.
20) Zhang, J.; Gandelman, M.; Shimon, L. J. W.; Rozenberg, H.; Milstein, D. *Organometallics* **2004**, *23*, 4026.
21) Tseng, K. T.; Rizzi, A. M.; Szymczak, N. K. *J. Am. Chem. Soc.* **2013**, *135*, 16352.
22) Zhang, Y; Fang, H; Yao, W; Leng, X; Huang, Z. *Organometallics* **2016**, *35*, 181-188.
23) Dobson, A.; Robinson, S. D. J. *Organomet. Chem.* **1975**, *87*, C52.
24) Zhang, J.; Balaraman, E.; Leitus, G.; Milstein, D. *Organometallics* **2011**, *30*, 5716.
25) Chen, T.; He, L.-P.; Gong, D.; Yang, L.; Miao, X.; Eppinger, J.; Huang, K.-W. *Tetrahedron Lett.* **2012**, *53*, 4409.
26) Field, L; Li, H; Dalgarno, S; McIntosh, R. *Inorg. Chem*. **2013**, *52*, 1570-1583.
27) Gilbert-Wilson, R; Field, L; Colbran, S; Bhadbhade, M. *Inorg. Chem*. **2013**, *52*, 3043-3053.
28) Gilbert-Wilson, R; Field, L; Bhadbhade, M. *Inorg. Chem*. **2012**, *51*, 3239-3246.
29) Gilbert-Wilson, R; Field, L; Bhadbhade, M. *Inorg. Chem*. **2014**, *53*, 12469-12479.

3.9: Crystal Data

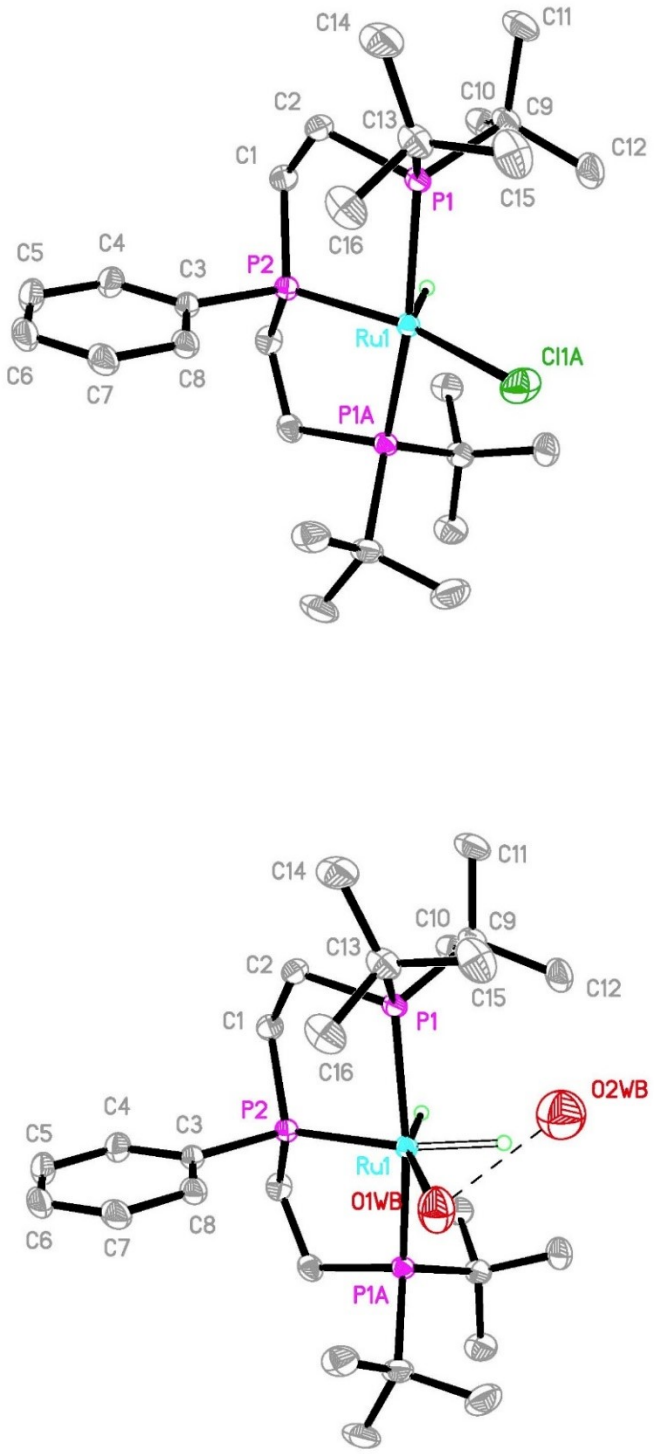

Figure 3.41: Structural Data for (^{tBu}PPP)RuHCl and (^{tBu}PPP)Ru(H_2)(H_2O)

Table 3.5. Crystal Data and Structure Refinement for (^{tBu}PPP)RuHCl

Identification code	RuP2CP_HCl_Pnma	
Empirical formula	C38 H63.25 Cl0.75 O0.50 P3 Ru	
Formula weight	748.70	
Temperature	120(2) K	
Wavelength	0.71073 Å	
Crystal system	Orthorhombic	
Space group	Pnma	
Unit cell dimensions	a = 20.9100(13) Å	$\alpha = 90°$.
	b = 19.4390(12) Å	$\beta = 90°$.
	c = 9.5217(6) Å	$\gamma = 90°$.
Volume	3870.3(4) Å^3	
Z	4	
Density (calculated)	1.285 Mg/m^3	
Absorption coefficient	0.607 mm^{-1}	
F(000)	1588	
Crystal size	0.510 x 0.310 x 0.270 mm^3	
Theta range for data collection	1.948 to 33.789°.	
Index ranges	-32<=h<=32, -30<=k<=28, -14<=l<=14	
Reflections collected	57132	
Independent reflections	7913 [R(int) = 0.0300]	
Completeness to theta = 25.242°	100.0 %	
Absorption correction	Semi-empirical from equivalents	
Max. and min. transmission	.9999 and .9369	
Refinement method	Full-matrix least-squares on F^2	
Data / restraints / parameters	7913 / 398 / 242	
Goodness-of-fit on F^2	1.133	
Final R indices [I>2sigma(I)]	R1 = 0.0301, wR2 = 0.0739	
R indices (all data)	R1 = 0.0327, wR2 = 0.0756	
Extinction coefficient	n/a	
Largest diff. peak and hole	0.667 and -0.706 e.Å^{-3}	

Table 3.6. Bond Lengths [Å] and Angles [°] for (^{tBu}PPP)RuHCl

Ru(1)-P(2)	2.1933(5)	C(9)-C(11)	1.5386(19)
Ru(1)-P(1)#1	2.3447(3)	C(10)-H(10A)	0.9800
Ru(1)-P(1)	2.3447(3)	C(10)-H(10B)	0.9800
Ru(1)-Cl(1A)	2.4352(7)	C(10)-H(10C)	0.9800
Ru(1)-H(1)	1.549(9)	C(11)-H(11A)	0.9800
Ru(1)-H(2B)	1.588(9)	C(11)-H(11B)	0.9800
O(1WB)-H(1WA)	0.831(9)	C(11)-H(11C)	0.9800
O(1WB)-H(1WB)	0.774(7)	C(12)-H(12A)	0.9800
O(2WB)-H(2WA)	0.843(10)	C(12)-H(12B)	0.9800
O(2WB)-H(2WB)	0.841(10)	C(12)-H(12C)	0.9800
P(1)-C(2)	1.8617(13)	C(13)-C(15)	1.535(2)
P(1)-C(9)	1.8963(12)	C(13)-C(14)	1.534(2)
P(1)-C(13)	1.8966(13)	C(13)-C(16)	1.5365(19)
P(2)-C(1)	1.8318(13)	C(14)-H(14A)	0.9800
P(2)-C(1)#1	1.8319(13)	C(14)-H(14B)	0.9800
P(2)-C(3)	1.8345(17)	C(14)-H(14C)	0.9800
C(1)-C(2)	1.5322(19)	C(15)-H(15A)	0.9800
C(1)-H(1C)	0.9900	C(15)-H(15B)	0.9800
C(1)-H(1D)	0.9900	C(15)-H(15C)	0.9800
C(2)-H(2C)	0.9900	C(16)-H(16A)	0.9800
C(2)-H(2D)	0.9900	C(16)-H(16B)	0.9800
C(3)-C(8)	1.389(2)	C(16)-H(16C)	0.9800
C(3)-C(4)	1.402(2)	C(17)-C(18)#1	1.378(2)
C(4)-C(5)	1.394(3)	C(17)-C(18)	1.378(2)
C(4)-H(4)	0.9500	C(17)-H(17)	0.9500
C(5)-C(6)	1.388(3)	C(18)-C(19)	1.376(3)
C(5)-H(5)	0.9500	C(18)-H(18)	0.9500
C(6)-C(7)	1.380(3)	C(19)-C(20)	1.382(2)
C(6)-H(6)	0.9500	C(19)-H(19)	0.9500
C(7)-C(8)	1.396(2)	C(20)-H(20)	0.9500
C(7)-H(7)	0.9500	C(21)-C(23)#2	1.380(2)
C(8)-H(8)	0.9500	C(21)-C(22)	1.386(2)
C(9)-C(12)	1.5340(19)	C(21)-H(21)	0.9500
C(9)-C(10)	1.5342(19)	C(22)-C(23)	1.383(2)

C(22)-H(22)	0.9500	C(23)-H(23)	0.9500
P(2)-Ru(1)-P(1)#1	84.099(8)	C(1)-C(2)-P(1)	112.23(9)
P(2)-Ru(1)-P(1)	84.100(8)	C(1)-C(2)-H(2C)	109.2
P(1)#1-Ru(1)-P(1)	163.215(17)	P(1)-C(2)-H(2C)	109.2
P(2)-Ru(1)-Cl(1A)	159.60(2)	C(1)-C(2)-H(2D)	109.2
P(1)#1-Ru(1)-Cl(1A)	97.613(8)	P(1)-C(2)-H(2D)	109.2
P(1)-Ru(1)-Cl(1A)	97.612(8)	H(2C)-C(2)-H(2D)	107.9
P(2)-Ru(1)-H(1)	75.83(18)	C(8)-C(3)-C(4)	118.65(16)
P(1)#1-Ru(1)-H(1)	82.783(16)	C(8)-C(3)-P(2)	119.98(13)
P(1)-Ru(1)-H(1)	82.784(16)	C(4)-C(3)-P(2)	121.37(14)
Cl(1A)-Ru(1)-H(1)	124.58(18)	C(5)-C(4)-C(3)	120.23(18)
P(2)-Ru(1)-H(2B)	153.9(5)	C(5)-C(4)-H(4)	119.9
P(1)#1-Ru(1)-H(2B)	92.67(6)	C(3)-C(4)-H(4)	119.9
P(1)-Ru(1)-H(2B)	92.68(6)	C(6)-C(5)-C(4)	120.20(18)
H(1)-Ru(1)-H(2B)	78.0(5)	C(6)-C(5)-H(5)	119.9
H(1WA)-O(1WB)-H(1WB)	109.5(14)	C(4)-C(5)-H(5)	119.9
H(2WA)-O(2WB)-H(2WB)	100.9(16)	C(7)-C(6)-C(5)	120.12(18)
C(2)-P(1)-C(9)	103.61(6)	C(7)-C(6)-H(6)	119.9
C(2)-P(1)-C(13)	100.73(6)	C(5)-C(6)-H(6)	119.9
C(9)-P(1)-C(13)	109.08(6)	C(6)-C(7)-C(8)	119.80(19)
C(2)-P(1)-Ru(1)	107.35(4)	C(6)-C(7)-H(7)	120.1
C(9)-P(1)-Ru(1)	114.12(4)	C(8)-C(7)-H(7)	120.1
C(13)-P(1)-Ru(1)	119.79(5)	C(3)-C(8)-C(7)	121.01(17)
C(1)-P(2)-C(1)#1	106.86(9)	C(3)-C(8)-H(8)	119.5
C(1)-P(2)-C(3)	103.06(5)	C(7)-C(8)-H(8)	119.5
C(1)#1-P(2)-C(3)	103.06(5)	C(12)-C(9)-C(10)	108.07(11)
C(1)-P(2)-Ru(1)	111.40(4)	C(12)-C(9)-C(11)	109.57(11)
C(1)#1-P(2)-Ru(1)	111.40(4)	C(10)-C(9)-C(11)	107.42(11)
C(3)-P(2)-Ru(1)	119.95(6)	C(12)-C(9)-P(1)	108.68(9)
C(2)-C(1)-P(2)	106.78(8)	C(10)-C(9)-P(1)	108.27(9)
C(2)-C(1)-H(1C)	110.4	C(11)-C(9)-P(1)	114.63(9)
P(2)-C(1)-H(1C)	110.4	C(9)-C(10)-H(10A)	109.5
C(2)-C(1)-H(1D)	110.4	C(9)-C(10)-H(10B)	109.5
P(2)-C(1)-H(1D)	110.4	H(10A)-C(10)-H(10B)	109.5
H(1C)-C(1)-H(1D)	108.6	C(9)-C(10)-H(10C)	109.5

H(10A)-C(10)-H(10C)	109.5	H(16A)-C(16)-H(16C)	109.5
H(10B)-C(10)-H(10C)	109.5	H(16B)-C(16)-H(16C)	109.5
C(9)-C(11)-H(11A)	109.5	C(18)#1-C(17)-C(18)	120.0(2)
C(9)-C(11)-H(11B)	109.5	C(18)#1-C(17)-H(17)	120.0
H(11A)-C(11)-H(11B)	109.5	C(18)-C(17)-H(17)	120.0
C(9)-C(11)-H(11C)	109.5	C(19)-C(18)-C(17)	119.96(16)
H(11A)-C(11)-H(11C)	109.5	C(19)-C(18)-H(18)	120.0
H(11B)-C(11)-H(11C)	109.5	C(17)-C(18)-H(18)	120.0
C(9)-C(12)-H(12A)	109.5	C(18)-C(19)-C(20)	120.36(16)
C(9)-C(12)-H(12B)	109.5	C(18)-C(19)-H(19)	119.8
H(12A)-C(12)-H(12B)	109.5	C(20)-C(19)-H(19)	119.8
C(9)-C(12)-H(12C)	109.5	C(19)#1-C(20)-C(19)	119.3(2)
H(12A)-C(12)-H(12C)	109.5	C(19)#1-C(20)-H(20)	120.3
H(12B)-C(12)-H(12C)	109.5	C(19)-C(20)-H(20)	120.3
C(15)-C(13)-C(14)	109.79(13)	C(23)#2-C(21)-C(22)	120.38(14)
C(15)-C(13)-C(16)	107.23(13)	C(23)#2-C(21)-H(21)	119.8
C(14)-C(13)-C(16)	107.75(12)	C(22)-C(21)-H(21)	119.8
C(15)-C(13)-P(1)	111.17(10)	C(23)-C(22)-C(21)	119.60(15)
C(14)-C(13)-P(1)	115.06(11)	C(23)-C(22)-H(22)	120.2
C(16)-C(13)-P(1)	105.41(9)	C(21)-C(22)-H(22)	120.2
C(13)-C(14)-H(14A)	109.5	C(21)#2-C(23)-C(22)	120.02(14)
C(13)-C(14)-H(14B)	109.5	C(21)#2-C(23)-H(23)	120.0
H(14A)-C(14)-H(14B)	109.5	C(22)-C(23)-H(23)	120.0
C(13)-C(14)-H(14C)	109.5		
H(14A)-C(14)-H(14C)	109.5		
H(14B)-C(14)-H(14C)	109.5		
C(13)-C(15)-H(15A)	109.5		
C(13)-C(15)-H(15B)	109.5		
H(15A)-C(15)-H(15B)	109.5		
C(13)-C(15)-H(15C)	109.5		
H(15A)-C(15)-H(15C)	109.5		
H(15B)-C(15)-H(15C)	109.5		
C(13)-C(16)-H(16A)	109.5		
C(13)-C(16)-H(16B)	109.5		
H(16A)-C(16)-H(16B)	109.5		
C(13)-C(16)-H(16C)	109.5		

Chapter 4

Exploring *para*-Benzoquinones as Potential Hydrogen Acceptors

Abstract:

(^{R}PCP)IrH_2 complexes are some of the most efficient homogenous catalysts for alkane dehydrogenation to date. However, one of the issues that prevents their use in a more practical application is the need for a sacrificial hydrogen acceptor. The necessity of stoichiometric quantities of acceptor leads to a high production of waste, especially if scaled up. One solution would be the use of an acceptor that could accept hydrogen and later be regenerated to its initial form for re-use. The regeneration could be done either in the same catalytic cycle or in a separate discrete step. Substituted *para*-benzoquinones were tested for their reactivity with (^{tBu}PCP)IrH_4. It was discovered that the benzoquinones are extremely efficient hydrogen acceptors; however, the excess quinone in reaction then binds to the iridium center preventing any catalysis. When using bulkier *para*-benzoquinones, the strength of the Ir-quinone bonds were weakened, allowing for some alcohol dehydrogenation to occur. While successful, this dehydrogenation occurred very slowly compared to other known hydrogen acceptors.

4.1 Introduction:

Since the first report of pincer-ligated metal complexes, research has shown a prodigious number of chemical applications they can be applied to, especially in the field of C-H activation. The ability to break C-H bonds selectively is one of the most researched topics in chemistry. Breaking specific C-H bonds on alkanes can allow for functionalization to make high value synthetic products. The main issue, however, is that the C-H bond is strong, meaning its relatively inert and hard to break.

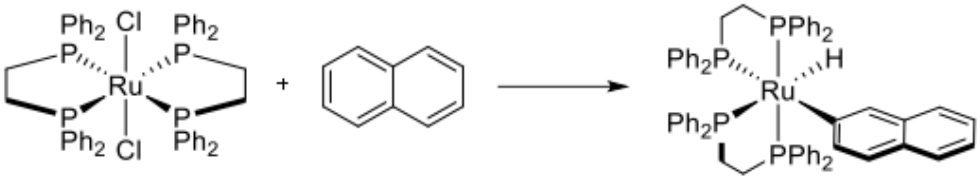

Scheme 4.1: C-H Oxidative Addition Reported by Chatt and Davidson in 1965

The first activation of C-H bonds using a transition metal was reported in 1965 by Chatt and Davidson.[1] However, it was not until almost 20 years later, that the individual reports by Bergman and Graham showed alkyl C-H activation using transition metals (Scheme 4.2 and 4.3).[2,3] Selectivity studies independently conducted by Bergman, Jones, and Bercaw all found that the selectivity for activation of the strongest C-H bond was most favorable despite the differences in their catalysts.[4-6]

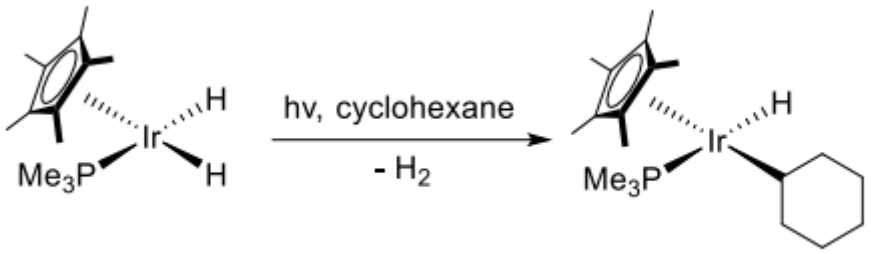

Scheme 4.2: C-H Oxidative Addition of Cyclohexane Reported by Bergman

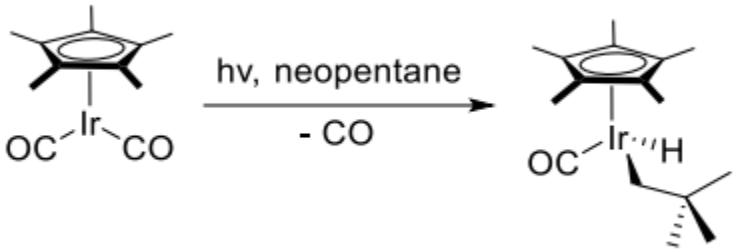

Scheme 4.3: C-H Oxidative Addition of Neopentane Reported by Graham

C-H bond activation is essential for many catalytic processes, especially alkane dehydrogenation, the conversion of alkanes to olefins. A continuous goal of chemistry is to take abundant, cheap materials and convert them into more valuable commodities. Using pincer-ligated metal complexes and their ability to C-H activate, alkanes (a cheap, abundant material) can be converted to alkenes (a valuable, versatile feedstock). The alkane dehydrogenation process is enthalpically unfavorable (ΔH ~ 30 kcal/mol),[7,8] however it is favorable entropically due to the loss of H_2. One way to lower the enthalpic barrier, and thus the overall barrier of the reaction, is to use a sacrificial hydrogen

acceptor such as *tert*-butylethylene (TBE) or norbornene (NBE). This process, known as transfer dehydrogenation, was first reported by Crabtree in 1979.[9]

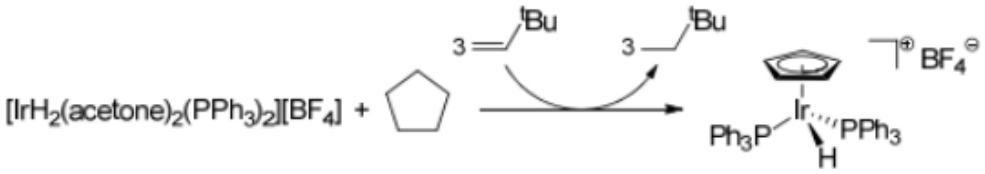

Scheme 4.4: Transfer Dehydrogenation Reported by Crabtree in 1979

Crabtree found that he could dehydrogenate cycloalkanes in the presence of TBE using an iridium catalyst to yield cyclic iridium diene complexes (Figure 4.4). Later in 1987, he reported the dehydrogenation of alkanes,[10] and then in 1989 our group reported the first efficient example of alkane dehydrogenation using photochemical dehydrogenation catalyzed by $RhCl(PMe_3)_2(CO)$ (Figure 4.1).[11,12] Numerous reports since 1989 have shown that pincer complexes are extremely efficient alkane dehydrogenation catalysts.

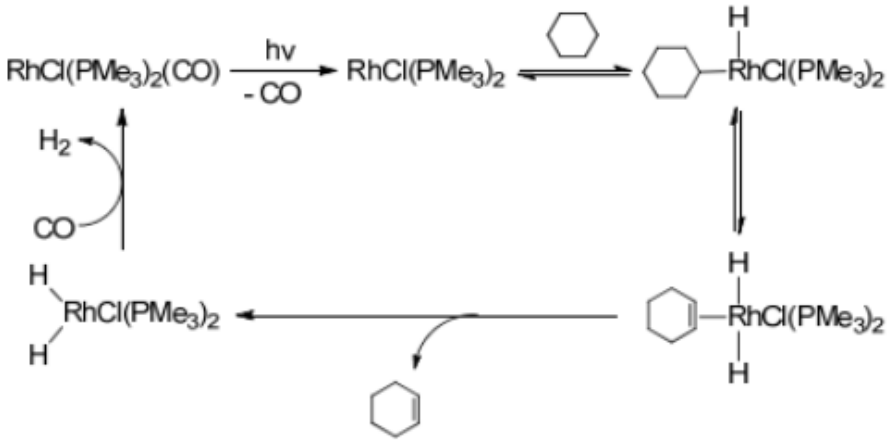

Figure 4.1: Photochemical Alkane Dehydrogenation Reported by Goldman in 1989

First discovered in 1996 by Kaska and Jensen,[13] (^{R}PCP)IrH$_2$ complexes are one of the most efficient series of homogenous catalysts for alkane dehydrogenation. However, one of the disadvantages of the alkane dehydrogenation reaction is the need for stoichiometric quantities of a sacrificial hydrogen acceptor. Using TBE as an acceptor, Kaska and Jensen were able to perform transfer dehydrogenation of cyclooctane (Figure 4.2). Not long after, our group reported the dehydrogenation of n-octane using TBE as well.[14]

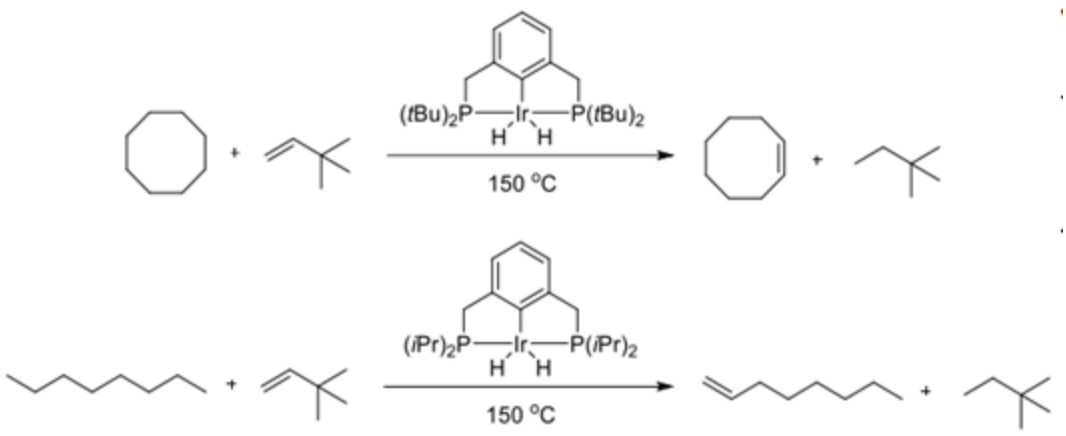

Figure 4.2: Examples of Transfer Dehydrogenation using TBE as an Acceptor

Since these reports, TBE has become a standard in dehydrogenation chemistry. It has been shown that when the (^{R}PCP)IrH$_2$ reacts with TBE, the acceptor is hydrogenated producing the (^{R}PCP)Ir 14 e$^-$ active species for catalysis and neohexane as waste. From here the catalyst can C-H activate the alkane, go through β-hydride elimination, and then release the olefin to reform the (^{R}PCP)IrH$_2$ species and repeat the cycle (Figure 4.3).[15,16] Previously our laboratory has shown that (^{R}PCP)IrH$_2$ can perform acceptorless

dehydrogenation. However, using DFT calculations and experimental data, it was determined that the rate determining step of hydrogen elimination, along with the positive reaction enthalpy of ~30 kcal/mol, prevents high conversion.[17,18]

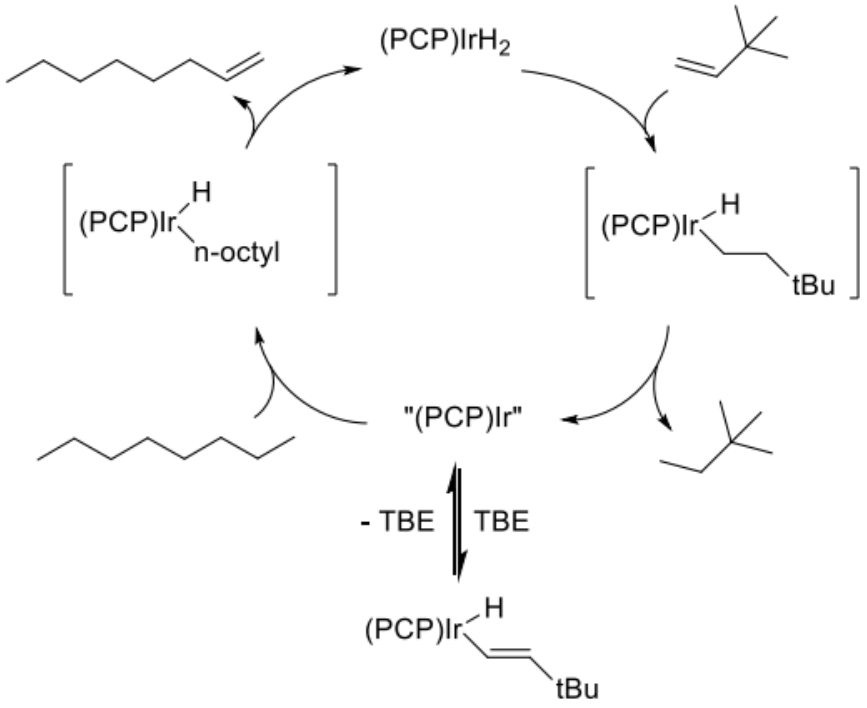

Figure 4.3: Mechanism for Alkane Dehydrogenation using (PCP)Ir

In order to keep the enthalpy low yet avoid the production of waste via the sacrificial acceptor, we explored the development of a renewable hydrogen acceptor; one that can accept hydrogen and then be regenerated through the loss of two protons and two electrons. This regeneration could be done in-situ via chemical means, or ideally, in an electrochemical system.

Para-benzoquinones are compounds that have been shown to hydrogenate easily and can be oxidized back to benzoquinone electrochemically or by using chemicals such as nitric acid and metal salts.[19-24] Additionally, hydroquinone can react with molecular oxygen in an aqueous solution to form benzoquinone, however the rate is strongly dependent on the pH of solution.[25] Due to the ease of hydrogenation and their ability to be regenerated electrochemically, we chose to study the ability of *para*-benzoquinones as hydrogen acceptors in the (^{R}PCP)Ir catalytic cycle (Scheme 4.5).

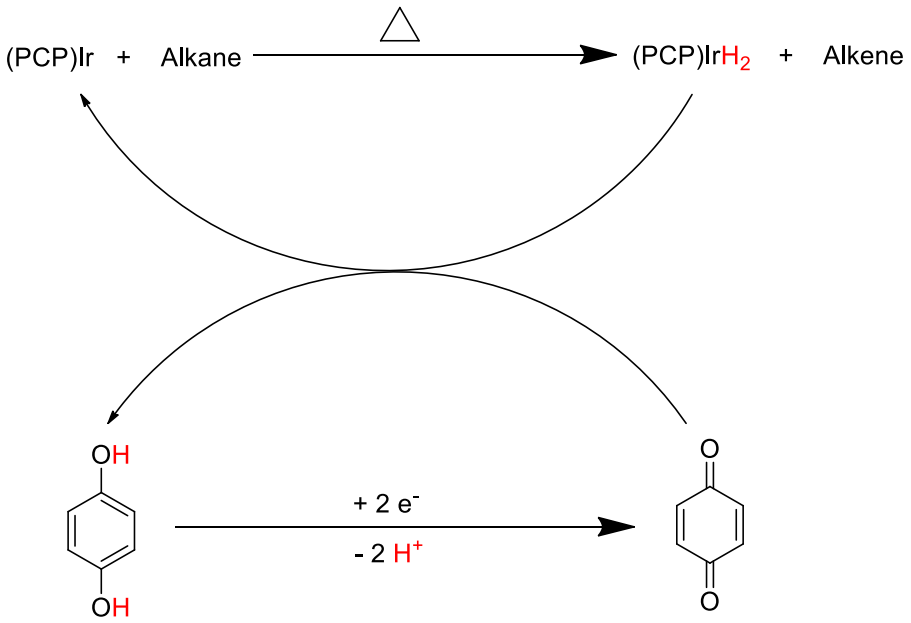

Scheme 4.5: Proposed Scheme for Electrochemical Alkane Dehydrogenation using Quinones

4.2 Study of the reactivity between (^{tBu}PCP)IrH$_4$ with four different *para*-benzoquinones

To study the potential of benzoquinones as hydrogen acceptors we first reacted (^{tBu}PCP)IrH$_2$ with substituted *para*-benzoquinones. Four different *para*-benzoquinones were chosen for study. We chose 2,5-di-tert-butylbenzoquinone and duroquinone to

study the effects of sterics on the reactivity of the quinone. Secondly, we chose tetrafluoro-1,4-quinone to rule out any potential C-H activation of the benzoquinone. These three *para*-benzoquinones were then compared to the unsubstituted, parent 1,4-benzoquinone.

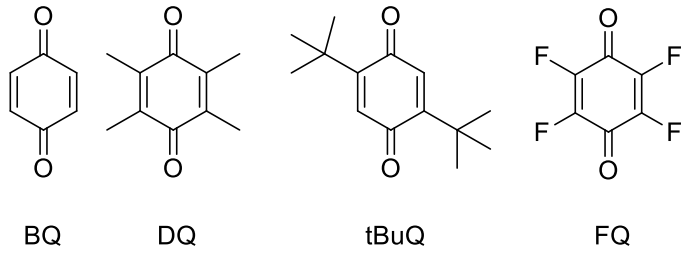

Figure 4.4: Types of Para-benzoquinones used for this Study (BQ=1,4-benzoquinone, DQ=duroquinone, tBuQ= 2,5-tert-butylquinone, FQ=2,3,5,6-tetrafluoroquinone)

1,4-Benzoquinone:

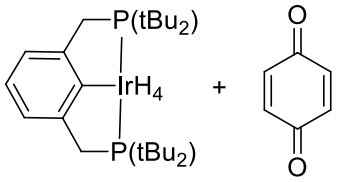

Scheme 4.6: Substrates for Reaction #1

The first quinone studied was the parent, unsubstituted 1,4-benzoquinone (BQ). Upon mixing of 6 eq. BQ with the (^{tBu}PCP)IrH_4 complex an instant color change to brown/purple was observed. One major species could be seen at 49.6 ppm in the ^{31}P NMR with a corresponding broad hydride at -36.35 ppm in the ^{1}H NMR. After stirring for 48 hrs. at room temperature, the color changed to brown and a new species at 44.0 ppm (82%) and two minor species around 47.1 ppm (18%) were observed in the ^{31}P NMR.

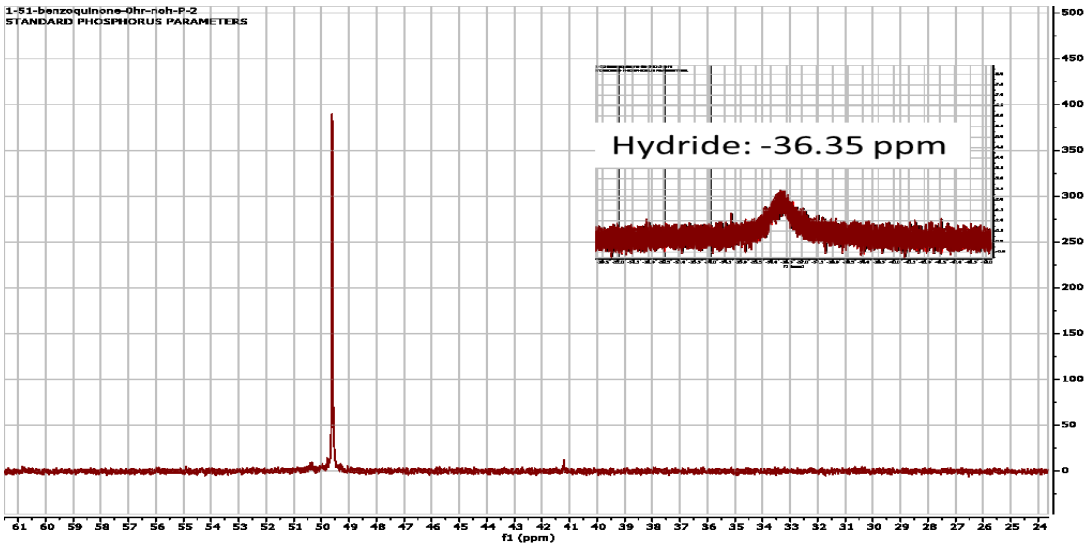

Figure 4.5: ^{31}P NMR of O-H Activated Product and Corresponding Hydride

We hypothesize that the BQ first acts as a hydrogen acceptor and turns into hydroquinone (HQ). At that point the 14 e$^-$ (^{tBu}PCP)Ir fragment O-H activates the hydroquinone and forms the species seen at 49.6 ppm early in the reaction (Scheme 4.7). The hydride observed at -36.35 ppm is consistent with other RO-H addition products seen with (^{tBu}PCP)Ir. The O-H activated product is the kinetic product in this reaction.

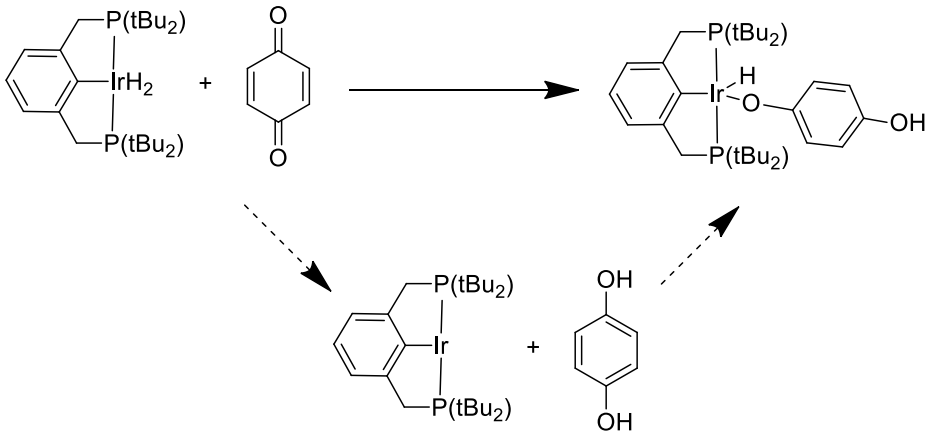

Scheme 4.7: Suggested scheme for O-H Activated Product

After 48 hours the complex converts to the more thermodynamically favored product, which we believe is the (^{tBu}PCP)Ir(BQ) "barber-chair" complex. Our collaborators at the University of Rochester found that when reacting (^{iPr}PCP)IrH_4 with BQ it forms a complex they named the "barber-chair" due to its geometry.[26] The BQ binds in a (bis)-η^2 fashion with the C-C double bonds of the benzoquinone (Figure 4.8). This binding fashion has been observed with other iridium complexes, however this was the first example of this type of (bis)-η^2 bond with a pincer-iridium complex.[27-29]

When comparing the two catalysts, it should be noted that the (^{iPr}PCP)Ir complex does not show the formation of the O-H activated product. The (^{tBu}PCP)Ir complex has significantly more steric bulk around the metal center. It is likely that the BQ has more difficulty binding to the metal center, which is why it prefers to react with the HQ over the BQ initially. However, over time the reaction ends up with the more stable BQ "barber-chair" complex. While we believe that we made the (^{tBu}PCP)Ir(BQ) "barber-chair" complex, we were not able to isolate crystals, so we were unable to confirm the exact structure.

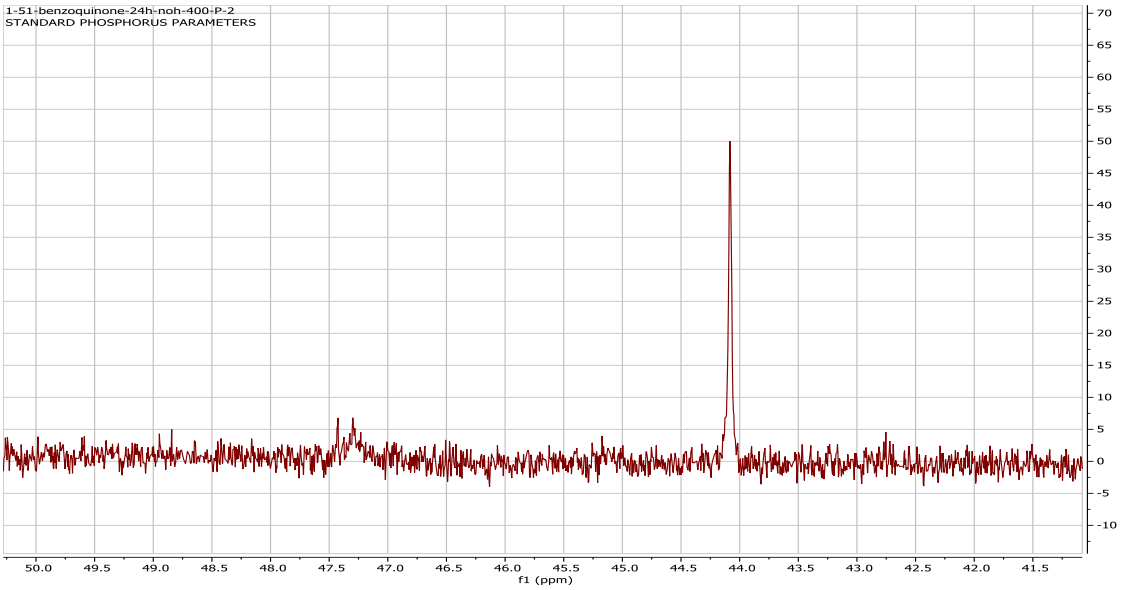

Figure 4.6: ^{31}P NMR of "Barber-Chair" Complex

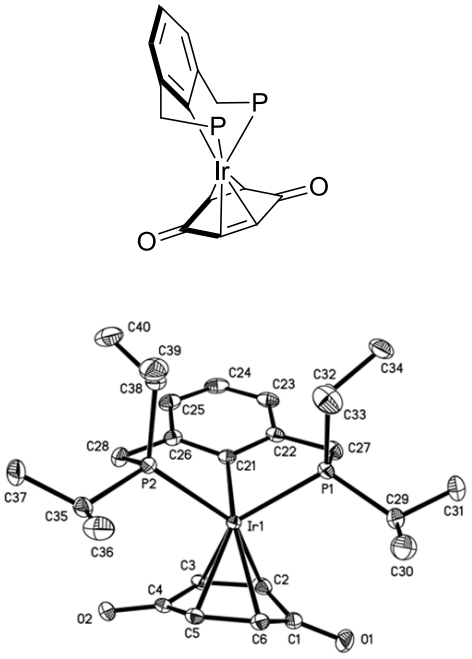

Figure 4.7: Top: Suggested structure for "Barber-Chair" Complex (*tert*-butyl groups are hidden for clarity) Bottom: Crystal Structure of (^{iPr}PCP)Ir(BQ) Complex Isolated by our Collaborators[28]

Duroquinone and 2,5-di-tert-butylquinone

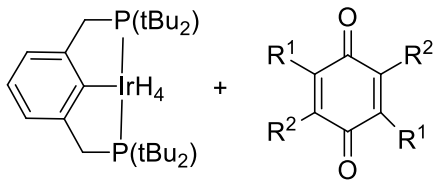

DQ: R^1, $R^2 = CH_3$
tBuQ: $R^1 = H$, $R^2 = C(CH_3)_3$

Scheme 4.8: Substrates for Reaction #2 and #3

In contrast to the parent HQ, duroquinone (DQ) and 2,5-di-tert-butylquinone (tBuQ) did not react with (^{tBu}PCP)IrH_4 at room temperature. When the reaction with 3 eq. DQ was heated at 40^{o}C for 24 hours, about 50% of the iridium was converted to a new species at 64.9 ppm in the ^{31}P NMR with a corresponding hydride at -34.7 ppm. The other 50% consisted of unreacted (^{tBu}PCP)IrH_4 and (^{tBu}PCP)IrH_2. Similar to the BQ, we believe that the DQ acted as a hydrogen acceptor and then the (^{tBu}PCP)Ir center O-H activated the durohydroquinone. However, the DQ in solution is too bulky to coordinate to the iridium center, therefore it never goes onto make the “barber-chair” complex, instead it stays as the O-H activated complex.

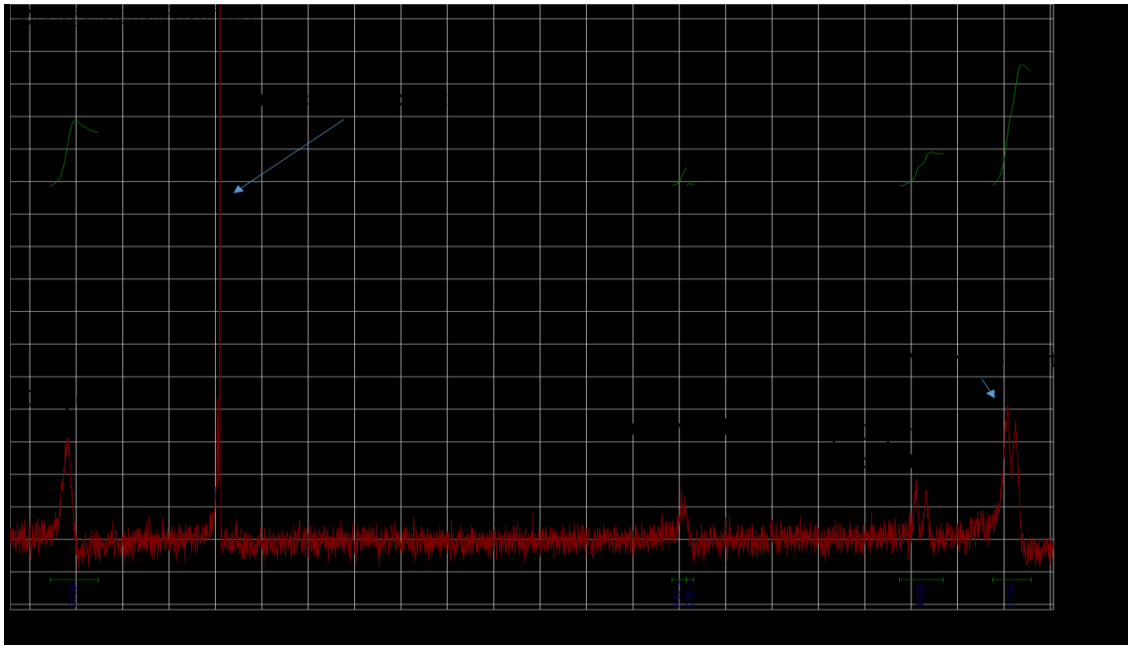

Figure 4.8: ^{31}P NMR of Reaction Mixture between (^{tBu}PCP)IrH$_4$ and DQ[††]

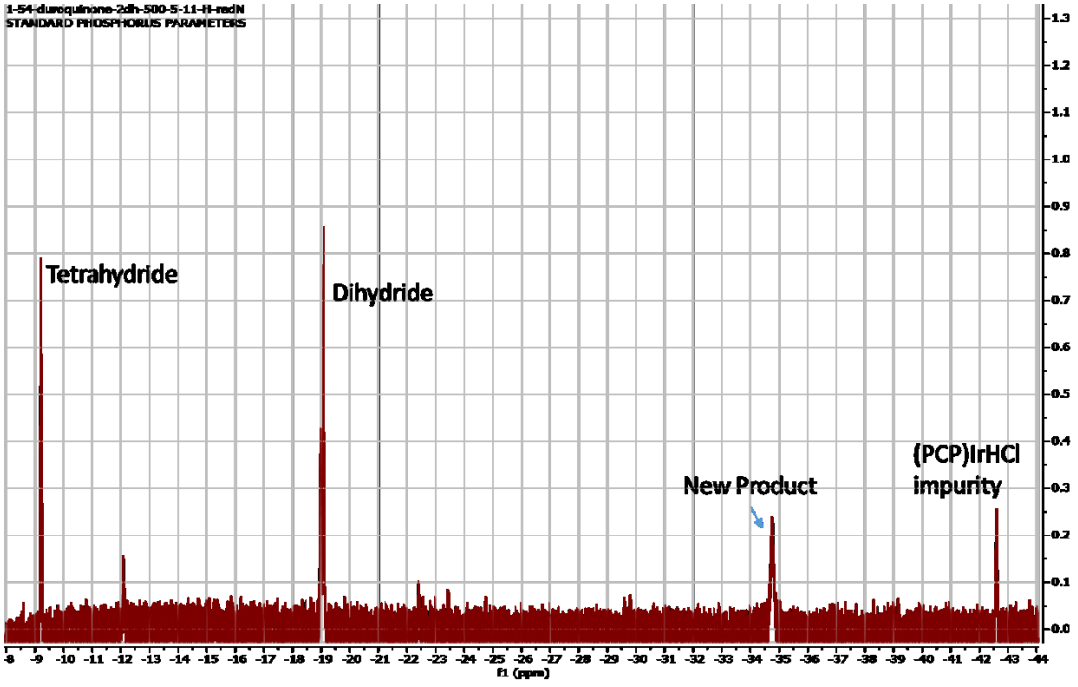

Figure 4.9: ^{1}H NMR: Hydrides of the Reaction Mixture Between (^{tBu}PCP)IrH$_4$ and DQ

[††] (PCP)IrHCl impurity came from unreacted (PCP)IrHCl in the synthesis of (PCP)IrH$_4$

In contrast, when the reaction with 3 eq. tBuQ was heated at 40°C for 24 hours, 85% of the iridium was converted to a new product at 51.2 ppm in the ^{31}P NMR. There were also two unknown products (13%) and small amount of unreacted (^{tBu}PCP)IrH_4 and (^{tBu}PCP)IrH_2 (<3%). There were no new hydrides in the NMR, suggesting the tBuQ acted as a hydrogen acceptor, however the Ir complex did not O-H activate the resulting hydroquinone. It is possible that the new product is the "barber-chair" complex, however all attempts to grow crystals were unsuccessful, so we cannot confirm this structure.

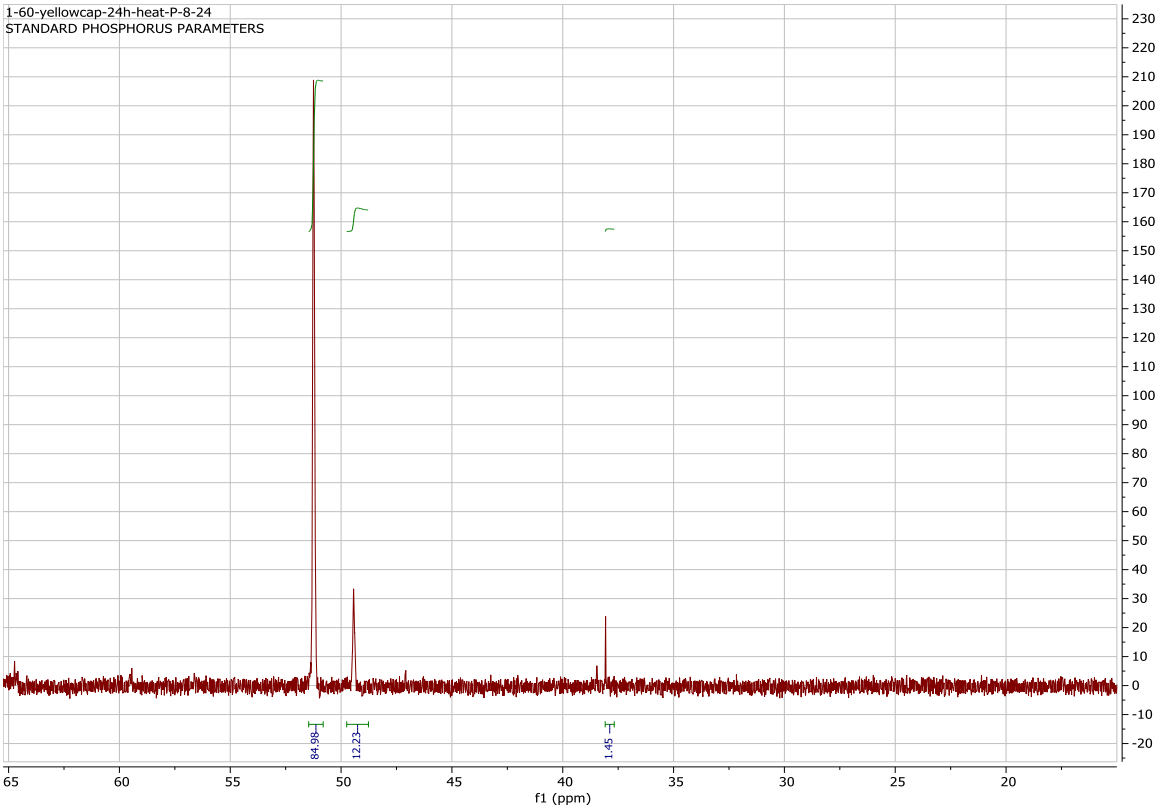

Figure 4.10: ^{31}P NMR of the Reaction Mixture Between (^{tBu}PCP)IrH_4 and tBuQ

Tetrafluoro-1,4-quinone

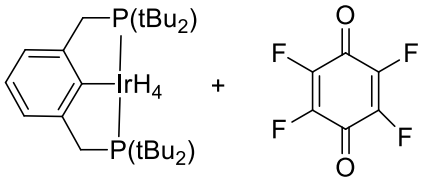

Scheme 4.9: Substrates for Reaction #4

In order to rule out any kind of C-H activation or interaction of the iridium center with the C-H bonds, we ran the same experiments with tetrafluoro-1,4-quinone (FQ). Upon mixing the FQ with the (^{tBu}PCP)IrH$_4$ the reaction turned purple. The ^{31}P NMR shows complete disappearance of the (^{tBu}PCP)IrH$_4$ and the production of three new peaks at 54.4 (15%), 49.6 (55%), and 32.3 ppm (30%), which we believe correspond to three new products. A single broad hydride can be observed at -41 ppm in the ^{1}H NMR. After 24 hours at room temperature, the three products can still be observed in slightly different amounts (54.4: 15%, 49.6: 81%, 32.3: 4%). The hydride peak remains relatively unchanged in intensity, suggesting it corresponds to the complex at 54.4 ppm. It is our hypothesis that the complex at 54.4 ppm is the O-H activated product and the complex at 49.6 ppm is the “barber-chair” complex. However due to the mix of products we were unable to do any further characterization to confirm this.

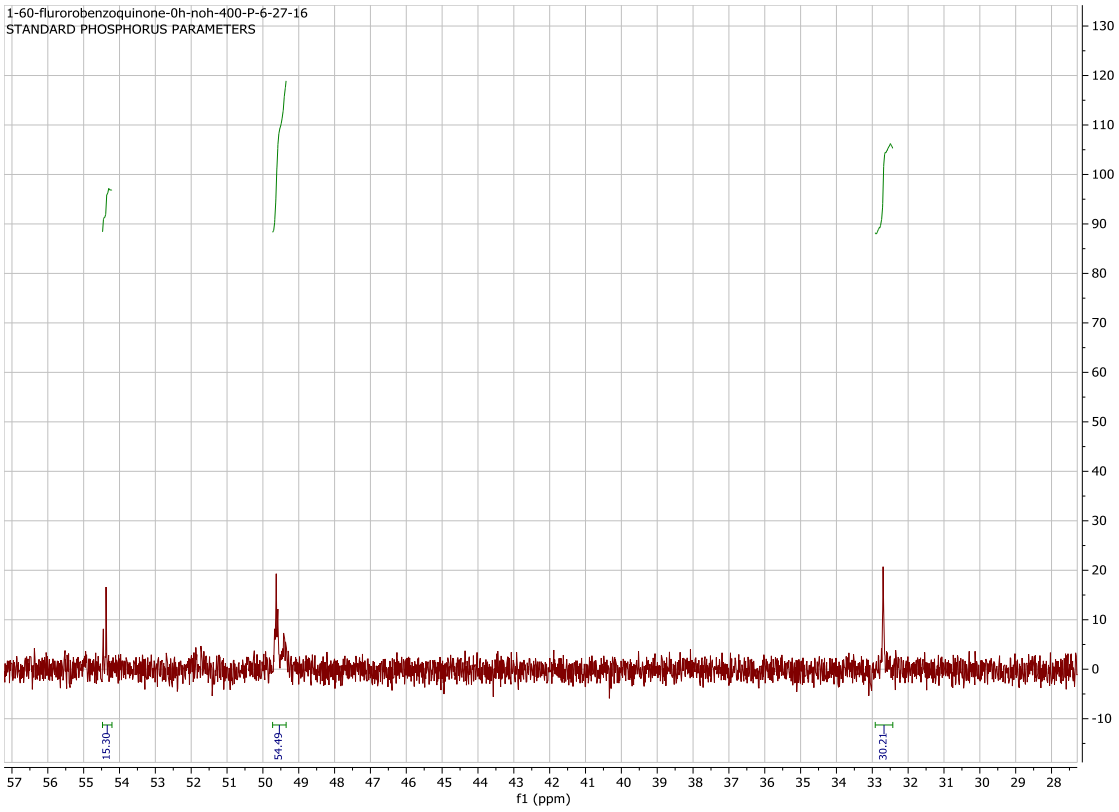

Figure 4.11: ^{31}P NMR of the Reaction Mixture Between (^{tBu}PCP)IrH$_4$ and FQ

4.3: Attempted Dehydrogenation Using 2,5-di-*tert*-butylbenzoquinone as an Acceptor

After results showed that *para*-benzoquinones can act as hydrogen acceptors, we attempted cyclooctane dehydrogenation. Even though the quinones complexed with the iridium center, we were hoping that in presence of an excess of alkane the iridium would preferably react with the alkane over the quinone in solution. With all four quinones we obtained the same results, with and without cyclooctane, showing that the iridium preferably O-H activates the hydroquinones or (bis)-η^2 binds the benzoquinone.

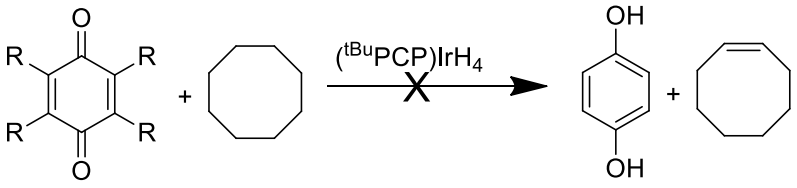

R= H, $C(CH_3)_3$, CH_3, or F

Scheme 4.10: Attempted Cyclooctane Dehydrogenation using Quinone Acceptors

At this point we were concerned that the iridium-quinone complexes were too stable to be reactive. To show that the quinone can dissociate from the iridium center, a trap experiment was set up using 2-phenylpyridine (ppy). We chose to study the (^{tBu}PCP)Ir complexes with tBuQ and FQ. We believed that the bulk of the tBuQ would cause its interaction with the iridium center to be weaker than the other quinones. Additionally, this quinone was also studied by our collaborators using (^{iPr}PCP)IrH_2.[28] We chose FQ because of the interesting binding interactions it has with the iridium (vide supra). Interestingly, when 3 eq. of phenylpyridine (ppy) was mixed with the (^{tBu}PCP)IrH_4 in presence of 3 eq. tBuQ, there was complete conversion to the (^{tBu}PCP)Ir(ppy)H complex. However, with FQ there was only complexing of the FQ to the (^{tBu}PCP)Ir center, no reaction with ppy was observed. As expected, the extra bulk of the tBuQ did weaken the quinone-iridium interactions, allowing the production of (^{tBu}PCP)Ir(ppy)H.

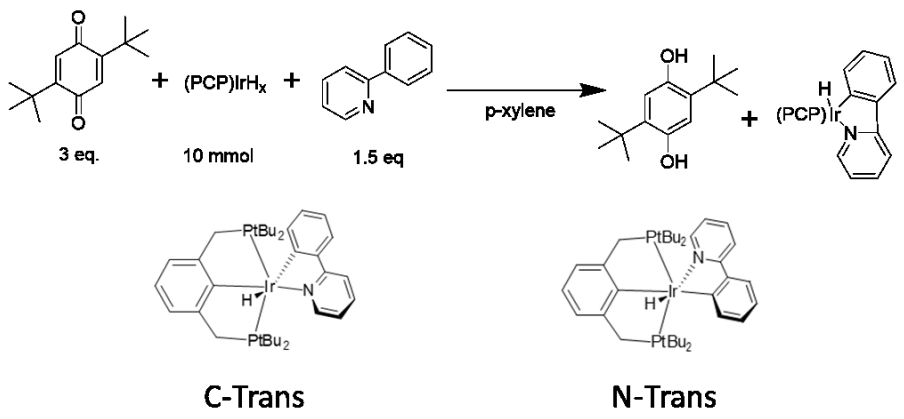

Scheme 4.11: Trap Experiment Performed using 2-phenylpyridine

It should be noted that we did not observe any (^{tBu}PCP)Ir(tBuQ) complexes at any point during the reaction. The only observed species were the (^{tBu}PCP)IrH$_4$, (^{tBu}PCP)IrH$_2$, and the final (^{tBu}PCP)Ir(ppy)H. We believe that the mechanism is the same when using other acceptors, such as TBE or NBE. After the quinone accepts the hydrogens, the 14 e$^-$ (^{tBu}PCP)Ir species preferably reacts with the ppy over the excess quinone, which is why no quinone complex is ever observed.

While the tBuQ was a successful hydrogen acceptor in the reaction of (^{tBu}PCP)IrH$_4$ with ppy, it was slower than using a more traditional hydrogen acceptor like norbornene (NBE). Using NBE as the acceptor allowed for 100% conversion to the (^{tBu}PCP)Ir(ppy)H after 12 hours, however with the tBuQ it took 72 hours. Even so, this experiment showed that the tBuQ could act as a hydrogen acceptor without inhibiting further reactivity.

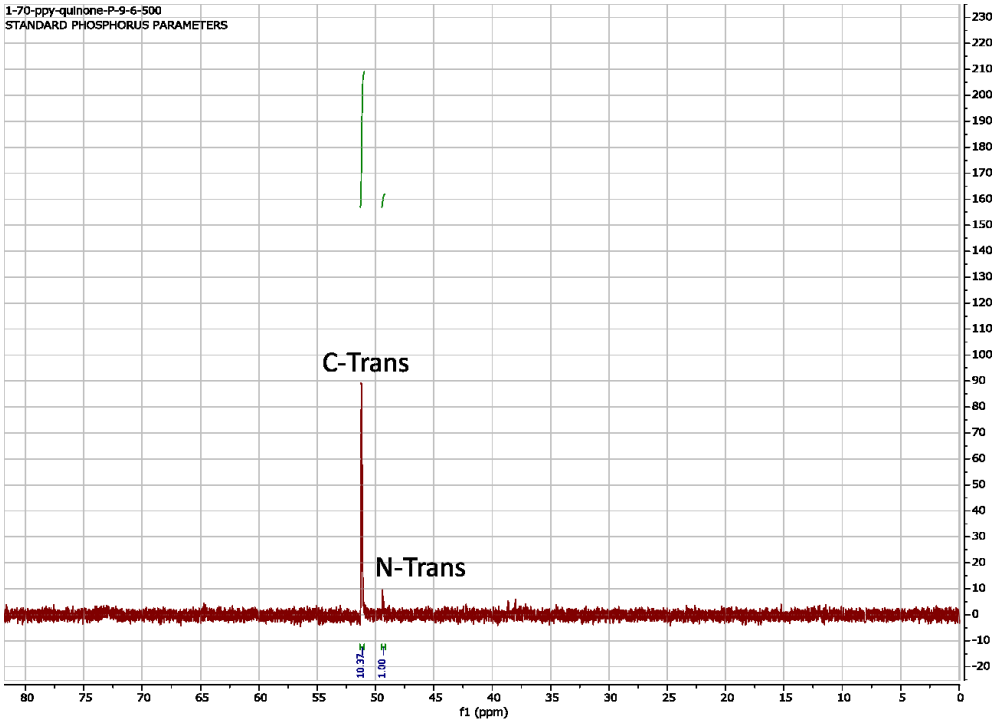

Figure 4.12: ^{31}P NMR of (^{tBu}PCP)Ir(ppy)H Produced from Trap Experiment

Since using tBuQ as a hydrogen acceptor for cyclooctane dehydrogenation was unsuccessful, we decided to attempt alcohol dehydrogenation. Alcohol dehydrogenation has been reported to be much easier than alkane dehydrogenation, so this was the best chance of attempting catalysis using tBuQ as a hydrogen acceptor.

Alcohol dehydrogenation studies were performed using 2-propanol as the substrate and tBuQ as the hydrogen acceptor. The reactions were set up in an NMR tube and heated in an oil bath. The TON was calculated based on the ratio of tBuQ to tBuHQ in the ^{1}H NMR and confirmed using the ratio of acetone to isopropanol on the GC. Reactions were attempted using only 10 eq. of tBuQ to prevent potential iridium-tBuQ interactions. After 24 hrs at 70^{o}C we were able to achieve 8 TON. The reaction could also work as low as 40^{o}C, however only 2 TON were observed.

Table 4.1: Results of Alcohol Dehydrogenation Attempts using tBuQ as an Acceptor

	mM Quinone	mM Hydroquinone	mM Isopropanol	mM Acetone	Total	TON
0hr r.t	200	0	500	0	700	0
24hr 40°C	152	48	475	25	700	2
24hr 70°C	40	160	467	33	667	8

Interestingly, it was very difficult to detect the acetone produced via NMR after the 24 hours at 70°C, but it could easily be seen in the 40°C reaction. GC shows that the acetone produced elutes somewhere in between proteo-acetone and acetone-d_6. It is possible that at the higher temperatures some H-D exchange occurs with the solvent leading to a partially deuterated acetone product.

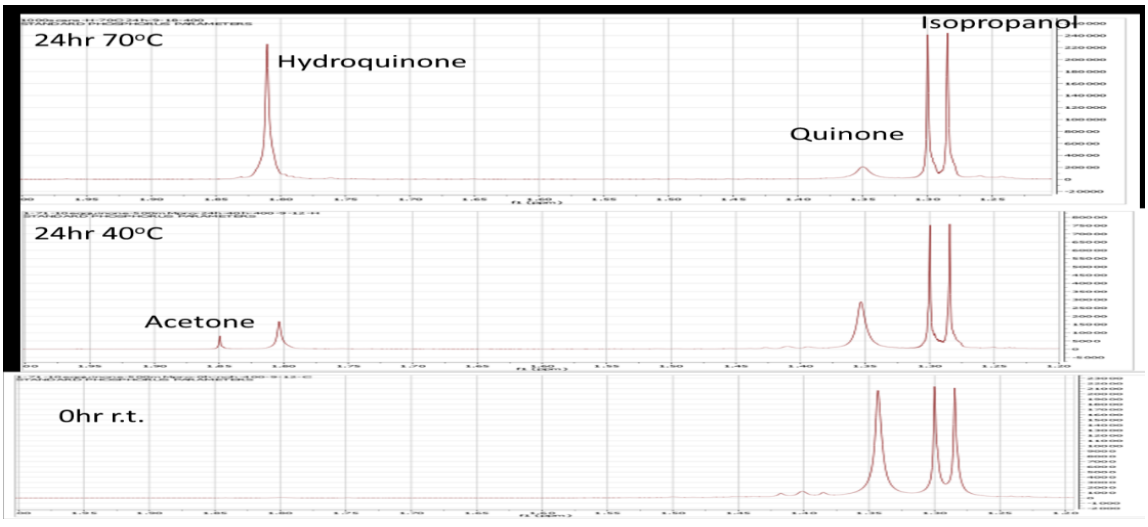

Figure 4.13: ^{1}H NMR Showing tBuQ Loss and tBuHQ Production

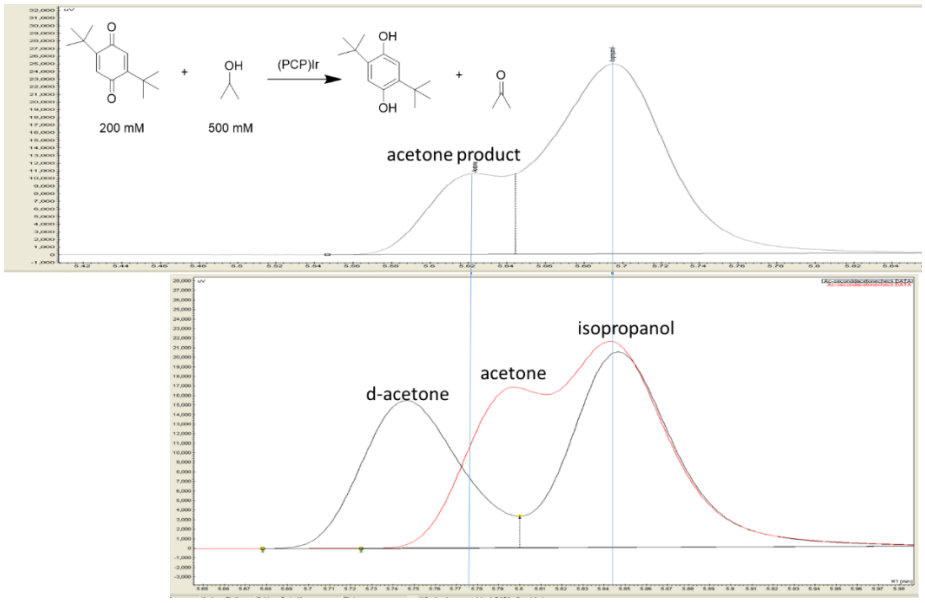

Figure 4.14: GC Scan Showing Acetone Product is in Between that of Proteo-acetone and Acetone-d_6

Based on our preliminary results, substituted *para*-benzoquinones are extremely good hydrogen acceptors, however without bulky groups they tend to bind to the iridium center and inhibit further reactivity. The alcohol dehydrogenation reactions with tBuQ were the most successful, reaching 80% conversion at 70°C after 24 hours. While going to higher temperatures may increase speed and reactivity of the catalyst, conducting electrochemistry at temperatures >100°C under inert atmosphere is very difficult. Our collaborators found that the (^{iPr}PCP)IrH_4 catalyst can perform alcohol dehydrogenation using the parent benzoquinone rapidly at room temperature.[26] Since the (^{iPr}PCP)IrH_4 catalyst was performing better at lower temperatures, all further work on this project was done by our collaborators focusing on the (^{iPr}PCP)IrH_4 system.

4.4: Summary

This brief study has shown that substituted *para*-benzoquinones are extremely good hydrogen acceptors. The parent benzoquinone and tetrafluoroquinone are able to accept hydrogen upon mixing with (^{tBu}PCP)IrH_4 at room temperature. As you add bulk to the quinones the reaction runs slower and needs heat to occur. However, the downside to using quinones is their ability to react strongly with the iridium center to create the "barber-chair" complexes. These "barber-chair" complexes are quite stable and inhibit alkane dehydrogenation from occurring. Again, adding bulk to the quinone helps prevent this iridium-quinone interaction and using 2,5-di-*tert*-butylquinone we were able to perform alcohol dehydrogenation of isopropanol achieving 80% conversion at 70°C after 24 hours.

4.5: Experimental

General Methods. All manipulations were carried out under argon using standard glovebox techniques. All experiments were carried out in a J-Young NMR tube. Deuterated solvents were degassed via freeze-pump-thaw cycles, dried over activated Al_2O_3, and stored over 3 Å molecular sieves prior to use. Reagents used as substrates for reactions with (^{tBu}PCP)Ir were purchased from commercial suppliers. (^{tBu}PCP)IrH_4 was synthesized following literature procedure.[30]

All ^{1}H and ^{31}P NMR spectra were recorded on 400 MHz and 500 MHz Varian spectrometers. Chemical shifts are reported in ppm. The ^{1}H NMR signals are referenced to the residual solvent signals, and the ^{31}P NMR signals are referenced to an external standard of $P(CH_3)_3$. GC analyses (FID detection) were conducted on a Varian 430 instrument equipped with a Varian FactorFour capillary column.

General Procedures for Reactions of (^{tBu}PCP)IrH_4 and quinones:

Inside the glovebox, 5 mg of (^{tBu}PCP)IrH_4 was mixed with 10 eq. of quinone in 0.5 mL p-xylene-d_{10} in a J-Young NMR tube. The reaction was then mixed at room temperature for 24 hours. For the DQ and tBuQ, the reactions were then heated to 40^{o}C and left to react for another 24 hours. All attempts to crystallize products and intermediates were unsuccessful.

General Procedure for Attempted Alkane Dehydrogenation:

Inside the glovebox, 6 mg of (^{tBu}PCP)IrH_4 was mixed with 3 eq. of quinone, 67 µL of cyclooctane, and 2.4 mg hexamethylbenzene standard in 433 µL p-xylene-d_{10} in a J-Young NMR tube. The reaction was then heated at 100°C 24 hours. No cyclooctene was observed by NMR or GC.

Procedure for Trap Experiment with 2-phenylpyridine:

Using tBuQ as an acceptor

5.8 mg of (^{tBu}PCP)IrH_4 was dissolved in 0.5 mL of p-xylene-d_{10}. To the reaction 7.65 mg of tBuQ and ~3.2 uL of 2-phenylpyridine were added. The reaction was heated at 70°C for 72 hours. Two isomers were observed by NMR in a 10:1 ratio (C-trans:N-trans). C-trans isomer: ^{31}P NMR (162 MHz, p-xylene-d_{10}) C-trans isomer: δ 47.19 (s) N-trans isomer: δ 45.51 (s). ^{1}H NMR (400 MHz, p-xylene-d_{10}) PCP aryl H peaks and some ppy H peaks are obscured by free substrate and solvent peaks. δ 9.34 (d, *J* = 5.6 Hz, ppy*H,* 1H),), 8.75 (d, *J* = 4.6 Hz, ppy*H,* 1H), 8.29 (d, *J* = 8.3 Hz, ppy*H,* 1H), 7.89 (d, *J* = 7.6 Hz, ppy*H,* 1H), 7.60 (t, *J* = 6.4 Hz, *ppyH, 2H*), 7.40 (d, *J* = 7.8 Hz, ppy*H,* 1H), 3.19 (dt, *J* = 16.0, 3.6 Hz, 2H, CH_2), 3.04 (dt, *J* = 15.9, 4.4 Hz, 2H, CH_2), 1.27 (t, *J* = 6.0 Hz, 18H, C(CH_3)$_2$), 0.51 (t, *J* = 6.1 Hz, 18H, C(CH_3)$_2$), -9.573 (t, *J* = 18.9 Hz, 1H, Ir-*H*). N-trans isomer. Due to very low concentration, only the hydride peak could be identified. -18.4 (t, *J* = 17.3 Hz, Ir-*H*).

Using FQ as an acceptor

The reaction above was also done with FQ. Same exact amounts and conditions were used. No (^{tBu}PCP)Ir(ppy)H was observed.

Alkane Dehydrogenation using tBuQ as an acceptor:

A mixture was made of 500 mM isopropanol, 10 eq. ditertbutylquinone, and 20 mM (^{tBu}PCP)IrH_4 in toluene. The reaction was heated at the desired temperature (40^{o}C or 70^{o}C) for 24 hours. The mixture was cooled to room temperature and the products were then identified/quantified using NMR and GC.

4.6: References

1) Chatt, J.; Davidson, J. M. *J. Chem. Soc.* **1965**, 843.
2) Janowicz, J. A.; Bergman, R. G. *J. Am. Chem. Soc*. **1982**, *104*, 352.
3) Hoyano, J. K.; Graham, W. A. G. *J. Am. Chem. Soc.* **1982**, *104*, 3723.
4) Buchanan, J. M.; Stryker, J.M.; Bergman, R. G. *J. Am. Chem. Soc.* **1986**, *108*, 1537.
5) Northcutt, T. O.; Wick, D.D.; Vetter, A. J.; Jones, W. D. *J. Am. Chem. Soc.* **2001**, *123*, 7257.
6) Bryndza, H. E.; Fong, L. K.; Paciello, R.A.; Tam, W.; Bercaw, J.E. *J. Am. Chem. Soc.* **1987**, *109*, 1444.
7) Crabtree, R.H.; Mellea, M. F.; Mihelcic, J. M.; Quirk, J. M. *J. Am. Chem. Soc.* **2012**, *134*, 9276.
8) Afeefy, H. Y.; Liebman, J. F.; Stein, S. E., "Neutral Thermochemical Data" In NIST Chemistry Webbook, NIST Standard Reference Database Number 69; Linstrom, P. J., Mallard, W. G., Eds. Gaithersburg, MD, http://webbook.nist.gov/chemistry/, (retrieved September 28, 2012).
9) Crabtree, R. H.; Mihelcic, J. M.; Quirk, J. M. *J. Am. Chem. Soc*. **1979**, *101*, 7738.
10) Burk, M. J.; Crabtree, R. H. *J. Am. Chem. Soc*. **1987**, *109*, 8025.
11) Maguire, J. A.; Boese, W. T.; Goldman, A.S. *J. Am. Chem. Soc*. **1989**, *111*, 7088.
12) Rosini, G. P.; Soubra, S.; Vixamar, M.; Wang, S.; Goldman, A. S. J. *Organomet. Chem.* **1998**, *554*, 41.
13) Gupta, M.; Hagen, C.; Flesher, R. J.; Kaska, W. C.; Jensen, C. M. *Chem. Commun.* **1996**, 2083.
14) Liu, F.; Pak, E. B.; Singh, B.; Jensen, C. M.; Goldman, A. S. *J. Am. Chem. Soc*. **1999**, *121*, 4086.
15) Kanzelberger, M.; Singh, B.; Czerw, M.; Krogh-Jespersen, K.; Goldman, A. S. *J. Am. Chem. Soc.* **2000**, *122*, 11017.
16) Renkema, K. B.; Kissin, Y. V.; Goldman, A. S. J. Am. Chem. Soc. 2003, 125, 7770.
17) Xu, W.; Rosini, G. P.; Gupta, M.; Jensen, C. M.; Kaska, W. C.; Krogh-Jespersen, K.; Goldman, A. S. Chem. Commun. 1997, 2273.
18) Liu, F.; Goldman, A. S. *Chem. Commun.* **1999**, 655.
19) Park, J; Kumar, V; Wang, X; Lee, P; Kim, W. *ACS Appl. Mater. Interfaces*, **2017**, *9*, 33728-33734.
20) Tashiro, M.; Koya, K.; Yamato, T.; *J. Am. Chem. Soc.* **1982**, *104*, 3707.
21) Koning, C. B.; Giles, R. G. F.; Knight, L. S.; Niven, M. L.; Yorke, C. S.; *J. Chem. Soc., Perkin Trans. 1* **1988**, 2477.
22) Mackenzie, A. R.; Moody, J. C.; Rees, C. W.; *Tetrahedron* **1986**, *42*, 3259.
23) Huynh, M. T.; Anson, C. W.; Cavell, A. C.; Stahl, S. S.; Hammes-Sciffer, S. *J. Am. Chem. Soc.* **2016**, *138*, 15903- 15910.
24) Chen, Q. *Chemical Engineering and Processing* **2008**, *47*, 787-792.
25) Sella, E; Shabat, D. *Org. Biomol. Chem.* **2013**, *11*, 5074-5078.
26) Wilklow-Marnell, M; Brennessel, W; Jones, W. *Polyhedron* **2017**, *143*.
27) Amouri, H; Vaissermann, J; Rager, M; Grotjahn, D. *Organometallics* **2000**, *19*, 1740-1748.

28) Moussa, J; Guyard-Duhayon, C; Herson, P; Amouri, H; Rager, M; Jutand, A. *Organometallics* **2004**, *23*, 6231-6238.
29) Hernandez-Juarez, M; Salazar, V; Garcia-Baez, E; Padilla-Martinez, I; Hopfl, H; Rosales-Hoz, M. *Organometallics* **2012**, *31*, 5438-5451.
30) (a) Gupta, M.; Hagen, C.; Flesher, R. J.; Kaska, W. C.; Jensen, C. M. *Chem. Commun.* **1996**, 2083-2084. (b) Gupta, M.; Hagen, C.; Kaska, W. C.; Cramer, R. E.; Jensen, C. M. *J. Am. Chem. Soc*. **1997**, *119*, 840-841. (c) Gupta, M.; Kaska, W. C.; Jensen, *C. M. Chem. Commun.* **1997**, 461-462.

Chapter 5

Exploring the use of (^{tBu}PCP)Ir Complexes

for Organic Light-Emitting Diode (OLED) Applications

Abstract:

One of the most integral parts of our everyday lives is the use of technology and electronics. Computers, phones, televisions, and gaming devices all have display technology primarily using liquid crystal displays. However, for the past few decades a significant amount of research has been dedicated to the development of organic-light emitting diode (OLED) displays. While there has been a decent amount of success with red and green diodes, an efficient "true-blue" diode has yet to be discovered. Herein we report the synthesis and characterization of (^{tBu}PCP)Ir(ppy)X, (^{tBu}PCP)Ir(fppy)X, and (^{tBu}PCP)Ir(nppy)X. (R = H or Cl, ppy = 2-phenylpyridine, fppy = 2-(2,4-difluorophenyl)pyridine, nppy=4-phenypyrimidine). Photoluminescence (PL) studies on these complexes in solution showed that the hydride complexes resulted in a green emission, while the chloride complexes resulted in a blue emission, near that of "true blue". PL and lifetime studies were then conducted on the three different chloride complexes in the solid state. However, preliminary results showed that the intensity of the complexes in the solid state decreased dramatically and could not be observed over the emission of the support material.

5.1: Introduction

Over the past two decades technology has become a constant in everyday life. Smartphones with high-resolution screens are in everyone's pockets and the large majority of the population looks at a computer or a television on a daily basis. As technology develops, electronics are becoming an indispensable staple of the modern world, and with this comes the necessary research to improve performance, reduce size, and increase durability/flexibility.

One of the most significant developments in electronics was the invention of liquid crystal displays (LCDs) in the 1960s.[1] Since their invention, extensive research has overcome many of the initial problems that faced LCDs and they are currently implemented in the majority of electronics. However, LCDs are non-emissive materials, meaning they require careful control and variation of voltage in order to produce various colors. They also require polarized glass to control the amount of light passing through the display.[2] The use of polarized glass means the screen and device are rigid and have little to no flexibility. Additionally, due to being non-emissive materials, they require a backlight.[1] This prevents a true black state, one that allows for better contrast and much better picture overall. Lastly, LCDs have a limited range of colors, however recent development of LCDs with quantum dot backlights have started to overcome this limitation.[3,4]

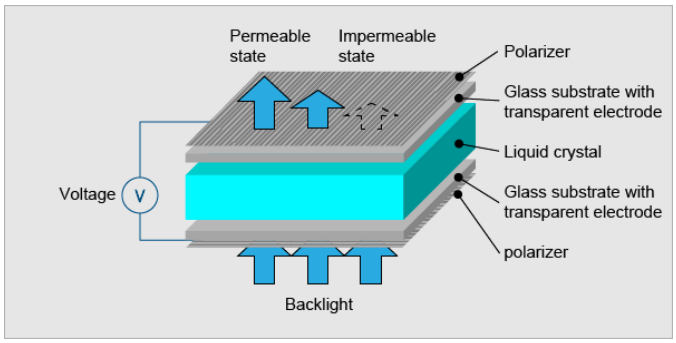

Figure 5.1: Typical Make-Up of a LCD Device[5]

The first proposed structure of an OLED display came from Tang and VanSlyke in 1987.[6] Their proposed structure was very simple in comparison to LCDs. The whole device consisted of two electrodes with organic emitting and hole-transporting layers in between. Organic layers can emit light on their own, so they do not require a backlight or polarized glass. Since this first proposal, OLED technology has come a long way. Now, it is more common to see multilayer OLED devices. Extra layers have been added to facilitate the transport of electrons for recombination in the organic layer, leading to higher quantum efficiency.

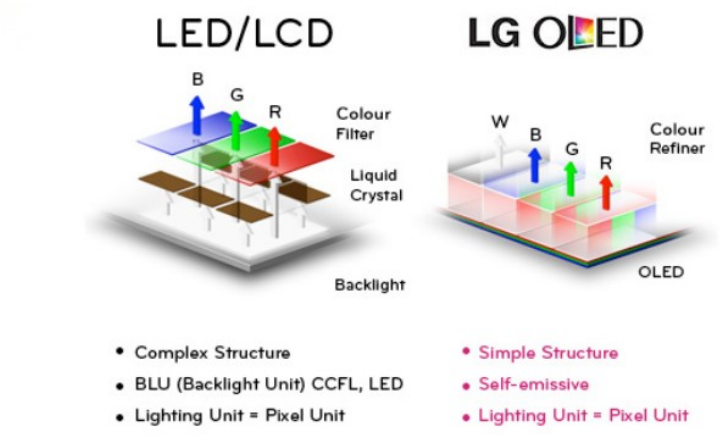

Figure 5.2: A Simple Comparison of LED/LCD and OLED devices[7]

Each layer of the OLED is extremely thin (the whole device is < 1 µm).[1] Since a rigid glass structure is no longer necessary in the construction of OLEDs, they are an ideal candidate for flexible displays. Additionally, due to their ability to self-emit light, the organic complexes used can be tuned to emit the ideal colors, leading to a significantly higher range of colors when compared to LCDs.[1,8] However, OLED displays have two major downfalls. The best reported fluorescent OLEDs only have theoretical internal quantum efficiencies (IQE) around 62% and as a result have a lower brightness than current LCDs.[1] Also, while red and green OLEDs have been developed with long lifetimes, the blue OLEDs have <25% of that lifetime.[8] This causes color distortions as the blue light degrades significantly faster than the red and green. Lastly, even though an OLED will consume only 40% of the power of a LCD device while displaying a black image, it can require three times as much to display a white image, using more power overall.[8] A full comparison of LCDs and OLEDs can be seen in Table 5.1.

Table 5.1: A Comparison of LCD and OLED Devices

LCDs	OLEDs
• Well developed • Well researched • Can reach black faster • Less screen "burn-in" • Less water sensitive • Longer life-time • Larger size • Cheaper	• Can use a plastic base (lighter and more durable) • Do not require backlighting • Can reach "true black" • Quicker response • More colors • Better picture • Thinner

To increase the IQE of OLEDs, researchers have begun introducing heavy metal atoms (such as Ir and Pt) into the emitters. By adding a metal, they can significantly reduce

the triplet lifetime, which results in phosphorescent emission. Additionally, the complex would now promote intersystem crossing from the singlet state to the triplet state. With the fast-intersystem crossing there is no longer a loss of energy, giving a theoretical IQE of 100%.[9]

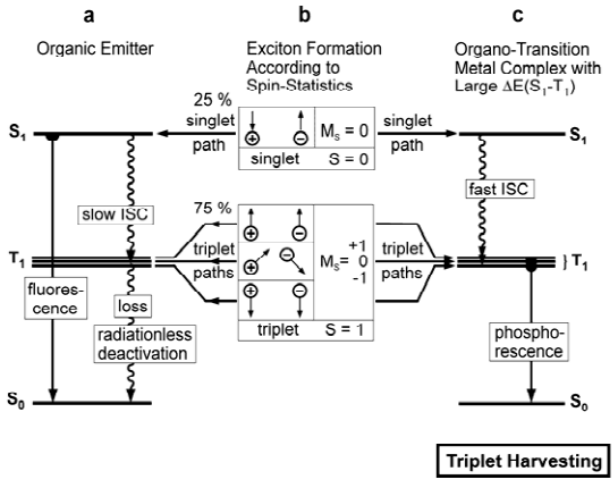

Figure 5.3: OLED Fluorescence vs PHOLED Phosphorescence[9]

The first iridium phosphorescent OLEDs (PHOLEDs) were proposed in 1999 and by the following year they showed nearly 100% IQE.[10,11] Since then, a wide range of iridium PHOLEDs have been studied for use in OLEDs of all colors, however the majority of research has focused on blue OLEDs. There are many reported iridium complexes that emit blue light, however almost 99% of them contain only monodentate and bidentate ligands. The first reported pincer-iridium complex for OLED study was an (NCN)Ir complex reported by Williams et. al. in 2006, seven years after the initial proposal of iridium PHOLEDs.[12] However, this complex emitted green light. Since then, the only report focusing on a blue-emitting pincer-iridium complex for OLEDs was in 2016 by Yun Chi et.

al.[13] In his more recent paper (2018), he shows that his pincer-ligated iridium complexes emitted in the blue-green range between 476 nm and 495 nm.[14] Closer than Williams, but not quite short-range enough for the desired “true blue” color.

Figure 5.4: (CNN)Ir Pincer Complexes Reported by Yun Chi in 2018[14]

Starting work in 2013, we were curious how our (^{tBu}PCP)Ir pincer complexes could perform in an OLED device. As stated above, at this time there were very few reports of pincer-ligated iridium complexes in the OLED literature, however pincer-ligated complexes containing platinum for OLEDs were first reported in 2001.[15] Following this, pincer complexes containing osmium and gold for OLEDs were first reported in 2012 and 2013 respectively.[16,17] The use of the pincer ligand added extra stability to the OLED and allowed for greater tunability of the emission wavelength. Following these literature examples, we decided to test our (^{tBu}PCP)Ir pincer complexes for their emission wavelength and potential use in OLED devices.

5.2: Synthesis and Characterization of (^{tBu}PCP)Ir Complexes for OLED Study

While much of literature you will find with pincer-metal complexes involves catalysis, their high stability makes them viable for other applications. Due to the

appearance of platinum, osmium, and gold pincer-complexes in the OLED literature, in addition to the numerous non-pincer iridium complexes,[18-23] we decided to synthesize several pincer-iridium complexes for comparison.

When combing through the literature on non-pincer iridium complexes for OLEDs, one common theme can be observed. In almost every complex, there is one or more bi- or tri-dentate ligands with nitrogens and/or carbons bound to the metal center.[18-22] The simplest ligand that fits this description is the phenylpyridine (ppy) ligand. For this reason, we started by synthesizing the (^{tBu}PCP)Ir(ppy)Cl complex and then went on to different phenylpyridine derivatives for comparison.

5.2.1 Synthesis of (^{tBu}PCP)Ir(ppy) Complexes

The synthesis of the (^{tBu}PCP)Ir(ppy)H complex was previously studied in our group.[24] (^{tBu}PCP)IrH_2/H_4 is mixed with an acceptor, such as norbornene, and in the presence of 2-phenylpyridine (ppy), the (^{tBu}PCP)Ir(ppy)H complex is produced. There are two different isomeric possibilities for the complex, one with the ppy carbon trans to the hydride (C-Trans) and one where the ppy nitrogen is trans to the hydride (N-trans). While attempting to optimize the reaction conditions and times, it was observed that when the reaction mixture is heated for shorter amounts of time (<5hrs), the C-Trans to N-Trans ratio is around 5:1. However, when heated longer (12 hrs) the ratio changes to 20:1, with the N-Trans complex barely visible via NMR. Each complex can be assigned via the hydride signals in the ^{1}H NMR. Due to the trans-influence of the nitrogen we expect the hydride signal to be further upfield, therefore we know it is the hydride signal seen

at -18.4 ppm whereas the C-Trans signal is only at -9.5 ppm. Additionally, the previous work done in our laboratory made a crystal of the C-Trans complex,[24] confirming the NMR.

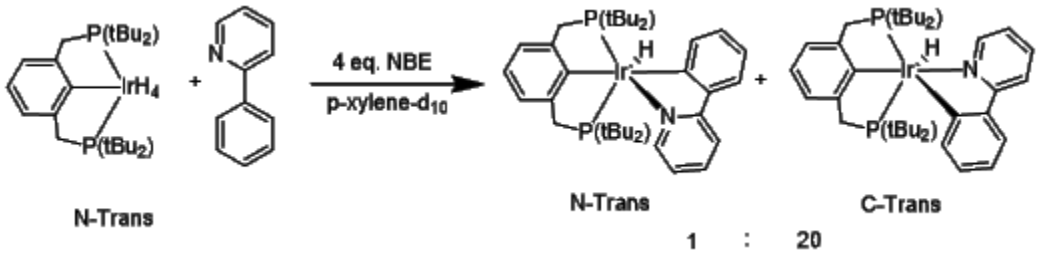

Scheme 5.1: Synthesis of (^{tBu}PCP)Ir(ppy)H N-Trans and C-Trans Complexes

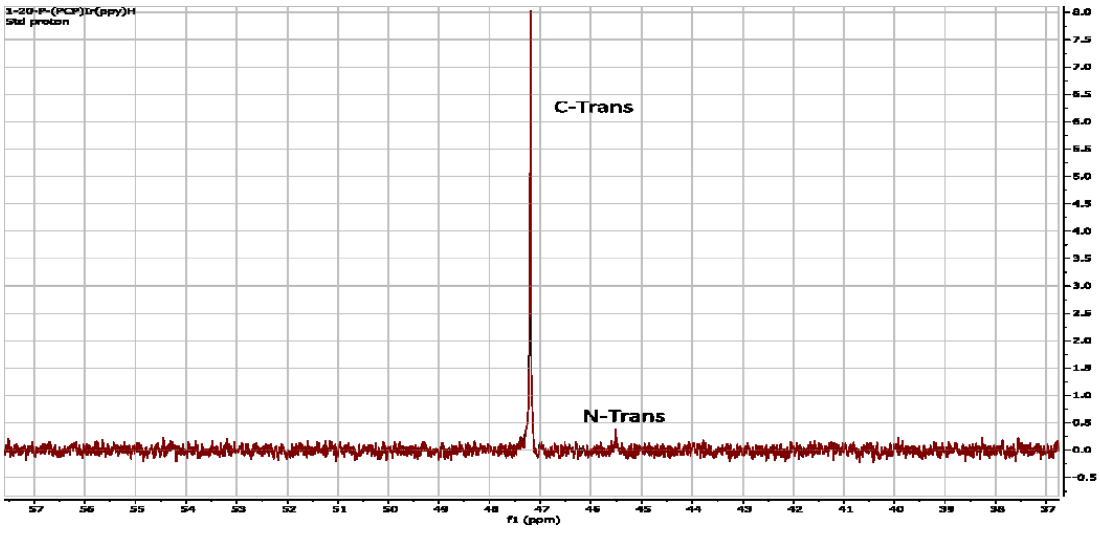

Figure 5.5: ^{31}P NMR of (^{tBu}PCP)Ir(ppy)H

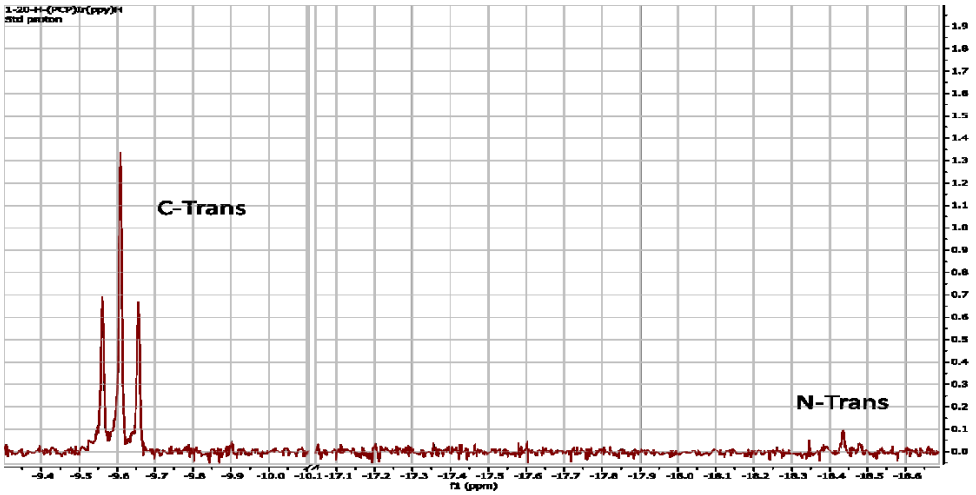

Figure 5.6: Hydride Peaks in ^{1}H NMR for (^{tBu}PCP)Ir(ppy)H

One of the desired qualities for OLED complexes is their high stability in a multitude of environments, which means ideally, they would be air-stable and water tolerant. The presence of a hydride on a pincer-iridum center could lead to the metal center reacting with small molecules such as oxygen, nitrogen, and water. Due to this, we decided to also synthesize the (^{tBu}PCP)Ir(ppy)Cl complex, hoping to prevent any reactivity.

Our first attempt to make the (^{tBu}PCP)Ir(ppy)Cl complex was done by adding HCl to a solution of the complex, however we observed no real reaction. Soon we discovered that adding CCl_4 to a hydride complex is a very efficient way to substitute the hydride with a chloride. Doing this we were able to obtain the (^{tBu}PCP)Ir(ppy)Cl complex in high purity for testing. When exposing the pure complex to air and wet solvent, no change occurred. This confirmed our hypothesis that the chloride would help prevent any reactivity. However, when we exposed the (^{tBu}PCP)Ir(ppy)H complex to air and wet solvent as well, in contrast to our hypothesis, no reactivity occurred. While unexpected, this showed us

that both the hydride and chloride complexes were very stable and had fit one of the highly preferred characteristics of OLED complexes.

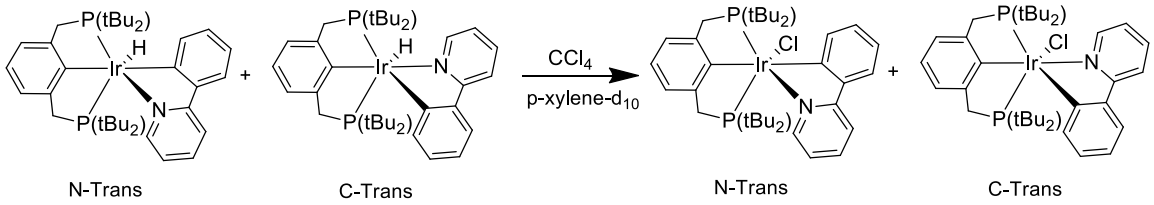

Scheme 5.2: Synthesis of (^{tBu}PCP)Ir(ppy)Cl N-Trans and C-Trans Complexes

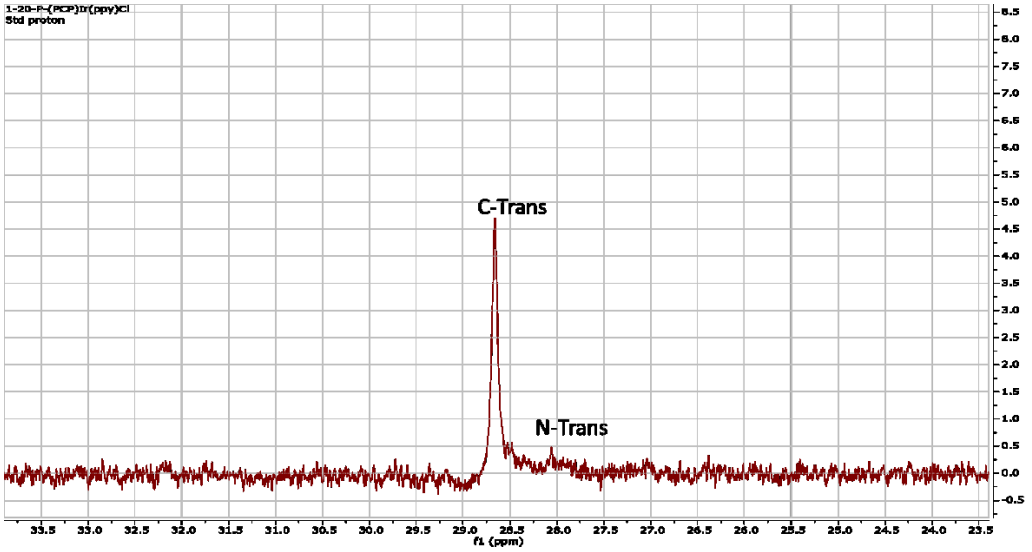

Figure 5.7: ^{31}P NMR of (^{tBu}PCP)Ir(ppy)Cl

5.2.2 Synthesis of (^{tBu}PCP)Ir(Xppy) Derivatives

In addition to the parent (^{tBu}PCP)Ir(ppy) complexes, we decided to synthesize two derivatives for comparison. This was done in order to learn more about the effect of the ppy ligand on the emission of the complex and hopefully provide some insight for future complexes.

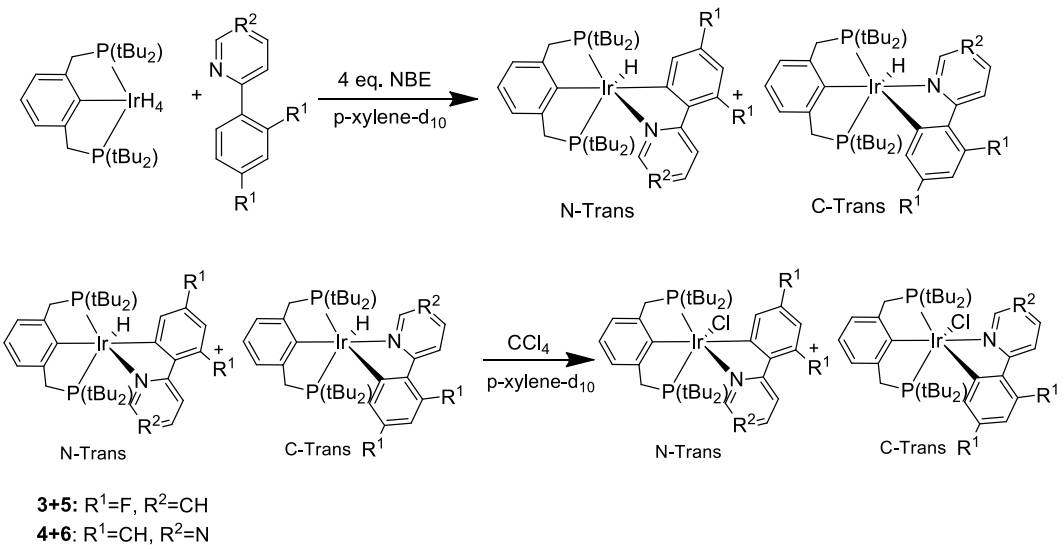

Scheme 5.3: Synthesis of (^{tBu}PCP)Ir(fppy) and (^{tBu}PCP)Ir(nppy) Complexes

The first derivative chosen was 2-(2,4-diflurophenyl)pyridine (fppy). This ligand was chosen because it was one of the derivatives most commonly observed in the literature. Similar to the (^{tBu}PCP)Ir(ppy) complexes, the reaction of (^{tBu}PCP)IrH_2/H_4 with the fppy ligand resulted in two isomeric species. However, in contrast to the ppy, the fppy had significantly less N-Trans product. Often the concentration was so low that we were unable to consistently observe it via NMR. Both the chloride and hydride complexes were synthesized.

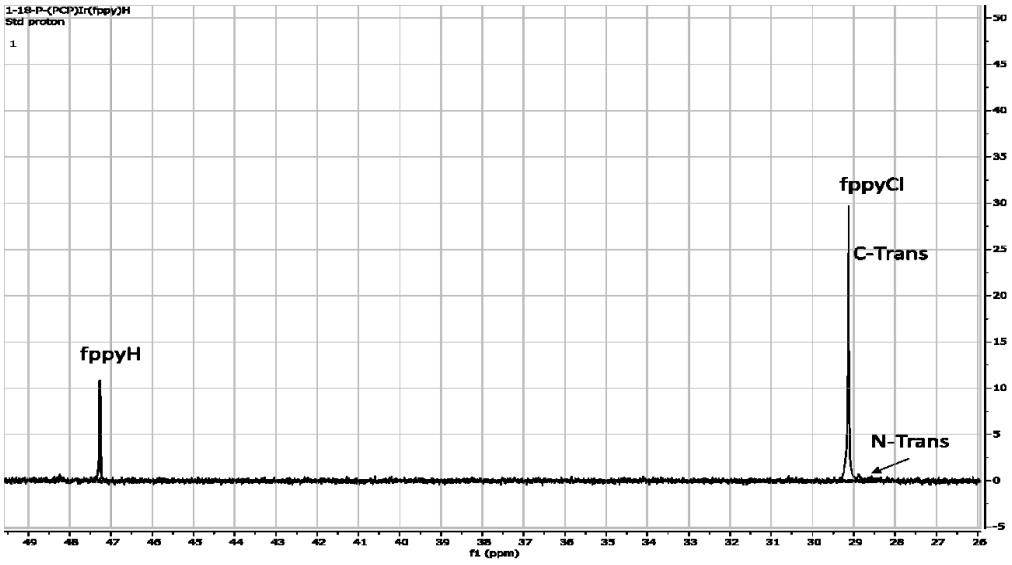

Figure 5.8: ^{31}P NMR of fppyH and fppyCl Complexes

The second derivative chosen was 4-phenylpyrimidine (nppy). This ligand was chosen because we were interested in how the addition of another nitrogen effected the emission. Unlike the other two complexes, upon initial heating, the solution immediately reacted and turned a dark green. The ^{31}P NMR shows one major species at 64.50 ppm with a corresponding hydride signal at -25.00 ppm in the ^{1}H NMR. We believe that this initial reaction is coordination of the nppy ligand via the nitrogen para to the phenyl ring (Figure 5.9). However, due to there being multiple species, we were unable to isolate this green complex to confirm.

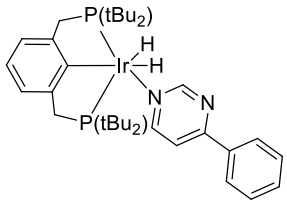

Figure 5.9: Hypothesized Configuration for Unknown Green (^{tBu}PCP)Ir(nppy) Complex

After heating the solution overnight, a color change from green to yellow is observed. When isolated the ^{31}P NMR shows that the products are primarily the C-Trans and N-Trans isomers. Both the chloride and hydride (^{tBu}PCP)Ir(nppy) complexes were synthesized and these complexes, along with the fppy and ppy versions, were sent to our collaborators for study.

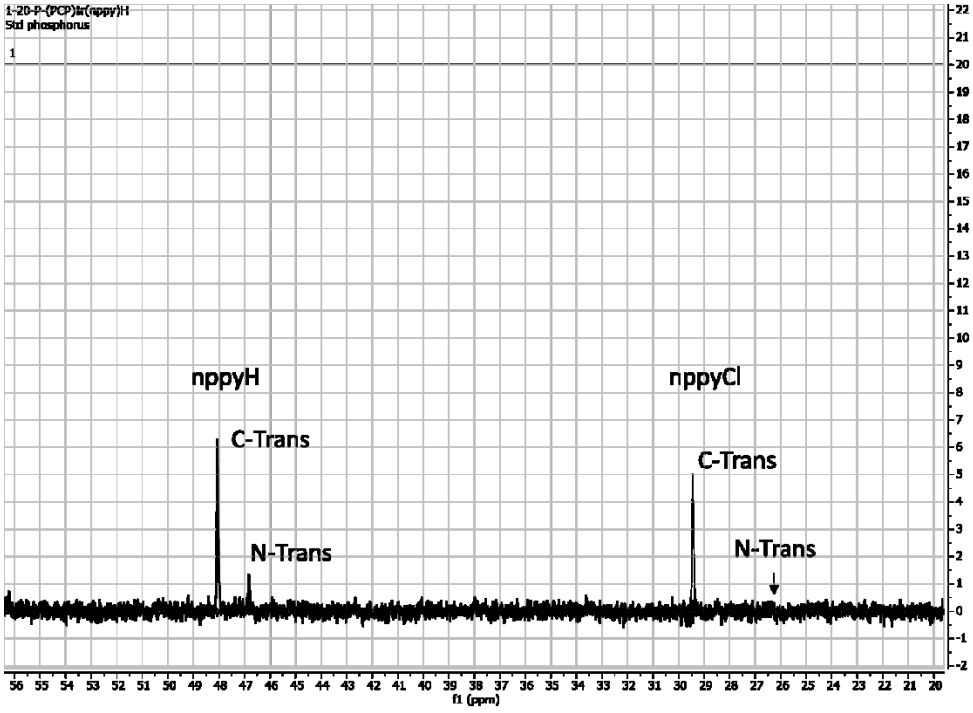

Figure 5.10: ^{31}P NMR of nppyH and nppyCl Complexes

5.3: Photoluminescence (PL) and Intensity Studies

All PL and absorbance studies were performed by the lab of our collaborator, Dr. Deirdre O'Carroll. A preliminary PL study showed that the complexes with a hydride emit at a wavelength in the green region. However, the chloride variants were more blue-shifted and emitted wavelengths in the desired blue region. Due to this, all further studies were performed on the chloride variants of each derivative.

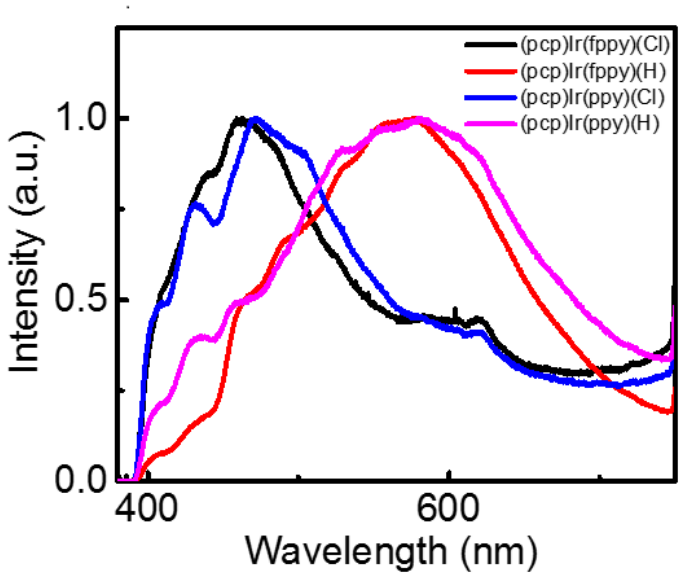

Figure 5.11: PL Study Performed on (^{tBu}PCP)Ir(ppy)H/Cl and (^{tBu}PCP)Ir(fppy)H/Cl

After the preliminary results, our collaborators did a more in-depth PL study on the three (^{tBu}PCP)Ir(Xppy)Cl complexes. Looking at the parent (^{tBu}PCP)Ir(ppy)Cl complex, an emission wavelength of 465 nm was observed. However, in comparison to the other two complexes the intensity of the emission was extremely low. The (^{tBu}PCP)Ir(fppy)Cl derivative emitted at 455 nm, slightly more blue-shifted than the parent complex, however the intensity of the emission was almost 4 times that of the parent complex. Lastly, the (^{tBu}PCP)Ir(nppy)Cl complex unexpectedly had two emissions at 460 and 510 nm. Other iridium complexes with the nppy ligand usually show a single emission. Also, the emission wavelengths of the -Cl complexes seem to be consistently around 460 nm. We believe that the 510 nm emission is most likely due to an impurity. However, new sample is needed to confirm this. Overall, the emission intensity was slightly lower than the fppy complex, however it was still much stronger than the parent complex.

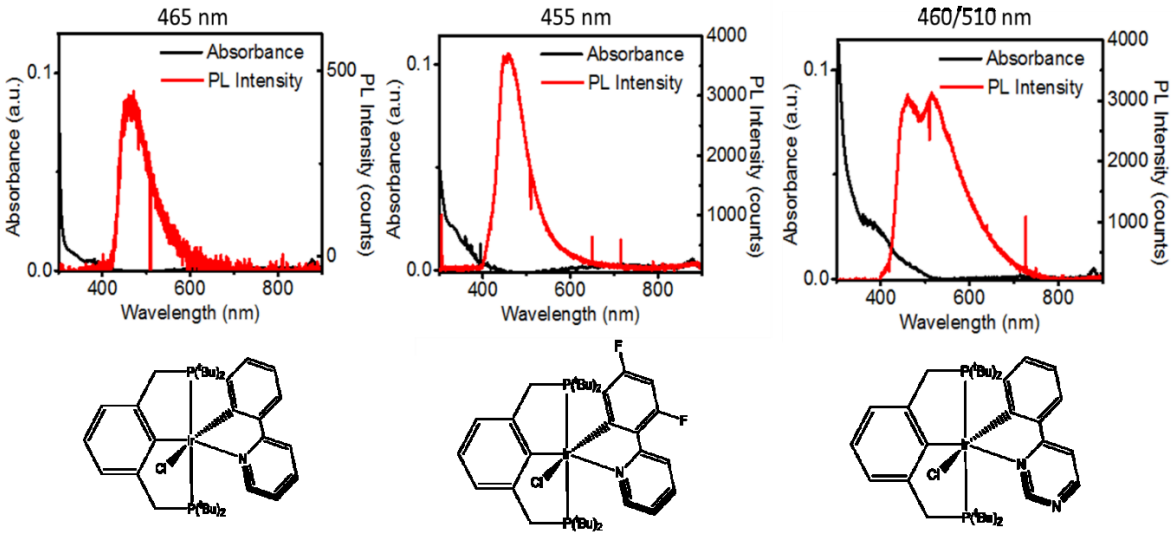

Figure 5.12: PL Study for (A) (^{tBu}PCP)Ir(ppy)Cl, (B) (^{tBu}PCP)Ir(fppy)Cl, and (C) (^{tBu}PCP)Ir(nppy)Cl

From these results we can derive several things. First, the addition of the second nitrogen to the complex has little impact on the shift of the blue wavelength, however it greatly increases its intensity. Secondly, the addition of the fluorine on the phenyl ring results in a 10 nm blue-shift and a significant intensity increase. A similar effect was observed by Nazeeruddin et. at. in 2012.[25] While exploring the influences of halogen atoms in Ir(Xppy) complexes, they observed that the addition of a fluorine resulted in a blue shift due to a stabilization of the HOMO. In their complex, the HOMO is spread over the fppy ligand while the LUMO is closer to the auxiliary picolinate ligand. Due to the proximity of the fluorine to the HOMO and LUMO orbitals, it lowers the energy of the HOMO more than the LUMO, resulting in a larger HOMO-LUMO gap, and therefore a blue-shift.

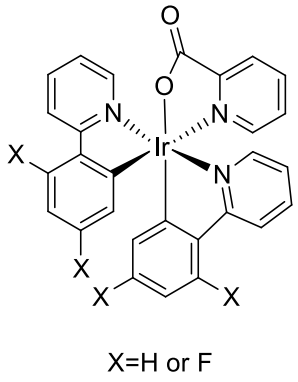

Figure 5.13: Complex Studied by Nazeeruddin et. al.

Another phenomenon we observed from the previous study is the transition from a -H ligand to a -Cl ligand has a significant effect. As previously stated, when the complexes had a -H ligand, they emitted a green wavelength and with a -Cl ligand they emitted a blue wavelength. In a more recent paper by Yun Chi in 2018, (CNN)Ir pincer-complexes were studied for their phosphorescence.[14] In contrast to our results, the substitution of an Ir-H bond for an Ir-Cl bond has minimal to no effect. However, in their complexes the HOMO and LUMO were spread over the pincer ligand and the chloride was in an axial position to the pincer. Another study by Kim et. al. showed similar results to Yun Chi. In his complex, the HOMO is primarily located over the phenyl ring and metal while the LUMO is over the pyridyl ring.[26] In contrast to Yun Chi, the chloride is equatorial to the ligand with the HOMO and LUMO orbitals, however there is still no effect on the emission wavelength.

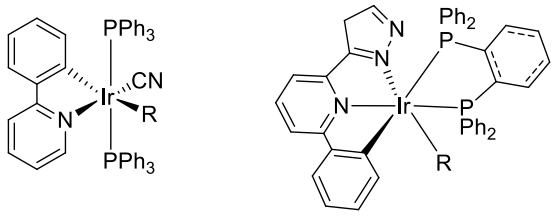

R= H or Cl
Kim et. al. 2008

R= H or Cl
Yun Chi et. al. 2018

Figure 5.14: Complexes Studied by Yun Chi and Young Kwan Kim

A comprehensive study of electron transfer in iridium-ppy complexes is reported in the dissertation of Johannes Klein.[27] In this dissertation they look into the HOMO and LUMO energies in different $Ir(Xppy)_2(L)$ derivatives. One thing they observed was that the primary HOMO-LUMO absorption for these complexes is metal-to-ligand charge transfer between the t_{2g}(Ir)-π(L)-orbital (HOMO) on the phenyl pyridine ligand to the π*(L') orbital (LUMO) of the ancillary ligand. These results are consistent with the reports previously discussed.

From these papers, it is difficult to hypothesize exactly why the chloride ligand in our complexes is having such a significant effect on the emission wavelength where in previous cases little to no effect is observed. The blue-shift of the wavelength shows an increase in the HOMO-LUMO gap. Following the report by Klein, we can hypothesize that our HOMO orbital is over the ppy ligand while the LUMO is spread over the PCP ligand. This suggests that the chloride ligand is either stabilizing the HOMO or destabilizing the LUMO. However, without in-depth modeling and electrochemical studies to determine the specific locations of the HOMO and LUMO, it is difficult to distinguish exactly what is happening.

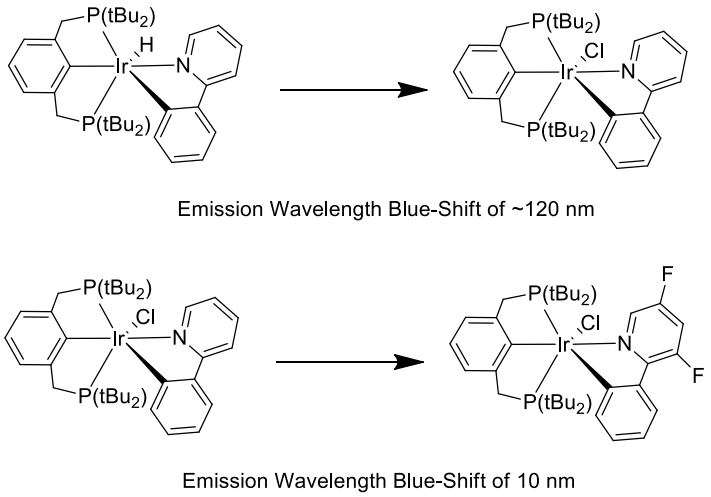

Figure 5.15: Effects of Fluorine and Chlorine on Emission Wavelength

Another observation we can make is that our complexes fall extremely close to the "true blue" wavelength of 470 nm. As stated in previously, the closest a reported pincer-ligated iridium complex has come to the "true blue" color is an emission wavelength in the blue-green range. Therefore, our complexes are the first pincer-ligated iridium complexes to emit the correct blue color. With some fine tuning using different electron-donating or withdrawing substituents, it is possible that we could achieve the ideal wavelength of 470 nm. With these exciting results in mind, we moved onto study the performance of our complexes in the solid-state.

5.4: Solid-state Performance Studies

In order to study the performance of each complex, a solution of complex in toluene was mixed with polymethylmethacrylate (PMMA) and spin coated onto a glass surface. PMMA was chosen because it is a substance that could easily support our complexes without reacting with them in any way. The coated glass was then studied

under a laser for 48 hours. It was immediately discovered that the intensity of emission from the complexes was significantly lower than that of PMMA. Due to this, no lifetime study could be performed because the emission of the complex was hidden under the emission signal from PMMA. This result was unexpected since in solution the complexes had a fairly high intensity (3700 counts in solution vs. <600 counts in the solid state).

(^{tBu}PCP)Ir(fppy)Cl in PMMA

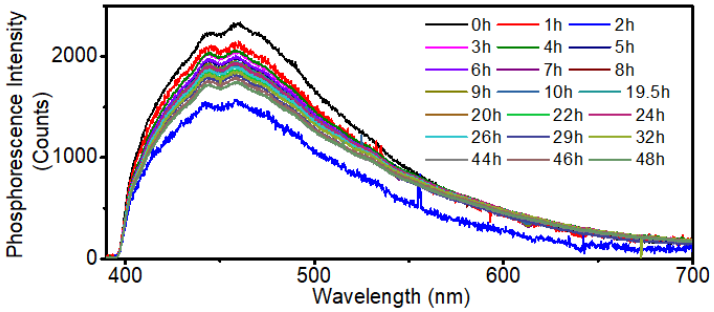

Only PMMA

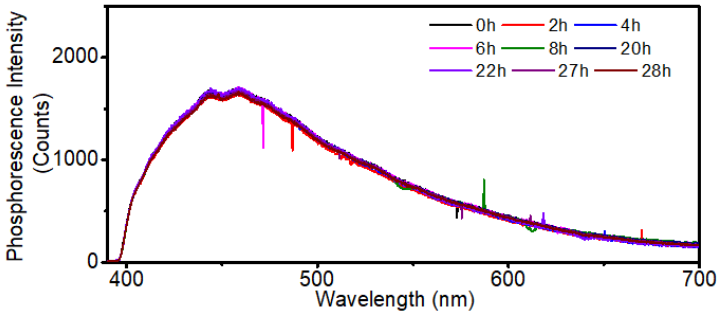

Figure 5.16: Lifetime Study on (^{tBu}PCP)Ir(fppy)Cl in PMMA vs Only PMMA

There are several possible reasons that the complex does not emit well in the solid state. In the solid state the molecular confirmation of the complex becomes less flexible and can potentially change compared to when it is in solution. Additionally, there is the possibility for aggregation and quenching of the complex when put into the solid state. It

is also possible that the complex is not very stable in solid support over a long time. However, this seems unlikely due to the complex's long lifetimes when stored as a solid. Lastly, there is a possibility that PMMA is not a very compatible host. However, when a reported emitter, FIrpic, was tested in identical conditions with PMMA, the emission could be observed with an intensity of nearly 8000 counts.

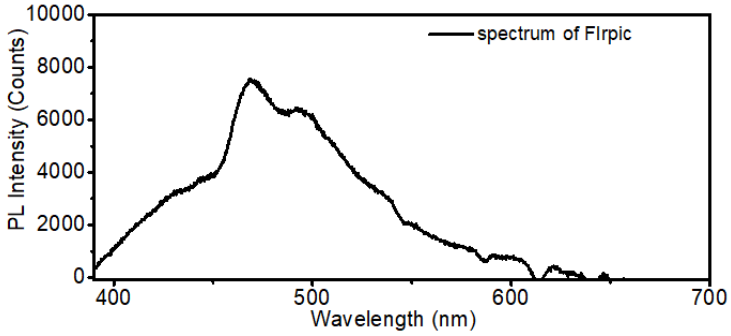

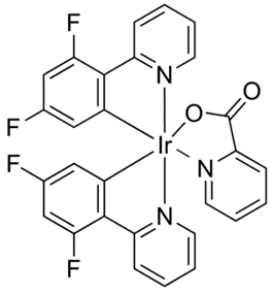

FIrpic

Figure 5.17: PL study of FIrpic in PMMA on Glass

5.5: Summary

The synthesis of several (^{tBu}PCP)Ir(ppy) derivatives were reported and studied for potential use in OLEDs. Initial studies on the complexes in solution showed a decent emission intensity. Also, the (^{tBu}PCP)Ir(ppy)X derivatives with a chloride ligand on the metal produced a blue emission wavelength, while the complexes with a hydride ligand on the metal produced a green emission wavelength. Furthermore, the addition of fluorine to the ppy ligand resulted in a blue-shift around 10 nm. The parent (^{tBu}PCP)Ir(ppy)Cl complex was the closest to the ideal "true blue" wavelength of 470 nm, emitting at 465 nm. This being the closest a pincer-ligated iridium complex has come to the ideal wavelength. Each complex was then tested in a PMMA support on a glass surface to observe the activity while in the solid state. In contrast to their performance in solution, the complexes had a very low intensity in the PMMA support and we were unable to perform any lifetime studies. While further research and optimization may have led to a better intensity in the solid state, the extremely poor performance in comparison to known iridium complexes led us to end this project.

5.6: Experimental

General Methods. All manipulations were carried out under argon using standard glovebox techniques. All experiments were carried out in a J-Young NMR tube. Anhydrous p-xylene was purchased from Sigma-Aldrich and degassed by purging with argon. Deuterated solvents were degassed via freeze-pump-thaw cycles, dried over activated Al_2O_3, and stored over 3 Å molecular sieves prior to use. Norbornene (NBE) was purified by sublimation. Reagents used as substrates for reactions with (^{tBu}PCP)Ir were purchased from commercial suppliers. All stock solutions (1M) were made with anhydrous p-xylene. (^{tBu}PCP)IrH_2/H_4 was synthesized following literature procedure.[28] The (^{tBu}PCP)Ir(ppy)H was synthesized via a modified literature procedure.[24]

All ^{1}H and ^{31}P NMR spectra were recorded on 400 MHz and 500 MHz Varian spectrometers. Chemical shifts are reported in ppm. The ^{1}H NMR signals are referenced to the residual solvent signals, and the ^{31}P NMR signals are referenced to an external standard of $P(CH_3)_3$. MestReNova software 12.0 was used to analyze NMR and predict spectra for help identifying PCP aryl and ppy peaks between 6.5 and 10.0 ppm.

Modified (^{tBu}PCP)Ir(ppy)H Synthesis:

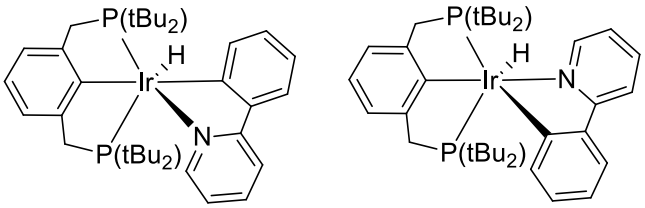

N-Trans C-Trans

20 microliters of a 1.0 M stock solution of (^{tBu}PCP)IrH_2/H_4 in p-xylene (0.020 mmol) was added to 0.378 mL of p-xylene-d_{10} tube at room temperature and 4 eq. of NBE were added from a 1.0 M stock solution. 2-Phenylpyridine (1.1 eq. 0.022 mmol) was added to the solution and after a few minutes the solution turned dark orange. After heating at 75^{o}C for 12 hr, the solution turned yellow. The solvent was evacuated resulting in a yellow solid. A mixture of C-trans (to the hydride) and N-trans isomers were observed in a 20:1 ratio. The complexes proved to be both air-stable and water tolerant. C-trans isomer: ^{31}P NMR (162 MHz, p-xylene-d_{10}) C-trans isomer: δ 47.19 (s) N-trans isomer: δ 45.51 (s). ^{1}H NMR (400 MHz, p-xylene-d_{10}) PCP aryl H peaks and some ppy H peaks are obscured by free substrate and solvent peaks. δ 9.34 (d, *J* = 5.6 Hz, ppy*H,* 1H),), 8.75 (d, *J* = 4.6 Hz, ppy*H,* 1H), 8.29 (d, *J* = 8.3 Hz, ppy*H,* 1H), 7.89 (d, *J* = 7.6 Hz, ppy*H,* 1H), 7.60 (t, *J* = 6.4 Hz, *ppyH, 2H*), 7.40 (d, *J* = 7.8 Hz, ppy*H,* 1H), 3.19 (dt, *J* = 16.0, 3.6 Hz, 2H, CH_2), 3.04 (dt, *J* = 15.9, 4.4 Hz, 2H, CH_2), 1.27 (t, *J* = 6.0 Hz, 18H, C(CH_3)$_2$), 0.51 (t, *J* = 6.1 Hz, 18H, C(CH_3)$_2$), -9.573 (t, *J* = 18.9 Hz, 1H, Ir-*H*). N-trans isomer. Due to very low concentration, only the hydride peak could be identified. -18.4 (t, *J* = 17.3 Hz, Ir-*H*).

Modified (tBuPCP)Ir(ppy)H Synthesis #2: In later experiments it was observed that the synthesis of (^{tBu}PCP)Ir(ppy)H could be performed acceptorless. The synthesis was performed in identical conditions to the one previously mentioned, however no NBE was added. Without acceptor the reaction rate was very similar, however eventual buildup of H_2 in the system inhibited the reaction from going to completion. Evacuating the H_2 buildup allowed for further reactivity. Like the previous reaction, the C-trans isomer was the major product in reaction.

Synthesis of (^{tBu}PCP)Ir(ppy)Cl:

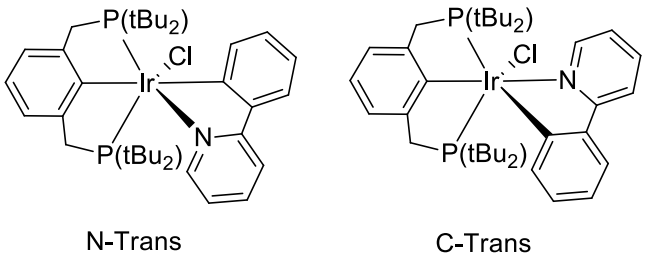

To the previous solution of (^{tBu}PCP)Ir(ppy)H, 10 microliters of carbon tetrachloride was added. The NMR tube was stirred at room temperature for 6 hr. The solution turned a lighter yellow and one complex was observable by phosphorous NMR. The solvent was removed, and the residue was dissolved in benzene. The solution was filtered and then an air-stable yellow solid was isolated after solvent removal. Both the C-trans and N-trans isomer could be seen in a 23:1 ratio. 34% Yield. ^{31}P NMR (162 MHz, Benzene-d_6) C-trans: δ 28.66 (s) N-trans: δ 28.06 (s). ^{1}H NMR (400 MHz, Benzene-d_6) C-trans: Most substrate and PCP aryl H peaks are obscured by free substrate and solvent peaks. δ 10.15 (d, J = 5.6 Hz, substrate H), 7.49 (d, J = 7.7 Hz, substrate H), 3.76 (dt, J = 15.1, 4.5 Hz, 2H, CH_2), 3.28

(dt, *J* = 15.1, 3.9 Hz, 2H, CH_2), 1.15 (t, *J* = 6.1 Hz, 18H, C(CH_3)$_2$), 0.32 (t, *J* = 5.8 Hz, 18H, C(CH_3)$_2$). N-trans concentration was too low to be clearly identified in proton NMR.

Synthesis of (^{tBu}PCP)Ir(fppy)H:

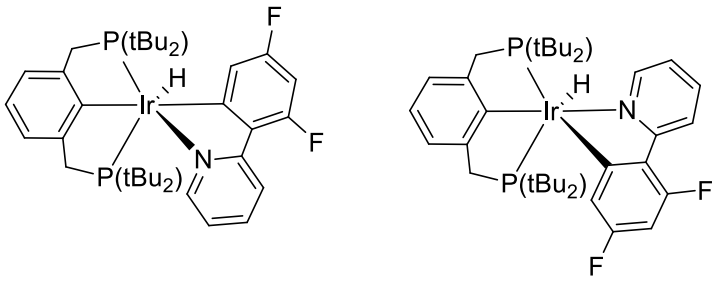

N-Trans C-Trans

20 microliter of a 1.0 M stock solution of (^{tBu}PCP)IrH_2/H_4 in p-xylene (0.020 mmol) was added to 0.378 mL of p-xylene-d_{10} in a J-Young NMR tube at room temperature and 4 eq. of NBE were added from a 1.0M stock solution in p-xylene. 2-(2,4-difluorophenyl)pyridine (1.1 eq. 0.022 mmol) was added to the solution and after a few minutes the solution turned dark orange. After heating at 75°C for 72 hr, the solution turned yellow. The solvent was then removed by vacuum to afford an air-stable yellow solid. Only the C-trans isomer was observed. 32% Yield. ^{31}P NMR (162 MHz, Benzene-d_6) δ 47.27 (s) ^{1}H NMR (400 MHz, Benzene-d_6) Most substrate and PCP aryl H peaks are obscured by free substrate and solvent peaks. δ 9.34 (d, *J* = 4.5 Hz, substrate H), 8.53 (dd, *J* = 5.0, 1.6 Hz, substrate H), 8.31 (d, *J* = 9.1 Hz, substrate H), 3.09 (dt, *J* = 16.0, 3.8 Hz, 2H, CH_2), 3.04 (dt, *J* = 16.2, 4.2 Hz, 2H, CH_2), 1.18 (t, *J* = 6.2 Hz, 18H, C(CH_3)$_2$), 0.47 (t, *J* = 6.2 Hz, 18H, C(CH_3)$_2$), -10.07 (t, *J* = 19.1 Hz, 1H, Ir-*H*). ^{19}F NMR (282 MHz, Benzene-d_6) δ -110.68 (qd, *J* = 8.7, 3.3 Hz), -110.83 – -110.99 (m).

Synthesis of (^{tBu}PCP)Ir(fppy)Cl:

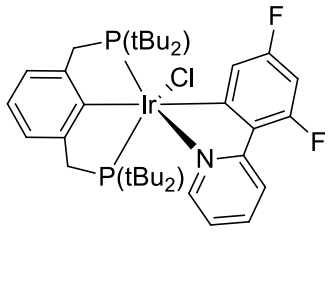

N-Trans

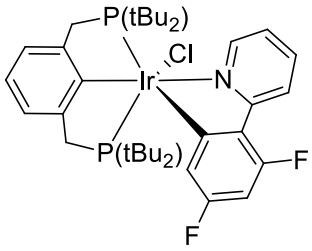

C-Trans

5.76 mg of (^{tBu}PCP)Ir(fppy)H was dissolved in 0.5 mL of p-xylene-d_{10} in a J-Young NMR tube. To this solution 0.08 mL of carbon tetrachloride was added. The NMR tube was heated overnight at 75°C. The solvent was then pulled by vacuum to afford an air-stable yellow crystalline solid. A very small amount of unknown hydride species was consistently observed in the proton NMR with a shift of -18.44 ppm (<2% of yield). In addition, both the C-trans (to the chloride) and N-trans isomer could be seen in a 33:1 ratio. ^{31}P NMR (202 MHz, Benzene-d_6) C-trans: δ 29.13 (s) N-trans 28.88 (s). ^{1}H NMR (400 MHz, Benzene-d_6) C-trans: Most substrate and PCP aryl H peaks are obscured by free substrate and solvent peaks. δ 10.13 (dd, *J* = 5.6, 1.8 Hz, C*H*, substrate H), 8.45 (d, *J* = 4.7 Hz, C*H*, 1H), 7.90 (d, *J* = 7.2 Hz, C*H*, 2H) 7.48 (dd, *J* = 5.7, 3.3 Hz, C*H*, 2H), 3.66 (dt, *J* = 15.6, 4.0 Hz, 2H, CH_2), 3.16 (dt, *J* = 15.1, 3.8 Hz, 2H, CH_2), 1.07 (t, *J* = 6.1 Hz, 18H, C(CH_3)$_2$), 0.31 (t, *J* = 5.9 Hz, 18H, C(CH_3)$_2$). N-trans was too low concentration to be clearly identified. ^{19}F NMR (470 MHz, Benzene-d_6) C-trans: δ -110.38 (q, *J* = 9.4 Hz), -110.70 (t, *J* = 11.6 Hz), N-trans: δ -110.33 (m), -110.62 (m).

Synthesis of (^{tBu}PCP)Ir(nppy)H:

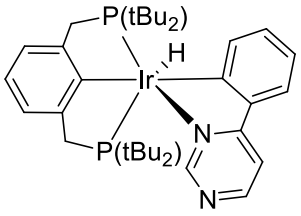

N-Trans

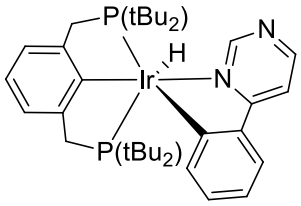

C-Trans

20 microliter of a 1.0 M stock solution of (^{tBu}PCP)IrH_2/H_4 in p-xylene (0.020 mmol) was added to 0.378 mL of p-xylene-d_{10} in a J-Young NMR tube at room temperature and 4 eq. of norbornene were added from a 1.0M stock solution in p-xylene. 4-Phenylpyrimidine (1.1 eq. 0.022 mol) was added to the solution. The NMR tube was placed in a 75^{o}C oil bath and within five minutes the solution turned dark green. The solution was left in heat overnight resulting in a yellow solution. Solvent was pulled by vacuum and a yellow solid was obtained. Both the C-trans and N-trans isomers were observed, in a 13:1 ratio, in addition to an unknown complex at 56.50 ppm in the ^{31}P NMR (15% of yield). ^{31}P NMR (162 MHz, Benzene-d_6) C-trans isomer: δ 48.33 (s) N-trans isomer: δ 47.11 (s). ^{1}H NMR (400 MHz, Benzene-d_6) C-trans isomer: Most substrate and PCP aryl H peaks are obscured by free substrate and solvent peaks. δ 8.61 (d, J = 4.6 Hz, substrate H), 8.17 (d, *J* = 5.4 Hz, substrate H), 8.12 (dd, *J* = 7.2, 1.7 Hz, substrate H), 7.63 (t, *J* = 7.0 Hz, substrate H), 3.19 (dt, *J* = 16.1, 3.6 Hz, CH_2, *2H*), 3.05 (dt, *J* = 15.9, 4.3 Hz, CH_2, 2H), 1.28 (t, *J* = 6.1 Hz, C(CH_3)$_2$, 25H), 0.56 (t, *J* = 6.1 Hz, C(CH_3)$_2$, 18H), -9.79 (t, *J* = 18.7 Hz, Ir-*H*, 1H). The N-trans and unknown complex were too low in concentration to be identified in the proton NMR.

Synthesis of (^{tBu}PCP)Ir(nppy)Cl:

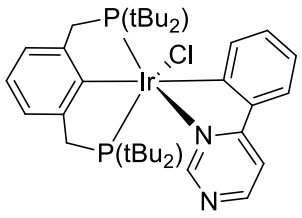

N-Trans

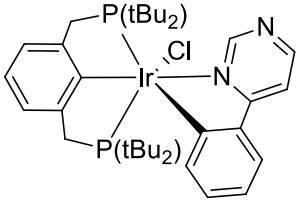

C-Trans

8.52mg of (^{tBu}PCP)Ir(fppy)H was dissolved in 0.5 mL of p-xylene-d_{10} in a J-Young NMR tube. To this solution 5 eq. of carbon tetrachloride was added. The NMR tube was heated overnight at 80°C. The solvent was then pulled by vacuum to afford an air-stable yellow crystalline solid. Both the C-trans and N-trans isomers were observed in a 62:1 ratio. ^{31}P NMR (162 MHz, Benzene-d_6) C-trans isomer: δ 29.44 (s) N-trans isomer: δ 26.33 (s). ^{1}H NMR (400 MHz, Benzene-d_6) C-trans isomer: Most substrate and PCP aryl H peaks are obscured by free substrate and solvent peaks. δ 9.26 (s, substrate H), 8.30 (d, *J* = 5.5 Hz, substrate H), 7.60 (d, *J* = 7.4 Hz, substrate H), 7.40 (dd, *J* = 7.3, 2.0 Hz, substrate H), 3.85 (dt, *J* = 15.0, 4.1 Hz, 2H, CH_2), 3.39 (dt, *J* = 15.2, 4.0 Hz, 2H, CH_2), 1.28 (t, *J* = 6.2 Hz, 18H, C(CH_3)$_2$), 0.49 (t, *J* = 5.9 Hz, 18H, C(CH_3)$_2$). N-trans isomer was in too low concentration to identify in the proton NMR.

5.7: NMR

(^{tBu}PCP)Ir(ppy)H

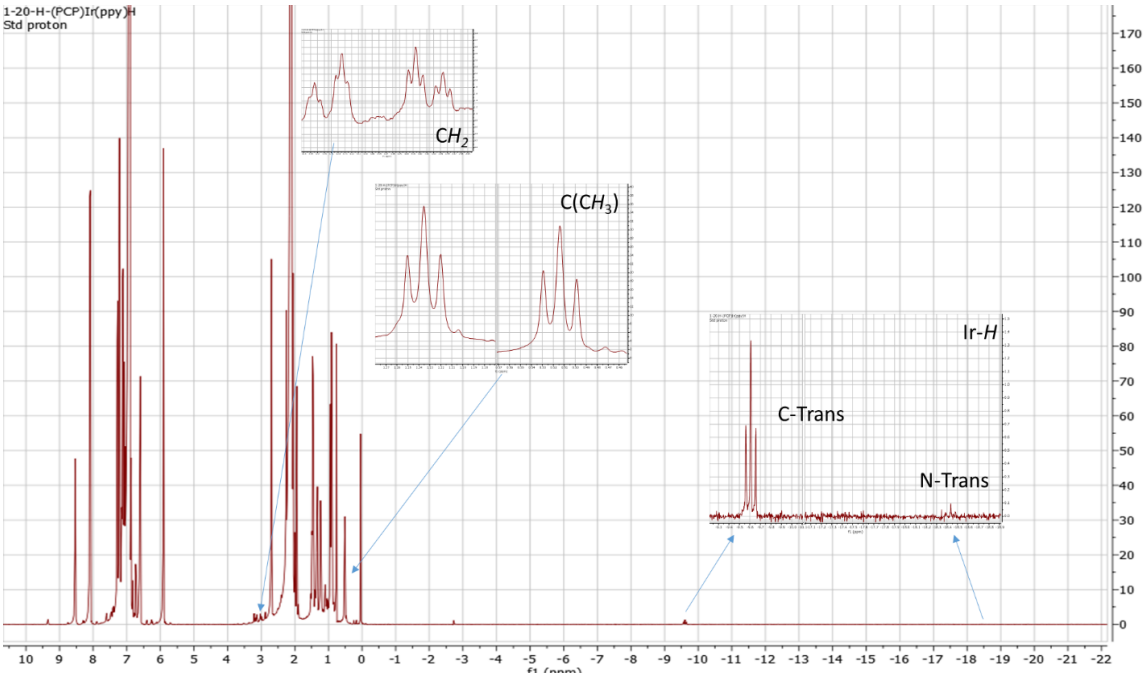

Figure 5.18: ^{1}H NMR of (^{tBu}PCP)Ir(ppy)H

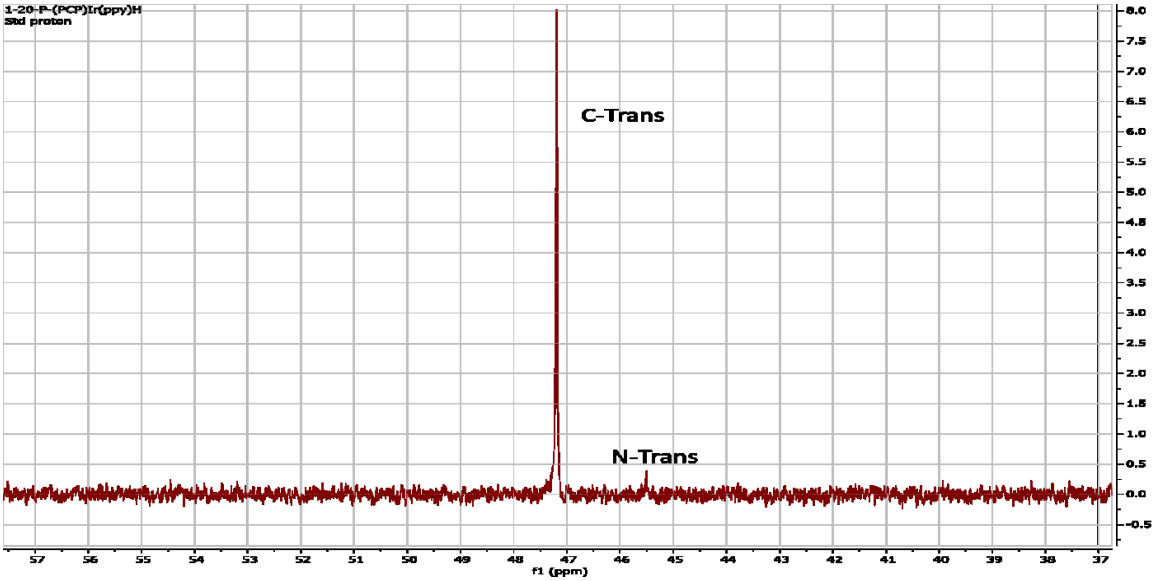

Figure 5.19: ^{31}P NMR of (^{tBu}PCP)Ir(ppy)H

(^{tBu}PCP)Ir(ppy)Cl

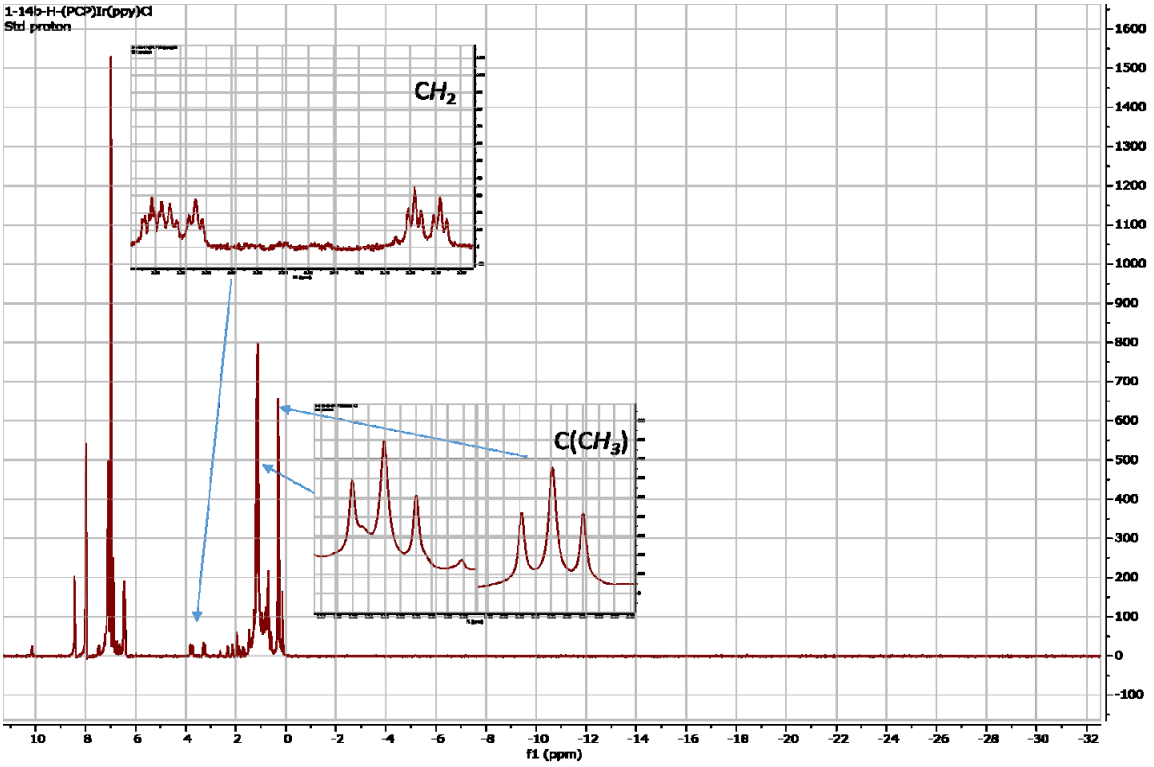

Figure 5.20: ^{1}H NMR of (^{tBu}PCP)Ir(ppy)Cl

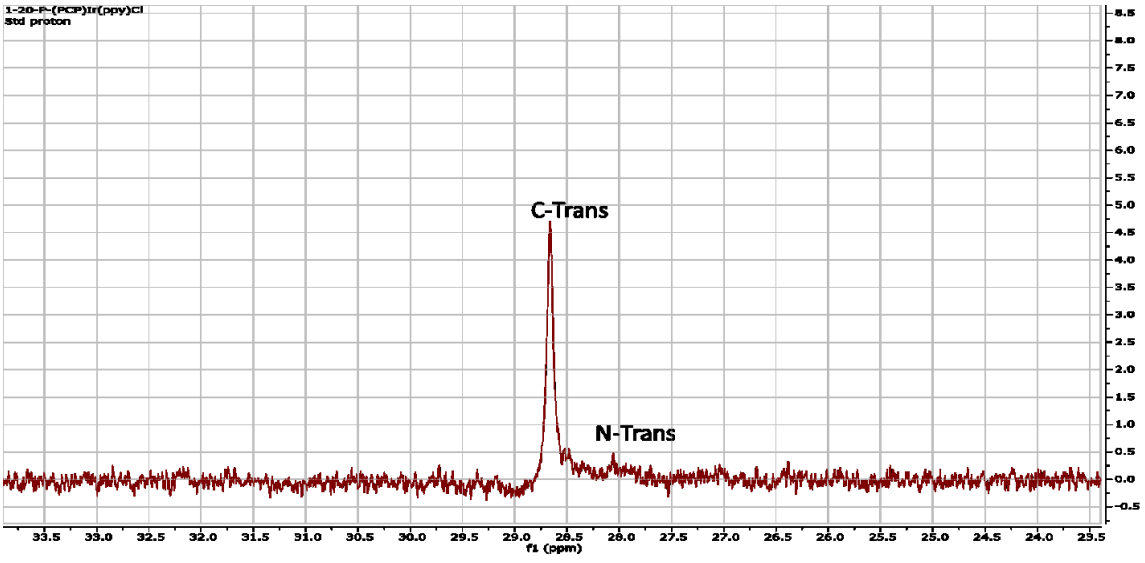

Figure 5.21: ^{31}P NMR of (^{tBu}PCP)Ir(ppy)Cl

(^{tBu}PCP)Ir(fppy)H

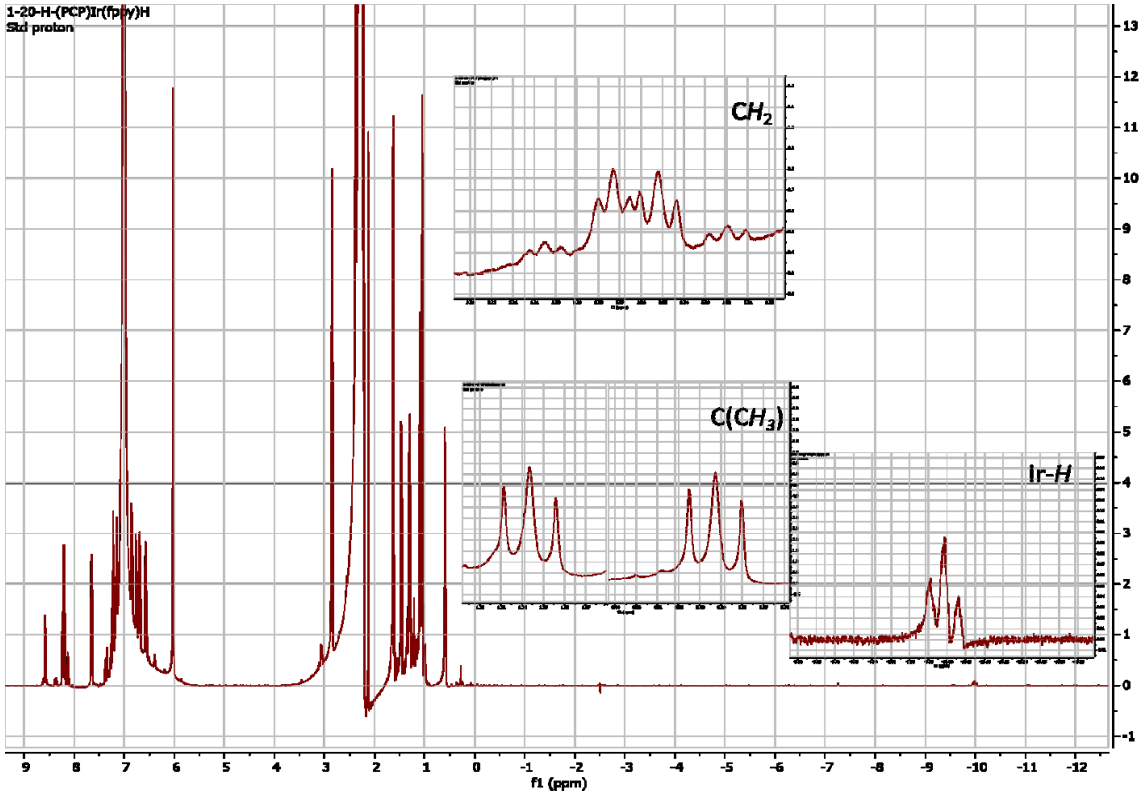

Figure 5.22: ^{1}H NMR of (^{tBu}PCP)Ir(fppy)H

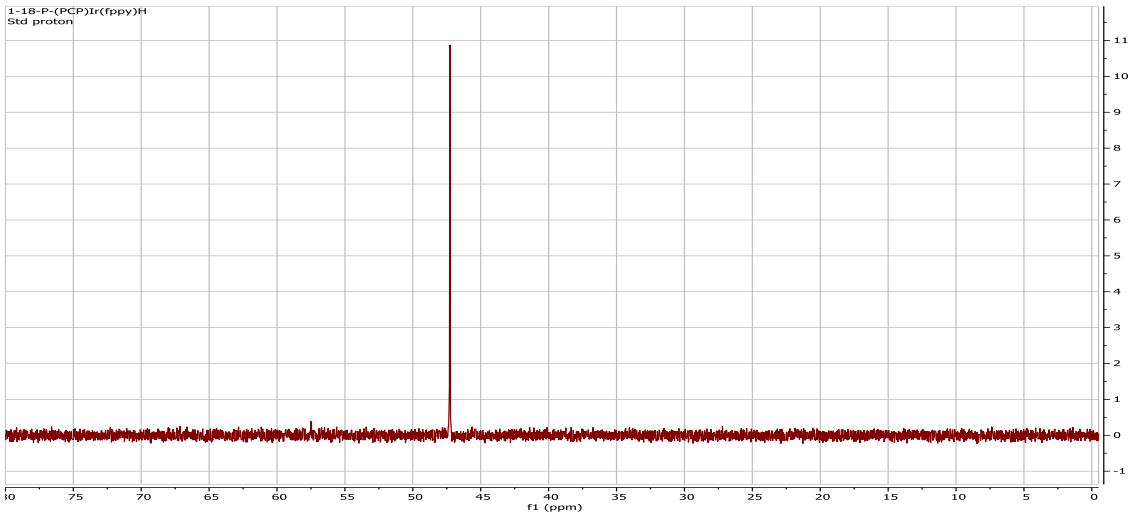

Figure 5.23: ^{31}P NMR of (^{tBu}PCP)Ir(fppy)H

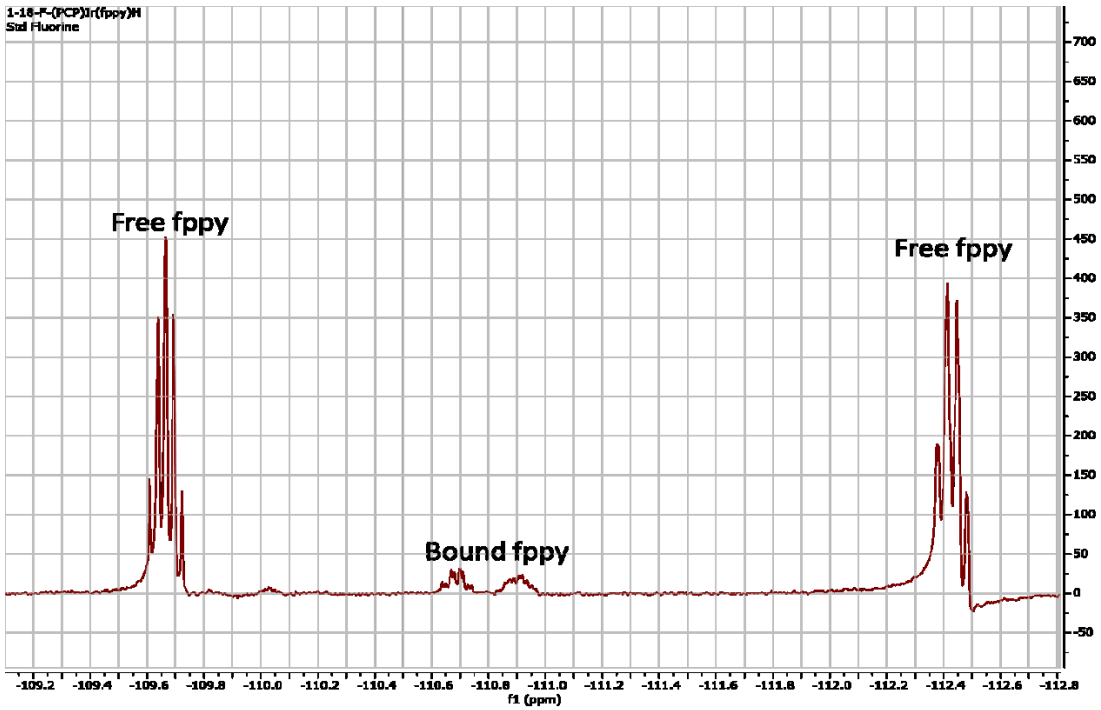

Figure 5.24: ^{19}F NMR of (^{tBu}PCP)Ir(fppy)H

(^{tBu}PCP)Ir(fppy)Cl

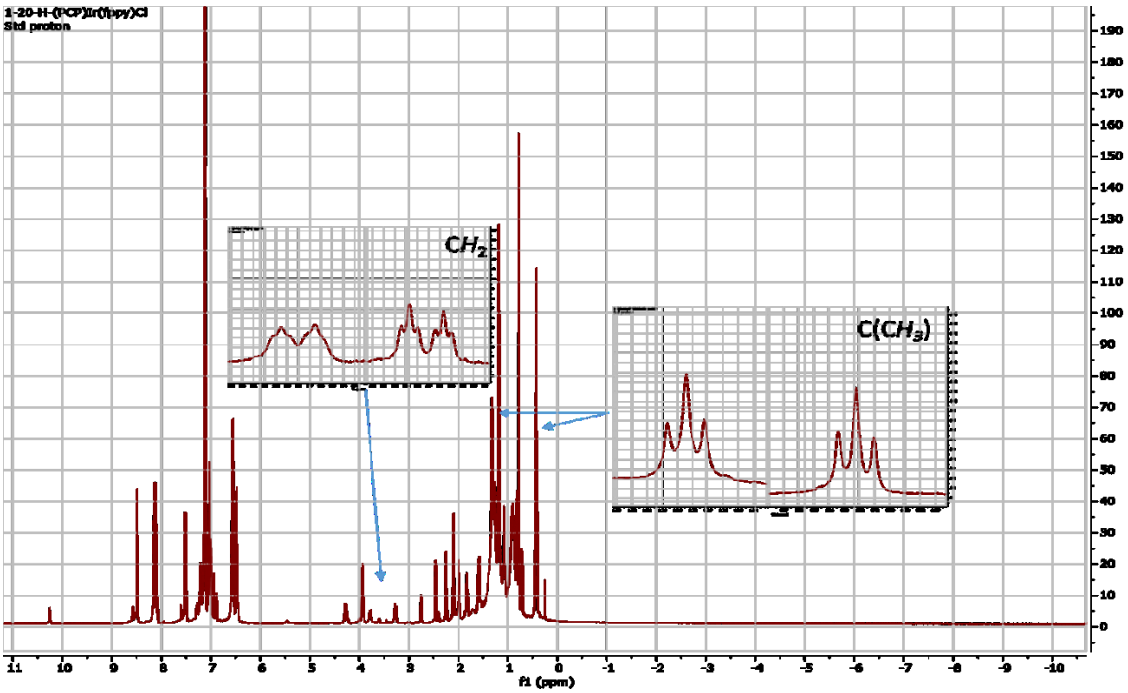

Figure 5.25: ^{1}H NMR of (^{tBu}PCP)Ir(fppy)Cl

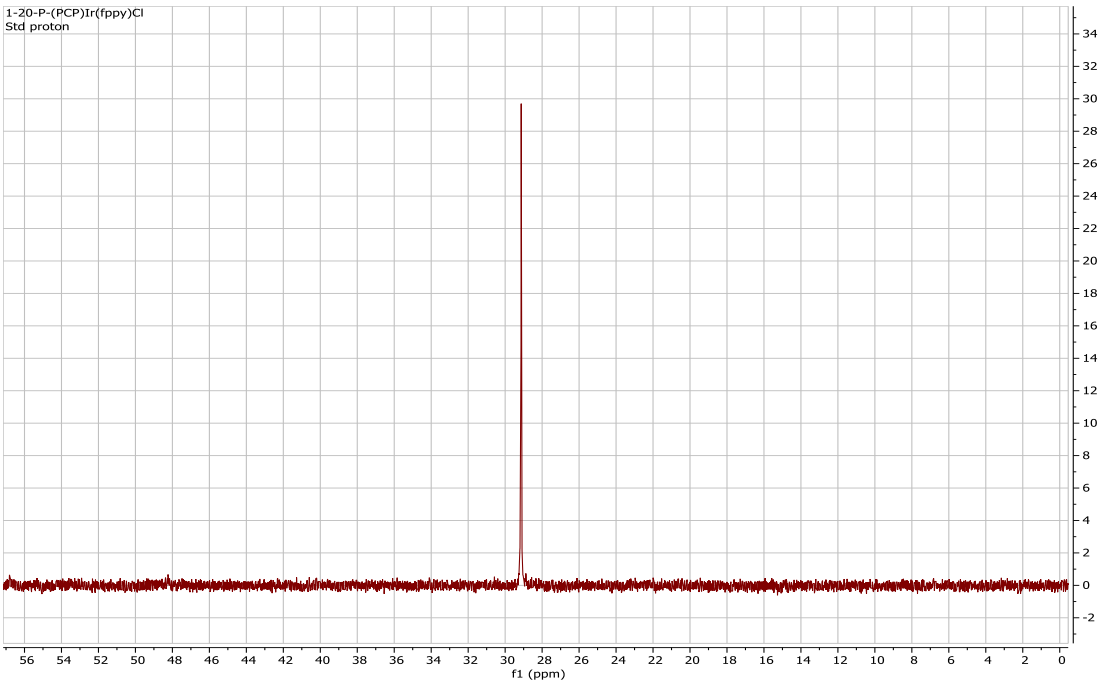

Figure 5.26: ^{31}P NMR of (^{tBu}PCP)Ir(fppy)Cl

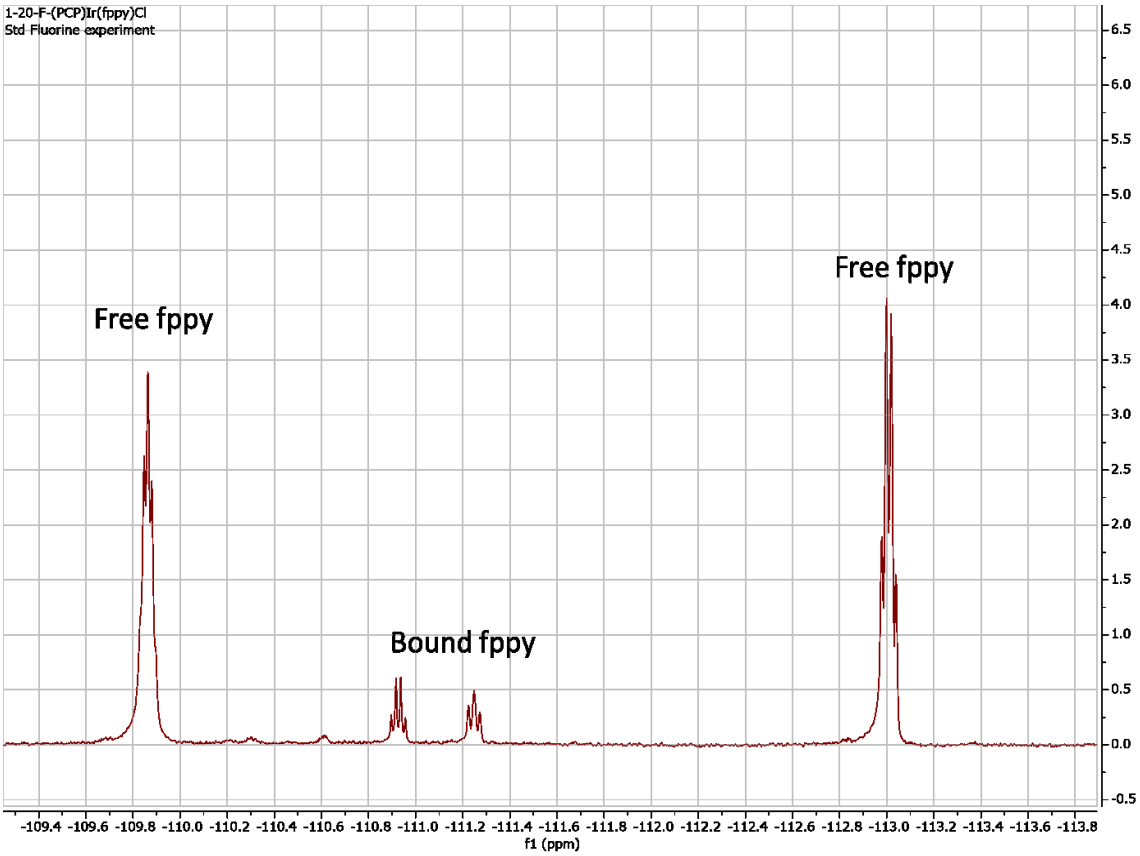

Figure 5.27: ^{19}F NMR of (^{tBu}PCP)Ir(fppy)Cl

(^{tBu}PCP)Ir(nppy)H

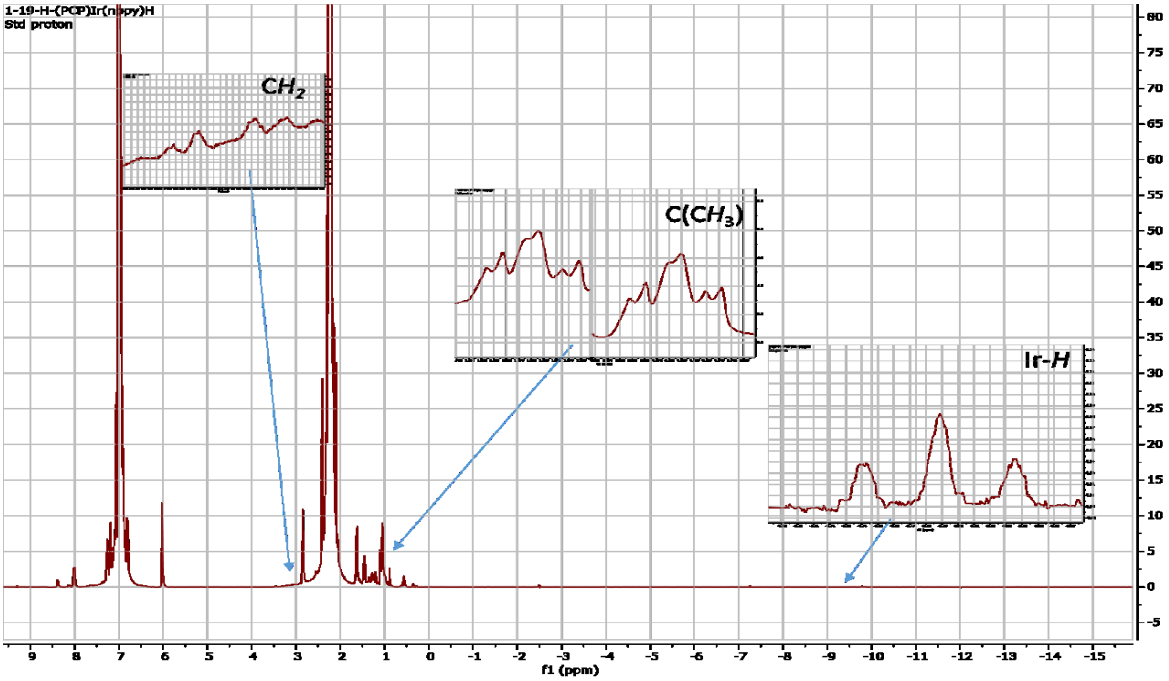

Figure 5.28: ^{1}H NMR of (^{tBu}PCP)Ir(nppy)H

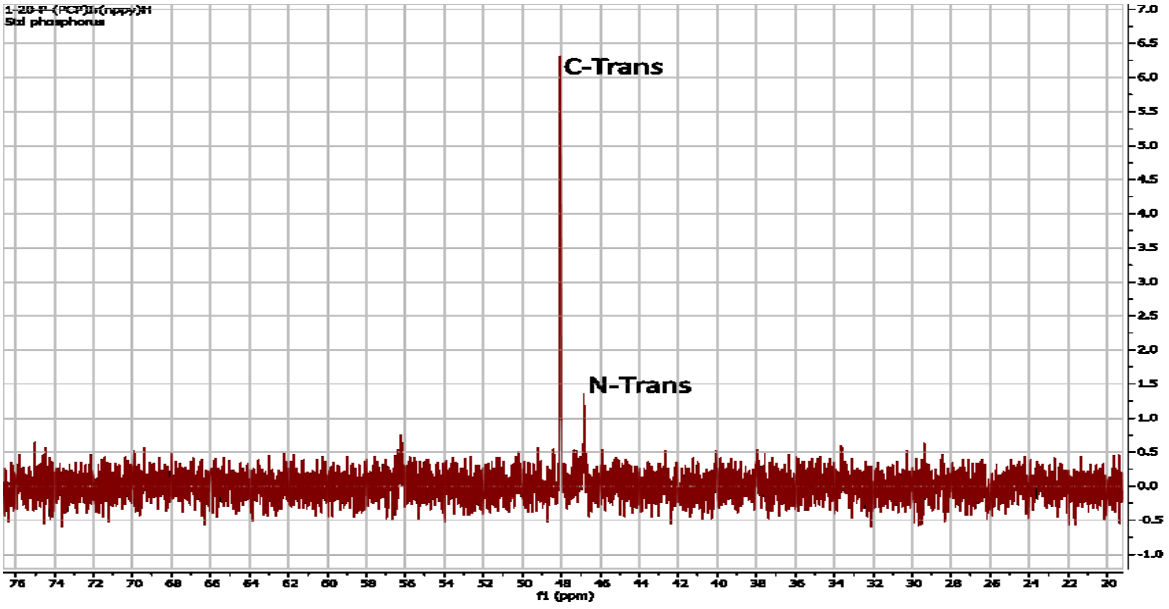

Figure 5.29: ^{31}P NMR of (^{tBu}PCP)Ir(nppy)H

(^{tBu}PCP)Ir(nppy)Cl

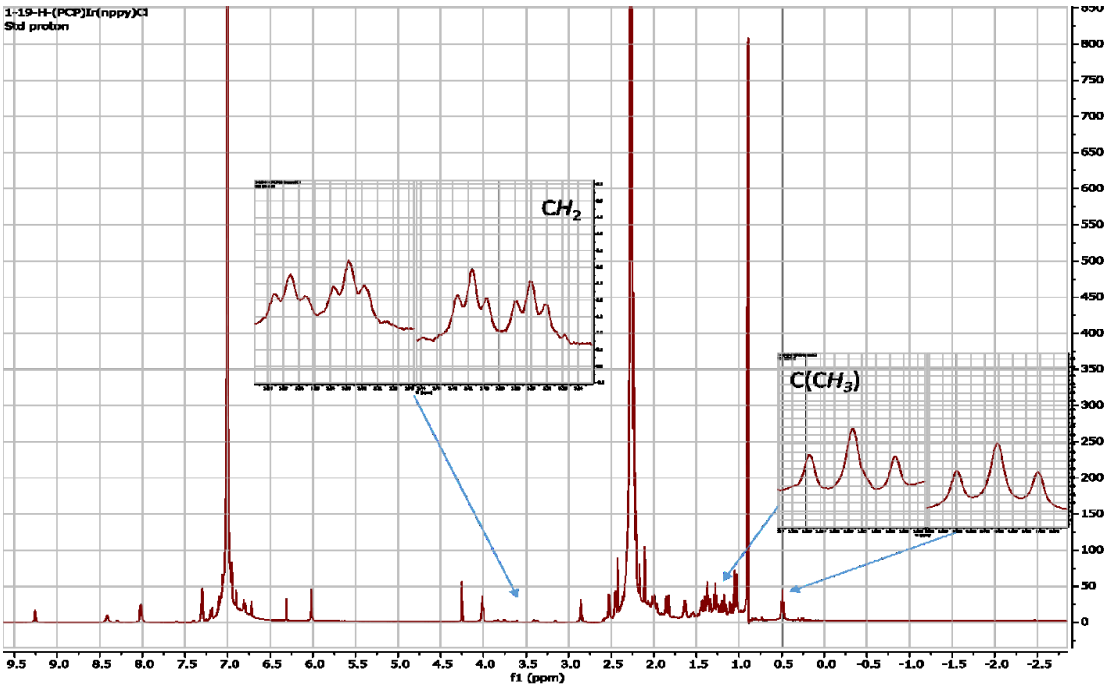

Figure 5.30: ^{1}H NMR of (^{tBu}PCP)Ir(nppy)Cl

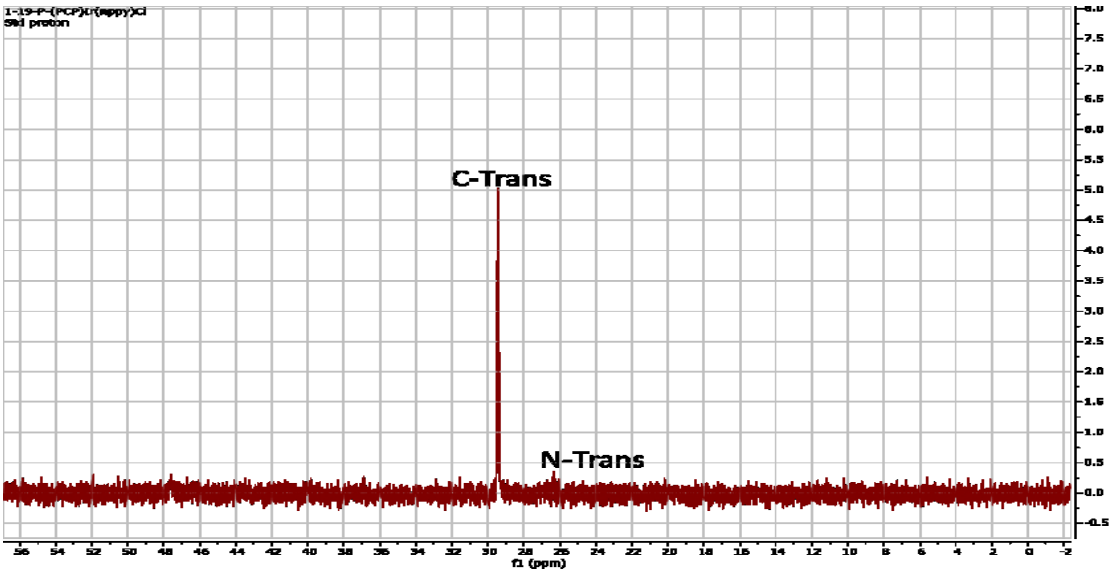

Figure 5.31: ^{31}P NMR of (^{tBu}PCP)Ir(nppy)Cl

5.8: References

1. Chen, H; Lee, K; Lin, B; Chen,S; Wu, S. *Light Sci. Appl.* **2018**, *7*, 17168.
2. Yang, D; Wu, S. *Fundamentals of Liquid Crystal Devices*. 2nd ed. John Wiley & Sons: New York, 2014.
3. Chen, J; Hardev, V; Hartlove, J; Hofler, J; and Lee, E. *SID Int. Symp. Dig. Tec.* **2012,** *43*, 895-896.
4. Chen, H; He, J; Wu, S. *IEEE J. Sel. Top. Quantum Electron.* **2017**, *23*, 1900611.
5.Japan Display Inc. LCD Basics.
https://www.j-display.com/english/technology/lcdbasic.html (Accessed Nov. 6, 2018).
6. Tang, C; VanSlyke, S. *Appl. Phys. Lett.* **1987**, *51*, 913–915.
7. 0

8. Essays, UK. Advantages and Disadvantages of Organic Light Emitting Diodes.
https://www.ukessays.com/essays/engineering/advantages-and-disadvantages-of-organic-light-emitting-diodes-engineering-essay.php (Accessed Nov. 6, 2018).
9. Lamansky, S.; Djurovich, P.; Murphy, D.; Abdel-Razzaq, F.; Lee, H.-E.; Adachi, C.; Burrows, P. E.; Forrest, S. R.; Thompson, M. E. *J. Am. Chem. Soc*. **2001**, *123*, 4304-4312.
10. Baldo M. A., Lamansky S., Burrows P. E., Thompson M. E., Forrest S. R. *Appl. Phys. Lett.* **1999,** *75*, 4–6.
11. Adachi C., Baldo M. A., Thompson M. E. & Forrest S. R. *J. Appl. Phys*. **2001,** *90*, 5048–5051.
12. Wilkinson, A; Puschmann, H; Howard, J; Foster, C; Williams, J. *Inorg. Chem*. **2006**, *45*, 8685-8699.
13. Lin, J; Chau, N; Liao, J; Wong, W; Lu, C; Sie, Z; Chang, C; Fox, M; Low, P; Lee, G; Chi, Y. *Organometallics* **2016**, *35*, 1813-1824.
14. Liao, J; Rajakannu, P; Liu, S; Lee, G; Chou, P; Jen, A; Chi, Y. *Inorg. Chem.* **2018**, *57*, 8287-8298.
15. Zhang, X; Wright, A; DeYonker, N; Hollis, T; Hammer, N; Webster, C; Valente, E. *Organometallics* **2012**, *31*, 1664-1672.
16. Chung, L; Chan, S; Lee, W; Wong, C. *Inorg. Chem.* **2012**, *51*, 8693-8704.
17. Au,V; Tsang, D; Wong, K; Chan, M; Zhu, N; Yam, V. *Inorg. Chem*. **2013**, *52*, 12713-12725.
18. Baranoff, E; Suarez, S; Bugnon, P; Barolo, C; Buscaino, R; Scopelliti, R; Zuppiroli, L; Graetzel, M; Nazeeruddin, Md. K. *Inorg. Chem.* **2008**, *47*, 6575-6577.
19. Li, H; Chou, P; Hu, Y; Cheng, Y; Liu, R. *Organometallics* **2005**, *24*, 1329-1335.
20. Jin, J; Shin, H; Park, J; Park, J; Kim, E; Ahn, T; Ryu, D; Son, S. *Organometallics* **2013**, *32*, 3954-3959.
21. Kim, J; Shin, I; Kim, H; Lee, J. *J. Am. Chem. Soc.* **2005**, *127*, 1615-1615.
22. Lo, S; Harding, R; Shipley, C; Stevenson, S; Burn, P; Samuel, I. *J. Am. Chem. Soc.* **2009**, *131*, 166181-16688.
23. The above papers were chosen to show some of the variety in iridium complexes studied for OLEDs. They in no way cover the complete scope of all reported OLED iridium complexes.

24. Laviska, D. A., Activation of Aryl C-H and C-X Bonds by a Pincer-Ligated 'PCP' Iridium Complex, Ph.D. Dissertation, Rutgers University-New Brunswick, New Brunswick, NJ, 2013.
25. Baranoff, E; Curchod, B; Monti, F; Steimer, F; Accorsi, G; Tavernelli, I; Rothlisberger, U; Rosario, S; Gratzel, M; Nazeeruddin, Md. K. *Inorg. Chem.* **2012**, *51*, 799-811.
26. Eum, M; Chin, C; Kim, S; Kim, C; Kang, S; Hur, N; Seo, J; Kim, G; Kim, Y. *Inorg. Chem*. **2008**, *47*, 6289-6295.
27. Klein, J.H. Electron Transfer and Spin Chemistry in Iridium-Dipyrrin Dyads and Triads, Ph.D. Dissertation, University of Wurzburg, Bavaria, Germany, 2015.
28. (a) Gupta, M.; Hagen, C.; Flesher, R. J.; Kaska, W. C.; Jensen, C. M. *Chem. Commun.* **1996**, 2083-2084. (b) Gupta, M.; Hagen, C.; Kaska, W. C.; Cramer, R. E.; Jensen, C. M. *J. Am. Chem. Soc*. **1997**, *119*, 840-841. (c) Gupta, M.; Kaska, W. C.; Jensen, *C. M. Chem. Commun.* **1997**, 461-462.